

DEVELOPMENT AND EVALUATION OF HIV gp120 RESPONSIVE MICROBICIDE
FORMULATION FOR THE PREVENTION OF HIV SEXUAL TRANSMISSION

A DISSERTATION IN
Pharmaceutical Sciences
and
Chemistry

Presented to the Faculty of the University
Of Missouri-Kansas City in partial fulfillment of
The requirements for the degree of

DOCTOR OF PHILOSOPHY

By
Fohona S. Coulibaly

B.S Chemical Engineering, INP-HB, Yamoussoukro, Ivory Coast, 2011

Kansas City, Missouri
2018

© 2018

FOHONA S. COULIBALY

ALL RIGHTS RESERVED

DEVELOPMENT AND EVALUATION OF HIV gp120 RESPONSIVE MICROBICIDE FORMULATION FOR THE PREVENTION OF HIV SEXUAL TRANSMISSION

Fohona S. Coulibaly, Candidate for the Doctor of Philosophy Degree

University of Missouri-Kansas City, 2018

ABSTRACT

Sexual transmission of HIV remains the primary route (75 to 85%) of HIV infection among all new infection cases. Furthermore, women represent the most vulnerable population and are more susceptible to HIV infections than their male counterpart. Thus, there is an urgent need to develop topical (vaginal/rectal) microbicide formulations capable of preventing HIV sexual transmission. The objective of this dissertation is to develop a mannose specific, lectin-based topical microbicide formulation capable of targeting HIV gp120 for the prevention of HIV sexual transmission. In Chapters 1 and 2, the general hypothesis, aims and scope of this work are introduced. Chapter 3 covers the literature review of anti-HIV lectins and current delivery approaches.

In Chapter 4, the binding interactions between the mannose specific lectin Concanavalin A (ConA) and glycogen from *Oster*, as well as mannan from *Saccharomyces cerevisiae*, were studied using a quartz crystal microbalance (QCM). The equilibrium dissociation constant describing the interaction between Con A and glycogen ($K_D = 0.25 \mu\text{M}$) was 12 fold lower than the equilibrium dissociation constant describing the binding between Con A and mannan ($K_D =$

2.89 μM). That is, Con A was found to have a higher affinity for the glucose-base polysaccharide, than for the mannose-based. This observation was mainly attributed to steric effects, the difference in molecular weight and branching pattern of both polysaccharides.

The knowledge gained in Chapter 4 was applied in Chapter 5 for the development of HIV-1 gp120 and mannose responsive particle (MRP) formulations. Thus, core dissolved MRP (C^-MRP) and core containing MRP (C^+MRP) were prepared through the layer-by-layer coating of calcium carbonate (CaCO_3) with the mannose specific lectin (Con A) and a polysaccharide cross-linker (Glycogen). Particles were characterized and tested *in vitro* on *Lactobacillus crispatus*, Human vaginal keratinocytes (VK2/E6E7) and murine macrophage [RAW 264.7 (TIB-71)] cell lines. C^+MRP average size and ζ -potential were 1130 ± 15.72 nm [PDI = 0.153] and -15.1 ± 0.55 mV, (n=3). Similarly, C^-MRP average size and ζ -potential were 1089 ± 23.33 nm (n=3) and -14.2 ± 0.25 mV (n=3). Tenofovir (TFV) encapsulation efficiency in CaCO_3 was 74.4% with drug loading of 16.3% w/w and 6.0% w/w in C^+MRP and C^-MRP , respectively. Both C^-MRP and C^+MRP were nontoxic to *L. crispatus* and did not induce any significant pro-inflammatory nitric oxide release in VK2 and RAW 264.7 cell culture. However, C^-MRP was found to significantly affect VK2 and RAW 264.7 cells viability at concentrations ≥ 100 $\mu\text{g/ml}$. Similarly, C^-MRP significantly increased pro-inflammatory cytokines (IL1 α , IL1 β , IL6, IL7, MKC and TNF α) release at concentrations ≥ 100 $\mu\text{g/ml}$. Conversely, C^+MRP did not induce any significant changes in VK2 and RAW 264.7 cells viability nor in pro-inflammatory cytokines' levels, in the concentration range tested (≤ 1000 $\mu\text{g/ml}$), for 24 h. C^+MRP was then selected for further *in vitro* drug release studies as well as *ex vivo* vaginal mucoadhesion studies. HIV gp120 triggered TFV release from C^+MRP in a concentration dependent manner, and following Hixson–Crowell and Hopfenberg kinetic models, consistent with drug release from diminishing surface or matrix

eroding drug particles. C^+MRP was further optimized by varying the number of Con A layer in the formulation, and in order to achieve lower HIV gp120 sensitivity ($\leq 100 \mu\text{g/ml}$). Furthermore, bioadhesion studies, performed *ex vivo* on porcine vaginal tissue, demonstrated that FITC- C^+MRP adheres to vaginal tissue at levels varying between $10\% \pm 1$ and $20\% \pm 2$, depending on the number of Con A layers in the formulation.

In chapter 6, C^+MRP preclinical safety was evaluated in 8-12 weeks old female C57BL/6 mice model. First, mice were treated with Depo-Provera® to maintain them in a diestrus-like state. Then the microbicide formulation was delivered vaginally at a dose of 100 mg/kg in PBS. Vaginal histology, immunohistochemistry evaluations, as well as pro-inflammatory cytokines release (vaginal lavage and tissue extract) were investigated after 24 h. The vaginal retention of FITC- C^+MRP was also evaluated, up to 24 h. Vaginal and major reproductive organs' histology did not show major damage of the epithelial layer. This result was also consistent with immunohistochemistry evaluation of CD45+ cells infiltration in the vaginal epithelial layer, unlike the positive control treated groups (BZK and N-9). Furthermore C^+MRP did not induce any significant changes in pro-inflammatory cytokines IL1 α , IL2, IL7, IP10 and TNF α . In addition, it was also observed that FITC labeled C^+MRP does not have a long-term retention in mice vaginal tract. This result suggested that a precoital or multiple vaginal application (i.e., BID) approaches of C^+MRP should be investigated.

Overall, this study demonstrates the feasibility of lectin-based microbicide formulations to target HIV gp120 for the prevention of HIV sexual transmission.

APPROVAL PAGE

The faculty listed below, appointed by the Dean of the School of Graduate Studies, have examined the dissertation titled “Development and Evaluation Of HIV gp120 Responsive Microbicide Formulation for the Prevention of HIV Sexual Transmission”, presented by Fohona S. Coulibaly, candidate for the Doctor of Philosophy Degree, and certify that in their opinion it is worthy of acceptance.

Supervisory Committee

Bi-Botti C. Youan, Ph.D., Committee Chair

Division of Pharmaceutical Sciences

William G. Gutheil, Ph.D.

Division of Pharmaceutical Sciences

Keith R. Buszek, Ph.D.

Department of Chemistry

Nathan A. Oyler, Ph.D.

Department of Chemistry

Zhu Da-Ming, Ph.D.

Department of Physics and Astronomy

CONTENTS

ABSTRACT	iii
LIST OF ILLUSTRATIONS	x
LIST OF TABLES	xv
LIST OF ABBREVIATIONS	xvi
ACKNOWLEDGEMENTS	xvii
CHAPTER	
1. INTRODUCTION	1
1.1 Problem statement	1
1.2 Research hypothesis	7
1.3 Objectives	7
2. STATE OF THE ART IN HIV MICROBICIDE DRUG DELIVERY	9
2.1 HIV life cycle	9
2.2 Vaginal physiology and HIV acquisition	12
2.3 HIV microbicides and classification	17
2.4 Topical microbicide candidates' formulation and delivery	21
2.5 Guidance for preclinical assessments of vaginal microbicide candidates' safety and efficacy	25
3. LITERATURE REVIEW OF HIV SURFACE GLYCOPROTEINS AND ANTI-HIV LECTINS	29
3.1 Introduction	29
3.2 HIV surface glycoproteins and glycans	30
3.3 Anti-HIV lectins	37

3.4 Challenges in anti-HIV lectins formulation development.....	43
3.5 Anti-HIV lectin nanoformulations	44
3.6 Conclusion.....	47
4. SCREENING OF CONCANAVALIN A - POLYSACCHARIDES BINDING AFFINITY USING A QUARTZ CRYSTAL MICROBALANCE	49
4.1 Introduction and rationale.....	49
4.2 Material and method.....	51
4.3 Results and discussion.....	57
4.4 Conclusion.....	66
5. DEVELOPMENT OF A MICROBICIDE LOADED HIV-1 gp120 TARGETED VAGINAL FORMULATION	68
5.1 Introduction and rationale.....	68
5.2 Material and method.....	71
5.3 Results and discussion.....	85
5.4 Conclusion.....	108
6. IN VIVO PRECLINICAL SAFETY EVALUATION OF A MICROBICIDE LOADED HIV-1 gp120 TARGETED VAGINAL FORMULATION IN FEMALE MOUSE REPRODUCTIVE TRACT	110
6.1 Introduction and rationale.....	110
6.2 Material and method.....	112
6.3 Results and discussion.....	122
6.4 Conclusion.....	131
7. SUMMARY AND FUTURE STUDIES	132

7.1 Summary.....	132
7.2 Future studies.....	135
APPENDIX.....	136
REFERENCES	138
VITA.....	196

LIST OF ILLUSTRATIONS

Figure	Page
1-1: Number of people living with HIV worldwide	2
1-2: HIV worldwide expenditure and proportion of infected people receiving treatment	3
1-3: HIV global prevalence by region	4
1-4: HIV global infection by gender	5
2-1: HIV virus life cycle.	9
2-2: Steps involved in HIV membrane fusion.	10
2-3: Vaginal mucosa and microbiota at different stages of women' life.....	14
2-4: Mechanism of HIV vaginal acquisition	16
Scheme 2-1: GO/NO-GO algorithm in vaginal microbicides products development.....	27
3-1: High mannose and complex glycan structures found in HIV gp120. Structures are adapted from the following references.....	33
3-2: High mannose and complex glycan structures in HIV gp41. Structures are adapted from the following references.....	35
Scheme 4-1: Step-by-step illustration of Con A immobilization onto the QCM gold surface. Special care should be taken in handling Piranha solution under a fume hood. Once the crystal is cleaned and dried under nitrogen, it is disposed in 5 mM of Mercaptoundecanoic acid for 48h for carboxylic acid functionalization. Con A is then immobilized by EDC chemistry using 2 mM EDC and 5 mM NHS in MES buffer (pH5.8). The reagent mixture is gently shaken to insure even distribution of reagents during EDC coupling.....	55
4-1: Typical single flow injection QCM200 experimental setup.....	56

4-2: (A) FTIR spectra of clean QCM gold crystal (a) followed by 11-mercaptoundecanoic acid (MUA) attachment (b), before EDC/NHS chemistry (c) and finally Con A immobilization (d) onto the QCM crystal. (B) Size exclusion chromatograms of sodium nitrate (NaNO ₃) (buffer), glycogen and yeast mannan	58
4-3: Frequency shift observed with polysaccharide injection after a baseline is reached with free buffer (0.05 M Tris-buffer saline, 1 mM Ca ²⁺ , 1 mM Mn ²⁺ , pH 8.0).....	59
4-4: Time dependent QCM resonance frequency shifts for glycogen (A) and mannan (B) at different concentrations	60
4-5: Saturation binding curves for glycogen (A) mannan (B) and their respective reciprocal curves (A') and (B') obtained from equation (4-4).....	61
4-6: Molecular branching pattern in glycogen from Oyster (A) and mannan from <i>Saccharomyces cerevisiae</i> (B). Mannan main chain's monomers are linked by 1→6 glycosidic bonds with several 1→3 linkages throughout the branches. Those linkages are shown in blue color in mannan's structure. Glycogen main chain's monomers are 1→4 linked with only few 1→6 glycosidic bonds occurring each 12 glucose residues. The 1→4 linkages are shown in blue in glycogen's structure and the 1→6 linkage in green. Hydroxyl groups at position 3, 4 and 6, shown in red are critical for Con A interaction with a greater requirement at position 6. Unavailability of the critical hydroxyl groups prevents binding to Con A.	63
4.7: Relationships (ΔR vs ΔF) between the motional resistance (ΔR) and the resonant frequency (ΔF) changes corresponding to specific glycogen (a) and mannan (b) adsorption on a Con A layer on QCM crystal surface.	66
Scheme 5-1: Illustration of MRP's layer-by-layer preparation.	73

5-1: Average particle size and cumulative size distribution for CaCO ₃ -PSS (A), C ⁺ MRP (B) and C ⁻ MRP (C), and their respective ζ-potential measurements (A', B' and C').....	86
5-2: Average size and ζ-potential fluctuation during C ⁺ MRP layer-by-layer preparation.	87
5-3: ³¹ P solid state NMR spectra of TFV standard, C ⁺ MRP and C ⁻ MRP.	89
5-4: TFV ³¹ P solution state NMR spectrum following layer-by-layer encapsulation	90
5-5: FTIR spectra for C ⁺ MRP, C ⁻ MRP, glycogen, Con A, CaCO ₃ -PSS core particle and Con A/Glycogen agglutinate	92
5-6: TEM (A & B), SEM (A' & B') and confocal microscopy (C & C') images of C ⁺ MRP, C ⁻ MRP. Scale bars are 2 μm for A, A', B, B' and 100 nm for C and C'	93
5-7: <i>L. crispatus</i> viability. Percent viability and standard deviations values are computed from quintuplicates (n=5). One-way anova test is performed in GraphPad (version 6.0) to determine statistical significance. * (P ≤ 0.05) shows statistically significant difference from the negative control (culture media).....	95
5-8: VK2 cytotoxicity. A, B and C shows the mitochondrial metabolism, cellular membrane integrity and nitric oxide production, respectively, for C ⁺ MRP and C ⁻ MRP. D and E represent the CC ₅₀ curves for C ⁺ MRP and C ⁻ MRP, respectively. Values are computed from quintuplicates (n=5). One-way anova test is performed in GraphPad (version 6.0) to determine statistical significance. * (P ≤ 0.05) shows statistically significant difference from the negative control (culture media). NS indicates non-significance (P > 0.05).	96
5-9: RAW 264.7 cytotoxicity. A, B and C shows the mitochondrial metabolism, cellular membrane integrity and nitric oxide production, respectively, for C ⁺ MRP and C ⁻ MRP. D and E represent the CC ₅₀ curves for C ⁺ MRP and C ⁻ MRP, respectively. Values are computed from quintuplicates (n=5). One-way anova test is performed in GraphPad (version 6.0) to determine statistical	

significance. * ($P \leq 0.05$) shows statistically significant difference from the negative control (culture media). NS indicates non-significance ($P > 0.05$).	97
5-10: IL1 α , IL1 β , TNF α , IL6, IL7, IP10 and MKC cytokines levels measured in RAW 264.7 cell culture supernatant for C^+MRP and C^-MRP . Values are computed from quintuplicates (n=5). One-way anova test is performed in GraphPad (version 6.0) to determine statistical significance. * ($P \leq 0.05$) shows statistically significant difference from the negative control (culture media). NS indicates non-significance ($P > 0.05$)	99
5-11: TFV release profiles from C^+MRP (3L) in the presence of Man (1000 $\mu\text{g/ml}$) and HIV-1 rgp120 (100-1000 $\mu\text{g/ml}$).....	101
5-12: TFV release profiles from C^+MRP (2L & 1L) in the presence of Man (1000 $\mu\text{g/ml}$) and HIV-1 rgp120.....	106
5-13: C^+MRP mucoadhesion to porcine vaginal tissue (A) with corresponding thin sections fluorescent images (B).	107
6-1: Model of HIV vaginal infection following mucosal disruption (b) from an intact mucosal layer (a).	112
6-2: Vaginal epithelial layer in different osmolality conditions	115
6-3: Mouse vaginal cytology representing each stage of estrous. The stages of estrous include proestrus (A), estrus (B), metestrus (C), diestrus (D). Three cell types are identified: leukocytes (circle), cornified epithelial (black arrow), and nucleated epithelial (white arrow).	116
6-4: C^+MRP average particle size (A), surface charge density (B) and SEM imaging (C). SEM image scale bar is 2 μm	123

6-5 Vaginal cytology assessment of the estrous stages in Depo-Provera treated and non-treated mice. Three cell types are identified: leukocytes (blue circle), cornified epithelial (red arrow), and nucleated epithelial (white arrow).	125
6-6: Histology (H&E staining) of mouse reproductive organs' tissues following treatment with C^+MRP for 24 h. Thinning and stripping of epithelial cell layer in positive controls is indicated by red arrows.....	126
6-7: Immunohistochemistry evaluation of vaginal tissue sections following treatment with C^+MRP for 24 h. Black boxes indicated by red arrows show significant leukocyte (CD45+ cells) infiltration.	127
6-8: Pro-inflammatory cytokines (IL1 α , IL1 β , IL6, IL7, IP10, MKC and TNF α) levels measured in mice cervicovaginal lavage and vaginal tissue extract, following C^+MRP treatment for 24 h, at a dose of 100 mg/kg. Values are computed from triplicates (n=3 animals). One-way anova test is performed in GraphPad (version 6.0) to determine statistical significance. * ($P \leq 0.05$) shows statistically significant difference from the negative control (PBS treated group). NS indicates non-significance ($P > 0.05$)	128
6-9: Vaginal retention of FITC labeled C^+MRP and HEC gel in mice after 24 h. C^+MRP was applied at a dose of 25 mg/kg.	130

LIST OF TABLES

Table	Page
2-1: FDA approved anti-HIV microbicide and formulations.	19
2-2: Current vaginal formulations for the prevention of HIV sexual transmission.	23
3-1: Example of natural anti-HIV lectins.	40
3-2: Summary of anti-HIV lectin nanoformulations	46
5-1: FDA similarity and dissimilarity factors for TFV release from C^+MRP (1L, 2L and 3L).	103
5-2: Kinetic models describing TFV <i>in vitro</i> release profiles from C^+MRP (3L)	104
6-1: Selected physico-chemical and biological properties of formulations tested	118

LIST OF ABBREVIATIONS

AH: Actinohivin	HIV gp160 : HIV glycoproteins precursor
AIDS : Acquired Immune Deficiency Syndrome	HIV gp41: HIV envelope glycoprotein 41
BanLec: Banana lectin	HIV : Human Immunodeficiency Virus
BzB: Benzoboroxole	HIV : Human Immunodeficiency Virus
C^+MRP : Core containing MRP	Man: Mannose
CBA: Carbohydrate Binding Agents	MHC: Major Histocompatibility Complex
C^-MRP : Core removed MRP	MHL: <i>Myrianthus holstii</i> lectin
Con A: Concanavalin A	MRC 1&2: Mannose Receptor C-Type 1&2
CVL: <i>Chaetopterus variopedatus</i> lectin	MRP: HIV-1 gp120 and mannose responsive particles
CV-N: Cyanovirin-N	MVL: <i>Microcystis viridis</i> lectin
DC-SIGN: Dendritic Cell-Specific Intercellular adhesion molecule-3-Grabbing Non-integrin	MVN: Microvirin
FIPV: Feline Infectious Peritonitis Virus	Neu5Ac: N-Acetylneuraminic acid (sialic acid)
Fuc: Fucose	NPL: <i>Narcissus pseudonarcissus</i> lectin
Gal: Galactose	OAA: <i>Oscillatoria agardhii</i> agglutinin
GlcNAc: N-acetylglucosamine	PBA: Phenylboronic acid
GRFT: Griffithsin	QCM: Quartz Crystal Microbalance
HexNAc: N-acetylhexoseamine (N-acetylglucoseamine, N-acetylgalactoseamine)	SARS: Severe Acute Respiratory Syndrome
HIV gp120: HIV envelope glycoprotein 120	SVL: <i>Serpula vermicularis</i> lectin
	SVN: Scytovirin
	TFV: Tenofovir

ACKNOWLEDGEMENTS

My wholeheartedly gratitude and thanks goes to my advisor and committee chair, Dr. Bi-Botti C. Youan, of the Division of Pharmaceutical Sciences, UMKC, for giving me the opportunity to make a life-long dream becomes a reality. I would like to sincerely thank him for his guidance, his unwavering support, and contagious determination and enthusiasm for the quest of science. His outstanding mentorship and critical reasoning have not only made this dissertation possible, but also raised the quality of this work. Dr. Youan' honest and constructive criticism and feedbacks throughout my Ph.D. studies have allowed me to grow as a pharmaceutical scientist.

I am also grateful to my committee members Dr. William G. Gutheil of the Division of Pharmaceutical Sciences, UMKC, Dr. Nathan A. Oyler and Dr. Keith R. Buszek of the Department of Chemistry, UMKC and Dr. Zhu Da-Ming of the Department of Physics and Astronomy, UMKC for their invaluable support, comments, guidance and insightful collaborations throughout my Ph.D. studies.

I am extremely thankful, to Dr. William G. Gutheil for his constant support and fruitful scientific discussions. His expertise in analytical chemistry and mass spectrometry have greatly advance this project and many other projects during my Ph.D. education. I would also like to thank him for serving in my Ph.D. advisory committee and dedicating time and efforts in reviewing this dissertation manuscript.

I would like to sincerely thank Dr. Nathan A. Oyler for his guidance and openness. His expertise in nuclear magnetic resonance spectroscopy and chemistry have helped me solve many analytical hurdles I faced throughout this project, and led to new NMR techniques for drug quantification and characterization in pharmaceutical sciences. I am also thankful to him for

serving in my Ph.D. advisory committee and dedicating time and efforts in reviewing this dissertation.

I am extremely grateful to Dr. Keith R. Buszek for his support and guidance in synthetic organic chemistry. I highly appreciate that he allowed me access to his lab to conduct synthetic reactions. I am truly honored to have met him, learned from him and to be called a friend. Dr. Keith R. Buszek' unique teaching of chemistry was remarkable and extremely helpful throughout my Ph.D. education. I am sincerely thankful to him for serving in my Ph.D. advisory committee and dedicating time and efforts in reviewing this dissertation.

I would like to express my sincere gratitude to Dr. Zhu Da-Ming for his support, guidance and interest in this project. Dr. Zhu Da-Ming guidance and flexibility have allowed me to overcome critical hurdles during my Ph.D. education. I am extremely thankful to him for serving in my Ph.D. advisory committee and providing honest and constructive reviews that have helped improve this manuscript.

My sincere gratitude to Dr. Agostino Molteni, Dr. Daniel C. Dim, Dr. Nilofer Qureshi, Tim Quinn and the late Dr. Betty L. Herndon of the School of Medicine, UMKC, for their kind help, guidance, and suggestions in histopathology, immunohistochemistry assays. I am extremely grateful for the scientific discussions and guidance I received from Dr. Betty L. Herndon before her passage.

I would also like to thank Dr. Russell B. Melchert, Dr. Ashim K. Mitra, and all the faculty and staff members of the School of Pharmacy, UMKC. The constant support, guidance and feedbacks I received from them have allowed me to hone my scientific skills and successfully navigate the Ph.D. labyrinth. I'm grateful for the constant financial support and scholarships from

the School of Pharmacy, UMKC, which allowed me to present my research at national and local scientific meetings.

I am extremely thankful to Dr. Denis M. Medeiros and Dr. Jennifer Friend for their vision and leadership during their tenure at the School of Graduate Studies, UMKC. Dr. Denis M. Medeiros unwavering engagement in helping graduate students discover their inner leader has been extremely helpful to me. My sincere thanks to the School of Graduate Studies, UMKC for its financial support and scholarships, which allowed me to explore my own scientific hypotheses, further my research and present my research findings at national and local scientific meetings.

Throughout my tenure at the School of Pharmacy, UMKC, I have had the opportunity to work with brilliant and highly skilled scientists and colleagues. My sincere thanks to Dr. Miezane Ezoulin, who taught me a great deal of cell culture techniques and bioanalytical methods. His guidance and leadership in the *in vivo* study were tremendously helpful, and I am extremely grateful for his friendship and brotherhood. I would like to thank Dr. Youm Ibrahima, Dr. Tao Zhang, Dr. Jianing Meng, Dr. Vivek Agrahari, Albert Ngo, Danielle Thomas, Omowumi Akinjole, Abdullah Alsalhi, Dr. Sudhaunshu Purohit, Abrar Alnafisah, Navid Ayon, Mark Rayhart, Dr. DJ Black for all the training, collaboration and friendship during my Ph.D. education.

I would like to extend a special thanks to my family, to whom I truly owe what I have become today. My moms Sanata Coulibaly, the late Mama Coulibaly and my late father Dramane Coulibaly, who have taught me the value of hard work and supported me and my siblings, even when they didn't have much. Their unconditional love, sacrifice and everyday struggle to support us is the most important lesson of my life. My heartfelt gratitude and thanks to Moussa ("Chef"), whose sacrifices and constant support have allowed the rest of us to fulfill our own dreams and educational goals. You are truly a role model for me. Thanks to Natenin, Ladjia, Drissa, Daouda,

Seidou, Madou, Souleymane, Tchemogo, Tata, Mangary, Fatou, Sali and Yoh for their selfless, love filled and constant support. I'm truly grateful for all you have sacrificed for me. I am also grateful for all my uncles, cousins and nephews constant love and support.

I would like to express my extreme gratitude and thanks to the love of my life, my friend and confident, Macouni Dore for her enduring love, unconditional support and her strategic thinking. You have truly been a great partner who have worked tirelessly to support our little oasis. Truly, you deserve as much credit for this achievement as I do. To our Bubble Guppies, Khalil and Raissa, I love you with all the strength in my soul; you are the boundless source of motivation that keeps the flame kindle in my heart.

My sincere gratitude to the Diomande for adopting my family and I, and making us feel truly at home. Thanks grandma!

I am immensely thankful to the National Institutes of Health (NIH) and the National Institute of Allergy and Infectious Diseases (NIAID) for providing the financial supports (R01AI087304) to carry out this project. Many thanks to Jennifer Robinson and the NIH AIDS reagent program for graciously supplying us with various HIV recombinant glycoprotein 120 (HIV-gp120) subtypes.

The acknowledgement presented here is not meant to be comprehensive at all. There were certainly many others who have contributed to my research experience and my enjoyment during these fulfilling years. Many thanks to you all!

CHAPTER 1

INTRODUCTION

1.1 Problem Statement

The Acquired Immunodeficiency Syndrome (AIDS) is an infectious disease caused by the Human Immunodeficiency Virus (HIV). AIDS is a debilitating condition in which a progressive failure of infected patients' immune system render them vulnerable to life-threatening opportunistic infections such as tuberculosis, pneumonia, salmonella infection, candidiasis, toxoplasmosis, and tuberculosis (TB). AIDS patients also have a higher risk of developing the so-called "AIDS-defining cancers" including Kaposi sarcoma, aggressive B-cell non-Hodgkin lymphoma, and cervical cancer.¹ In fact, on average, people infected with HIV have been shown to be 500 times more likely to develop Kaposi sarcoma, 12 times more likely to be diagnosed with non-Hodgkin lymphoma, and 3 times more likely to develop cervical cancer, among women.² Furthermore, HIV patients have a higher risk of developing several other types of cancers known as "non-AIDS-defining cancers" including, Hodgkin lymphoma, liver cancer, anal cancer, oral cavity/pharynx cancer and lung cancer.^{3, 4} It was shown that people living with HIV are eight times more likely to be diagnosed with Hodgkin lymphoma, three times as likely to be diagnosed with liver cancer, nineteen times more likely to be diagnosed with anal cancer, twice as likely to be diagnosed with oral cavity/pharynx cancer and about two times as likely to be diagnosed with lung cancer.¹⁻³ Besides their higher risk of developing various cancers, HIV patients have an increased risk of dying from cancer.⁵

⁶ According to the 2017 UNAIDS fact sheet, 36.7 million [30.8 million–42.9 million] of people were living with HIV/AIDS worldwide in 2016. On average, 1.8 million [1.6 million–2.1

million] new HIV infection were recorded in 2016.⁷ According to the same report, 1 million [830 000–1.2 million] people died from AIDS-related illnesses in 2016. Despite a steady increase in the proportion of HIV infected people receiving anti-HIV treatment and the increase in the global HIV expenditure, the overall number of people living with HIV has continue to grow over the years.⁸ More alarmingly, the rate of new HIV-1 infections is believed to be outpacing the rate of new individuals receiving antiretroviral therapy by an average of 2.5:1.⁹ Figure 1-1 represents the number of HIV global infection since 1990. Figure 1-2 is a representation of HIV global expenditure and the percentage of HIV infected people receiving HIV treatment worldwide.

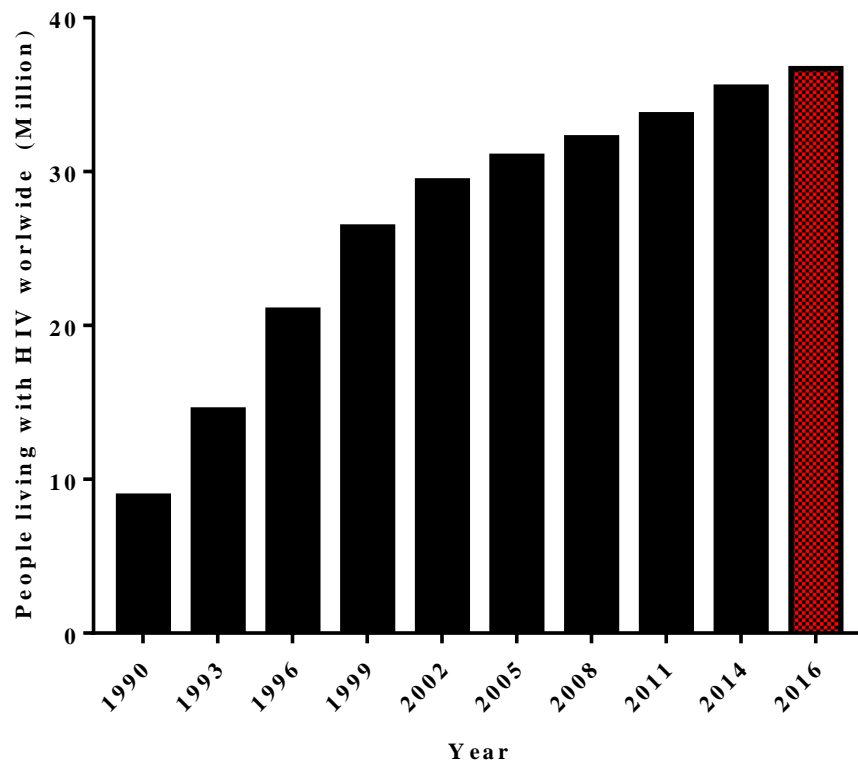


Figure 1-1: Number of people living with HIV worldwide.

Although HIV/AIDS is a worldwide pandemic disease, the African continent remains the most affected with Sub-Saharan African regions accounting for about 70% of the worldwide HIV infections in 2016.⁸ This could be due to many factors including difficulties in raising awareness among rural communities, inter-generational relationships, cultural and social believes. In fact, the widely promoted “ABC” approach, (abstinence, being faithful, using condoms) aimed at fostering HIV prevention and reducing the rate of infection spread, has shown some limitations, especially in third world countries.¹⁰ Cohen stated that the practice of abstinence “is only theoretical, since one can only be certain of one’s own behavior, not the behavior of one’s partner”.¹¹ Although HIV infection declines in Uganda and Thailand were attributed to reduction in partner number, its long term application remains a challenge in rural areas, where polygamy is often deeply rooted in traditional and religious believes.^{12, 13}

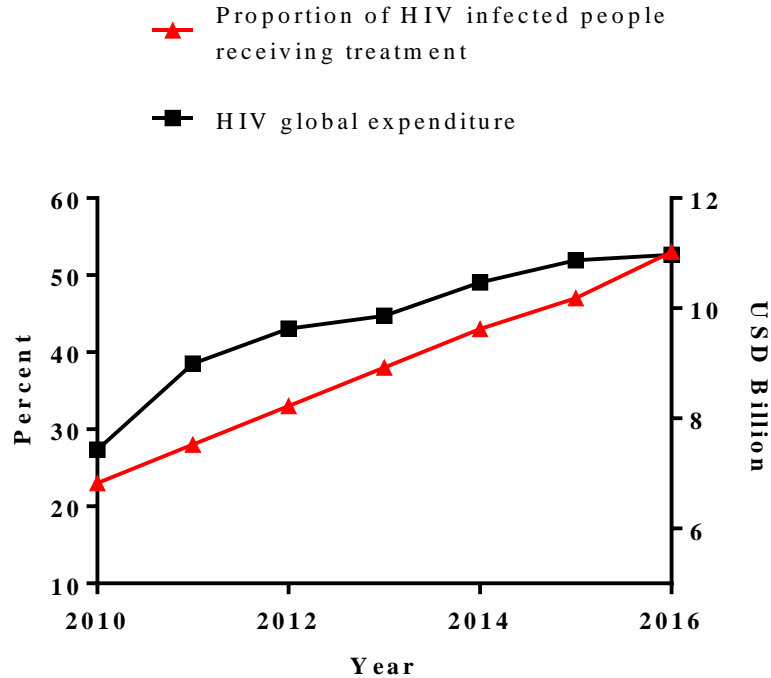


Figure 1-2: HIV worldwide expenditure and proportion of infected people receiving treatment.

Condoms, which are known to be effective when used consistently and correctly, still face a strong rejection from certain users who often report reduced physical pleasure, embarrassment of purchasing condoms, and a general perception that condom use represents a sign of infidelity and/or HIV/STD-seropositive status.¹⁴ Figure 1-3 is a statistical representation of HIV global prevalence by region.

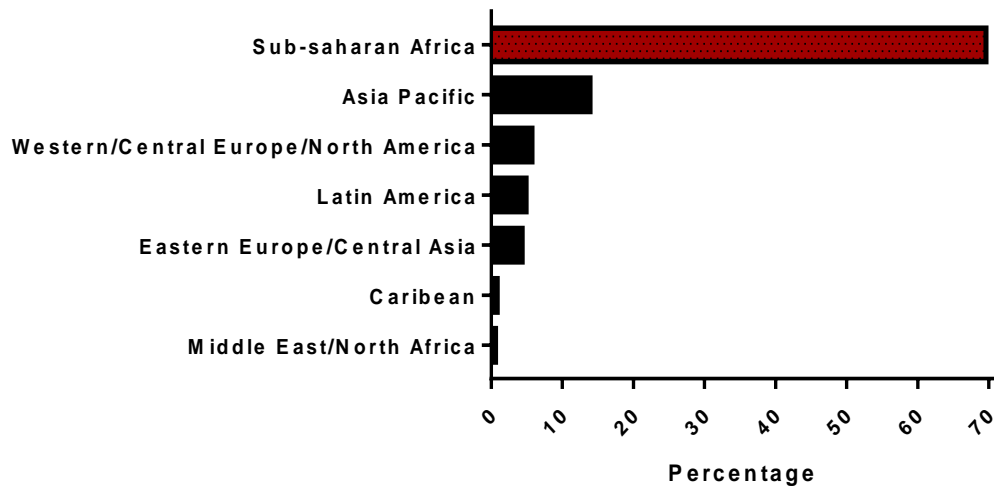


Figure 1-3: HIV global prevalence by region.

Since 2006, there has been noticeable gender gap in the global proportion of HIV infection. In fact, there has been a steady increase in the global proportion of women infected with HIV, which was estimated at 51.59%, in 2016.⁸ In Sub-Saharan Africa regions, the proportion of women infected with HIV was estimated at 59% in 2016.¹⁵ Figure 1-4 represents HIV global infection by gender. According to Ramjee and Daniels, biological, social, behavioral, cultural, economic and structural reasons might explained the gender gap in HIV infection, especially in Sub-Saharan Africa. In fact, women have a greater mucosal surface area exposed to pathogens and infectious fluid for longer periods during sexual intercourse and

are likely to face increased tissue injury than men.¹⁶ Furthermore, women hormonal cycle was shown to increase their vulnerability to HIV infection due to the suppressing influence of sex hormones on the innate, humoral and cell-mediated immune systems.¹⁷ The slowing economic growth affecting Sub-Saharan Africa is also known to be a driving force of women vulnerability in the region. In fact poverty has been associated with earlier sexual experience, lower condom use at last sex act, having multiple sex partners, increased chances that the first sex act is non-consensual, and a greater likelihood of having had transactional sex or physically forced sex, which increase their risk of HIV infection.¹⁸ Structural gender roles in Sub-Saharan Africa, including male sexual entitlement, the lack of social value and power for women, and ideas of manhood being linked to the control of women usually lead to lower levels of education, few public roles, the lack of family, social and legal support for women, which increase their vulnerability to HIV infections.^{16, 19, 20}

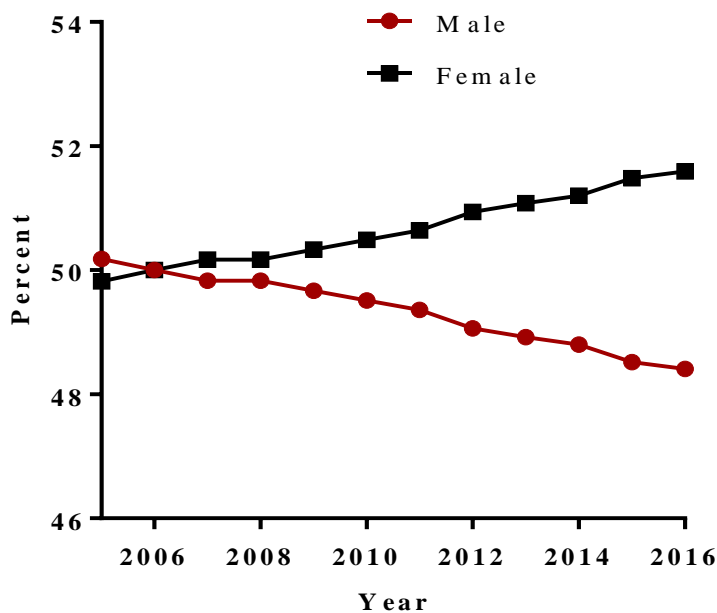


Figure 1-4: HIV global infection by gender.

In addition to women's vulnerabilities to HIV infection, sexual transmission of HIV is known to be the major route of the overall HIV infections. In fact, 75% to 85% of all HIV infections are believed to be occurring through sexual contact.²¹ In addition to having multiple sexual partners and the lack of male circumcision, another major reason for the increase in HIV sexual transmission is that 6 out of 10 people living with HIV do not know their HIV positive status making them a risk to other sexual partners.^{22, 23} Therefore, there is a crucial need to develop a safe, effective and compliant topical (vaginal/rectal) nanomicrobicide capable of preventing HIV sexual transmission. One expected benefit of such topical nanomicrobicides is their potential use as pre-exposure prophylaxis (PrEP) for women.

The proof of concept for PrEP is primarily based on the success of oral antiretroviral therapy in the prevention of mother-to-child transmission of HIV and on animal studies, involving rhesus macaques and humanized mice, that show the efficacy of PrEP against mucosal and parenteral infection.²⁴ Due to limited success and failure shown by oral PrEP clinical trials such as iPrEx, FEM-PrEP and CDC 4323, latest efforts in the field have shifted toward the vaginal and rectal application of anti-HIV microbicide drugs as "topical PrEP". Thus, various microbicide drug delivery strategies (gels, films, rings, etc.) have been proposed, attempting to address this need, with limited success. Semisolid dosage forms (gels) which are the most common microbicide drug delivery systems, present major challenges of messiness, leakage and lack of controlled release.²⁵ Besides their lack of retention, which constantly leads to leakages and therefore patient adherence and compliance issues, topical microbicide loaded gel formulation, such as CAPRISA 004, have shown minimal effectiveness against HIV.^{26, 27} Vaginal films, which are less untidy than gels, are fast dissolving with rapid drug clearance by mucus renewal cycle.²⁵ Moreover, the ASPIRE study states that the silicone based

vaginal ring Dapivirine, although promising, still needs to address compliance issues with undesirable drug release kinetics.²⁸ In fact, the major concern of a ring-based delivery system is a constant drug release even in the absence of HIV virus, which could eventually lead to drug waste, drug resistance issues, and potential side effects.

1.2 Research hypothesis

To address the problem mentioned above, the present study hypothesizes that Concanavalin A (Con A)-based topical vaginal and rectal nanomedicine formulation is capable of the safe and effective release of a pre-encapsulated HIV microbicide, "on-demand", in the presence of HIV gp120. Such an HIV specific microbicide delivery system will not only protect the active agent but may ultimately protect women, since more than half of all new HIV infections worldwide occur in females.²⁹

1.3 Objectives

The objectives of this work are:

- 1- To engineer a Con A biosensor to investigate the binding interactions of the mannose binding lectin to a mannose based polysaccharides (Mannan from *Saccharomyces cerevisiae*) and a glucose based polysaccharides (Glycogen from Oyster) using a quartz crystal microbalance.
- 2- To develop and optimize a layer-by-layer engineered, Con A-based, mannose responsive drug delivery system capable of encapsulating the HIV reverse transcriptase inhibitor Tenofovir (TFV). Physico-chemical parameters including, particle mean

diameter, surface charge, morphology, percent encapsulation efficiency (%EE), percent loading efficiency (%LD) and chemical composition will also be assessed. Furthermore, percent mucoadhesion to porcine vaginal tissue will also be investigated. *In-vitro* cytotoxicity of the nanomicrobicide will also be investigated on *Lactobacillus crispatus*, Human vaginal keratinocytes (VK2/E6E7) and murine macrophage [RAW 264.7 (TIB-71)] cell lines.

- 3- To test the hypothesis that HIV gp120 and mannose can trigger TFV release from the Con A-based layer-by-layer engineered drug delivery system. Time and concentration dependent TFV release will be investigated in vaginal and seminal fluid simulants mixture. Drug release mechanism from the layer-by-layer drug delivery system will be investigated by fitting various kinetic models.
- 4- To evaluate the preclinical safety of the mannose and HIV gp120 responsive microbicide formulation in C57BL6 mice. Vaginal and major reproductive organ's tissues will be assessed for damage, inflammation signs and immune response. Furthermore, pro-inflammatory cytokines' level in cervicovaginal lavage and tissue extracts will be assayed.

CHAPTER 2

STATE OF THE ART IN HIV MICROBICIDE DRUG DELIVERY

2.1 HIV life cycle

Engineering an HIV targeted drug delivery system requires a thorough understanding of the steps involved in HIV life cycle. As represented in figure 2-1, HIV life cycle can be divided in seven (7) critical steps.

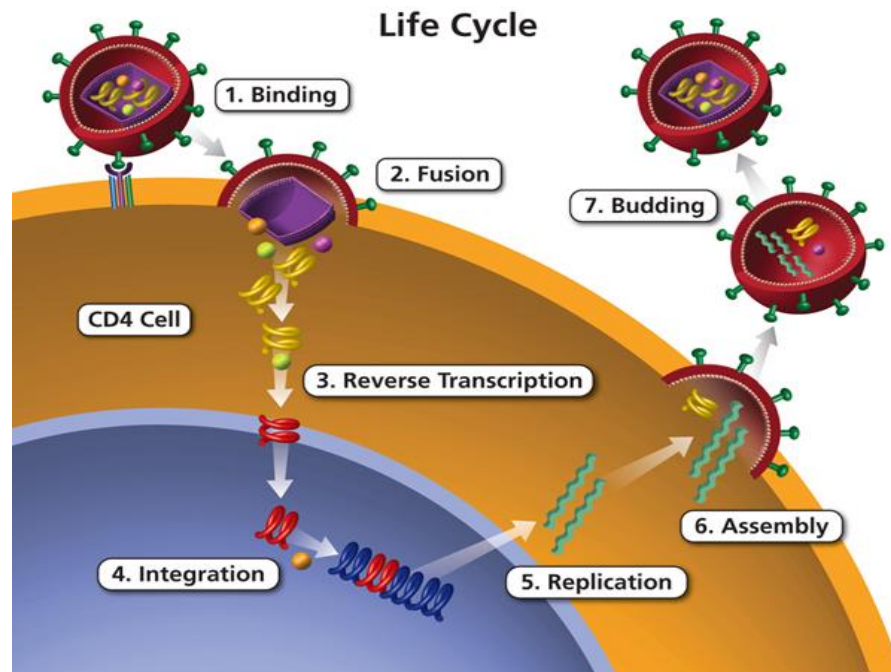
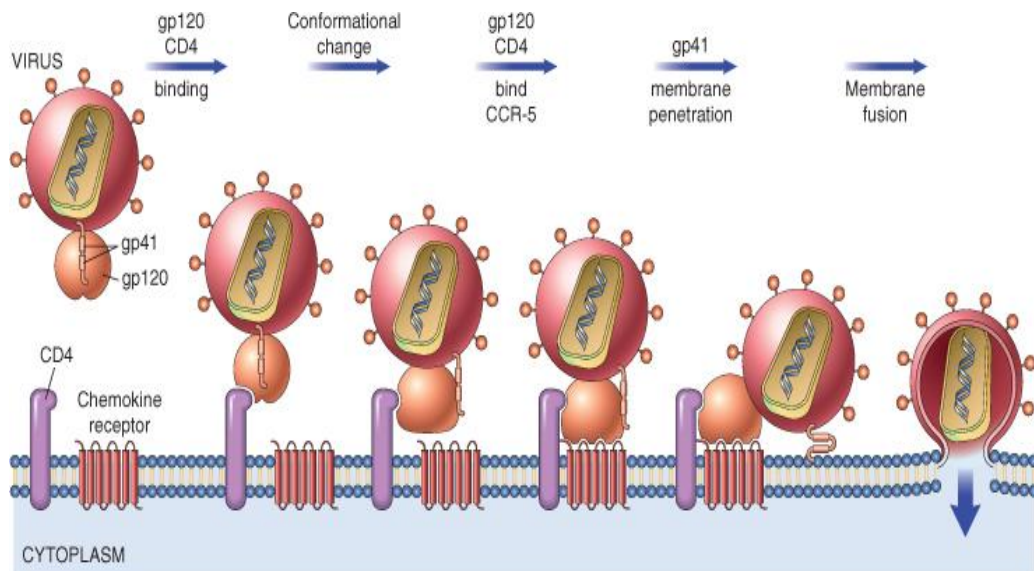


Figure 2-1: HIV virus life cycle.³⁰

- 1- Binding and fusion: The first step in HIV life cycle is the binding to target cells (CD4+ cell). HIV binding is mediated through a specific interaction between the viral envelope glycoprotein (HIV gp120) and the CD4 receptor on target cells' surface. This binding triggers a conformational change in HIV gp120 which, in turn, enhances its affinity to chemokine coreceptors CXCR4 and CCR5. This secondary binding to chemokine

coreceptor is considered to be the trigger for the following steps. In fact, in its original state, HIV transmembrane glycoprotein (HIV gp41) is thought to be in a high energy state, with its fusion peptide buried inwards. However, following the chemokine coreceptor binding, HIV gp41 undergoes a conformational change, which releases it from its high energy state, and the previously buried fusion peptide extends towards the host cell membrane, bridging the gap between the virus and the host cell membrane. Therefore, HIV gp41 transiently becomes a component of both the viral membrane, which it is anchored in, and the host cell membrane, which it is grafted to. Following the insertion of the fusion peptide into the host cell membrane, HIV gp41 refolds itself in order to shorten the distance between the virus and host cell membranes. This refolding leads to the formation of a thermodynamically stable six helix bundle due to interaction between three (3) pairs of the so-called "heptad-repeat (HR)" regions HR1 and HR2.



© Elsevier 2005

Figure 2-2: Steps involved in HIV membrane fusion.

The refolding, which finally brings the viral and cell membranes in even closer proximity, leads to the formation of a hair-pin structure or “hemifusion stalk”, where the outer membranes have fused but not the inner membranes. The fusion process is completed with the formation of the fusion pore, where previously semi-fused viral and host cell membranes become a single lipid bilayer.^{31, 32}

- 2- Reverse transcription: A direct result of HIV membrane fusion process is the internalization of key viral proteins and the viral capsid into host cells cytoplasm.³³ The viral capsid, which contains HIV viral RNA and critical enzymes such as HIV integrase and HIV reverse transcriptase, is believed to undergo a cytoplasmic uncoating upon entry into the host cell cytoplasm. Several models have been proposed to elucidate the exact mechanism of HIV capsid uncoating and, to date, three major theories have emerged. Early models have suggested a rapid and complete disassembly of HIV capsid in host cell cytoplasm. Other imaging-based studies show both uncoated and partially uncoated HIV capsid. Other recent studies suggest an intact capsid structure that only disassembled at the nuclear pore complex (NPC). This mechanism is also referred to as NPC uncoating. Regardless of the model considered, HIV reverse transcriptase generates a double-stranded HIV complementary DNA (cDNA) from the single-stranded HIV RNA in the process known as reverse transcription.³⁴
- 3- Integration: In the integration phase, which occurs in the nucleus, the newly generated double-stranded HIV cDNA is incorporated into the host cells’ genome. The process of cutting host cells’ genome and clipping the viral cDNA is catalyze by the HIV integrase enzyme. Once completed, the integration process, which is non-reversible, leads to the so-called proviral DNA.³⁵

- 4- Replication: In the replication phase, the proviral DNA, essentially serving as a template, is transcribed into new viral RNA copies by host cells' enzymes, in the nucleus. In the cytoplasm, some of the viral RNA are further spliced into mature viral RNA copies (mRNA). The viral mRNA are further translated into long, non-functional polypeptide chains, which are, in turn, cleaved into functional viral proteins (HIV integrase, reverse transcriptase, HIV envelope glycoproteins, etc.) by HIV protease.³⁶
- 5- Assembly and budding: This represents the last step of HIV viral replication that leads to the generation of new virion particles. In the assembly and budding process, critical viral proteins and copies of viral RNA are packaged into new virion particles that are then excreted from host cells through the process known as budding. New virion particles' surface are decorated with HIV envelope glycoproteins required to initiate binding and entry into new target cells. This cycle of viral binding/entry to the production of new virion particles sustains an increasing HIV viral count and eventually spreads the infection to other parts of the body. HIV viral burst, which represents the total number of virus particle produced from a single infected target cell, was shown to be 4.0×10^4 and 5.5×10^4 for the first and second inoculations, respectively.³⁷ Eventually, the hijacked host cells die by apoptosis or pyroptosis, after few cycle of HIV virion production.³⁸

2.2 Vaginal physiology and HIV acquisition

Normal vaginal physiology

The development of appropriate vaginally applicable microbicide formulations intended for the prevention of HIV sexual transmission requires an understanding of the normal

vaginal physiology and its environment. The vagina is a highly expandable, slightly s-shaped, fibromuscular tube roughly 8 to 10 centimeters (3 to 4 inches) long across the posterior wall (rear), and about 7.5 centimeters (2.5 to 3 inches) long across the anterior wall (front).^{39, 40} It is located between the rectum, which lies posterior to it, and the urethra and bladder, which lies anterior to it, and extends from the vulva to the uterus. From the lumen outwards, the vaginal wall is composed of three distinctive tissue layers: the mucosa, the muscularis, and the tunica adventitia.³⁹ Numerous studies have established that the vaginal epithelial layer remains relatively constant throughout the menstrual cycle in adult women (postpubertal and premenopausal).³⁹ Nonetheless, the structure of the vaginal epithelium changes throughout the lifespan of women, and is also affected by hormonal and environmental conditions.⁴¹ One of the most striking changes observed among women of different ages, is the vaginal epithelium thickness (figure 2-4).⁴² In prepuberal girls and postmenopausal women, the vaginal epithelium is thin and mainly composed of basal and parabasal cells layers. In reproductive, adult women, the vaginal epithelium is thick and composed of a multicellular layer of nonkeratinized squamous cells. Cervical glands and local epithelial cells secrete a mucus that provides an innate barrier to invading pathogens. In fact, pathogens entrapped in the mucus layer could potentially be cleared through the natural mucus turnover cycle. Various immune cells, including Langerhans cells (LCs), $\gamma\delta$ CD4⁺ T cells, CD4⁺ T cells, dendritic cells (DCs), Natural Killer cells (NK) and macrophage, are located in and underneath the epithelial cell. Furthermore, hormonal differences, such as estrogen level, in women of different ages, have been associated with glycogen storage and level in the vaginal epithelium. Glycogen serves as substrate for *lactobacilli*, a major component of vaginal microbiota, in the production of lactic acid, which maintains the vaginal acidic pH in adult women.⁴¹ In fact, differences in the vaginal

microbiota as well as the vaginal pH are other noticeable structural changes in the vaginal mucosa during different stages of women's life. During childhood, the vaginal microbiota is mainly composed of gram-negative anaerobe bacteria such as *Fusobacteria*, *Veillonella*, *Bacteroides* and a subpopulation of Gram-negative cocci as well as Gram-positive anaerobe bacteria including *Bifidobacteria*, *Peptococcus*, *Propionibacterium*, *Actinomyces* and *Peptostreptococcus*.^{43, 44} The vaginal microbiota in healthy adult women is mostly dominated by *Lactobacillus* including *L. crispatus*, *L. gasseri*, *L. iners*, and *L. jensenii*.⁴⁵ In postmenopausal women, the vaginal microbiota is primarily dominated by *L. iners* and *G. vaginalis* and a lower abundance of *Candida*, *Mobiluncus*, *Staphylococcus*, *Sneathia*, *Bifidobacterium*, and *Gemella*. This stage is particularly characterized by a low lactobacilli bacteria population.^{46, 47} In prepubertal girls and postmenopausal women, the significant reduction in glucose-fermenting microorganisms, including lactobacilli, facilitates an increase in the vaginal pH (6.5 -7.5), while the vaginal pH in healthy pubertal women is acidic and vary between 3.5-4.5.^{42, 48} The acidic vaginal pH in reproductive adult women has been shown to significantly prevent HIV sexual transmission.^{49, 50} Furthermore, H₂O₂-producing

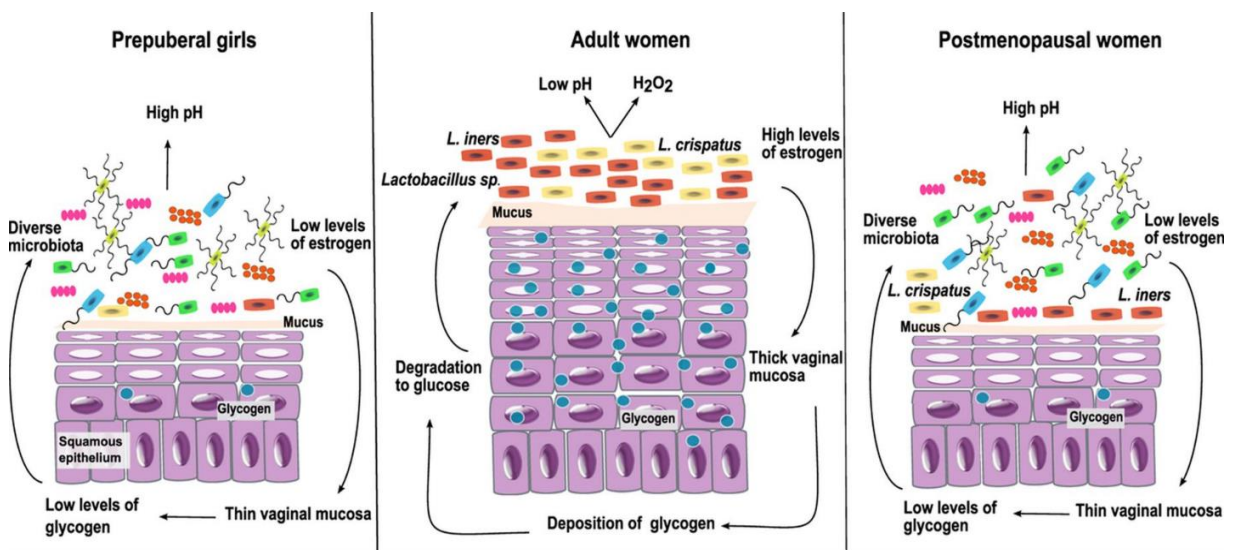


Figure 2-3: Vaginal mucosa and microbiota at different stages of women's life.⁴²

Lactobacillus species, such as *L. crispatus* and *L. jensenii* provide an additional antimicrobial protective layer in adult women, compared to prepuberal girls and postmenopausal women.⁵¹

52

Vaginal acquisition of HIV

Unprotected vaginal intercourse is a high-risk route of HIV transmission for both men and women, in the case where one partner carries the virus.^{53, 54} Nonetheless, numerous studies established that women have a greater risk to contract HIV infection through sexual intercourse than their male partners.⁵⁵ In addition to biological, social, behavioral, cultural, economic and structural differences explained in chapter I, this could also be due to male circumcision. In fact, it is now evident that male circumcision offers significant protections against HIV transmission in men.⁵⁶ The model of HIV vaginal transmission presented in figure 2-5 considers the primary infection of female from an infected sexual partner. Typically, HIV vaginal transmission can occur through six (6) main routes (figure 2-5).⁴²

- 1- First, mature HIV virion particles can be trapped in the vaginal mucus layer and migrate within gaps, intercellular spaces, in the epithelial cell layer to reach the stroma or the submucosa. Similarly, infected donor cells could be trapped in the mucus and release more HIV virion. These virions could reach and infect LCs which could then carry them to the submucosa.
- 2- Moreover, HIV virion could infect $\gamma\delta$ CD4⁺ T cells in the epithelium.
- 3- Free HIV virions or those released from infected donor cells can be transferred through the epithelial cell layers by transcytosis. These virions could either infect epithelial

cells or migrate to the stroma where they could infect stroma DCs and seed the production of new virions.

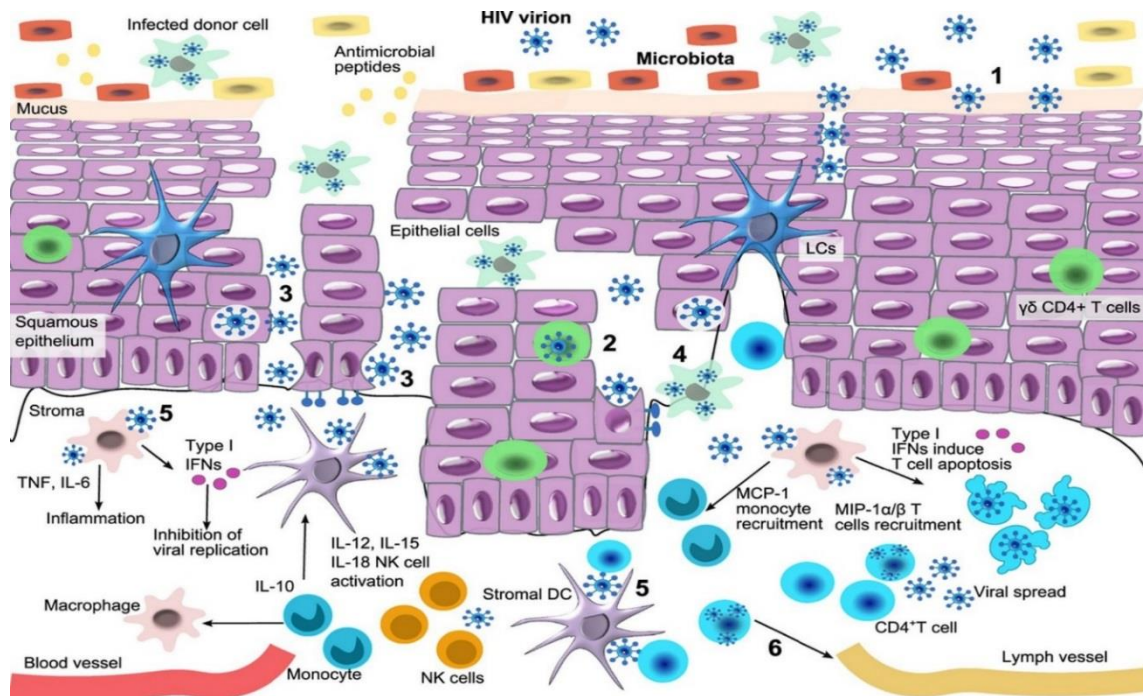


Figure 2-4: Mechanism of HIV vaginal acquisition.⁴²

- 4- Furthermore, free HIV virion particles and infected donor cells could migrate through lesions within a damage epithelial cell layer and reach the stroma. In the stroma region, donor cells may release more HIV virions.
- 5- Free HIV virions that reach the stroma can further infect CD4⁺ T cells and macrophages. Infected DCs may also transport these virions to underlying CD4⁺ T cells.
- 6- Infected immune cells including DCs, CD4⁺ T cells, macrophages, and LCs further spread the infection in the submucosa and to local lymph nodes and blood vessels.

2.3 HIV microbicides and classification

Before FDA approval of Indinavir, Nevirapine and Ritonavir in 1996, very few antiretroviral treatment options existed for HIV infection, and clinical management primarily consisted of prophylaxis against opportunistic diseases and AIDS related diseases.⁵⁷ Today, nearly forty (40) HIV approved microbicides are marketed and many more are being investigated in ongoing clinical trials.⁵⁸ HIV microbicides can be classified into six (6) main drug class based on their therapeutic target or mechanism of action.

- 1- Entry inhibitors: HIV entry inhibitors prevent viral entry into target cells through interactions with either HIV or host proteins involved in the entry process. HIV entry inhibitors can be subdivided into five (5) distinct classes including gp41 inhibitors, gp120 inhibitors, CXCR4 inhibitors, CCR5 antagonists and CD4 inhibitors. Entry inhibitors such as Enfuvirtide and Sifuvirtide, mimic heptad-repeat (HR) of HIV gp41, thus blocking the formation of the six-helix bundle structure critical for the membrane fusion process between HIV and host cells. CCR5 antagonist such as maraviroc bind the chemokine coreceptor CCR5 inducing a conformational change in the receptor which, in turn, prevents HIV gp120 binding to the coreceptor.^{57, 59}
- 2- Reverse-transcriptase inhibitors (RTI): RTI exert their microbicide activity by blocking the reverse transcription of HIV single-stranded RNA into its complementary double-stranded cDNA. RTI are classified into two subgroups including nucleoside/nucleotide reverse transcriptase inhibitors (NRTI) and non-nucleoside reverse transcriptase inhibitors (NNRTI). NRTI, such as TFV and Zidovudin, which lack the 3'-hydroxyl group at the sugar (2'-deoxyribose) moiety, induce the proviral cDNA chain termination by preventing the formation of 3'-5'-phosphodiester bond between the

- NRTIs and incoming 5'-nucleoside triphosphates. NNRTI such as Nevirapine and Etravirine are non/uncompetitive inhibitors of the reverse transcriptase enzyme. NNRTI essentially limit the special conformational flexibility of the reverse transcriptase, which in turn, reduces the polymerase activity.^{57, 59}
- 3- Integrase inhibitors: Integrase inhibitors (INI) prevent the integrase enzyme from catalyzing the formation of covalent bonds between the viral and host DNA. INI, such as Raltegravir and Elvitegravir, essentially block three steps required for viral DNA incorporation into the host chromosome, which generally occurs within the first 15–20 h of infection. INI prevent the assembly with the viral DNA, the endonucleolytic processing of the 3' ends of the viral DNA, and the strand transfer or joining of the viral and cellular DNA.^{57, 59}
 - 4- Protease inhibitors: Protease inhibitors (PI) exhibit their mechanism of action late in the HIV replication cycle by binding and inhibiting HIV proteases. Binding of PI, such as Ritonavir and Nelfinavir, blocks the proteolytic activities of the enzyme, which, in turn, prevents the formation of functional viral Gag and Gag-Pol proteins, resulting in the inability of formation of mature, infectious HIV virions.^{57, 59}
 - 5- Capsid inhibitors: HIV capsid inhibitors interfere with the assembly and disassembly of the viral capsid that encloses the viral genome. Currently, there is no FDA approved capsid inhibitors. However, GS-CA1, a preclinical capsid inhibitor from Gilead, has shown potent inhibition of HIV-1 replication, with EC50 of 140 picomolar in peripheral blood mononuclear cells.⁶⁰

Table 2-1: FDA approved anti-HIV microbicide and formulations.⁶¹

Drug class	Microbicide	Formulation	
Entry inhibitors	Enfuvirtide (Fuzeon)	Injection	
	Maraviroc (Selzentry)	Oral tablet	
	NRTI	Zidovudine (Retrovir)	Oral capsule, oral tablet, oral syrup, and injection.
		Didanosine (Videx)	Capsule
		Delayed-release didanosine (Videx EC)	Capsule
		Stavudine (Zerit)	Capsule
		Emtricitabine (Emtriva)	Capsule, oral solution
		Lamivudine (EpiVir)	Oral tablet and oral solution
		Lamivudine and zidovudine (Combivir)	Oral tablet
		Abacavir sulfate (Ziagen)	Oral tablet, oral solution
		Abacavir and lamivudine (Epzicom)	Oral tablet
		Abacavir, zidovudine, and lamivudine (Trizivir)	Oral tablet
	Tenofovir disoproxil fumarate (Viread)	Oral tablet	
	Tenofovir disoproxil fumarate and Emtricitabine (Truvada)	Oral tablet	
NNRTI	Rilpivirine (Edurant)	Oral tablet	
	Etravirine (Intelence)	Oral tablet	
	Delavirdine mesylate (Rescriptor)	Oral tablet	
	Efavirenz (Sustiva)	Oral tablet, capsule	

Drug class	Microbicide	Formulation
NNRTI	Nevirapine (Viramune)	Oral tablet, oral suspension
	Nevirapine extended-release (Viramune XR)	Oral tablet
INI	Raltegravir (Isentress)	Oral tablet, oral powder
	Dolutegravir (Tivicay)	Oral tablet
	Elvitegravir (Vitekta)	Oral tablet
PI	Tipranavir (Aptivus)	Capsule, oral suspension
	Indinavir (Crixivan)	Capsule
	Nelfinavir (Viracept)	Oral tablet, oral powder
	Atazanavir (Reyataz)	Oral capsule, oral powder
	Atazanavir/cobicistat (Evotaz)	Oral tablet
	Saquinavir (Invirase)	Oral tablet, oral capsule
	Lopinavir/ritonavir (Kaletra)	Oral solution, oral tablet
	Ritonavir (Norvir)	Oral tablet, capsule, oral suspension
	Fosamprenavir (Lexiva)	Oral tablet, oral suspension
	Darunavir (Prezista)	
	Darunavir/cobicistat (Prezcobix)	Oral tablet, oral suspension
Caspase inhibitor	N/A ^a	N/A ^a

^aN/A: Note available

Lessons learned from HIV high susceptibility for mutation in microbicide monotherapy, has led to antiretroviral combination therapies. Today the highly active antiretroviral therapy (HAART) is a standard HIV treatment regimen which combines a “backbone” of 2-NRTI, plus one of these classes of drugs – PI (usually boosted with ritonavir), NNRTI, INI, or CCR5 antagonist. Since its first use in 1995, HAART has dramatically improved HIV infected patient health and survival.^{59, 62}

2.4 Topical microbicide candidates’ formulation and delivery

Given the elevated rate of HIV sexual transmission among all new HIV infections, vaginally applicable microbicide formulations have received a special attention in the past decades. Topical microbicide agents can be classified into two major groups or generations, based on their mechanism of action.⁶³

The first generation topical microbicide agents includes surfactants, polyanions and acid buffering agents. These agents are non-specific, with a broad spectrum of antimicrobial activity as well as contraceptive properties. Surfactants represent the first topical microbicides investigated for their ability to prevent HIV sexual transmission. They exert their mechanism of action by disrupting viral and cellular membranes.⁶⁴ Surfactants such as Nonoxynol 9 (N-9), a non-ionic surfactant, and C31G (SAVVY), an amphoteric surfactant, have been tested in this group. Despite success shown *in vitro*, both N-9 and C31G showed lack of effectiveness and possible harm in clinical trials, possibly linked to inflammatory changes in the cervicovaginal mucosa.^{63, 65} Polyanions-based topical microbicides prevent viral attachment to target cells via electrostatic interactions with viral envelope glycoprotein (HIV gp120). Cellulose sulfate (UsherCell), carrageenan (Carraguard), and sulfonated naphthalene

derivative (PRO 2000) are some of the Polyanions-based topical microbicides that have been clinically investigated. Similar to surfactants, these products did not demonstrate any protection against HIV-1 acquisition and in some cases enhanced HIV transmission instead. Polyanions failure was attributed to various factors including low potency (in comparison to antiretrovirals), negligible mucosal absorption, reduced activity in seminal plasma, short duration of effect, and induction of mucosal and microflora changes facilitating HIV-1 initial infection.⁶³ Buffering microbicide agents were developed to maintain an acidic pH in the vaginal environment, inactivate HIV (due to the acidic pH) and immobilized and killed potential HIV vectors, such as lymphocytes and macrophages. BufferGel® and lime juice are few acid buffering agents that have been studied clinically. Both products did not show any significant anti-HIV protection and lime juice was found to induce pronounce cervicovaginal epithelial toxicity.^{66, 67} Amphora™ (Acidform™) is an approved sexual lubricant gel that is being considered as a candidate microbicide given its acid-buffering and bioadhesive properties.^{63, 64}

Second generation topical microbicides are essentially composed of antiretrovirals formulations and are currently the main focus in topical microbicide development. They have emerged following repeated and significant setbacks observed with first generation topical microbicides. Thus, semi-solid (films, creams and gel), vaginal tablet as well as nanofibers and intravaginal ring (IVR) formulations are being investigated. Although many second generation topical microbicides have shown excellent safety profiles, only few formulations have been proven effective, to date. For example, although dapivirine film (a NNRTI) has demonstrated a reduced cervical tissue infectivity post HIV challenge, vaginal films are generally fast-dissolving with a rapid clearance.^{68, 69} Dapivirine vaginal film potential to prevent HIV vaginal

transmission in women still needs to be tested, in addition to compliance issues that this formulation faces.⁷⁰ TFV (NRTI) vaginal gel formulation is currently one of two vaginal microbicides that have demonstrated effectiveness in preventing HIV vaginal transmission in human. In fact, besides the lack of controlled release, the messiness and leakage associated with vaginal gels, 1% TFV (CAPRISA 004) was shown to reduce HIV acquisition by 39% and 54% over 18 months period among women, and depending on the level of adherence.⁶⁵ However, a larger clinical trial study (FACTS 001) of 1% TFV, designed to confirm the effectiveness identified in CAPRISA 004, did not show any reduction in HIV infections.⁷¹ The IVR formulation of Dapivirine is the second vaginal microbicide that was recently shown to significantly prevent HIV transmission in a clinical trial (ASPIRE).²⁸ Similar to CAPRISA 004, the ASPIRE team identified women adherence to the microbicide formulation to be a critical factor affecting the level of effectiveness observed. Table 2 is a summary of first and second generation vaginal microbicides formulations.

Table 2-2: Current vaginal formulations for the prevention of HIV sexual transmission.⁷²

Mechanism of action	Microbicide	Dosage form	Clinical trial outcome	Current status
Surfactants	Nonoxynol-9	Gel	Not safe	Rejected
		Film	Not effective	
	Savvy gel®	Gel	Safe	Rejected
Acidifier	BufferGel®	Gel	Not effective	
			Safe	Rejected
Polyanions	Carraguard®	Gel	Not effective	
			Safe	Use as carrier being assessed

Mechanism of action	Microbicide	Dosage form	Clinical trial outcome	Current status
Polyanions	PRO 2000®	Gel	Safe	Rejected
			Not effective	
	VivaGel®	Gel	Not safe	Rejected
	gp120-neutralizing monoclonal antibody	Vitamin B12	Gel	ND ^a
	Cyanovirin-N	Gel	ND ^a	Candidate for clinical trials It has been expressed and purified from transgenic plants
		Probiotics (genetically modified <i>Lactobacillus jensenii</i> strain)	ND ^a	In clinical trials
Entry inhibitors	Maraviroc	Gel (Hydroxyethyl Cellulose)	ND ^a	Its period of effectiveness must be increased
		Gel (silicone)	ND ^a	Candidate for clinical trials
		IVR	ND ^a	Controlled release over 28 days
Viral enzyme inhibitors	Tenofovir/tenofovir disoproxil fumarat	Gel	Safe Effective	The first microbicide that demonstrated efficacy in women

Mechanism of action	Microbicide	Dosage form	Clinical trial outcome	Current status
Viral enzyme inhibitors	Tenofovir/ disoproxil fumarat	IVR	Safe	In clinical trials. Provides lasting protection in animal.
		Nanoparticles (into a film)	ND ^a	Controlled release over 24 hours. Further evaluation needed.
	MIV-150	Gel	Safe	In clinical trials
		IVR	ND ^a	Candidate for clinical trials
	Dapivirine	Gel	Safe	In clinical trials
		IVR	Safe Effective	Controlled release over 28 days. Has demonstrated efficacy in women
	Film	Safe	In clinical trials	

^aND: Note determined

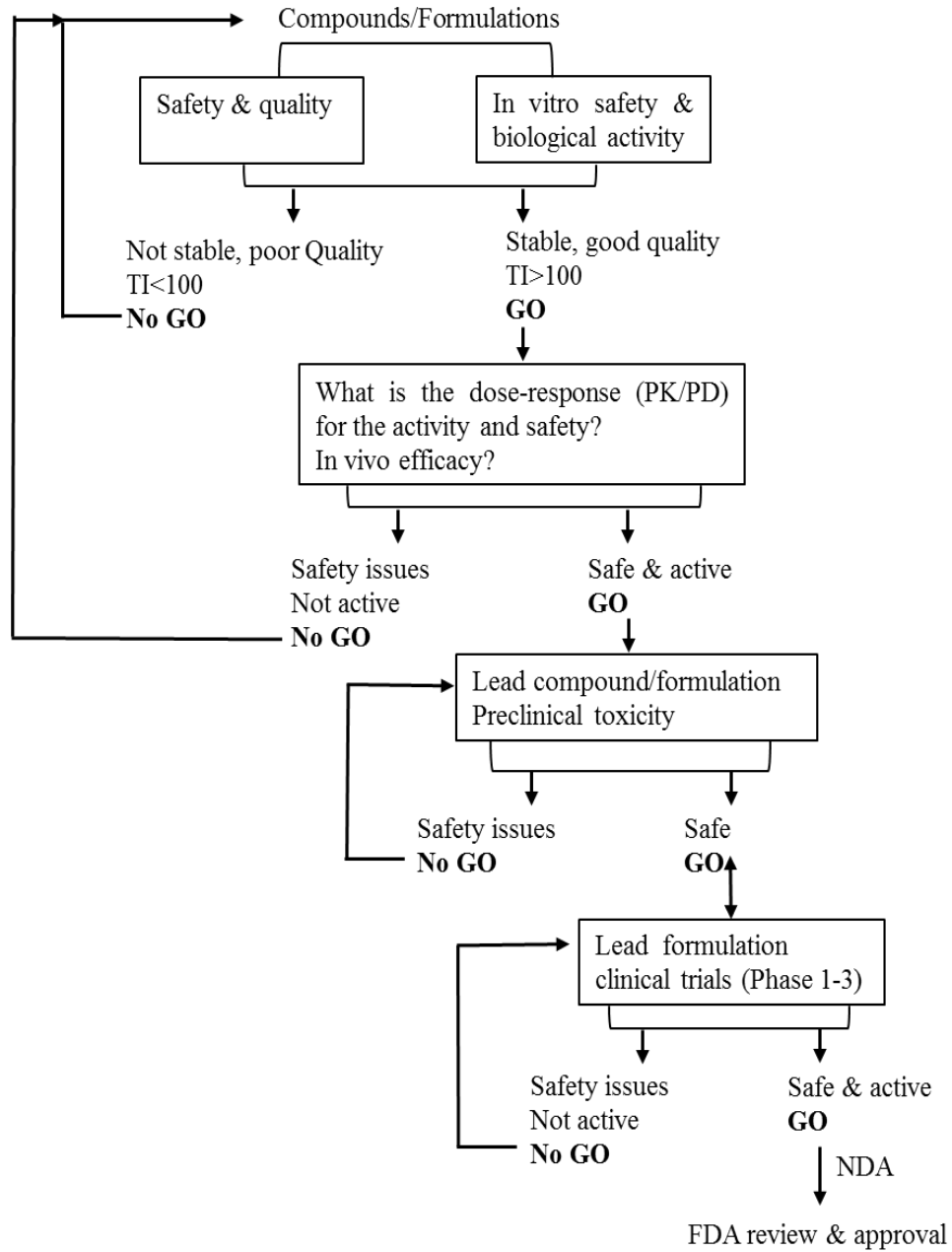
2.5 Guidance for preclinical assessments of vaginal microbicide candidates' safety and efficacy.

Similar to other therapeutics administered ocularly, orally or by injection; vaginal microbicides candidates need to demonstrate their preclinical safety and efficacy in order to be considered for clinical trials. The growing number of investigational vaginal microbicides formulations, partly governed by the urgent and critical need of topical formulation capable of preventing HIV sexual transmission, necessitate uniform guidelines for these products assessment and approval. To investigate their safety and efficacy, vaginal microbicide

formulations candidates are subject to rigorous preclinical evaluations in both cell based and animal subjects. These studies are mostly guided by prerequisites suggested or imposed by regulatory agencies that approve studies in humans, and help to follow a rational and ethical approach that will finally allow the start of clinical trials.⁷³

One of the first steps in the development of vaginal microbicides is to identify active pharmaceutical ingredients (APIs) that can block HIV entry or replication processes. Extensive evaluation of the physical and chemical properties of the unformulated and formulated API(s), as well as API compatibility with formulation excipients and chemical stability also need to be investigated. Additional tests and specifications on formulations include pH, osmolality, vaginal retention, rheological properties (in the case of a gel), appearance, odor, content uniformity of drugs, impurities, dose volume, product dimensions, and drug release kinetics.⁷³ Ideal candidate microbicide formulations need to demonstrate excellent safety profile, including lack of localized and systemic toxicity, not disrupt the vaginal epithelium, not induce inflammation or pro-inflammatory cytokine release, be inert towards the normal vaginal microbiota, and show no-effect on fertility and/or fetal abnormalities. These formulations also need to demonstrate evidence of anti-HIV activity and efficacy by efficiently preventing HIV infection of target cells, be active against a range of sexually transmitted pathogens, be fast acting with long-term efficacy, demonstrate irreversible efficacy and should not induce drug resistance. From both the safety and efficacy studies, some of the endpoints generally determined are the median effective concentration (EC_{50}), the average cytotoxic concentration (CC_{50}), and the therapeutic index (TI, or CC_{50}/EC_{50}). The 90% viral inhibition concentration (EC_{90}) is also determined to inform a rational dose selection when formulating candidate microbicide. EC_{90} is also an important parameter to consider in pharmacokinetic (PK) and

pharmacodynamic (PD) studies. Typically, a minimum acceptable TI value ranges from 10 to 100.⁷³



Scheme 2-1: GO/NO-GO algorithm in vaginal microbicides products development.⁷³

Vaginal microbicide candidates must also be stable under diverse environmental conditions, such as, the vaginal acidic pH (3-4.5) and neutral pH values (7-8), which typically occur during sexual intercourse, due to the strong buffering capacity of human seminal fluid.⁷⁴

⁷⁵ Products must have adequate shelf life, with minimal need of cold chain distribution and storage that might limit their practical use in third world countries. Furthermore, ideal vaginal microbicide products should provide controlled, sustained and significant drug release (level) at the target site. Finally, microbicides candidates production must be economic, scalable and should be affordable in high-risk populations and should not interfere with sexual pleasure.⁷⁶

⁷⁷ In their study on the Preclinical assessments of vaginal microbicide candidate safety and efficacy, Fernández-Romero et al.⁷³ have established a possible go/no-go algorithm relevant for vaginal microbicide development. Scheme 2-1 is a modified version of the algorithm of Fernández-Romero et al.

CHAPTER 3
LITERATURE REVIEW OF HIV SURFACE GLYCOPROTEINS AND ANTI-HIV
LECTINS

(AIMS Molecular Science, 2018, 5(1): 96-116)

3.1 Introduction

Among the different classes of anti-HIV microbicides currently in use, agents targeting and preventing viral entry into target cells have shown remarkable promises, partly favored by fewer barriers that could potentially hinder their mechanism of action. HIV entry inhibitors are subdivided into three main groups composed of attachment inhibitors, co-receptor binding inhibitors, and fusion inhibitors.⁷⁸ Attachment inhibitors such as zintevir, BMS-378806 and BMS-488043 block a non-specific adsorption step between HIV virions and target cells' membrane, which is due to an interaction between the positively charged regions of the envelope glycoprotein gp120 and oppositely charged proteoglycans on cell surface. Co-receptor binding inhibitors are generally CCR5 antagonists such as aplaviroc, vicriviroc and maraviroc that bind to CCR5 and prevent further HIV gp120/CCR5 interaction, which is critical for viral entry into host cells. Fusion inhibitors such as tifuvirtide, enfuvirtide and sifuvirtide prevent the formation of the fusion pore by mimicking either heptad repeat sequences (HR1 or HR2) in HIV gp41. These sequences block the formation of a six-helix bundle structure necessary for HIV entry into host cells.⁷⁸

Lectins, which are carbohydrate binding proteins, have long being considered for their diagnostic and therapeutic potentials, as well as their pathogenic implication in many human diseases and conditions, including various cancers,⁷⁹ type 2 diabetes,^{80, 81} cardiovascular

disease,⁸² weight management,^{83, 84} and HIV/AIDS.⁸⁵ The ability of lectins to recognize and bind several mannose oligosaccharides was long considered a viable example of anti-HIV therapeutic strategy.⁸⁶ Primarily, anti-HIV lectins act as viral entry inhibitors by binding to oligosaccharides epitopes on HIV surface glycoproteins, which either hinder a proper interaction between HIV and receptors on target cells' membrane or affect post-binding conformational alterations of key viral envelope and transmembrane glycoproteins (HIV gp120/ HIV gp41). In this chapter, we report on the current trend in anti-HIV lectins research and emerging lectins formulations aiming at improving the delivery of these sugar-binding proteins.

3.2 HIV surface glycoproteins and glycans

HIV surface glycoproteins (HIV gp120 and HIV gp41) mediate host cell entry through interaction with CD4 receptor and CCR5/CXCR4 coreceptors on target cells. These glycoproteins are first expressed as HIV gp160 precursor, before the proteolytic cleavage in the trans-Golgi by cellular furin or furin-like proteases that leads to the formation of the envelope glycoprotein HIV gp120 and the transmembrane glycoprotein HIV gp41. In mature HIV viruses, HIV gp120 and HIV gp41 remain linked by noncovalent interactions.³³ Most anti-HIV lectins target and bind specific glycan structures on HIV envelope glycoproteins. Understanding the glycosylation pattern of these glycoproteins is useful not only for anti-HIV vaccine design, but also for the selection of appropriate lectins for potential vaginal microbicides formulation development. Glycans found on HIV surface glycoproteins may also help in understanding anti-HIV lectins overall mechanism of action. Moreover, the extent and variation in glycosylation pattern between HIV strands, as well as changes in the glycosylation

pattern during HIV maturation may help explain resistance to certain anti-HIV vaccines and lectins, as well as the lack of broad activity usually observed with anti-HIV lectins.^{87, 88}

HIV gp120 glycans and their function

HIV gp120 is the external envelope glycoprotein of HIV. It is a homotrimer with each subunit having a nominal molecular weight of 120 kDa. HIV gp120 plays an essential role in HIV entry into host cells. In fact, HIV host cell entry is initiated by the binding of gp120 to CD4 receptor. This binding triggers a conformational change in HIV gp120 which, in turn, enhances its affinity to chemokine receptors CXCR4 or CCR5. This secondary binding induces another conformational change in the transmembrane glycoprotein HIV gp41 resulting in an intimate contact and fusion of both viral and host cell membranes. The membrane fusion process leads to the internalization of HIV viral capsid, containing the viral mRNA and key viral proteins, into host cells cytoplasm. Ultimately, new HIV virus particles are produced which then propagate the infection.^{32, 89} Literature abound of HIV gp120 biosynthesis, trafficking, and incorporation. Rather than the underlying biological mechanism involved in these processes, this section focuses on the nature of HIV gp120 glycosylation and its role in the membrane fusion.

Ratner et al.,⁹⁰ Allan et al.⁹¹ and Montagnier et al.⁹² have published some of the first studies that explored HIV gp120 glycosylation. Although these pioneering studies did not investigate HIV gp120 glycan structures in detail, they did report HIV gp120 glycosylation to account for approximately 27 to 50% of the overall glycoprotein molecular weight. Some of these early investigations also demonstrated the presence of 31⁹¹ or 32⁹³ potential N-glycosylation sites on HIV gp120. Subsequent studies by Mizuochi et al.^{94, 95} further

investigated HIV gp120 glycan structures. Mizuochi's findings showed in part that HIV gp120 is unique in its diversity of oligosaccharide structures. These studies also reported HIV gp120 glycans to be predominantly oligomannoses that are mostly comprised of five to nine mannose residues accounting for approximately 33% of the overall glycoprotein's carbohydrate structures.⁹⁶ Furthermore, this study projected the number of potential N-glycosylation sites on HIV gp120 to be around 20. Besides the high-mannose type glycans, Mizuochi et al. also identified complex type glycan chains (34% of carbohydrate structures) mainly composed of four categories: mono-, bi-, tri- and tetra-antennary, with or without N-acetylglucosamine repeats, and with or without a core fucose residue.^{94, 96-98} A previous study by Geyer et al.⁹⁷ reported similar findings and showed that predominant oligomannose glycans in HIV gp120 are composed of seven to nine mannose residues, depending on whether the glycoprotein is excreted or expressed intracellularly. Geyer et al. also showed that HIV gp120 complex-type oligosaccharide are fucosylated with partial sialylated bi- and triantennary structures. Recent advances in glycoscience, genomics, proteomics and mass spectrometry have led to more detailed and in depth characterization studies of HIV gp120 glycosylation. In fact, recent mass spectrometry studies have confirmed HIV gp120 high mannose proportion for various viral clades and expression systems,⁹⁸⁻¹⁰² and it is widely accepted that HIV N-glycosylation sites number range from 20-35.³³ Following a matrix-assisted laser desorption/ionization (MALDI) time-of-flight (TOF) analysis, Bonomelli et al. showed that HIV gp120 oligosaccharides, derived from virus [clade A (92RW009), clade B (JRCSF), and clade C (93IN905)] isolated from infected peripheral blood mononuclear cells (PBMCs), are almost entirely oligomannoses and varies from 62–79% for virion-associated, versus 30% for recombinant, monomeric HIV gp120.^{99, 103} These studies also identified an “intrinsic” mannose patch in HIV gp120

composed essentially of $\text{Man}_5\text{-}\beta\text{-GlcNAc}_2$ and conserved across primary isolates and geographically divergent HIV clades. Many other studies have confirmed the presence of the mannose patch on HIV gp120 and its relevance in the development of a successful anti-HIV vaccine and microbicides.¹⁰⁴⁻¹⁰⁷ HIV gp120's main glycan structures are summarized in figure 3-1. HIV gp120's heavy glycosylation is believed to play four (4) key roles: host immune evasion, pathogenesis, proper glycoproteins folding and host cell surface recognition.¹⁰⁸ In fact, several studies have compared HIV gp120 extensive glycosylation to a protecting shield that prevents antibodies access to underlying amino acid sequences and therefore limits their efficacy.^{106, 109-112} More specifically, Sanders et al. determined that the carbohydrate at asparagine 386 on HIV-1 gp120 enhances HIV immune evasion.¹¹³ Furthermore, the general role of HIV gp120 glycosylation in HIV pathogenesis has widely been reported.¹¹⁴ Besides its major implication in HIV gp120 proper folding and lysosomal degradation, Francois et al.¹¹⁵ and Mathys et al.¹¹⁶ showed that cleavage of glycan at asparagine 260 of HIV-1 gp120 results in loss of viral infectivity.

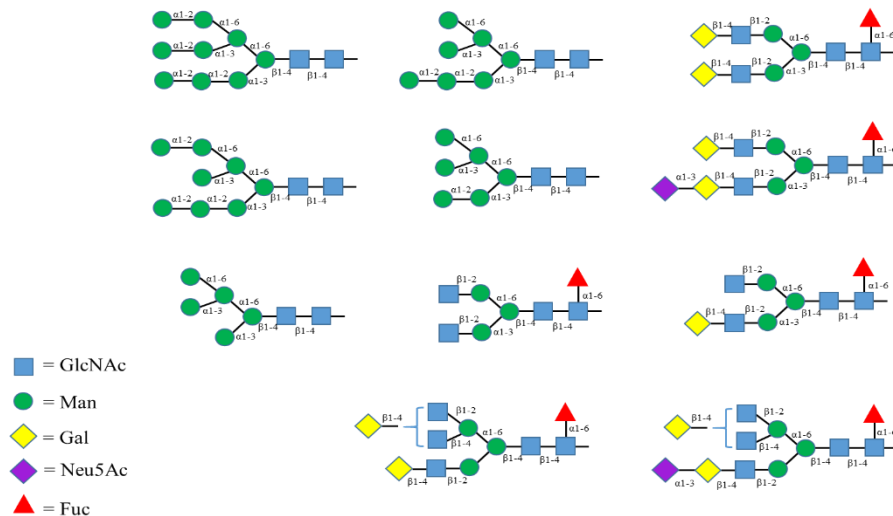


Figure 3-1: High mannose and complex glycan structures found in HIV gp120. Structures are adapted from the following references.^{94, 96, 97, 117, 118}

Similarly, Huang et al. demonstrated that deletion of HIV gp120 glycans from asparagine proximal to the CD4-binding region (156, 262 and 410) impairs HIV viral infectivity.¹¹⁹ The essential role of glycosylation in proper HIV gp120 folding was also elucidated by numerous reports.^{116, 120} For example, Li et al. showed that N-linked glycosylation is highly essential for a proper conformation of HIV gp120 capable of binding to CD4 receptor.¹²¹ In a separate study, Li et al. determined that deletion of the glycan at asparagine 448 can profoundly influence CD4⁺ T cell recognition of HIV-1 gp120.¹²²

HIV gp41 glycans and their function

HIV gp41 is composed of 345 amino acid that are organized into three (3) major domains: extracellular domain (ectodomain), transmembrane domain, and C-terminal cytoplasmic tail.^{33, 123, 124} Unlike HIV gp120, the transmembrane glycoprotein contains fewer N-glycosylation sites. Nonetheless, there is an inconsistency pertaining to the number of N-glycosylation sites in HIV gp41, as various communications often report different numbers. This may be due to differences in expression systems, cell lines and HIV strands. According to the current literature, the number of potential N-glycosylation sites in HIV gp41 vary between 3-8. In fact, Perrin et al. reported a poor glycosylation of HIV gp41 ectodomain with only 4 or 5 potential glycosylation sites.¹²⁵ Following the screening of ten HIV-1 amino acid sequences, Johnson et al. determined that HIV gp41 typically contains 3 or 4 N-glycosylation sites, localized within a short stretch (20 to 30 amino acid residues) of the C-terminal half of the ectodomain.¹²⁶ The same number of HIV gp41 potential N-glycosylation sites was reported by Fenouillet et al.^{127, 128}, Lee et al.¹²⁹, Ma et al.¹³⁰ and Wang et al.¹³¹ Furthermore, citing the work of Montefiori et al.¹¹⁴, Checkley et al. reported HIV gp41 N-glycosylation sites to vary

between 3-5.³³ The work of Balzarini et al. reported some of the highest number of HIV gp41 potential N-glycosylation sites, which was thought to be 7 with only 4 seemingly glycosylated.¹³² Further studies by Mathys and Balzarini have reported N-glycosylation sites in HIV gp41 between 4-8 with all 4 to 5 N-glycans on the ectodomain composed of complex-type glycans.^{133, 134}

In contrast to HIV gp120, the transmembrane glycoproteins' glycans are known to be primarily composed of more complex carbohydrate types. In fact, following the analysis of HIV gp41 expressed from two different producer cells (Chinese hamster ovary cells and human embryonic kidney cells [293T]), Pritchard et al. determined that, in combination with the presence of less oligomannose glycans (19%–34%) compared to HIV gp120 (60%–65%), HIV gp41 contains large populations of complex-type glycans on its ectodomain.¹¹⁸ Regardless of the expression system, HIV gp41 oligomannose population was also found to be composed of

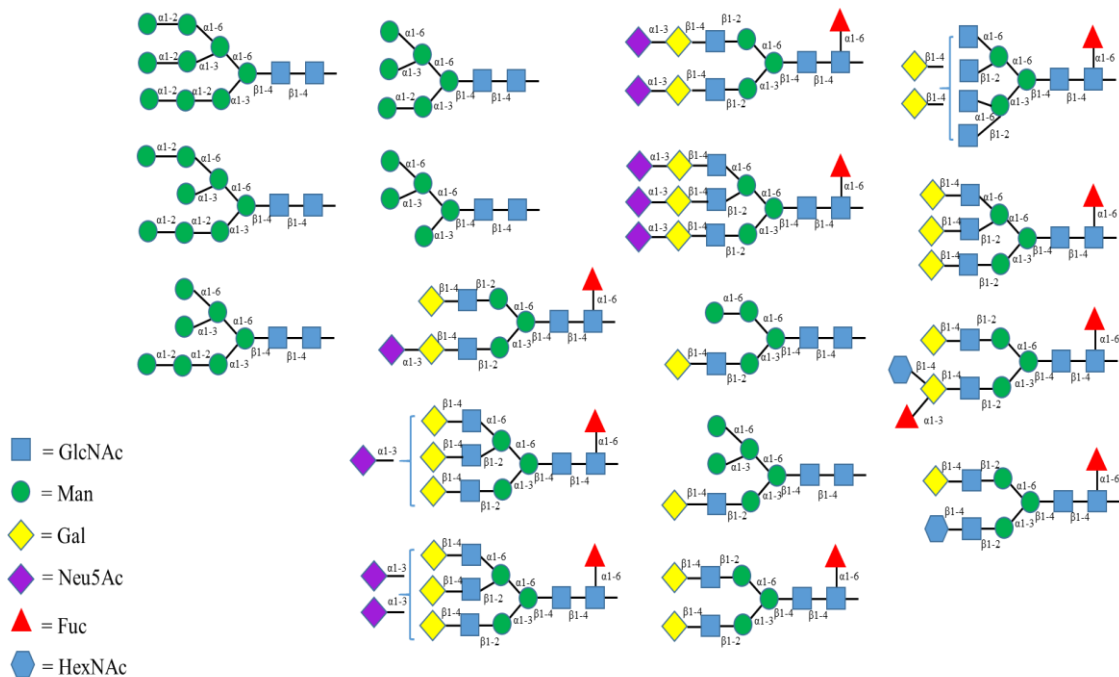


Figure 3-2: High mannose and complex glycan structures in HIV gp41. Structures are adapted from the following references.^{100, 117, 118}

Man₅₋₉GlcNAc₂. Like HIV gp120, complex glycans in HIV gp41 are composed of sialylated and asialylated bi-, tri- and tetra-antennary structures usually containing N-lactosamine repeats, with or without core fucose residue.^{100, 117, 118} HIV gp41 main glycan structures are summarized in figure 3-2.

HIV gp41 plays an equally critical role in HIV entry into target cells by mediating the membrane fusion process required for the internalization of the HIV viral capsid.³² Glycans in HIV gp41 are reported to play key roles in viral entry, immune evasion, and infectivity. In fact, Fenouillet et al., reported a loss of HIV ability to enter target cells after complete removal of the glycan cluster from asparagines at positions 621, 630, and 642 in HIV gp41.¹³⁵ A follow up study by Perrin et al., determined the critical role of HIV gp41 glycosylation for an effective membrane fusion process.¹²⁵ This study also reported that out of the 4 or 5 glycosylation sites in HIV gp41, only 2 sites are sufficient for efficient membrane fusion with a single site, at asparagine 621, being the most critical of all positions. Yuste et al. have also suggested that the function of HIV gp41 glycosylation, from both HIV and SIV, might be mainly for shielding underlying epitopes sequences, thereby allowing the virus to escape neutralizing antibodies.¹³⁶ Furthermore, Wang et al. reported that the glycan at asparagine 637 in HIV gp41 is composed of Man₉GlcNAc₂ and play a critical role in immune evasion through a facilitation of the membrane fusion process.¹³¹ A later study by Mathys and Balzarini lead to a rather different conclusion regarding the importance of the glycan at asparagine 637.¹³⁴ In fact, by following the generation of several HIV-1 mutants, lacking HIV gp41 *N* glycans and assessing their influence on viral infectivity, this study determined that besides the glycan at asparagine 616 that when deleted leads to a complete loss of HIV-1 infectivity, deletion of glycans on asparagine at position 611 and 637 displayed marginal effect on overall viral infectivity. In

addition, this study concluded that glycans on asparagines 625 and 674 do not play any significant role in HIV infectivity, since their deletion did not influence viral infectivity.

3.3 Anti-HIV lectins

Natural lectins

Owing to HIV-gp120 high mannose content, various mannose binding natural lectins have been investigated as potential HIV entry inhibitors. Primarily, these lectins specifically bind mannose oligosaccharides on HIV-gp120, thus hindering a proper interaction between the envelope glycoprotein and its host cell receptor (CD4). This may ultimately prevent the membrane fusion step and the production of new HIV virions. Actinohivin (AH), a prokaryotic lectin derived from the gram-positive bacteria actinomycete *Longispora albida* (K97-0003T) successfully prevented HIV-1 entry into CD4⁺ T lymphocytes (IC₅₀ ≈ 2–110 nM).¹³⁷ It was determined that AH binds α(1-2)-mannose oligosaccharides present in HIV gp120 and HIV gp41. Furthermore, AH did not induce any mitogenic activity, or cytokine/chemokine production in PBMC cultures, suggesting that this lectin could be a safe and potentially effective microbicide candidate.¹³⁸ Recently, Zhang et al. reported that Man₁ and Man₂ residues, found in HIV gp120 high-mannose-type glycans structures, occupy 2 of the three carbohydrate binding sites of AH while Man₃ residues interact with conserved hydrophobic amino acid residues Tyr and Leu of AH.¹³⁹ Cyanovirin-N (CV-N) is a cyanobacterial lectin with broad-spectrum antiviral activity. The potential use of CV-N as anti-HIV microbicide has widely been reported (IC₅₀ ≈ 3.9-31 nM).¹⁴⁰⁻¹⁴⁴ CV-N inhibits HIV replication, in part, by binding to HIV-gp120 high mannose glycans, thus preventing the envelope glycoprotein binding to its cell surface receptor (CD4), thereby blocking the glycoprotein-mediated

membrane fusion process required for HIV-1 entry.¹⁴⁵ Hu et al. have determined that CV-N binding interaction is mediated through 3-5 high-mannose residues from 289 to 448 in the C2-C4 region of HIV gp120 and deglycosylation of these residues resulted in a resistance to CV-N.^{146, 147} It was also shown that CV-N inhibits HIV replication by interacting with the chemokine receptors CXCR4 and CCR5.¹⁴⁸ Recently, a CV-N oligomer (CV-N₂) was designed and demonstrated an increased HIV-1 neutralization activity by up to 18-fold compared to the wild-type CV-N (IC₅₀ ≈ 0.1-41 nM).¹⁴⁷ *Oscillatoria agardhii* agglutinin (OAA) is a newly discovered cyanobacterial lectin that was shown to prevent HIV transmission, replication and syncytium formation between HIV-1-infected and uninfected T cells (IC₅₀ ≈ 24-30 nM).¹⁴⁹ OAA is known for having two sugar binding sites that recognize Man α (1-2)Man, Man α (1-6)Man and the branched core unit of Man₉ (3 α ,6 α -mannopentaose).¹⁴⁹⁻¹⁵² Like OAA, scytovirin (SVN) is a cyanobacterium lectin isolated from *Scytonema varium*.¹⁵³ SVN was also shown to possess potent anti-HIV activity through its binding interaction with HIV gp160, HIV gp120 and HIV gp41 and binds Man α (1-2)Man α (1-6)Man α (1-6)Man tetrasaccharide in high mannose type oligosaccharides (IC₅₀ ≈ 24.1 nM).¹⁵⁴⁻¹⁵⁶ In addition, MVL, a lectin isolated from the cyanobacterium *Microcystis viridis* also showed strong anti-HIV activity in nanomolar concentration by binding to Man α (1-6)Man β (1-4)GlcNAc β (1-4)GlcNAc oligosaccharides on the surface of HIV gp120 (IC₅₀ ≈ 30 nM).^{157, 158} Another cyanobacterial lectin, microvirin (MVN), isolated from *Microcystis aeruginosa* has shown anti-HIV activity comparable to CV-N with a much better cytotoxicity profile (IC₅₀ ≈ 2-12 nM).¹⁵⁹ It was further shown that MVN bind Man α (1-2)Man residues on HIV gp120.^{159, 160} Plant lectins such as *Narcissus pseudonarcissus* lectin (NPL) (EC₅₀ ≈ 0.17-2.76 μ g/ml)^{161, 162} and *Myrianthus holstii* lectin (MHL) (EC₅₀ ≈ 150 nM)¹⁶³ have also shown potential HIV

inhibition *in vitro*. Concanavalin A (Con A), one of the most studied plant lectins, is a mannose binding lectin extracted from jack bean. Con A binds sugars, glycoproteins, and glycolipids, containing internal and nonreducing terminal α -D-mannosyl and α -D-glucosyl groups ($K_D \approx 0.05 \mu\text{M}$ to $1.5 \mu\text{M}$).^{164, 165} Several studies have demonstrated the ability of Con A to bind HIV gp120 and inhibit the fusion process during HIV infection ($EC_{50} \approx 98 \text{ nM}$).¹⁶⁶⁻¹⁶⁹ Furthermore, BanLec is a lectin isolated from the banana fruit (*Musa acuminata*), which has shown potent anti-HIV activity ($IC_{50} \approx 2.5\text{-}694 \text{ nM}$).¹⁷⁰ Similar to Con A, BanLec inhibits HIV by binding to high mannose carbohydrate structures found in HIV gp120, thus blocking the virus entry into the host cells. In fact, in a comparative study, BanLec showed similar inhibitory activity like T-20 and maraviroc, two FDA approved HIV entry inhibitor microbicides.⁹

Griffithsin (GRFT), a lectin isolated from the red algae *Griffithsia* inhibited cell-to-cell fusion between HIV infected and uninfected cells ($IC_{50} \approx 4 \text{ nM}$).¹⁷¹ GRFT also inhibited HIV-1 transmission by binding to glucose, mannose, and *N*-acetylglucosamine residues in HIV glycoproteins (HIV gp120, HIV gp41 and HIV gp160).¹⁷² Emau et al.¹⁷³ have also established that GRFT strongly blocked CXCR4 and CCR5-tropic viruses at concentrations less than 1 nM, with low cytotoxicity, rapid onset of antiviral activity and long-term stability in cervical/vaginal lavage. GRFT tandemers recently reported by Moulaei et al. have shown anti-HIV activities 5 to 10 fold higher than native GRFT ($IC_{50} \approx 0.02\text{-}0.274 \text{ nM}$).¹⁷⁴

Chaetopterus variopedatus lectin (CVL) is a β -galactose-specific lectin extracted from the marine worm *Annelida*. CVL was shown to inhibit both HIV attachment to host cells and the fusion process between HIV and target cells ($EC_{50} \approx 73 \text{ nM}$)¹⁷⁵; suggesting that CVL might be exerting its action through interaction with complex glycan type found in HIV gp120 and HIV gp41.¹⁷⁶ In addition, Mermaid, a calcium (Ca^{2+}) dependent lectin isolated from the marine

nematode (*Laxus oneistus*) was shown to have structural similarities and similar glycan specificity with the Dendritic Cell-Specific Intercellular Adhesion Molecule-3-Grabbing Non-integrin (DC-SIGN). Mermaid, which bind mannose oligosaccharides on HIV gp120, prevented HIV-1 binding to DC-SIGN on dendritic cells, which ultimately blocked HIV transmission ($IC_{50} \approx 3.1 \mu\text{g/ml}$).^{177, 178} Another marine lectin *Serpula vermicularis* lectin (SVL) isolated from the sea worm *Serpula vermicularis* was also shown to bind GlcNAc and inhibited the production of viral p24 antigen and cytopathic effect induced by HIV-1 ($EC_{50} \approx 0.15\text{-}0.23 \mu\text{g/ml}$).^{179, 180}

Table 3-1: Example of natural anti-HIV lectins.

Lectin	Glycan preference	Target	Origin	References
AH	Man α (1-2)Man, Man α (1-3)Man, Man α (1-6)Man, GlcNAc	gp120 and gp41	<i>Actinomycete</i> <i>Longispora albida</i>	138
	Man α (1-2)Man in Man ₈ or Man ₉	gp120, CXCR4 and CCR5	<i>Nostoc</i> <i>elliposporum</i>	146, 147
OAA	Man α (1-6)Man, 3 α ,6 α - mannopentaose	gp120	<i>Oscillatoria</i> <i>agardhii</i>	149-152
SVN	Man	gp120	<i>Scytonema varium</i>	154, 155

Lectin	Glycan preference	Target	Origin	References
	Man α (1-6)Man β (1-			
MVL	4)GlcNAc β (1- 4)GlcNAc	gp120	<i>Microcystis viridis</i>	157
MVN	Man α (1-2)Man	gp120	<i>Microcystis aeruginosa</i>	159, 160
NPL	Man α (1-3)Man; Man α (1-2)Man	gp120	<i>Narcissus Pseudonarcissus</i>	161, 162
MHL	GlcNAc	gp120	<i>Myrianthus Holstii</i>	163
Con A	α -D-Man and α -D- Glc	gp120	Jack bean	164
BanLec	Man	gp120	<i>Musa acuminata</i>	9
GRFT	Glc, Man and GlcNAc	gp120, gp41, gp160, CXCR4 and CCR5	<i>Griffithsia</i>	172
CVL	β -Gal	gp41, gp120	<i>Chaetopterus variopedatus</i>	176
Mermaid	Man α (1-3)Man α (1- 6)Man	gp120	<i>Laxus oneistus</i>	177, 178
SVL	GlcNAc	gp41, gp120	<i>Serpula vermicularis</i>	179

Synthetic lectins

Carbohydrate binding agents (CBA) can bind to carbohydrate residues on viral envelope proteins, such as HIV gp120. This binding could lead to an inhibition of viral entry. Moreover, mutations of the envelope glycoproteins can improve drug pressure and lead to viral neutralization by host's immune response. Because manufacturing natural plant-based lectins can be expensive, synthetic lectins have been considered as potential inhibitory alternative.¹⁸¹ Synthetic lectins are cheaper to mass-produce as compared to their plant-based counterparts. As a response to the high cost and potential mitogenicity of natural lectins, Mahalingan et al. developed a benzoboroxole (BzB) polymeric synthetic lectin. Like natural plant-based lectins, BzB targets and binds carbohydrates on HIV viral envelope. At pH 7, BzB demonstrated increased binding efficiency to reducing sugars, such as fructose and weak binding affinity to non-reducing sugars, such as galactopyranose, a terminal sugar found on the surface of HIV gp120 complex glycans. This study further showed that BzB polymers of high molecular weight increased antiviral activity, proving that polyvalent interactions between inhibitor and glycosylated sites on HIV viral envelope improved with increased molecular weight. For example, increasing the mole percent of BzB functionalization showed an increase in EC_{50} [$EC_{50}=15\mu\text{M}$ (25 mol%); $EC_{50}=15\text{nM}$ (75 mol%)]. Moreover, substituting the polymer backbone with 10% sulfonic acid, resulted in an increased synergistic anti-HIV activity, as well as a 50 fold increase in aqueous solubility of the polymer. Furthermore BzB-sulfonic acid showed an improved selectivity to HIV gp120, and the presence of fructose from seminal fluid did not decrease its anti-viral activity.¹⁸² Similarly, synthetic lectins containing phenylboronic acid (PBA) could potentially exhibit carbohydrate recognition similar to that of CBA. For instance, Trippier et al. synthesized mannose selective PBA-based synthetic lectins that were

tested for binding affinity against HIV gp120.¹⁸³ Because the mono-PBA synthetic lectins tested did not bind HIV gp120 and were not good antiviral candidates, bis-PBA synthetic lectins were further investigated.¹⁸⁴ Although the bis-PBA did not demonstrate pronounced antiviral activity, these compounds were however found to be relatively noncytotoxic. It was also suggested that the lack of HIV gp120 binding could be due to the lack of multivalency and the small size of the PBA compounds.

3.4 Challenges in anti-HIV lectins formulation development

The clinical translation of anti-HIV natural lectins faces numerous challenges including stability, solubility, resistance, toxicity and manufacturing. These factors have seriously limited the progress in the field and often overshadowed the potential benefits that anti-HIV lectins may have. For example, BanLec has been shown to partially dissociate into its monomeric forms in acidic conditions (pH 2) while maintaining a dimeric structure at neutral pH. The monomeric form of BanLec also offered more resistance towards chemical denaturation than the native dimeric form.¹⁸⁵ In addition, AH was shown to display low solubility in neutral buffer solutions with an enhanced solubility in acidic conditions¹⁸⁶. This lack of solubility in neutral pH conditions could dramatically limit AH use as a topical microbicide for the prevention of HIV sexual transmission, given that vaginal pH increases from acidic (pH \approx 4.5) to neutral (pH \approx 7.5) during intercourse.⁷⁵ Furthermore, lectin resistant HIV strands have been reported.⁸⁷ The mutation of certain glycan structures in HIV gp120 was shown to be responsible for CV-N and Con A resistant HIV strands.¹⁶⁶ Although the development of HIV resistance to lectins may ultimately undermine the potency of these proteins, this is however viewed as an indirect route for exposing underlying amino acid

sequences that could potentially be targeted by antibodies.¹⁴⁶ Anti-HIV lectins have also been associated with strong toxicity. In particular, Con A was shown to be mitogenic toward T-cells and induced cytotoxicity at high concentrations (>10mg/ml).^{187, 188} Similarly, CV-N and BanLec induced pronounced mitogenic activities on PBMCs and T-cells respectively.^{189, 190} Nonetheless, by replacing histidine 84 with a threonine in BanLec, Swanson et al. have demonstrated the possibility to bioengineer anti-HIV lectins in order to suppress their mitogenicity while maintaining their antiviral activity.¹⁷⁰ The high cost of natural anti-HIV lectins mass production and purification presents another particularly difficult challenge.¹⁹¹ Although recombinant technology was proposed to overcome this limitation, improving fermentation yield, controlling mutation and addressing potential immune system insults need to be studied.¹⁹² Besides their ability to address some of the limitations aforementioned and inhibit HIV transmission with relatively good safety profiles, synthetic lectins usually lack carbohydrate specificity and often require extensive optimizations to improve their binding affinity for HIV surface glycoproteins.^{183, 184, 191}

3.5 Anti-HIV lectin formulations

A potential barrier in developing antibody based vaccines against HIV is the oligosaccharide layer that provide a protective covering to the underlying antigens on the viral envelope surface.¹⁹³ Carbohydrate-lectin complexes are a promising therapeutic strategy because various proteins interact with oligosaccharides on the surface of many human cells. Glycoproteins and glycolipids can also interact with lectins and enhance mucosal absorption of drugs and vaccines.¹⁹⁴ Taking advantage of the so-called “lectin direct targeting”, potential efficacious HIV vaccine nanoformulations have targeted endogenous lectins for antigen

delivery to immune cells.¹⁹⁵ Dendritic cell lectins are often targeted in this strategy. Those anti-HIV vaccines strategy activate various receptors on antigen presenting cells or C-type lectins, in order to illicit immune responses.

The mannose receptor, a C-type lectin found on the vaginal epithelium, is known to bind HIV gp120.^{196, 197} Binding of the mannose receptor to HIV gp120 allows the virus to cross the vaginal epithelium.¹⁹⁶ Humans have two types of mannose receptors, type 1 (MRC1) and type 2 (MRC2) and both can stimulate active and adaptive immunity. Because mannose receptors are highly expressed on dendritic cells as well as macrophages, these receptors are important for antigen recognition. Mannose receptors on dendritic cells take up antigen, which stimulates robust T-cell activation via both major histocompatibility complexes (MHC) I and II molecular uptake mechanisms. This T-cell activation plays a critical role in the successful anti-HIV vaccine development.¹⁹⁶ When HIV-1 DNA was encapsulated in mannan coated-cationic liposomes targeting MRC, the nanoformulation successfully activated immunological responses, such as cytotoxic T cells, IgA, and other hypersensitivity responses.¹⁹⁶ These cationic nanoparticles showed 50% higher uptake than non-coated mannan nanoparticles in the macrophage cell line J774E.¹⁹⁸ Similarly, Espuelas et al. showed that a liposome nanoformulation containing mono-, di-, and tetraantennary mannosyl lipid derivatives could potentially achieve identical mannose receptor targeting on dendritic cells for a potential mannose-targeted vaccination strategy.¹⁹⁹ Nonetheless, this study proved that liposome formulations containing higher mannose density result in more efficient interactions with mannose receptors. Furthermore, DC-SIGN, a Ca^{2+} binding adhesion lectin present on the surface of immature dendritic cells, plays an important role in modulating host response to infection and inflammatory stimuli.²⁰⁰ Because of its implications for antigen targeting and

stimulation of T cell responses, DC-SIGN has been considered a potential receptor for HIV vaccine targeting. In fact, DC-SIGN recognizes various high mannose oligosaccharides on HIV gp120.²⁰¹ *In vitro* studies using DC-SIGN-targeted PLGA nanoparticles have shown that these nanoformulations deliver antigens to human dendritic cells.²⁰² DC-SIGN also increased antigen presentation, which translated into an improved activation of CD4+ and CD8+ T-cells.

Table 3-2: Summary of anti-HIV lectin nanoformulations.

Formulation	Lectin	Target	Reference
Mannan coated-cationic liposomes	Mannose receptors, C type lectins	MRC (Dendritic cells)	196, 198
Mannosylated liposome	Mannose receptors, C type lectins	MRC (Dendritic cells)	199
PLGA nanoparticles	DC-SIGN	Dendritic cells	202
High density enveloped HIV glycoprotein liposomes	N/A	BRC (B cells receptor)	203
Con A immobilized polystyrene nanospheres	Con A	HIV gp120	204
Con A immobilized polystyrene/methacrylate nanospheres	Con A	HIV gp120	205

The development of additional HIV nanovaccine immunogens utilized envelope glycoprotein mimetics. Ingale et al. investigated liposomes-grafted high density enveloped HIV glycoprotein trimers that were recognized by anti-HIV-1 antibodies and activated B cells.²⁰³ These liposome constructs may lead to a promising HIV neutralization vaccine. Moreover, He et al. designed nanoparticles containing native like trimeric structures of V1V2 and gp120. These nanoformulations presented a variety of gp140 trimers that displayed 20 spikes similar to that of other virus like particles. This study achieved high B cell stimulation, which may lead to further investigations in the development of a multivalent HIV vaccine.²⁰⁶

Other lectin based anti-HIV strategies have focused on “lectin indirect targeting” instead. In this case, lectins (natural or synthetic) are included in formulations to target HIV envelope glycoproteins. This “virion capture” approach may lead to a successful HIV prevention by hindering a proper interaction between HIV virus and its targets. Virion and HIV gp120 antigen capture could potentially lay the foundation for a mucosal anti-HIV vaccine. Akashi et al. proposed Con A immobilized polystyrene nanospheres capable of capturing HIV virions through binding interactions with HIV gp120 high mannose glycans.²⁰⁴ A similar strategy was investigated by Hayakawa et al. using nanoparticles prepared via copolymerization of polystyrene and poly methacrylate.²⁰⁵

3.6 Conclusion

In general, the field of lectinology has greatly contributed in the structural elucidation, the mechanistic understanding and the advancement of lectin based alternative antiviral therapy for various enveloped viruses including HIV, zika, ebola, marburg, herpes, hepatitis-C, influenza severe acute respiratory syndrome (SARS), feline infectious peritonitis virus

(FIPV) and many more.²⁰⁷⁻²¹⁴ Despite test tube promises shown by lectins (natural and synthetic) against these pathogens, lectin-based antiviral clinical translation still faces great challenges including, resistance, cytotoxicity, immunogenicity, antigen specificity, and limited stability.²¹⁵ Nonetheless, advance research on selected lectin candidates inclusion BanLec and Griffithsin may potentially lead to the first clinically available lectin-based antiviral therapy in the near future.^{9, 216} Even though anti-HIV lectins research is projected to grow, future investigations in the field would likely have to address novel delivery strategies to significantly improve CBAs clinical translation.

CHAPTER 4

SCREENING OF CONCAVALIN A - POLYSACCHARIDES BINDING AFFINITY USING A QUARTZ CRYSTAL MICROBALANCE

(Biosensor and Bioelectronics, 2014, 59: 404–411)

4.1 Introduction and rationale

The design of core-shell novel drug delivery systems relies mostly on the interaction between a coating agent and a triggering element. In the case of using Con A, such delivery systems rely primarily on a competitive binding between a free carbohydrate/glycoprotein and a carbohydrate crosslinker.²¹⁷ This then makes the binding constants a fundamental parameter for a rational design of lectin based drug delivery systems, especially when a control release is expected. The binding of Con A to mannose and glucose containing oligosaccharides has been extensively studied, and to date, several carbohydrate binding constants to Con A are known.²¹⁸⁻²²¹ Yet, a thorough investigation of the binding constants of polysaccharides to Con A remains to be investigated. Particularly, it is crucial to understand the interaction of Con A and glycogen considering the emerging interest in drug delivery systems using such interaction as a design strategy.²²²⁻²²⁶ In addition, this study intends to provide binding affinity constants, based on the determined molecular weights by Size Exclusion Chromatography (SEC), for a thorough characterization of ConA-glycogen and Con A-mannan interactions. Furthermore, the present study may provide a model for a better understanding of protein-polysaccharides *in vitro* interaction.

In this study, it is hypothesize that a Quartz Crystal Microbalance (QCM) can be used in a flow injection setting to monitor the binding affinities of polysaccharides (glycogen and

mannan) to an immobilized lectin, Con A. The binding constants of Con A to these polysaccharides could then be utilized rationally in the design of stimuli-sensitive drug delivery systems to target high mannose or glucose containing glycoproteins or surfaces, such as HIV gp120.

Introduced in 1959 by Sauerbrey, the basic QCM theory correlates the mass change per unit area at the QCM electrode surface to the observed change in oscillation frequency of the crystal.²²⁷ QCMs have been proven to be reliable in the field of electrochemistry,²²⁸⁻²³⁰ in petroleum characterization,^{231, 232} in environmental chemistry,²³³ material science²³⁴ and more interestingly in the development of biosensors,²³⁵⁻²³⁸ which are valuable for disease diagnosis. QCMs have also found a great interest in the study of binding affinity constants defining substrate-ligand interactions.²³⁹⁻²⁴² Besides the fact that it does not require any calibration, one of the most exciting features of the QCM is its ability to quantify a mass change at the nanogram level. This makes QCM an easy to setup and robust technique for bioaffinity analysis. Data obtained from QCMs are shown to be in accordance with other well-established techniques such as surface plasmon resonance (SPR),^{243, 244} fluorescence spectroscopy,^{217, 245} atomic force microscopy^{246, 247} and photoelectron microscopy.²⁴⁸

Polysaccharides and glycoconjugates are known to play crucial roles in biological processes, such as, cell activation, differentiation and apoptosis,²³⁹ but also in cellular recognition, transmission of information, immunity and tumorigenesis.^{241, 249-252} Glycogen, known as "animal starch" for its resemblance with starch found in plants, is the principal storage form of glucose (energy) in animal cells.²⁵³ It is a highly branched polymer in which small chain of glucose molecules are linked by α -D-(1 \rightarrow 4) linkage and α -D-(1 \rightarrow 6) branching

points.²⁵⁴ In human, glycogen is mostly found in the liver but can also be found in muscles and brain glial cells where its proportion is significantly lower.²⁵⁵⁻²⁵⁷

Originally extracted from jack bean, Con A is a member of the legume lectin family and binds to sugars, glycoproteins, and glycolipids, containing internal and nonreducing terminal α -D-mannosyl and α -D-glucosyl groups.^{221, 258-260} Like most lectins, Con A is a homotetramer with each subunit composed of 235 amino acids and having a molecular weight of 26.5 kDa. At pH below 6, Con A exists as a dimer and is in its tetrameric form at pH above 6. To depict its binding activity, the protein requires metal ions. Agrawal and Goldstein have shown that each subunit has one Ca^{+2} and Mn^{2+} binding sites.^{258, 261}

4.2 Material and methods

Quartz Crystal Microbalance

Stanford Research System (SRS) QCM200 apparatus (Sunnyvale, CA, USA) is used in this experiment. The QCM200 System is a stand-alone instrument with a built-in frequency counter and resistance meter. It includes controller, crystal oscillator electronics, crystal holder, and quartz crystals. In this study, 1 inch diameter, 5 MHz AT-cut, plano-plano Chromium/gold (Cr/Au) quartz crystals from SRS are used for each measurement in a flow injection mode. Two single injection syringe pumps are used to deliver the analytes (polysaccharides) and the free buffer (Tris Buffer Saline). Series resonance frequency and resistance are measured and displayed directly on the front panel. However, Labview V7.0 software (Sunnyvale, CA, USA) is installed on a computer for real-time data collection, display, analysis and storage.

Chemicals

Concanavalin A (Con A) from *Canavalia ensiformis* (Jack bean) Type VI, glycogen from Oyster, mannan from *Saccharomyces cerevisiae*, N-Hydroxysuccinimide (NHS), 11-mercaptoundecanoic acid (MUA, 95%), 4-Morpholineethanesulfonic acid sodium salt (MES), sulfuric acid (H₂SO₄, puriss. p.a., 95-97% (T)), hydrogen peroxide solution (H₂O₂, 30 wt. % in H₂O, ACS reagent), 200 proof absolute ethanol, hydrochloric acid (ACS reagent, 37%), calcium chloride dehydrate (CaCl₂•2H₂O, ACS reagent, ≥99%) and manganese (II) chloride tetrahydrate (MnCl₂•4H₂O, Reagent Plus®, ≥99%), phosphate buffered saline (PBS) pH 7.4 and Tris Buffer Saline (TBS) pH 8.0 were purchased from Sigma-Aldrich (Milwaukee, WI, USA). 1-ethyl-3-[3-dimethylaminopropyl]carbodiimide hydrochloride (EDC) was purchased from Thermo Scientific (Rockford, IL, USA). PBS and TBS were prepared according to the manufacturer protocol and the pH was verified before any experiment. TBS was supplemented with Mn²⁺ and Ca²⁺ and used as running buffer without any further treatments.

Methods

Fourier Transform Infrared Spectroscopy (FTIR)

Agilent Cary 630 FTIR instrument (Newark, DE) equipped with a diamond crystal having a single reflection and a nominal angle of 45° is used in its Attenuated Total Reflectance (ATR) mode for the acquisition of all IR spectra. A resolution of 4 cm⁻¹ and a sample scan of 32/s is set as parameters and the effective pathlength is 1.1 μm. Prior to any IR analysis, QCM crystals are dried under a nitrogen gas stream and allowed to make an intimate contact with the ATR diamond crystal surface by pressing them with a pressure clamp. FTIR spectra are

collected and analyzed with MicroLab PC and MicroLab Lite softwares (versions 4.0, Newark, DE, USA), respectively.

Size Exclusion Chromatography (SEC)

Glycogen and mannan molecular weight are determined by size exclusion chromatography. Briefly, seven (7) dextran standards covering a molecular weight range from 5.2 kDa to 668 kDa are run on SEC (Waters, Milford, MA, USA) equipped with a differential refractometer detector to draw a calibration curve. The equation of the calibration curve is $Y = -0.3367X + 10.351$ with a coefficient of determination of $R^2 = 0.9877$ indicating a strong correlation between the retention time (X) and the base 10 logarithm (\log_{10}) of the molecular weights (Y). Samples are dissolved in 0.1M of sodium nitrate (NaNO_3) at pH 7 and each experiment is conducted at a flow rate of 1 ml/min on a 7.8×300 mm WAT011525 Ultrahydrogel column (Waters, Milford, MA, USA). Data are acquired and analyzed on Millennium³² software version 3.20 (Waters, Milford, MA, USA). Glycogen and mannan molecular weights are derived from their respective retention time using the calibration curve.

QCM measurement

Preparation of the gold crystal surface

Prior to any experiment, a Cr/Au QCM crystal is cleaned by exposing it to a piranha cleaning solution. Basically, the cleaning solution is prepared in an appropriate container by carefully adding 1 part per volume of hydrogen peroxide to 3 parts per volume of sulfuric acid to reach a ratio of 1:3.²⁴⁶ **Caution:** *Piranha solution should be handled with extreme care and only small volume should be prepared at any time.* For safety purposes, the piranha solution should be prepared under a well-functioning hood and crystals should be handled with

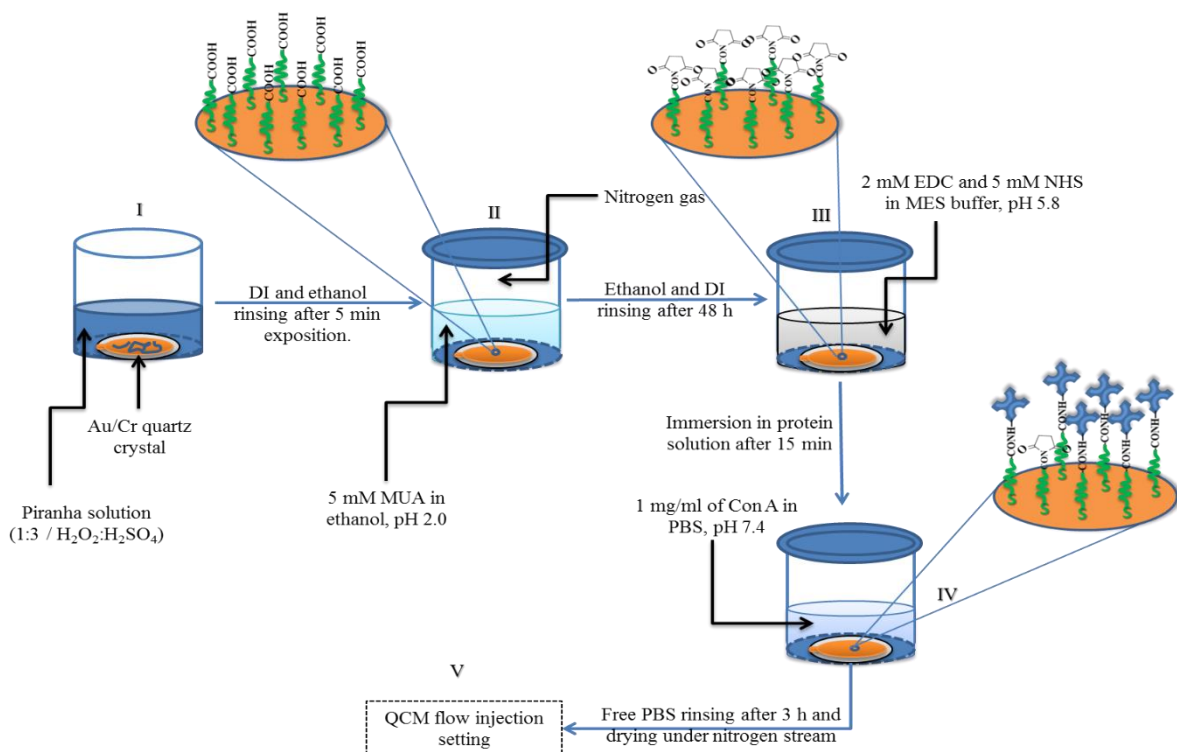
appropriate tweezers. After 5 minutes in the piranha solution, the crystals are removed and cleaned twice with Millipore Q water (DI water) and ethanol before drying under a nitrogen stream.

Con A immobilization

To study the binding kinetics of the polysaccharides to Con A, the lectin is first immobilized onto a gold crystal by EDC chemistry and the immobilization is validated by Fourier Transform InfraRed spectroscopy (FTIR). As shown earlier by Lebed et al.²³⁹, Con A can readily adsorb onto a clean gold crystal surface. Even though the mechanism involved in such physisorption is not fully explained, it appears that the lectin binds loosely and can easily be detached off the crystal's surface when the free buffer is allowed to flow onto the surface. To avoid such an undesirable effect, a covalent attachment of the lectin is performed through zero linker (EDC/NHS) chemistry by coupling the N-terminal of the protein with the carboxylic head group of MUA.

To immobilize Con A on the quartz crystal, the method of Caruso et al.²⁴⁶ is used with minor adaptations. Briefly, in order to provide the gold surface with the carboxylic acid function, a clean gold crystal is incubated in an ethanolic solution of 5 mM of MUA at pH 2.0 for 48 h. To avoid thiol oxidation and ensure the success of the self-assembling, the container is tightly sealed and backfilled with dry nitrogen prior to storage. The success of MUA attachment relies on the intrinsic property of the alkanethiols moieties to chemisorb onto gold surfaces.²⁶² Love et al.²⁶³ have proven that the sulfur atom of the alkanethiol forms a dative bond with the gold metal surface. After 48 h of incubation, the crystal is removed and thoroughly rinsed with ethanol and DI water before immersion in a 0.1 M MES buffer

containing 0.5 M NaCl at a pH 5.8. EDC and NHS are subsequently added to the buffer to reach a concentration of 2 mM and 5 mM, respectively. The mixture is allowed to react for at least 15 minutes (min). The crystal is then retrieved and redispersed in 1 mg/ml of Con A in PBS for 3 hours, after which the surface is cleaned again with free PBS buffer and placed in the flow cell chamber for QCM frequency acquisition. Scheme 4.1 shows an illustration of the steps involved in the lectin immobilization.



Scheme 4-1: Step-by-step illustration of Con A immobilization onto the QCM gold surface.

Special care should be taken in handling Piranha solution under a fume hood. Once the crystal is cleaned and dried under nitrogen, it is disposed in 5 mM of Mercaptoundecanoic acid for 48h for carboxylic acid functionalization. Con A is then immobilized by EDC chemistry using 2 mM EDC and 5 mM NHS in MES buffer (pH5.8). The reagent mixture is gently shaken to insure even distribution of reagents during EDC coupling.

QCM frequency acquisition

QCM200 is used in a flow injection mode to monitor the lectin and polysaccharides interaction (figure 4-1). Briefly, two injection pumps, one for the free running buffer and the second for the polysaccharide solutions, are connected to a dual flow connector. The flow rates are set to 3 ml/h in each measurement. The free buffer is first run to rule out the buffer effect and the flow is switched to the polysaccharide solution after a baseline is reached. Five different concentrations covering a range from 0.1 to 1mg/ml are prepared in the running buffer for both glycogen and mannan, and the relative frequency shifts and mass increases following the binding are recorded on a computer through the QCM200 software. The Sauerbrey's equation 4-1 is used to fit the frequency shift to the mass change onto the crystal surface.

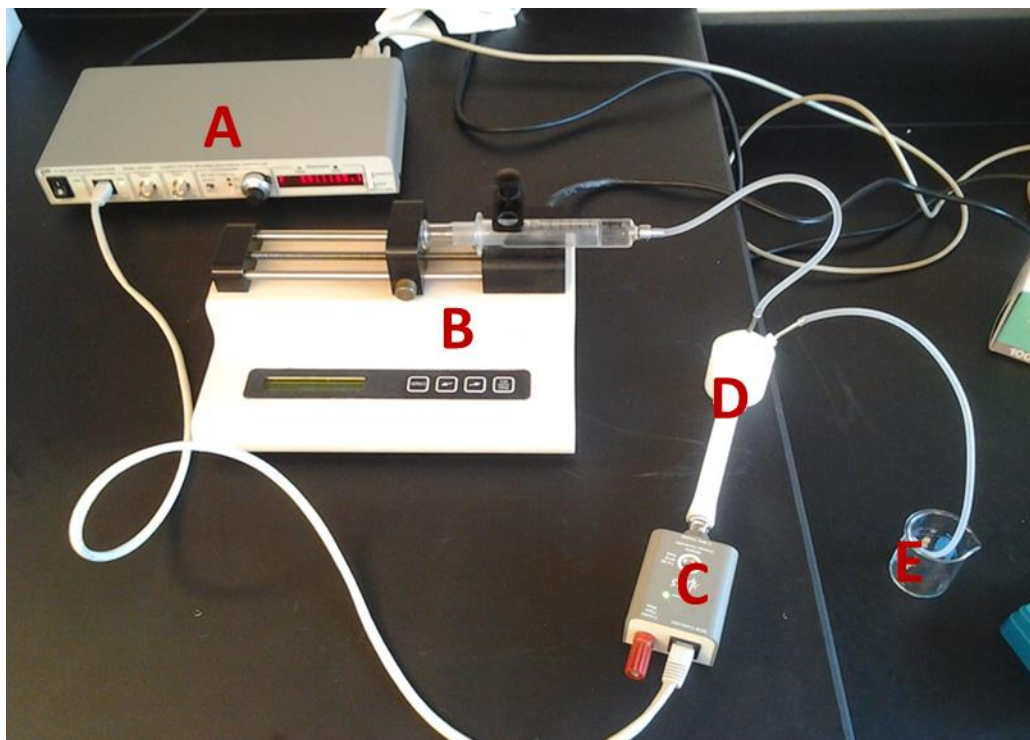


Figure 4-1: Typical single flow injection QCM200 experimental setup. (A) QCM200 digital controller, (B) syringe pump, (C) crystal controller, (D) crystal holder and (E) waste collector.

$$\Delta F = -C_f \times \Delta m \quad (4-1)$$

Where ΔF , C_f and Δm are respectively the frequency shift (resonance frequency change), the crystal sensitivity factor, and the relative mass change. C_f is a fundamental property of the quartz crystal and is expressed by equation 4-2.

$$C_f = \frac{2nf_0^2}{(\rho_q\mu_q)^{0.5}} \quad (4-2)$$

In equation 4-2, n is the number of harmonic at which the crystal is driven, f_0 the resonant frequency of the fundamental mode of the crystal, ρ_q the density of quartz and μ_q the shear modulus of quartz. In this experiment, these parameters are $n = 1$, $f_0 = 5.0 \text{ MHz}$, $\rho_q = 2.648 \text{ g cm}^{-3}$ and $\mu_q = 2.947 \times 10^{11} \text{ g cm}^{-1} \text{ s}^{-2}$, respectively. The sensitivity factor C_f is $56.6 \text{ Hz } \mu\text{g}^{-1} \text{ cm}^2$.

4.3 Results and discussion

Figure 4-2A summarizes the FTIR spectra obtained at each step of the lectin immobilization process. The spectrum A-a is obtained from the clean and unmodified QCM gold crystal. The FTIR spectrum acquired after MUA attachment (A-b) onto the gold crystal shows distinctive peaks between 2980 and 2850 cm^{-1} , which are due to the symmetric and asymmetric stretch mode of CH_2 in MUA backbone.^{264, 265} Furthermore, features at around 1440 and 1700 are related to the COOH groups in MUA.²⁶⁶ The spectrum obtained after the EDC/NHS chemistry (A-c) shows two bands at around 1715 cm^{-1} and 1650 cm^{-1} , which are bands responsible for the carbonyl stretch mode of the COO-NHS ester moiety.^{264, 265} After Con A attachment, amide I and amide II bands at 1540 and 1640 cm^{-1} can be distinguished and are indicative of a successful Con A covalent attachment on the gold surface (A-d).^{267, 268}

Glycogen and mannan molecular weights, determined by SEC/GPC, are found to be 604 ± 4.852 kDa and 54 ± 6.562 kDa ($n=3$), respectively. Typical chromatograms from these analyses are shown in figure 4-2B.

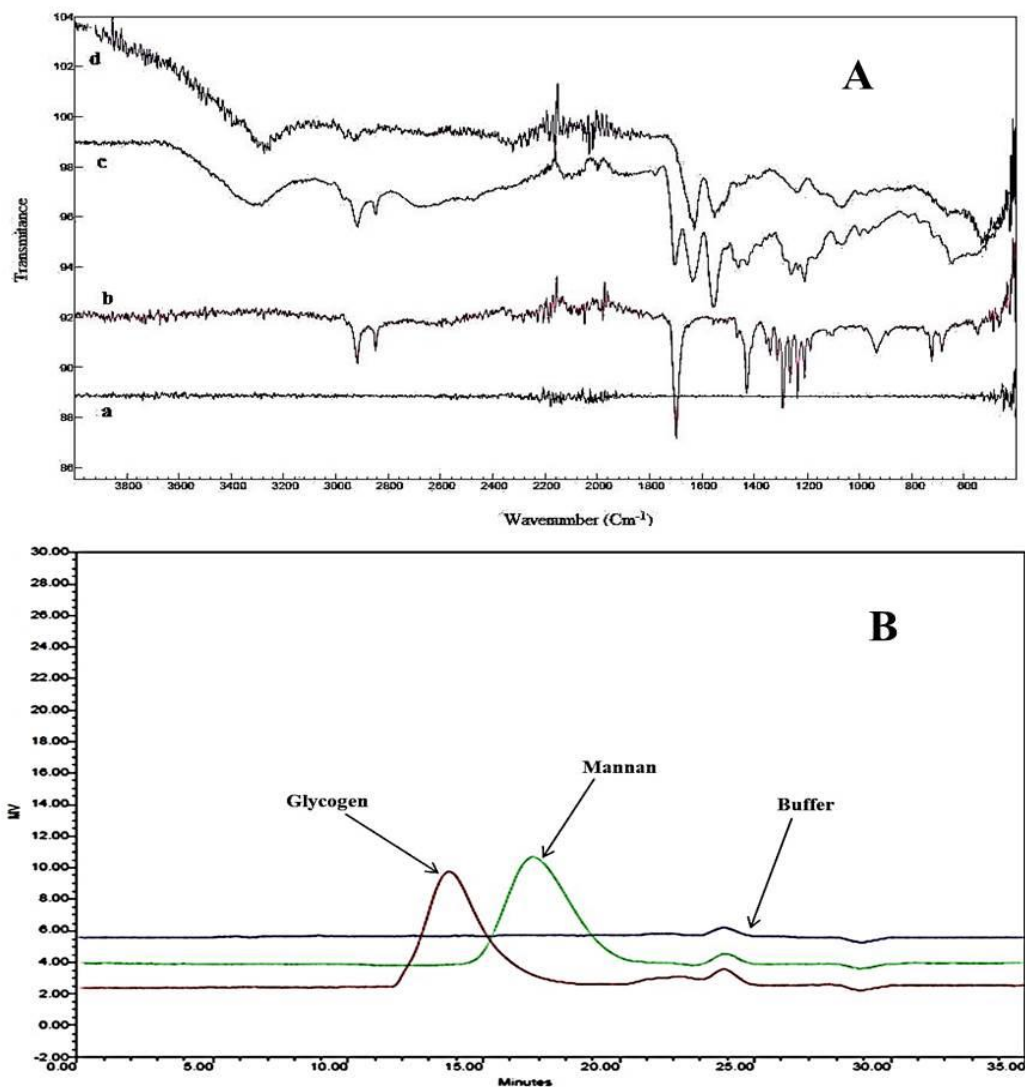


Figure 4-2: (A) FTIR spectra of clean QCM gold crystal (a) followed by 11-mercaptoundecanoic acid (MUA) attachment (b), before EDC/NHS chemistry (c) and finally Con A immobilization (d) onto the QCM crystal. (B) Size exclusion chromatograms of sodium nitrate (NaNO₃) (buffer), glycogen and yeast mannan.

Once Con A is immobilized onto the gold surface, different analyte concentrations are flowed on the Con A-immobilized QCM crystal. In this work, each experiment is run on a separate crystal and the polysaccharide solutions are injected when a stable baseline is reached, as shown in figure 4-3. The resonance frequency is gradually decreasing while increasing the glycogen and mannan concentration as displayed in figure 4-4 (A&B) and are found to be following a Langmuir-type adsorption isotherm (equation 4-3) as shown in figure 4-5 (A&B).

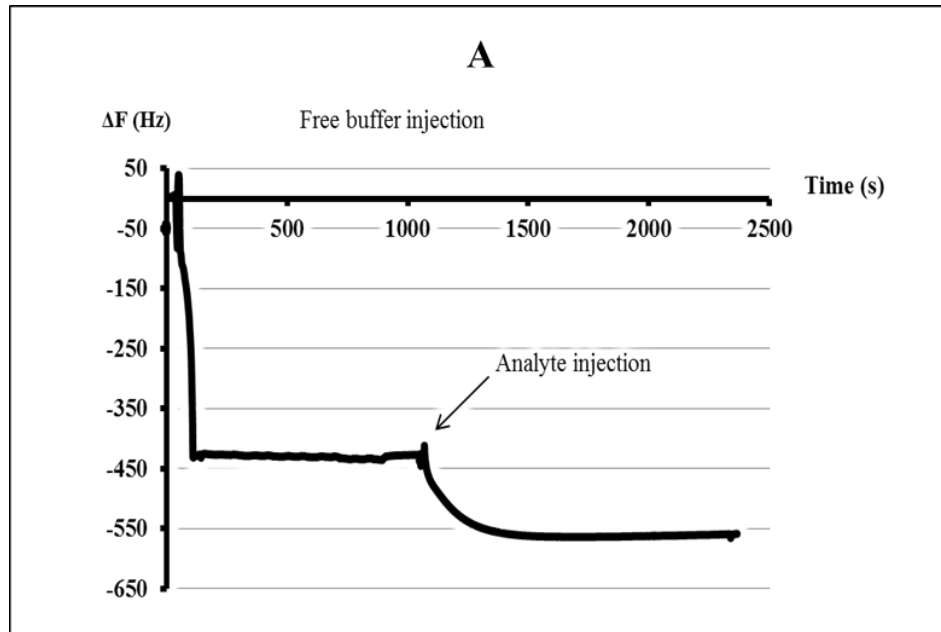


Figure 4-3: Frequency shift observed with polysaccharide injection after a baseline is reached with free buffer (0.05 M Tris-buffer saline, 1 mM Ca²⁺, 1 mM Mn²⁺, pH 8.0).

$$\Delta F = \Delta F_{max} \frac{K_A[\text{analyte}]}{1+K_A[\text{analyte}]} \quad (4-3)$$

In equation 4-3, ΔF represents the frequency shift observed on the QCM frequency counter, ΔF_{max} the maximum frequency shift at saturation, and K_A represents the equilibrium

association constant and [analyte] the concentration of polysaccharide. At saturation, the binding and dissociation rates of analytes to the available binding sites of the lectin are identical and reach a steady state.²⁶⁹

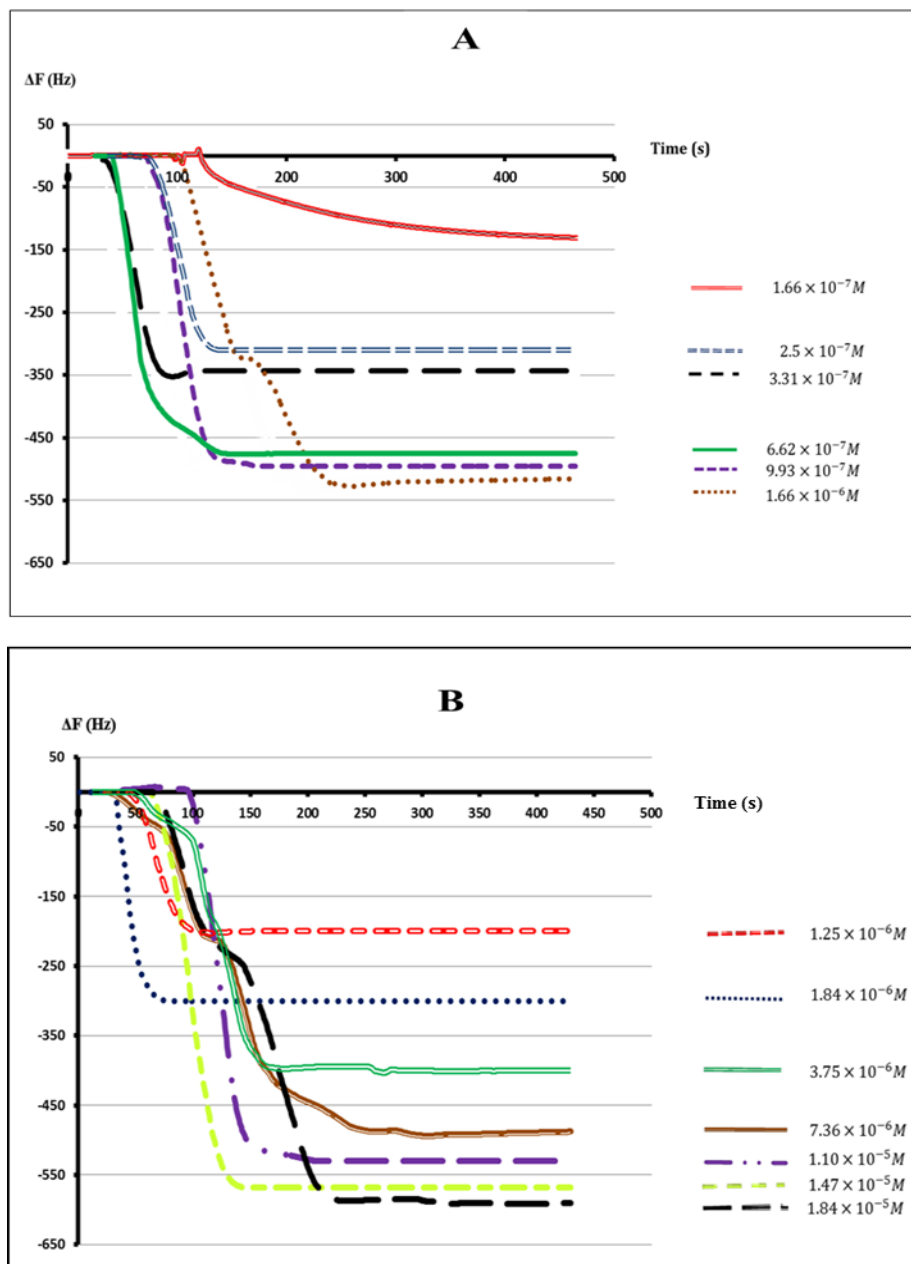


Figure 4-4: Time dependent QCM resonance frequency shifts for glycogen (A) and mannan (B) at different concentrations.

The reciprocal of equation 4-3 gives the equation of a straight line (equation 4-4) from which one can derive ΔF_{\max} from the y-intercept and the equilibrium association constant (K_A) from the slope, as shown in figure 4-5 (A'&B'). The equilibrium dissociation constant is obtained from equation 4-5 which is the reciprocal of K_A .

$$\frac{1}{\Delta F} = \frac{1}{K_A \times \Delta F_{\max} \times [\text{analyte}]} + \frac{1}{\Delta F_{\max}} \quad (4-4)$$

$$K_D = \frac{1}{K_A} \quad (4-5)$$

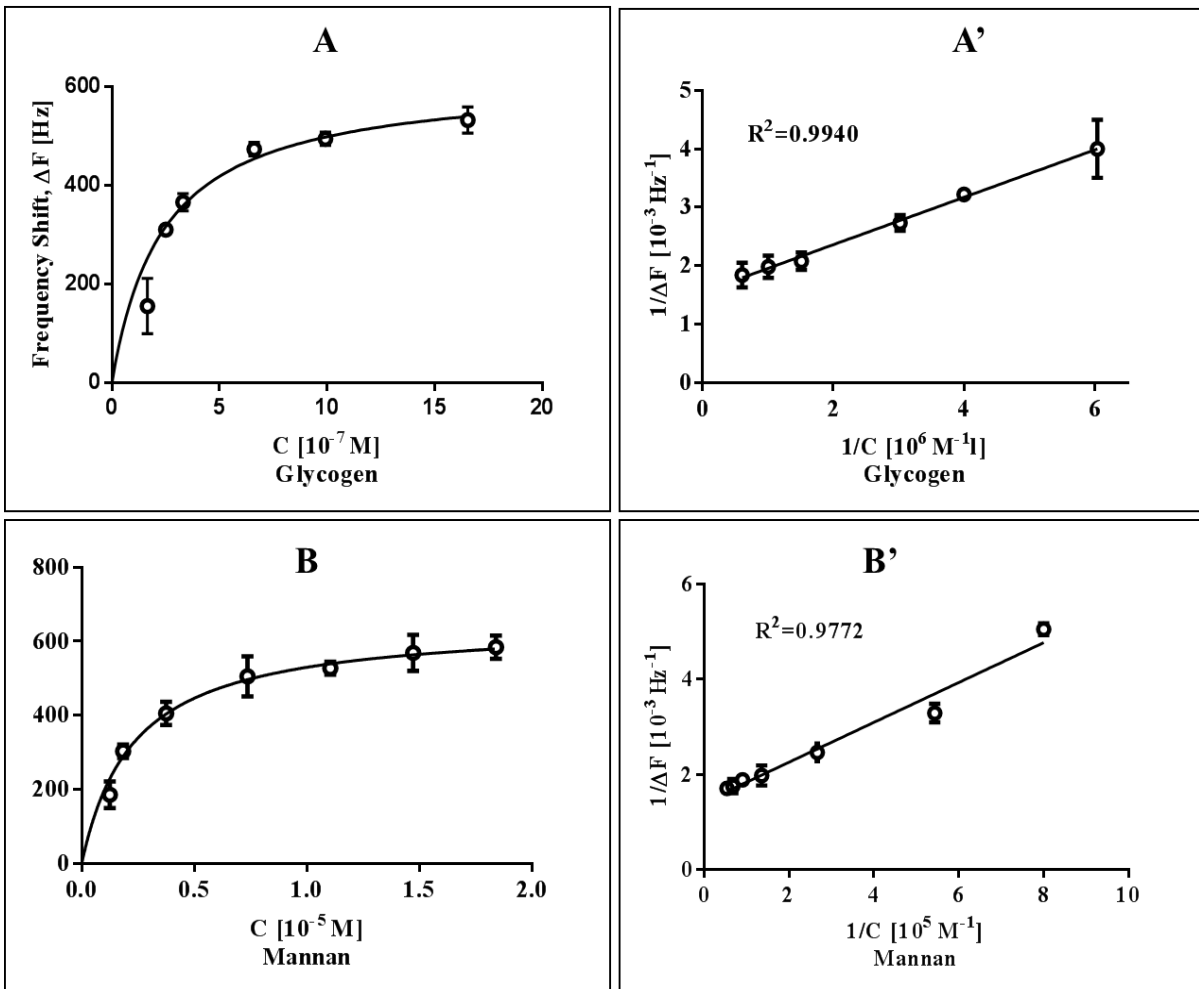


Figure 4-5: Saturation binding curves for glycogen (A) mannan (B) and their respective reciprocal curves (A') and (B') obtained from equation (4-4).

The expression of equation 4-4 for glycogen is $Y = 4 * 10^{-10}X + 1.57 * 10^{-3}$ with a coefficient of determination of $R^2 = 0.9940$ indicating a very good correlation for this polysaccharide. The calculated ΔF_{\max} is 637 Hz and the equilibrium association and dissociation constants value are $K_A = 3.93 * 10^6 M^{-1}$ and $K_D = 0.25 \mu M$, respectively. These values are found to be consistent with those of Tan et al.²⁷⁰ obtained using an electrochemical piezoelectric quartz crystal impedance (EPQCI) method ($K_A = 1.48 * 10^6 M^{-1}$ and $K_D = 0.4 \mu M$).

For mannan, the fitted equation 4-4 is $Y = 4.15 * 10^{-9}X + 1.43 * 10^{-3}$ with a coefficient of determination of $R^2 = 0.9772$, suggesting a good correlation. ΔF_{\max} is found to be 697 Hz and the equilibrium association and dissociation constants are $K_A = 3.46 * 10^5 M^{-1}$ and $K_D = 2.89 \mu M$, respectively. Equilibrium dissociation constants (K_D) reported so far for the interaction of the yeast mannan with Con A measured on QCM are in the range of 0.1-1.1 μM .^{271, 272} The binding affinity (K_A) obtained for the binding between Con A and an immobilized yeast mannan is reported to be 0.4 μM .²⁴⁹ Compared to our study, in which the lectin was immobilized, Pei et al. opted instead for a method in which yeast mannan was immobilized onto the gold crystal, which might explained the slight difference in affinity values. In fact, Duverger et al.²²⁰ have proven that different affinity values can be obtained in SPR experiments for the same interaction, considering whether the lectin or the ligand is immobilized onto the crystal.

Con A is known to have higher affinities to mannose containing oligosaccharides compared to glucose containing moieties.^{241, 273} However, in this study, a greater affinity was found for Con A to glycogen compared to yeast mannan. Initially observed by Tan et al.²⁷⁰ using a EPQCI method, this pattern may be partly due to the greater compaction of the

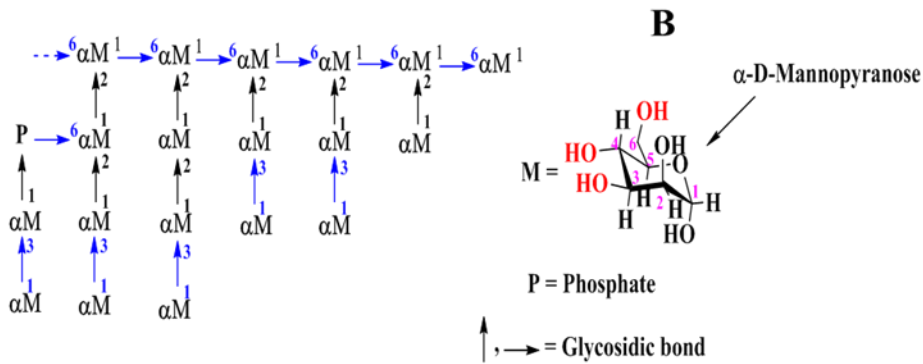
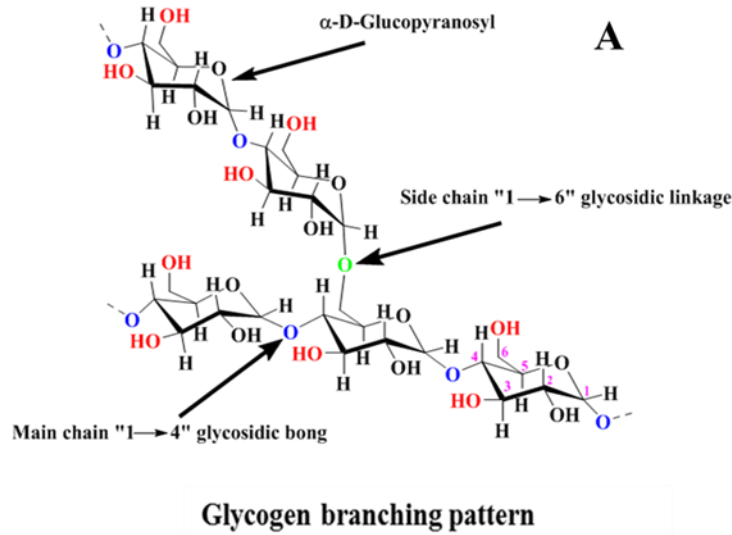


Figure 4-6: Molecular branching pattern in glycogen from Oyster (A) and mannan from *Saccharomyces cerevisiae* (B). Mannan main chain's monomers are linked by 1→6 glycosidic bonds with several 1→3 linkages throughout the branches. Those linkages are shown in blue color in mannan's structure. Glycogen main chain's monomers are 1→4 linked with only few 1→6 glycosidic bonds occurring each 12 glucose residues. The 1→4 linkages are shown in blue in glycogen's structure and the 1→6 linkage in green. Hydroxyl groups at position 3, 4 and 6, shown in red are critical for Con A interaction with a greater requirement at position 6. Unavailability of the critical hydroxyl groups prevents binding to Con A.

association between Con A and glycogen compare to mannan and Con A. The steric hindrance caused by the glycogen macromolecule is also thought to have an influence on the combination between Con A and glycogen. In addition to the steric effect, the huge difference in the polysaccharides molecular weights could explain the result obtained in this study. Indeed, Mueller et al.²⁷⁴ observed that the binding affinity of glucans polymers to (1→3)-β-D-glucan receptors in a human monocyte-like cell line is in part dependent on their molecular weights. In fact, this group observed that higher glucan molecular weights resulted in higher affinity values. Similar results are reported by Kojima et al. in their study on the antitumor activity of Schizophyllan.²⁷⁵

Furthermore, the higher affinity to glycogen could be due to the branching pattern of both glycogen and yeast mannan (figure 4-6). Indeed, in the past decades, it has been extensively proven that sugar residues must obey a set of criteria in order to interact with Con A. Thus, it is generally accepted that hydroxyl groups at the C-3, C-4 and C-6 positions are critical in Con A and a sugar residue interaction, with a higher requirement at the C-6 position, as shown by Goldstein and others.^{258, 276} Moreover, glycogen main chain's glucose monomers are connected by 1→4 glycosidic bonds, with only few 1→6 branches linkages at every 12 glucose residues.²⁷⁷ This branching arrangement allows more glucose residues to be available for interaction with Con A. Unlike for glycogen, yeast mannan main chains monomers are linked by 1→6 glycosidic bonds with several 1→3 glycosidic linkages found throughout the branches of the macromolecule.²⁷⁸⁻²⁸⁰ Kwiatkowski and Kwiatkowski²⁸¹ have also shown the presence of 1→4 glycosidic bonds in yeast mannan. This arrangement, in contrast, does not allow a wide range of mannose residues to successfully interact with Con A because of a higher unavailability of the C-6, C-4 and C-3 hydroxyl groups compared to glycogen.

Along with the frequency shift, the motional resistance shift following the binding of the polysaccharides to Con A is recorded in each experiment. The motional resistance expresses the loss in mechanical energy dissipated to the medium and the quartz interior and is induced by viscoelasticity changes occurring onto the quartz surface and changes of solution viscosity and density.²³⁹ Using a Butterworth-Van Dyke equivalent circuit model Stephan et al.²⁸² derived a linear relationship (equation 4-6) between the change in series resonance resistance (ΔR) of the quartz oscillator and the liquid density and viscosity during a liquid loading.

$$\Delta R = \frac{n \cdot \omega_s \cdot L_u}{\pi} * \sqrt{\frac{2 \omega_s \cdot \rho_L \cdot \eta_L}{\rho_q \cdot \mu_q}} \quad (4-6)$$

Where ΔR represents the change in series resonance resistance in Ω , n the number of sides in contact with the liquid, ω_s the angular frequency at series resonance ($2\pi f_s$) and L_u the induction for the unperturbed (dry) resonator. ρ_L and η_L are the density and shear viscosity of the liquid, respectively. ρ_q and μ_q are the density and shear modulus of quartz. In our study, the resistance is recorded from the frequency counter as the experiment progresses.

Figure 4-7 shows the relationship between the motional resistance change and the resonant frequency shift (ΔR vs ΔF) corresponding to the polysaccharides binding to Con A. The fitting equations are $Y = 0.027 * X + 0.303$ for glycogen and $Y = 0.029 * X - 0.086$ for mannan and the coefficients of determination are $R^2 = 0.9908$ and $R^2 = 0.9963$, respectively. From the fitting curves, it is found that the reciprocal of the slopes ($\Delta F/\Delta R$) are $37.29 \text{ Hz} \cdot \Omega^{-1}$ for glycogen and $34.86 \text{ Hz} \cdot \Omega^{-1}$ for mannan. Lebed et al.²³⁹ found a $\Delta F/\Delta R$ value of $29.41 \text{ Hz} \cdot \Omega^{-1}$ for the interaction of carboxypeptidase Y to an immobilized Con A on a 5 MHz QCM gold electrode in Tris-buffered saline. Characterizing the interaction between Con A and

glycogen, Tan et al. found $\Delta F/\Delta R$ values ranging from 41.6 to 43.2 Hz. Ω^{-1} for the adsorption of glycogen, BSA and Con A onto a 9 MHz quartz crystal in PBS.²⁷⁰ Low $\Delta F/\Delta R$ values are generally associated with viscoelastic or damping effects.²³⁹ However, the values obtained in this study, as compared to others, are typical of a bulk liquid effect instead of the process related to the association of the polysaccharides to Con A.^{239, 270} That is, the frequency shift observed is primarily due to the mass effect, and Sauerbrey's rigidity approximation is valid.²⁸³

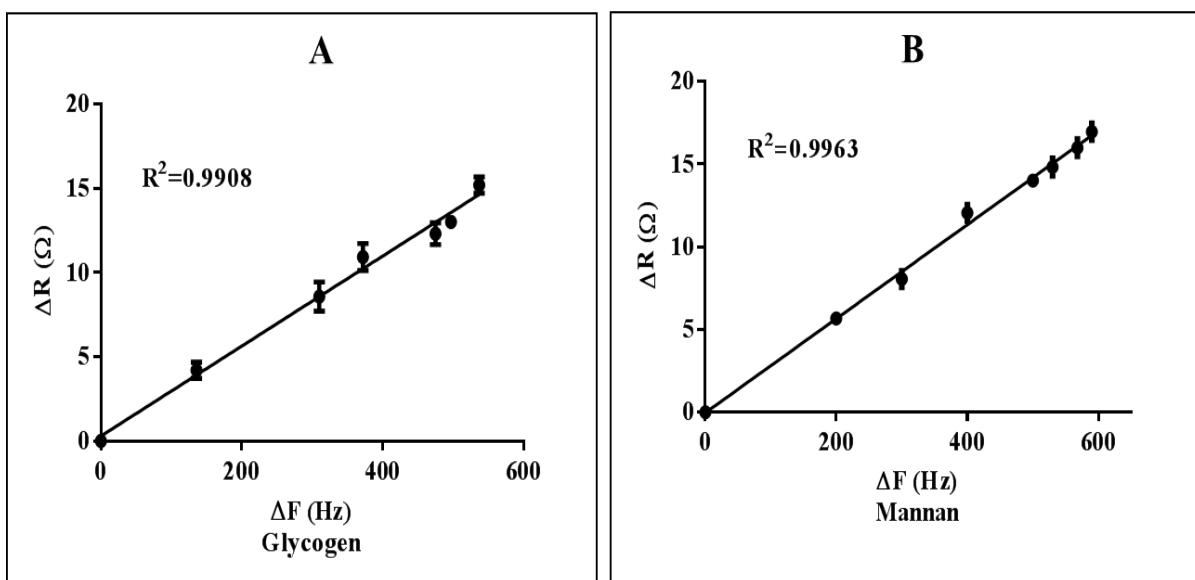


Figure 4-7: Relationships (ΔR vs ΔF) between the motional resistance (ΔR) and the resonant frequency (ΔF) changes corresponding to specific glycogen (a) and mannan (b) adsorption on a Con A layer on QCM crystal surface.

4.4 Conclusion

Using a Quartz crystal microbalance in its flow injection mode, we have been able to obtain affinity binding constants describing the interaction between two polysaccharides (glycogen and mannan) and Con A. The equilibrium dissociation constant for the interaction Con A-glycogen is $K_D = 0.25 \mu\text{M}$ which is about 12 fold lower than the equilibrium

dissociation constant describing the interaction Con A-mannan ($K_D = 2.89 \mu\text{M}$). That is, Con A, a mannose specific lectin, is found to have a higher affinity to glycogen from Oyster, a glucose base polysaccharide, than to mannan from *Saccharomyces cerevisiae*, a mannose based polysaccharide. This observation was mainly due to a steric effect, the molecular weight and the branching pattern of both polysaccharides. Based on the underlying results, as for Con A/glycogen agglutinate, it is hypothesized that carbohydrate responsive drug delivery system could also be designed based on Con A/mannan interaction. Nonetheless, due to the lower binding affinity between Con A and mannan, the stability of such system will need to be thoroughly investigated in various pH and thermal conditions.

CHAPTER 5

DEVELOPMENT OF A MICROBICIDE LOADED HIV-1 gp120 TARGETED VAGINAL FORMULATION

(Molecular Pharmaceutics, 2017, 14(10): 3512–3527)

5.1 Introduction and rationale

Since its discovery in 1983, Human Immunodeficiency Virus infection and Acquired Immune Deficiency Syndrome (HIV/AIDS) has remained a global threat, given that a complete eradication strategy is yet to be effective.^{284, 285} According to the 2016 UNAIDS fact sheet, it is estimated that 36.7 million [34. million – 39.8 million] of people are currently living with HIV worldwide.²⁸⁶ Owing to the Highly Active Antiretroviral Therapy (HAART), which decreases the risk of opportunistic infections and maintains the immune system function, HIV patients can now live longer. However, sexual transmission of HIV, which accounts for 75 to 85 % of the overall HIV infections, is still a major hurdle in the complete eradication of HIV.²¹ In addition to having multiple sexual partners and the lack of male circumcision, another major reason for the increase in HIV transmission is that 6 out of 10 people living with HIV do not know their HIV positive status, making them a risk to their sexual partners.^{22, 23} Therefore, there is an urgent and crucial need to develop a safe, effective and patient compliant topical drug delivery system capable of preventing HIV sexual transmission. Recently, various microbicide drug delivery strategies (gels, films, rings, etc.) have been proposed, attempting to address this need with limited success. Semisolid dosage forms (gels), which are the most common microbicide drug delivery systems, present major challenges of messiness, leakage and lack of controlled release.²⁵ Besides their lack of retention, which constantly leads to

leakages and therefore patient adherence and compliance issues, topical microbicide loaded gel formulation, such as CAPRISA 004, have shown a lack of effectiveness against HIV.^{26, 27} Vaginal films, which are less untidy than gels, are fast dissolving with rapid drug clearance by mucus renewal cycle.²⁵ Moreover, the ASPIRE study states that the silicone based vaginal ring Dapivirine, although promising, still has to address compliance issues with undesirable drug release kinetics.²⁸ In fact, the major concern of a ring-based delivery system is a constant drug release even in the absence of HIV virus, which will eventually lead to drug waste, drug resistance issues, and potential side effects. To address this problem, the present study hypothesizes that Concanavalin A (Con A) based topical vaginal and rectal nanomedicine formulation is capable of the safe and effective release of a pre-encapsulated HIV microbicide, "on-demand". Such a microbicide delivery system would not only protect the active agent but could ultimately protect women, since more than half of all new HIV/AIDS infections worldwide occur in females.²⁹

Carbohydrate-binding agents (CBA) are a class of proteins that have high affinities for sugar moieties. They have been shown to be highly effective against HIV, as microbicides.²⁸⁷⁻²⁸⁹ Lectins, which represent a subclass of CBA, are proteins that specifically recognize carbohydrate (glycan) structures.^{290, 291} One of the most studied lectins is *Canavalia ensiformis* (Con A), extracted from jack beans. Con A is known to bind sugars, glycoproteins, and glycolipids, containing internal and nonreducing terminal α -D-mannosyl and α -D-glucosyl groups.^{258, 260, 292} Like most lectins, Con A is a homotetramer with each subunit composed of 235 amino acids and having a molecular weight of 26.5 kDa. At pH below 6, Con A exists as a dimer, and is in its tetrameric form at pH above 6. Con A has an isoelectric point (PI) that ranges from 4.5 to 5.5, depending on its isoforms. Like all proteins, above its pI, Con

A is negatively charged, and bears a positive charge at pH values below the pI value. Con A has previously been shown to bind HIV-1 and HIV-2 viruses' envelope glycoprotein 120 (HIV gp120).¹⁶⁷ More recently, Con A-immobilized polystyrene nanospheres were successfully designed for HIV-1 virions captured through Con A/HIV-1 gp120 binding interactions.²⁰⁵ HIV gp120 plays a critical role in HIV infection. In fact, the binding of HIV gp120 (on HIV virus' membrane) to CD4 receptors (on host cells' membrane) represents the first step in the course of HIV attachment and host cells entry. This leads to the fusion of both membranes and the incorporation of the viral material into the host cell cytoplasm.²⁹³ This process ultimately leads to the production of new HIV virions and the spreading of the disease.

In the last few decades, HIV gp120 has been extensively studied. To date, more is known about its structure and composition than ever before. Several groups have shown that HIV gp120 is composed of high proportions of carbohydrates. It is estimated that 50% of the apparent molecular mass of HIV gp120 is composed of carbohydrates.²⁹⁴ More specifically, Mizuochi et al. found that about 40% of the total oligosaccharide structures released from HIV gp120 are hybrid and/or high mannose-type oligosaccharides and 60% are of the complex type.^{94, 95} These studies also highlighted the unique and high mannose oligosaccharides content in recombinant HIV-1 envelope glycoprotein gp120 (HIV-1 rgp120) compared to other Chinese hamster ovary-cell-derived glycoproteins. Furthermore, Geyer et al.⁹⁷ found that high mannose-type oligosaccharides account for approximately 50% of the carbohydrate structures of HIV gp120. More recently, Bonomelli et al.⁹⁹ reported that HIV gp120 derived from virions prepared by infecting peripheral blood mononuclear cells (PBMC) with viruses from clade A (92RW009), clade B (JRCSF), and clade C (93IN905), show a predominantly oligomannose glycan composition (62–79%) $\text{Man}_{5-9}\text{GlcNAc}_2$ with a predominant population of

Man₅GlcNAc₂. These oligomannoses bind to Con A with equilibrium dissociation constant (K_D) values ranging from 0.05 μ M to 1.5 μ M.²⁹⁵ Binding of Con A to HIV gp120 glycans either prevent HIV virus binding to receptors on target cells membrane or affect key conformational changes of HIV gp120 following binding.⁸⁵ Our group recently published Con A binding affinities to glycogen from Oyster (0.25 μ M) and mannan from *Saccharomyces cerevisiae* (2.89 μ M).¹⁶⁴

In the present study, we intend to engineer an HIV-1 gp120 responsive, Con A cross-linked polysaccharide, drug delivery system to deliver a pre-encapsulated microbicide. In the long term, we envisage this drug delivery system to address some of the deficiencies shown by previous approaches in HIV prevention including undesired drug release, retention and effectiveness.

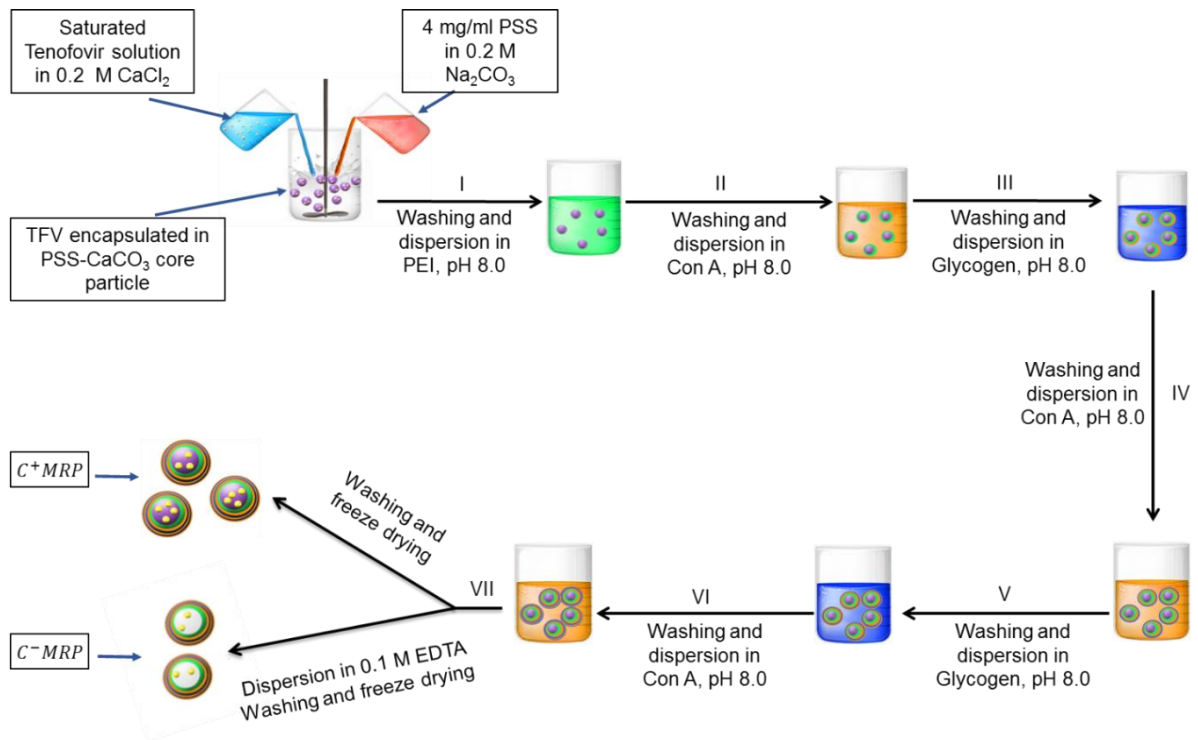
5.2 Materials and methods

Reagents. The following reagents were purchased from Sigma-Aldrich (St. Louis, MO, USA); Concanavalin A (Con A) from *Canavalia ensiformis* (Jack bean) type VI, glycogen from Oyster, polyethylenimine (PEI) 50 wt. % solution in water, poly(sodium 4-styrenesulfonate) (PSS) average Mw ~70.000 powder, calcium chloride dehydrate ($\text{CaCl}_2 \cdot 2\text{H}_2\text{O}$, ACS reagent, $\geq 99\%$), sodium carbonate anhydrous ($\geq 99\%$), fluorescein isothiocyanate labeled Concanavalin A (FITC-Con A) type IV lyophilized powder, tetramethylrhodamine isothiocyanate–Dextran (TRITC-Dextran), manganese (II) chloride tetrahydrate ($\text{MnCl}_2 \cdot 4\text{H}_2\text{O}$, Reagent Plus, $\geq 99\%$), methyl α -D-mannopyranoside (Man) ($\geq 99\%$), Tris Buffer Saline (TBS) pH 8.0, resazurin sodium salt, neutral red (NR), sodium nitroprusside dehydrate (SNP), Dulbecco's Phosphate-Buffered Saline (DPBS), acetic acid,

ethyl alcohol (ethanol) pure 200 proof ACS reagent ($\geq 99.5\%$), Triton™ X-100 and lipopolysaccharides (LPS). Fluorescein Isothiocyanate Isomer I (FITC) 90% pure ACROS Organics™, Dulbecco's Modified Eagle Medium (DMEM) and keratinocyte serum-free medium (1X) (K-SFM) were purchased from Thermo Fisher Scientific (Waltham, MA, USA). 3-(4,5-dimethylthiazol-2-yl)-5-(3-carboxymethoxyphenyl)-2-(4-sulfophenyl)-2H-tetrazolium inner salt (MTS) was purchased from Promega Corporation (Madison, WI, USA). Human Immunodeficiency Virus type 1 recombinant envelope glycoprotein (HIV-1 gp120) was purchased from Sino Biological Inc. (Beijing, China). Tenofovir (TFV) (99%) was purchased from Zhongshuo Pharmaceutical Co. Ltd. (Beijing, China).

Layer-by-layer preparation. The potential for layer-by-layer engineered particles to deliver therapeutics has previously been investigated.²⁹⁶⁻²⁹⁹ In the present study, HIV-1 gp120 and mannose responsive particles (MRP) were prepared via the layer-by-layer coating of a core template with the mannose specific lectin (Con A) and a polysaccharide cross-linker (Glycogen).^{300, 301} The core particle [calcium carbonate (CaCO_3)] was prepared by mixing equal volume (15 ml) of 0.2 M CaCl_2 and 0.2 M sodium carbonate (Na_2CO_3) in the presence of a dispersant (PSS), and under vigorous stirring at 13,500 rpm for two (2) minutes with the IKA Ultra-Turax model T25 homogenizer (Wilmington, NC, USA). A preliminary screening had led to the selection of PSS as the optimal dispersant at a concentration of 4 mg/ml (data not shown). TFV was encapsulated into the core particle by dissolving the microbicide in CaCl_2 (3 mg/ml) prior to the addition of Na_2CO_3 /PSS solution. Core particles prepared in the presence of PSS depicted a negative charge and were subsequently dispersed in a positively charged layer initiator solution (4 mg/ml PEI in 0.5 M NaCl, pH 8.0) for at least 30 minutes. This

allowed the negatively charged lectin (1 mg/ml Con A in TBS, pH 8.0) to adhere to the previous molecular assembly after 1 h exposure time. After a washing step in deionized water (DI water) and centrifugation at 1000 rpm, Con A coated particles were redispersed in glycogen solution (1 mg/ml in TBS, pH 8.0), for 1 h, to allow the addition of the first polysaccharide layer. After a washing step, glycogen coated particles were further dispersed in Con A solution, and the process was repeated until a desired number of layer was attained. After each layer addition, average particles size and ζ -potential were measured by Dynamic Light Scattering (DLS), as explained below. In order to visualize MRP by confocal microscopy, FITC-Con A was used for the first lectin layer addition and TRITC-Dextran for the last polysaccharide layer. After this initial preparation phase, part of the layer-by-layer assembled MRP are dispersed in 0.1 M EDTA solution under gentle stirring to dissolve the CaCO_3 core. Core dissolved MRP (C^- MRP) are then washed twice with DI water to remove



Scheme 5-1: Illustration of MRP's layer-by-layer preparation.

residual EDTA and are then freeze dried for twelve (12) hours (Labconco FreeZone 1 Liter Benchtop Freeze Dry System, Kansas City, MO). Scheme 1 summarizes the layer-by-layer preparation procedure for core containing MRP (C^+MRP) and core dissolved MRP (C^-MRP). A regular increase in average particle size after each layer addition and the change in ζ -potential were critical parameters to ensure a successful preparation. After preparation, MRP was freeze-dried for 12 h (Labconco FreeZone 1 Liter Benchtop Freeze Dry System, Kansas City, MO) and stored at 4 °C.

Average particle size and zeta potential determination. MRP' [both (C^+MRP) and (C^-MRP)] particle size and zeta potential (ζ -potential) measurements were conducted on Malvern instrument 3600 Zetasizer Nano (Worcestershire, UK). Briefly, 1 ml of sample suspension, in distilled water, was prepared in the measurement cuvette and sonicated by bath sonication (Qsonica LLC, Newtown, CT, USA). The cuvette was then placed in the cell area and experiments were performed at 25 °C on the Zetasizer. Data acquisition and analysis were conducted using Zetasizer software (version 6.01, Worcestershire, UK).

Encapsulation and loading efficiency determination. TFV percent encapsulation efficiency (%EE) and loading efficiency (%LD) in MRP were estimated by liquid state and solid state phosphorus (^{31}P) nuclear magnetic resonance (NMR), respectively. Previous reports by our group have established 1H NMR and ^{31}P NMR methods for TFV quantification.^{302, 303}

^{31}P solution state NMR: TFV %EE was measured by quantifying the free drug amount in the supernatant by ^{31}P solution state NMR. Equation 5-1 was then used to compute %EE.

$$\%EE = \frac{\text{Total amount of TFV-Free TFV}}{\text{Total amount of TFV}} \times 100 \quad (5-1)$$

³¹P solution state NMR experiment was carried out on a Varian (Palo Alto, California) 400 MHz spectrometer with a Varian two channel probe and operated by Vnmrj 2.2. Typically, spectra were acquired with a 45° pulse length of 5.05 μs. The relaxation delay and the number of scans were 5 and 256 seconds, respectively. The spin-lattice relaxation time (T1) of the target phosphorus in TFV was 5 s and typically required up to 25 s (5 × T1) for relaxation. Shimming was applied to every sample to obtain a similar linewidth in each spectrum. Baseline correction, phase adjustment, and integral calculations were carried out using MestReNova Lite 5.2.5-4731 software (Escondido, CA, USA) and Matlab 6.1 (Natick, MA, USA), and all experimental measurements were conducted at 37°C. To determine TFV amount in the supernatant, a standard curve was performed across a concentration range of 0-500 μg/ml in DI water. Equation 5-2 describing the calibration curve was Y = 9675.2 X - 29.677 and the coefficient of determination R² = 0.9999, indicative of a strong correlation between ³¹P solid state NMR peak area (Y) and TFV concentration (X).

³¹P solid state NMR: After freeze drying, TFV %LD was determined by comparing MRP' ³¹P solid state NMR peak area to a pure TFV standard of the same mass. Thus, solid state NMR spectra for 30 mg of MRP and pure TFV samples were taken at room temperature in triplicates, and signals were represented as chemical shift value δ: ppm. Equation 5-3 was used to compute %LD.

$$\%LD = \frac{{}^{31}\text{P NMR peak area for 30 mg MRP}}{{}^{31}\text{P NMR peak area for 30 mg TFV standard}} \times 100 \quad (5-3)$$

Practically, ³¹P-P90 Solid-State Magic Angle Spinning (MAS SS) NMR spectra was acquired on a Tecmag Apollo console (Houston, TX, USA) operated by NTNMR software package (v.2.4.29, Houston, TX, USA) with 8.45 T magnet and a 3 mm, homebuilt, 2-channel,

wide-bore NMR probes. The ^1H and ^{31}P Larmor frequencies were 357.2 MHz and 144.596 MHz, respectively. The MAS spinning frequency and 45° pulse length were 8 KHz and 2 μs , respectively.

Fourier transform infrared spectroscopy. IR spectroscopy was conducted following a published method.¹⁶⁴ Briefly, Agilent Cary 630 Fourier transform infrared spectroscopy (FTIR) instrument (Newark, DE, USA), equipped with a diamond crystal with a single reflection and a nominal angle of 45° , was used in the Attenuated Total Reflectance (ATR) mode for IR spectra acquisition. A resolution of 4 cm^{-1} , a sample scan of 32/s and an effective pathlength of 1.1 μm were selected as parameters. IR spectra were acquired between 4000 and 400 cm^{-1} . For better spectral resolution, all samples were allowed to make intimate contact with the ATR diamond crystal surface by pressing them with a built-in pressure clamp. FTIR spectra were collected and analyzed with MicroLab PC and MicroLab Lite softwares (versions 4.0, Newark, DE, USA), respectively.

Morphological analysis of MRP. To confirm the inclusion of both the lectin and polysaccharide in the self-assembly, C^+MRP (3 Con A layers formulation/3L) prepared using FITC-Con A and TRITC-Dextran was imaged by confocal microscopy. Briefly, few drops of the fluorescently labeled MRP solution were placed on a microscope glass slide ($25\times 75\times 1.0\text{ mm}$) and sealed with a nail varnish after covering with a coverslip. Z-stack imaging was then performed on Leica TCS SP5 II confocal microscope (Mannheim, Germany) at 100X magnification. LAS-AF lite software (version 3.x, Buffalo Grove, IL) was used for data

collection and analysis. Furthermore, MRP (3L) was visualized by transmission electron microscopy (TEM) and scanning electron microscopy (SEM).³⁰³

***L. crispatus* viability assay.** *L. crispatus* viability assay was performed following a published method.³⁰⁴ Although vaginal microbiota is composed of different species, *Lactobacillus* are the dominant bacterial species in majority of women (73% of bacterial community).³⁰⁵ Briefly, *L. crispatus* was grown overnight at 37 °C in broth culture media. The density was adjusted to an OD670 value of 0.06, corresponding to 0.5 McFarland Standard or 108 CFU/ml.³⁰⁶ Then, hundred microliters (100 µl) of the adjusted *L. crispatus* culture were placed in 96-well plates before addition of MRP (3L) suspension. *C*⁺MRP and *C*⁻MRP concentrations ranging from 1 to 1000 µg/ml were prepared by successive log₁₀ dilutions of the working standard solution in broth culture media, and homogenized before addition to *L. crispatus*. Broth media and 1% Triton X-100 were used as negative (untreated) and positive controls, respectively. Plates were initially incubated at 37 °C for 24 h before addition of 20 µl of MTS reagent to each well and further incubated at 37 °C for 4 h. This allowed the reduction of MTS compound by viable *L. crispatus* into the colorful formazan product. Bacterial viability was determined by measuring the absorbance at a wavelength of 490 nm on a microplate reader (Beckman Coulter DTX 880 Multimode Detector, Fullerton, CA, USA). Percent viability was calculated using equation 5-4.

$$Viability (\%) = \frac{ABS_{Test} - ABS_{Background}}{ABS_{Negative\ control} - ABS_{background}} \times 100 \quad (5-4)$$

All experiments were conducted in triplicates and cytotoxicity results were rated according to ISO-standard 10993-5 as non-cytotoxic (cell viability higher than 75%), slightly cytotoxic (cell

viability ranging from 50% to 75%), moderately cytotoxic (cell viability ranging from 25% to 50%), and severely cytotoxic (cell viability lower than 25%).^{307, 308}

Cell culture conditions. Human vaginal keratinocytes cell line (VK2/E6E7, ATCC Number CRL-2616) was obtained from the American Type Culture Collection (Manassas, VA, USA). VK2/E6E7 cell line was used as model epithelial cell types of the female reproductive tract with relevance for vaginal drug delivery and topical microbicide development. Its differentiation pattern and immune responses closely resemble those of the normal tissues of origin.³⁰⁹ Cells were cultured in antibiotic-free K-SFM supplemented with 0.1 ng/ml of EGF human recombinant, 0.05 mg/ml of bovine pituitary extract and 0.4 mM CaCl₂. Culture medium was replaced every 2–3 days. Before confluence, cultures were washed with DPBS and subsequently detached by enzymatic treatment with 0.25% trypsin/EDTA solution for 3-5 minutes at 37 °C. After trypsin inhibition by soybean inhibitor at a molar ratio of 1:1, cells were washed, and seeded in new flasks or 96-well plates. All experiments were performed on cells in the logarithmic growth phase. Murine macrophage [RAW 264.7 (TIB-71)] cell line was purchased from the American Type Culture Collection (Manassas, VA) and cultured in antibiotic-free DMEM media supplemented with 10% heat-inactivated fetal bovine serum (FBS). All incubations were performed in the same conditions (37 °C in a humidified atmosphere of 5% carbon dioxide (CO₂), 95% air) throughout the experimental studies unless otherwise specified.

Experimental procedure for cell exposure to MRP.

VK2/E6E7 cells. C^+MRP and C^-MRP suspensions were prepared in concentrations ranging from 1 to 1000 $\mu\text{g/ml}$ by successive \log_{10} dilutions of a working standard (1000 $\mu\text{g/ml}$) in K-SFM medium. Suspensions were homogenized by vortexing immediately before exposure to VK2 cells. Cells (100 μl per well, 2.0×10^5 cells/ml) were seeded into 96-well flat-bottomed plates (TPP, Switzerland; growth surface: 0.32 cm^2 per well; Thermo Fisher Scientific (Waltham, MA, USA)) and incubated as explained above, for 48 h. Culture medium was subsequently substituted with 100 μl of fresh culture medium containing increasing MRP concentrations (1 to 1000 $\mu\text{g/ml}$), and cells were further incubated for 24 h. Complete culture medium was used as negative controls while various positive controls of 1% Triton X-100 and 1 mg/ml SNP were used as benchmarks against MRP.

RAW 264.7 cells. C^+MRP and C^-MRP working standard suspensions were freshly prepared in DMEM with 5% FBS at 1000 $\mu\text{g/ml}$, and a range of concentrations from 1 to 1000 $\mu\text{g/ml}$ was prepared. Cells (100 μl per well, 2.0×10^6 cells/ml) were seeded into 96-well flat-bottomed plates and incubated, as explained above. Cells were subsequently exposed to 100 μl of fresh medium containing increasing C^+MRP and C^-MRP concentrations (1 to 1000 $\mu\text{g/ml}$) and incubated for 24 h. Culture medium and LPS (10 $\mu\text{g/ml}$), were used as negative and positive controls, respectively.

Assessment of cell membrane integrity. Dose-response effect of C^+MRP and C^-MRP on plasma membrane integrity was assessed using the uptake and specific accumulation of the vital dye neutral red (NR) in lysosomes.^{310, 311} NR is a weak cationic dye that penetrates viable cells membrane and accumulates intracellularly in lysosomes where it binds with anionic sites of the lysosomal matrix.³¹² Cell membrane alterations are generally

irreversible and result in the loss of the NR from the lysosome.³¹³ After exposure to C^+MRP and C^-MRP , cells were washed twice with DPBS and supplemented with fresh culture medium (100 μ l) containing 50 μ g/ml NR. Assay plates were incubated for 3 h to allow viable cells to accumulate NR in their lysosomes. After the incubation time, cells were further washed twice with DPBS followed by membrane disruption with an aqueous solution of 1% acetic acid/50% ethanol (100 μ l/well). Fluorescence intensity (FI) measurement (530-560 nm excitation, 590 nm emission) was performed on Cary Eclipse Fluorescence Spectrophotometer and membrane integrity was determined using equation 5-5. Membrane integrity result was analyzed following ISO-standard 10993-5.

$$Membrane\ Integrity\ (\%) = \frac{FI_{Test} - FI_{Background}}{FI_{Negative\ Control} - FI_{Background}} \times 100 \quad (5-5)$$

Assessment of mitochondrial metabolism. Resazurin assay is based on the ability of viable, metabolically active cells to convert the redox dye resazurin from the oxidized (non-fluorescent) dark blue form to the reduced (highly fluorescent) pink form, resorufin.³¹⁴ This conversion occurs intracellularly by a pool of oxidoreductase or diaphorase-type enzyme derived from mitochondria by accepting electrons from nicotinamide adenine dinucleotide phosphate (NADPH), flavin adenine dinucleotide (FADH), flavin mononucleotide (FMNH), nicotinamide adenine dinucleotide (NADH), as well as from numerous cytochromes.³¹⁵ After exposure to C^+MRP and C^-MRP , cells were washed twice with DPBS and supplemented with fresh culture medium (100 μ l). Ten (10) microliters of resazurin working solution (0.1 mg/ml, DPBS) was added directly to each well and plates were incubated for 3h to allow viable cells to convert resazurin into resorufin. Then, fluorescence intensity (FI) measurement (530-560 nm excitation, 590 nm emission) was performed on Cary Eclipse Fluorescence

Spectrophotometer, and cell viability was calculated using equation 5-6. Mitochondrial metabolism result was analyzed following ISO-standard 10993-5.

$$\text{Mitochondrial metabolism (\%)} = \frac{FI_{\text{Test}} - FI_{\text{Background}}}{FI_{\text{Negative Control}} - FI_{\text{Background}}} \times 100 \quad (5-6)$$

Determination of nitric oxide production. Nitric oxide (NO) production in culture supernatant, a measure of inducible NO Synthase (iNOS) activity, was assessed by measuring nitrite accumulation, the stable end product of the autoxidation of NO in aqueous solution.³¹⁶ After cells were incubated with different concentrations of C^+MRP and C^-MRP , for 24 h at 37 °C; supernatants were collected, centrifuged (1000 rpm) and NO content was determined using Griess reagent system kit (Promega Corp., Madison, WI, USA). Briefly, 50 μ l of supernatant was placed in a new 96 well plate and mixed with Griess reagents according to the manufacturer.³¹⁷ Absorbance was measured at 540 nm on DTX 880 microplate reader. NO concentration was calculated using the sodium nitrite standard curve, according to the manufacturer. Equation 5-7, describing the calibration curve, was $Y = 0.0045 X$, where Y and X represent the absorbance value and NO concentration (μ M), respectively. The coefficient of determination was $R^2 = 0.9991$, suggesting a good correlation between absorbance value and NO content. As positive controls, the generation of NO was achieved for RAW 264.7 with LPS and 1 mg/mL SNP for VK2/E6E7 cells.³¹⁸

Multiplex immunoassay analysis of cytokines secretion. After macrophages RAW 264.7 exposure to C^+MRP and C^-MRP , cell free supernatants were harvested and analyzed for various cytokines susceptible to enhance HIV infectivity. The cytokines level were assayed using a high-sensitivity multiplexed bead-based immunoassay (Milliplex MAP Mouse

Cytokine/Chemokine Magnetic Bead Panel, Millipore Corp., Billerica, MA; and Luminex MAGPIX instrument, Luminex Corp., Austin, TX, USA). Supernatants from untreated cells (negative control) and LPS-treated cells (positive control) were also evaluated. Seven cytokines including IL-1 α , IL-1 β , IL-6, IP10, MKC, TNF- α and IL-7 were measured according to the manufacturer's procedure.³¹⁹ Pre-mixed magnetic beads conjugated to antibodies for all 7 analytes were mixed with equal volumes of supernatants (25 μ l) in 96-well plates. Plates were protected from light and incubated on a microplate shaker overnight at 4 °C. Then, magnetic beads were washed twice with 200 μ l of washing buffer. The detection antibodies were added to each well and the mixtures incubated at room temperature for 1 h. Streptavidin-phycoerythrin conjugate compound was added to each well, and the mixtures were incubated for an additional 30 min at room temperature. The magnetic beads were subsequently washed and resuspended in the washing buffer for 5 min. Plates were then assayed on the Magpix system with Luminex xPONENT software (version 4.2, Austin, TX). Median fluorescence intensities were analyzed using a 5-parameter logistic method from a standard curve of respective analytes to determine cytokines concentration in the supernatants. All assays were conducted in duplicate.

Drug release conditions and kinetics. Based on initial cytotoxicity indicators for both C^-MRP and C^+MRP (see results and discussion section), drug release experiments were conducted only for C^+MRP . Thus, TFV release from several C^+MRP formulations (1L, 2L and 3L corresponding to 1, 2 and 3 Con A layers in formulation) was performed in the presence of Man and HIV-1 rgp120. TFV level was quantified using a previously published LC/MS/MS method.³²⁰ TFV was detected with electrospray ionization (ESI)-MS/MS in the positive ion

mode using 288/176.2 m/z transition. The mobile phase consisted of 30% H₂O (0.1 % FA)/70% Acetonitrile (0.1% FA). Flow rate was maintained at 0.3 ml/min, and a calibration curve relating TFV concentration to 176.2 m/z ion peak area was used to determine the concentration of unknowns. Equation 5-8 describing the calibration curve was $Y = 595.6 X$ with $R^2 = 0.9946$. This suggested a strong correlation between 176.2 m/z ion peak (Y) area and TFV concentration (X), in the range of 0-500 µg/ml. The average volume of human vaginal fluid (VFS, pH 4.2) and seminal fluid (SFS, pH 7.6), during intercourse, have previously been reported to be 0.75 ml and 3.4 ml, respectively.³⁰² Therefore, to mimic the intercourse situation, for each time point, 6 mg of MRP was weighed and dispersed in 4.15 ml of SFS:VFS (4.5v:1v) mixture under gentle stirring at room temperature. Vaginal and seminal fluids simulant were prepared following the method of Owen et al.^{321, 322} The release media was then filtered on a 0.2 µm whatman syringe filter before any MS spectral acquisition. In the current study, HIV-1 rgp120 was tested at *in vitro* concentrations ranging from 25 µg/ml to 1000 µg/ml, which is consistent with other reported studies [1 pM to 1 µM (0.12 ng/ml to 120 µg/ml)].³²³ The model-independent method was used to determine whether TFV release profile was similar or different from the control condition (SFS:VFS; taken as reference). Thus, to assess the significance level in the drug release profiles, a pair-wise comparison of the release profiles was conducted using the US FDA similarity factor (f_2) and dissimilarity factor (f_1).³²⁴ f_1 measures the percent error while f_2 measures the sum-squared error between a test and reference compound's overall time points.

$$f_1 = \left(\frac{[\sum_{j=1}^n |R_j - T_j|]}{[\sum_{j=1}^n R_j]} \right) \times 100 \quad (5-9)$$

$$f_2 = 50 \times \log \left\{ \left[1 + \left(\frac{1}{n} \right) \sum_{j=1}^n |R_j - T_j|^2 \right]^{-0.5} \times 100 \right\} \quad (5-10)$$

In equations 5-9 and 5-10, n is the sampling number, R and T are the percent dissolved of the reference and test products, respectively at each time j. Furthermore, to elucidate the drug release mechanism, zero order, first order, Higuchi, Hixson–Crowell and Hopfenberg kinetic models, given by equation 5-11, 5-12, 5-13, 5-14 and 5-15, respectively, were applied to the release profiles.

$$Q_t = Q_0 + K_0t \quad (5-11)$$

$$\log Q_t = \log Q_0 + \frac{K_1t}{2.303} \quad (5-12)$$

$$Q_t = K_H t^{\frac{1}{2}} \quad (5-13)$$

$$(1 - f_t)^{1/3} = 1 - K_\beta t \quad (5-14)$$

$$f_t = 1 - [1 - K_2 t^x] \quad (5-15)$$

In the above equations, Q_t is the amount of drug dissolved in time t, Q_0 represents the initial amount of drug in solution (usually, $Q_0 = 0$) and K_0 is the zero order release constant. K_1 is the first order release constant. K_H is the Higuchi dissolution constant and f_t represents the fraction of drug dissolved in time t. K_β represents the Hixson–Crowell release constant and K_2 , indicative of the erosion rate, is the Hopfenberg release constant. The parameter x, describing the drug particle shape, is 1, 2, or 3 for slab, cylinder and spheres, respectively. In the present study, the Hopfenberg's drug particle shape parameter was $x = 3$.

Bioadhesion test. C^+ MRP mucoadhesion was tested *ex vivo*, on porcine vaginal tissue, following the immersion method, according to previously published reports.^{325, 326} Briefly, fluorescently labeled MRP (1L, 2L and 3L) were prepared using FITC-Con A, as explained above. Fresh porcine tissue was obtained from the local abattoir (Fairview Farm Meat Co., Topeka, KS, USA), within 2 h of the animal death. The tissue was washed with normal saline,

frozen in liquid nitrogen, and kept at $-80\text{ }^{\circ}\text{C}$. Frozen porcine tissue were thawed at $4\text{ }^{\circ}\text{C}$ and cut into pieces of $8\text{ cm}/1\text{ cm}$ (L/W) for mucoadhesion assessment. Cyanoacrylate glue (water resistant and safe to porcine tissue) was used to stick sample tissues onto microscope slides, with luminal side facing up. The tissue slides were further immersed into tubes containing FITC labeled C^+MRP (10 mg/ml) in 10 ml of VFS. A control experiment was conducted with FITC alone. The tubes were kept in a shaking water bath ($37\text{ }^{\circ}\text{C}$) at 100 rpm , and removed for analysis of the remaining fluorescence in the VFS at 4 h and 24 h . The difference in VFS fluorescence, before and after treatment, was analyzed on Cary Eclipse Fluorescence Spectrophotometer ($\lambda_{\text{ex}}\ 490\text{ nm}/\lambda_{\text{em}}\ 520\text{ nm}$) operated by Cary Eclipse advance reads application (Version 1.1 (132), Santa Clara, CA, USA). Tissue images were also acquired on Nikon Labophot-2 microscope (Nikon Instruments, Inc., Melville, NY, USA) equipped with PAXCam digital microscope camera and PAX-it! image management and analysis software (version 7.9, Midwest Information Systems, Inc., Villa Park, IL, USA). The percent mucoadhesion was determined using equation 5-16, where F_i and F represent VFS initial and final fluorescence, respectively.³²⁶

$$\text{Mucoadhesion (\%)} = \frac{(F_i - F)}{F_i} \times 100 \quad (5-16)$$

5.3 Results and discussion

Layer-by-layer preparation of MRP.

Figure 5-1 summarizes size and ζ -potential measurement for MRP and CaCO_3 -PSS core particle. The average size (diameter) of CaCO_3 -PSS core particles was $259.1 \pm 1.87\text{ nm}$ ($n=3$) with a polydispersity index (PDI) of 0.250 (figure 5-1A). The ζ -potential of freshly

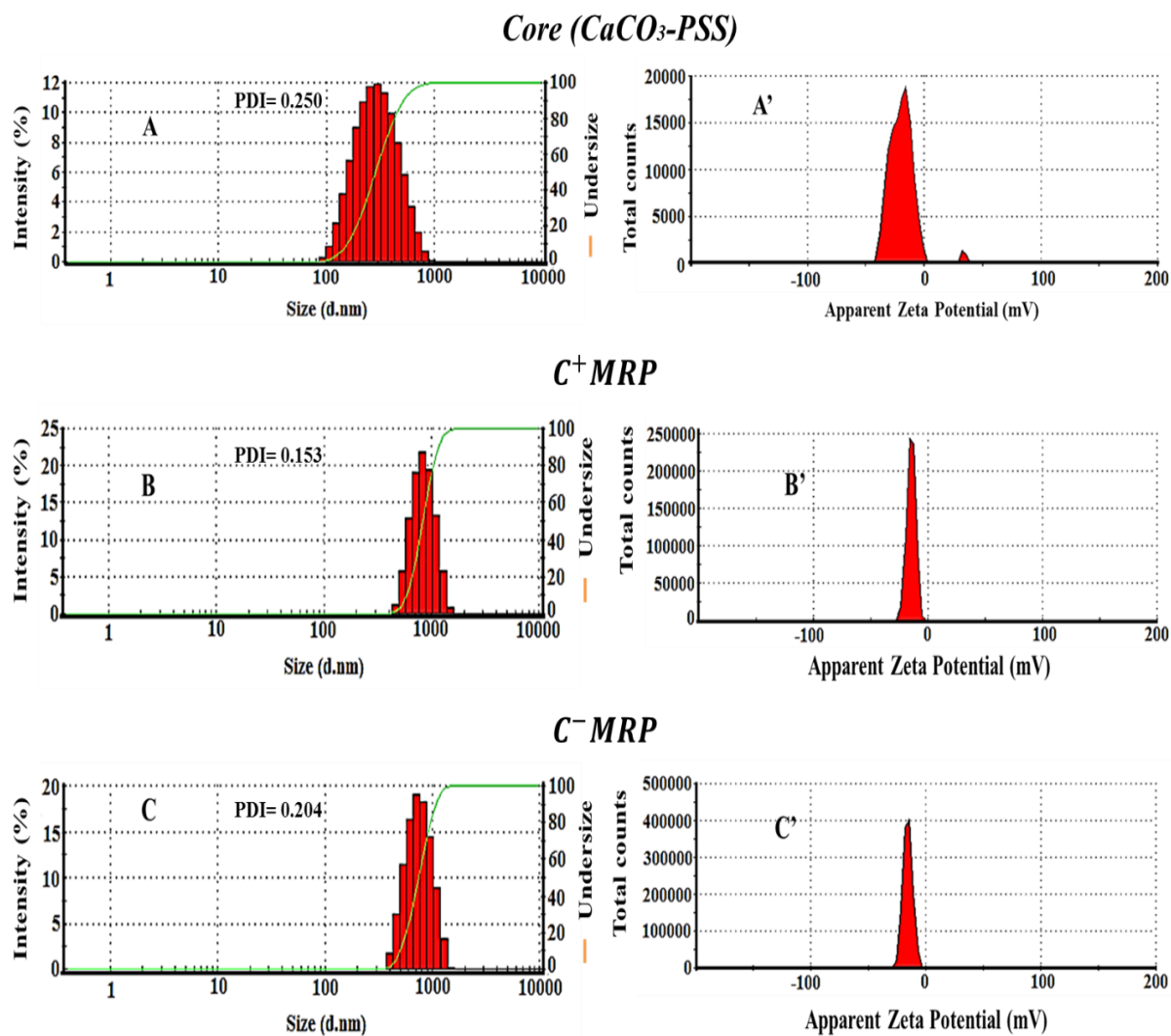


Figure 5-1: Average particle size and cumulative size distribution for CaCO₃-PSS (A), C⁺MRP (B) and C⁻MRP (C), and their respective ζ -potential measurements (A', B' and C').

prepared CaCO₃-PSS particles was -26.9 ± 2.14 mV ($n=3$) (figure 5-1A'), partly due to the negatively charged PSS present onto the particles surface. C⁺MRP average size and ζ -potential were 1130 ± 15.72 nm [PDI = 0.153] and -15.1 ± 0.55 mV, ($n=3$). Similarly, C⁻MRP average size and ζ -potential were 1089 ± 23.33 nm ($n=3$) and -14.2 ± 0.25 mV ($n=3$) (Fig.1-C'). The

shrinking from C^+MRP to C^-MRP could be due to a rearrangement of the layers upon removal of the supporting inner core. Similar observations have been reported by Gao et al.³²⁷

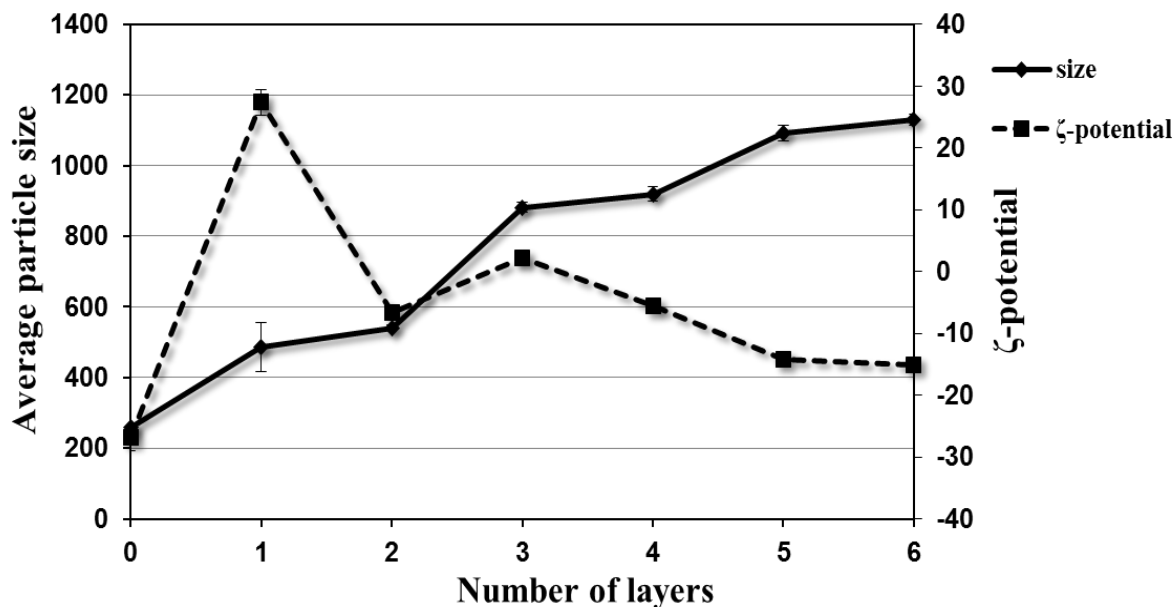


Figure 5-2: Average size and ζ -potential fluctuation during C^+MRP layer-by-layer preparation.

Figure 5-2 summarizes the overall average size and zeta potential variations during the layer-by-layer preparation of C^+MRP . After addition of the positively charged PEI layer (layer 1) onto the negatively charged $CaCO_3$ -PSS, the average size increased from 259.1 ± 1.87 nm to 486.3 ± 70.18 nm [PDI = 0.314] and the ζ -potential switched from -26.9 ± 2.14 mV to $+27.4 \pm 2.08$ mV. This suggested the success of PEI layer adsorption onto the particles surface, through electrostatic attractions between the negatively charged core and the positively charged PEI. The addition of Con A layer (layer 2) brought the average particle size to 540.8 ± 6.62 nm [PDI = 0.261] and the ζ switched back from positive to a negative value (ζ -potential = -6.74 ± 1.11 mV). The first lectin layer successfully adhered to the assembly through

electrostatic interactions between the positively charged PEI and the negatively charged Con A. Both the size increase and the change in ζ -potential were due to the addition of the Con A layer to the molecular assembly. With the adsorption of glycogen layer (layer 3), the average particle size increased by 63% and was 881.7 ± 15.45 nm [PDI = 0.341], while the ζ -potential became $+2.23 \pm 0.3$ mV. The glycogen layer was successfully added through the specific binding between Con A and α -D-glucose moieties in glycogen²⁵⁸. The addition of the next, Con A layer (layer 4) increased the average particle size to 918.6 ± 132.6 nm [PDI = 0.284] and the ζ -potential was -5.53 ± 0.73 mV. The second glycogen layer (layer 5) induced an overall 20% increase in average particle size, which was 1091 ± 21.07 nm [PDI = 0.254], and the ζ -potential decreased roughly from -5.53 ± 0.73 mV to -14.3 ± 0.21 mV. The third Con A layer (layer 6) brought the average particle size to 1130 ± 15.72 nm (n=3) [PDI = 0.153] (figure 5-1B) and the ζ -potential to -15.1 ± 0.55 mV (n=3) (figure 5-1B'). Percent increase or decrease in particle size was estimated using equation 5-17.

$$\text{Change in size (\%)} = \frac{\text{Final size} - \text{Initial size}}{\text{Initial size}} \times 100 \quad (5-17)$$

TFV entrapment in MRP. TFV %EE in CaCO₃-PSS core particle was 74.4% and %LD obtained for C^+ MRP (3L) and C^- MRP (3L) were $16.3\% \pm 0.1$ w/w and $6.0\% \pm 0.1$ w/w, respectively. TFV %LD in C^+ MRP was ~ 3 folds higher than C^- MRP. This difference in %LD is probably due to a lost in Tenofovir during core dissolution because of its relatively high water solubility (13.4 mg/mL). Figure 5-3 and 5-4 show the ³¹P solid state NMR spectra (figure 5-3) and a typical supernatant' ³¹P solution state NMR spectrum (figure 5-4). The TFV phosphorus chemical shifts values were 15.7 ppm and 13 ppm for ³¹P solid state NMR and ³¹P

solution state NMR, respectively. TFV encapsulation in CaCO₃-PSS particles was possible due to two major factors. First, after the nucleation phase, leading to the formation of CaCO₃-PSS crystal precursors, the crystal growth phase involved a coprecipitation. Thus, drug molecules can be physically entrapped in CaCO₃-PSS particles during the crystallization process. Coprecipitation has previously been used to successfully load both small molecule and protein drugs in CaCO₃.³²⁸⁻³³⁰ However, coprecipitation alone does not explain the overall TFV entrapment in MRP. In fact, along with aluminum hydroxide [Al(OH)₃], calcium acetate [Ca(C₂H₃O₂)₂], lanthanum carbonate [La₂(CO₃)₃] and magnesium carbonate [MgCO₃];

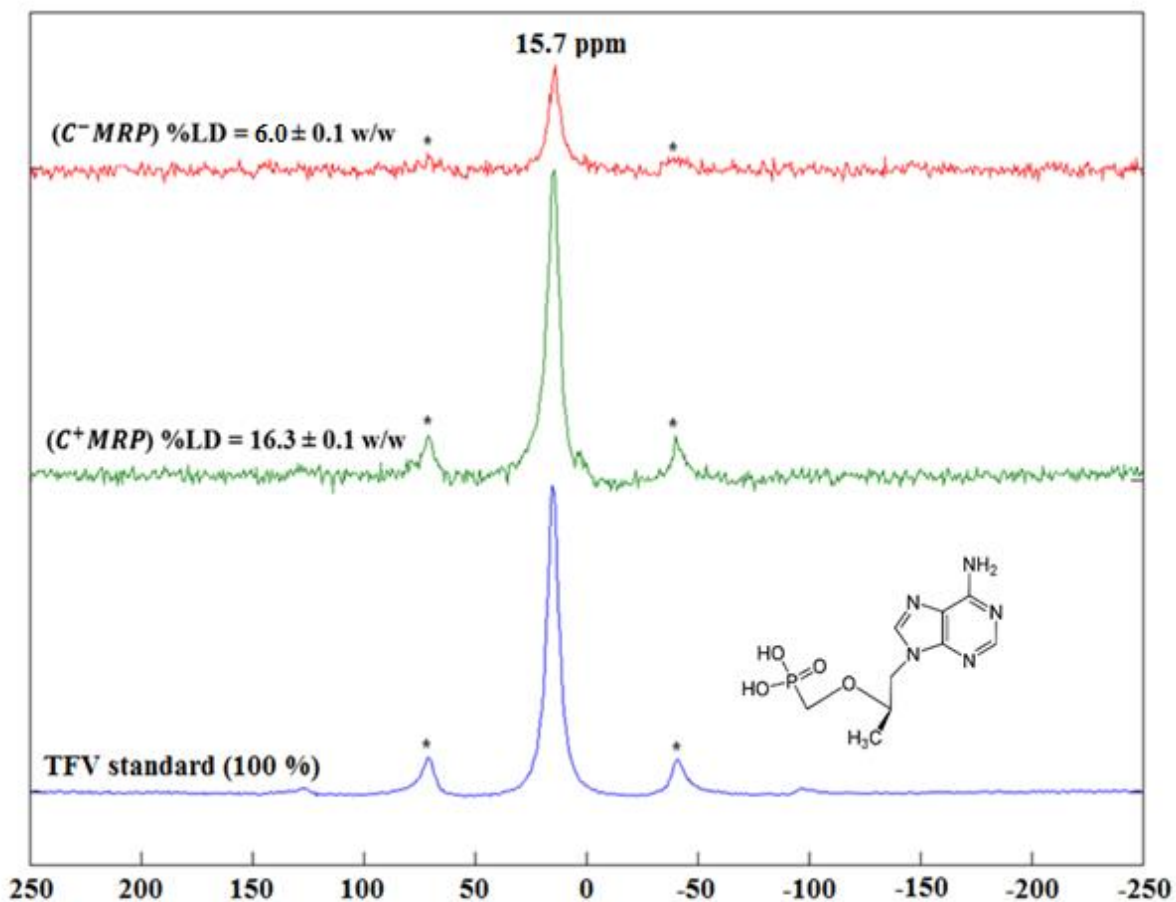


Figure 5-3: ³¹P solid state NMR spectra of TFV standard, C⁺MRP and C⁻MRP.

CaCO₃ is a member of the phosphate binders family.³³¹⁻³³⁴ Phosphate binders form complexes with phosphorus atoms through ionic interactions. In CaCO₃, it is the calcium ion (Ca²⁺) that interacts with the phosphate group. Therefore, it was expected that TFV, which structure contains a phosphate group (figures 5-3 & 5-4), would be entrapped in the core particles. Taking advantage of this principle, Ueno et al. were able to achieve 90% loading of betamethasone phosphate into CaCO₃ nanoparticles.³³⁵

TFV payload in MRP could provide satisfactory drug strength capable of exerting desired therapeutic activity. In fact, it was previously shown that vaginal suppositories' weight vary from 1000-2000 mg.^{336,337} Potential MRP suppositories weighing between 1000-2000 mg

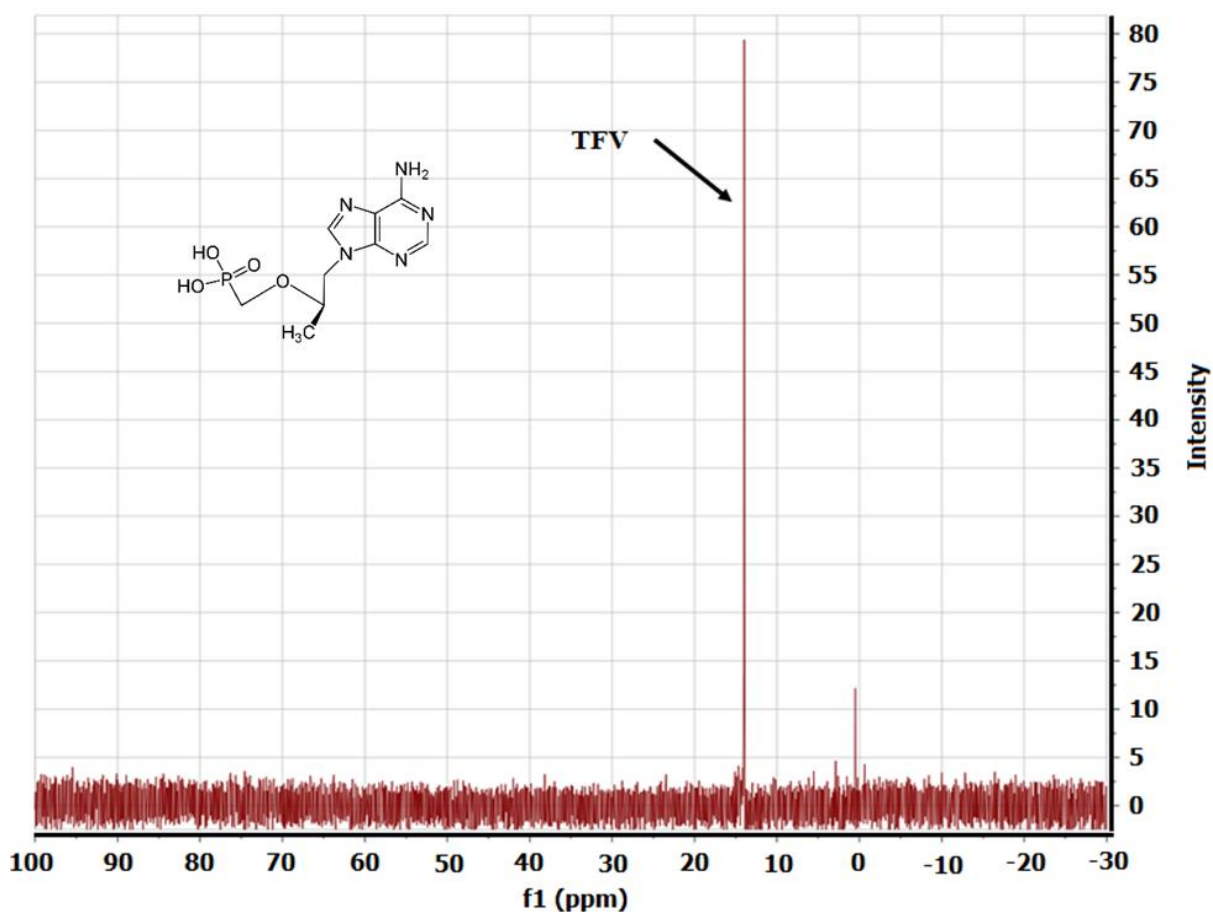


Figure 5-4: TFV 31P solution state NMR spectrum following layer-by-layer encapsulation.

would have TFV strength ranging from 163 – 326 mg, respectively. These TFV strengths are 4 to 8 fold higher than TFV strength tested in both 1% TFV vaginal gel and TFV reservoir intravaginal ring (40 mg).^{338, 339}

FTIR analysis. In order to characterize and confirm the composition of the coating layers, FTIR spectra of C^+MRP , C^-MRP , glycogen, Con A, $CaCO_3$ -PSS core particle and Con A/Glycogen agglutinate were acquired (figure 5-5). Glycogen IR spectrum showed distinctive weak peaks at 1160 cm^{-1} , 1080 cm^{-1} and a strong absorption at 1000 cm^{-1} characteristic of polysaccharides C-O-C, C-O and C-H stretches, respectively.^{340, 341} The bands at 3300 cm^{-1} and 2900 cm^{-1} were due to OH and CH_2 stretches in glycogen, respectively. Con A IR spectrum showed strong bands at 1620 cm^{-1} and 1520 cm^{-1} , attributed to amide I and II, respectively.^{164, 342} Spectrum obtained for $CaCO_3$ -PSS core particle showed a strong peak at 870 cm^{-1} , characteristic of carbonate band in $CaCO_3$.³⁴³ Features at 1400 cm^{-1} - 1480 cm^{-1} were attributed to both $CaCO_3$ and S=O asymmetric stretching vibration mode in $CaCO_3$ -PSS.^{298, 344} C^+MRP spectrum showed a distinctive Con A amide I band at around 1620 cm^{-1} and glycogen C-O-C, C-O and C-H stretches at 1160 cm^{-1} , 1080 cm^{-1} and 1000 cm^{-1} , confirming the presence of both the lectin and the polysaccharide in the layer-by-layer assembly. These features were similar to bands observed in Con A/Glycogen agglutinate spectrum. The bands between 1400 cm^{-1} - 1480 cm^{-1} , as well as the strong absorption at 870 cm^{-1} in C^+MRP IR spectrum further confirmed the presence of $CaCO_3$ -PSS core particle in the assembly. As expected, bands attributed to the carbonate band are not seen in C^-MRP IR spectrum. The band at 1000 cm^{-1} and the amide I stretching band at 1620 cm^{-1} further confirm the presence of Con A/Glycogen agglutinate in C^-MRP assembly.

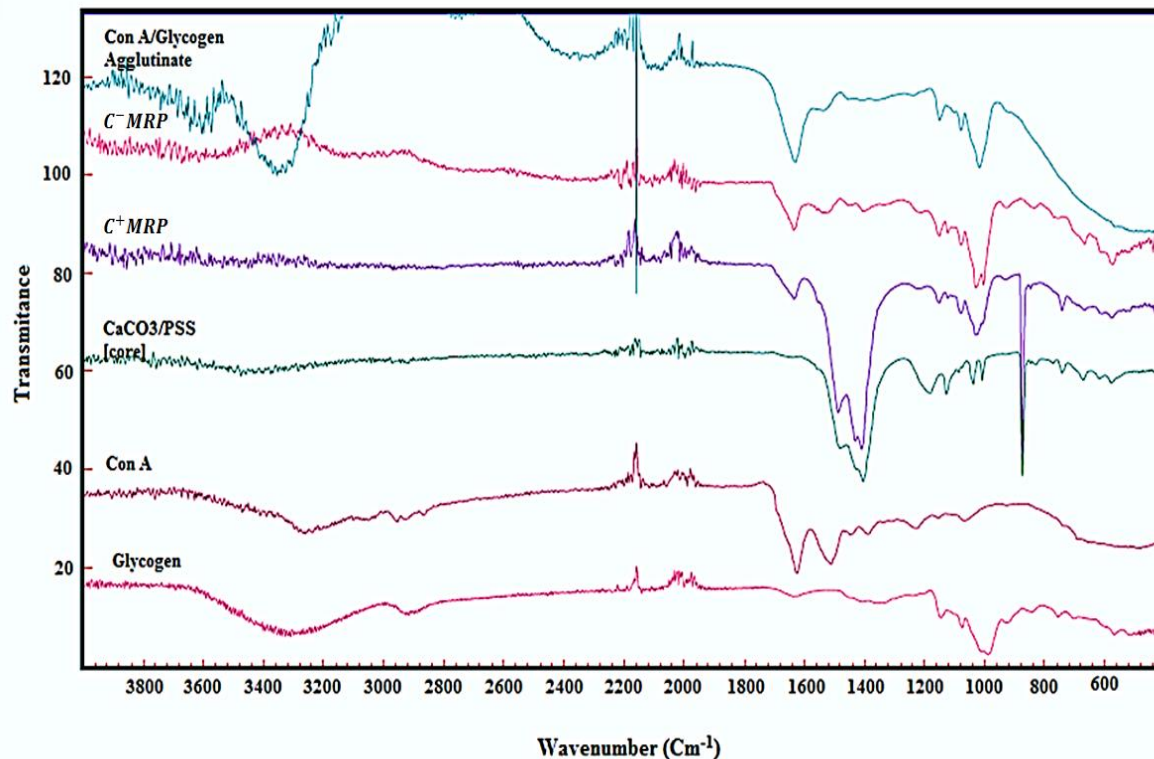


Figure 5-5 : FTIR spectra for C^+MRP , C^-MRP , glycogen, Con A, $CaCO_3$ -PSS core particle and Con A/Glycogen agglutinate.

Morphological analysis. Figure 5-6 shows TEM (A & B) and SEM (A' & B') images of C^+MRP and C^-MRP particles. These images suggested that individual MRP particles exhibit spherical shape with diameter ranging from 800-1100 nm ($n=5$). C^+MRP SEM image (A') showed a distinctive layer covering the core particle and the TEM image (A) showed an optically dense core of $CaCO_3$ -PSS surrounded by less dense layers of Con A/Glycogen agglutinate, confirming C^+MRP core shell structure and the success of the layer-by-layer preparation procedure. For C^-MRP , the SEM image (B') shows particles with a rough surface, probably due to the removal of the supporting $CaCO_3$ -PSS core particles. The absence of the electron dense cores in C^-MRP TEM images (B) suggest the complete or partial removal

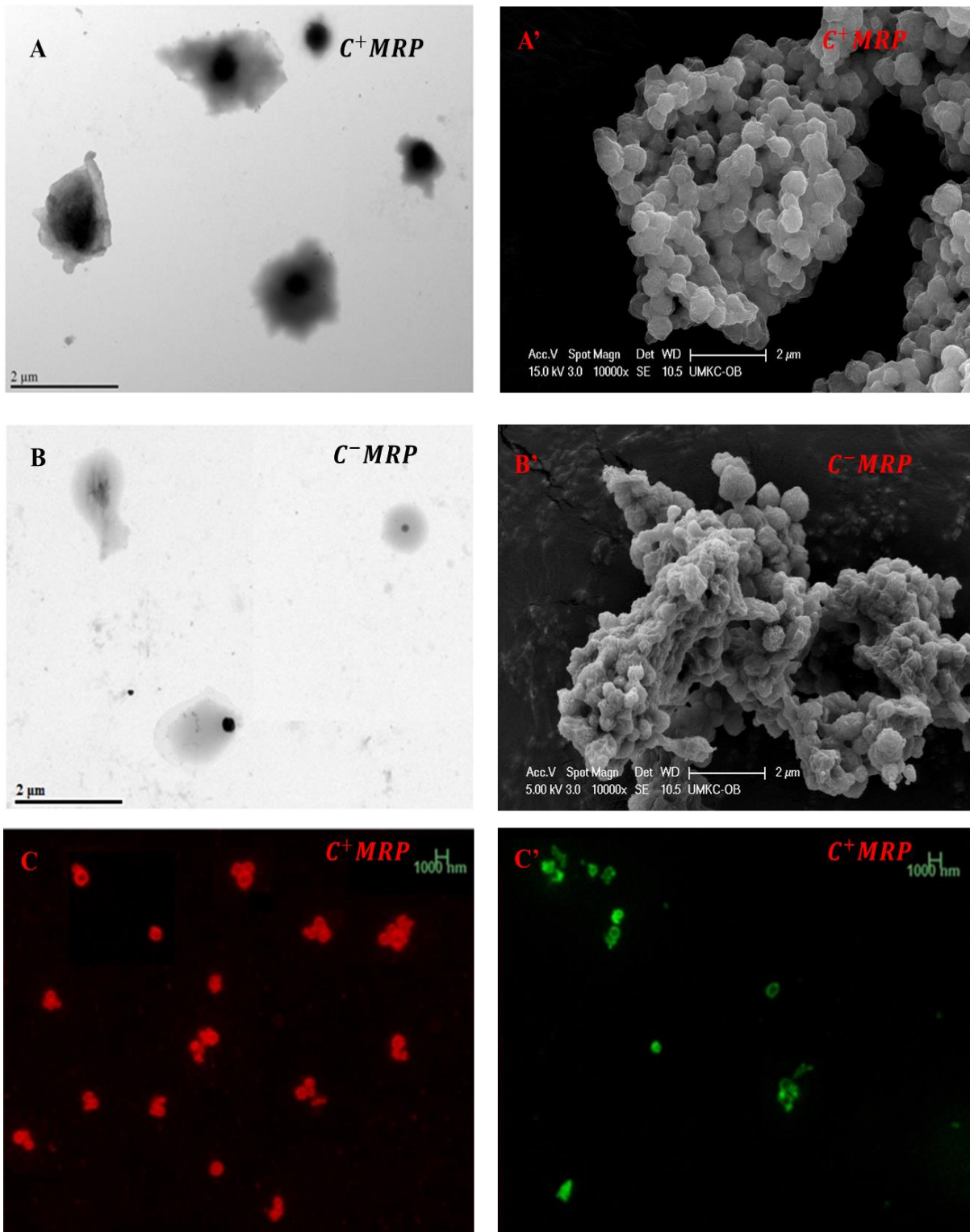


Figure 5-6: TEM (A & B), SEM (A' & B') and confocal microscopy (C & C') images of C^+MRP , C^-MRP . Scale bars are 2 μm for A, A', B, B' and 100 nm for C and C'.

of the CaCO₃-PSS. The difference in optical density was due to a difference in material properties between the core and shell, as previously shown by Dahl et al.³⁴⁵ These morphological descriptions were consistent with the work of Zhu et al.³⁴⁶ When FITC-Con A and TRITC-dextran were used in *C*⁺*MRP* preparation, fluorescent particles were prepared and visualized under a confocal microscope. The presence of both TRITC (red fluorescence C) and FITC (green fluorescence C') in *C*⁺*MRP* layers confirmed the success of Con A and the polysaccharide attachment in the assembly. These fluorescent images further confirmed *C*⁺*MRP* particles size, geometry, and ultrastructure.

***In vitro* cytotoxicity analysis.** The normal vaginal flora represents a critical natural barrier against HIV transmission, by contributing to the vaginal acidic pH and hydrogen peroxide (H₂O₂) production.^{347, 348} *Lactobacillus* is a predominant vaginal floral species that produces H₂O₂.³⁴⁹ To be considered safe for vaginal delivery, microbicide formulations should not disturb the normal vaginal flora, therefore should not be toxic to *Lactobacillus*.³⁰⁶ As summarized in figure 5-7, both *C*⁺*MRP* and *C*⁻*MRP* are non-cytotoxic to *Lactobacillus crispatus* suggesting that both MRPs might be safe for vaginal microbicide delivery. Furthermore, inflammation has been shown to increase HIV transmission because of the increase in the body innate and specific immune response at an inflammation sites^{350, 351}. That is, there is a high recruitment of HIV receptive cells at the inflammation site which increases HIV infectivity. Because it is an important pro-inflammatory mediator^{352, 353}, nitric oxide released upon incubation of vaginal keratinocytes cells (VK2) with MRP is determined. For both *C*⁺*MRP* and *C*⁻*MRP*, no significant nitric oxide release is observed compared to the negative control (culture media) in the concentration range tested, suggesting that no

inflammation of VK2 cells is associated with both MRPs' treatment (figure 5-8C), up to 24h. Figure 5-8 also summarizes the *in vitro* safety profile of C^+MRP and C^-MRP on VK2 cells. It appears that across the concentration range tested, C^+MRP is non-cytotoxic on VK2 cells with a CC_{50} value of 1433 $\mu\text{g/ml}$. Moreover, this formulation did not induce any loss in cell membrane integrity up to 1000 $\mu\text{g/ml}$ in 24h. However, C^-MRP is non-cytotoxic up to 10 $\mu\text{g/ml}$, slightly cytotoxic at 100 $\mu\text{g/ml}$ and severely cytotoxic at 1000 $\mu\text{g/ml}$. The cytotoxicity observed at 1000 $\mu\text{g/ml}$ is consistent with a significant decrease in cell membrane integrity at the same concentrations. The CC_{50} value for C^-MRP on VK2 cells is 200 $\mu\text{g/ml}$.

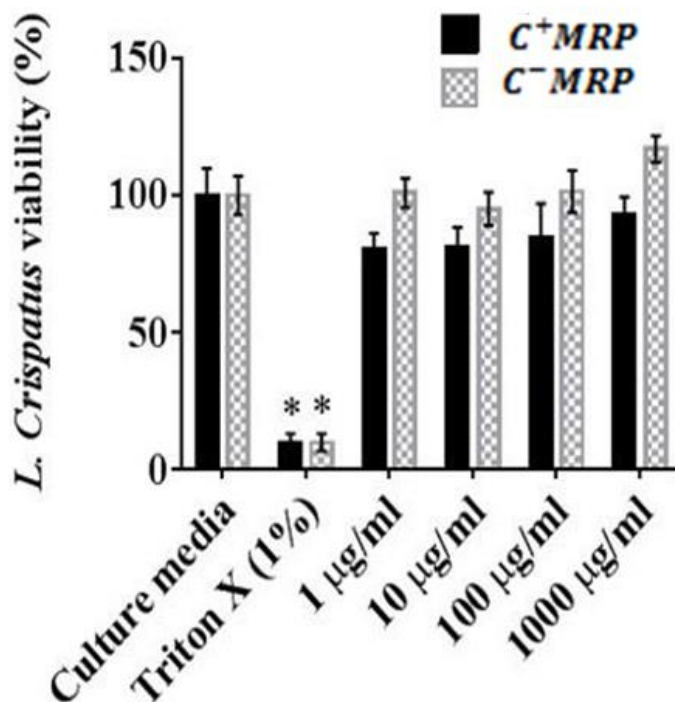


Figure 5-7: *L. crispatus* viability. Percent viability and standard deviations values are computed from quintuplicates (n=5). One-way anova test is performed in GraphPad (version 6.0) to determine statistical significance. * ($P \leq 0.05$) shows statistically significant difference from the negative control (culture media).

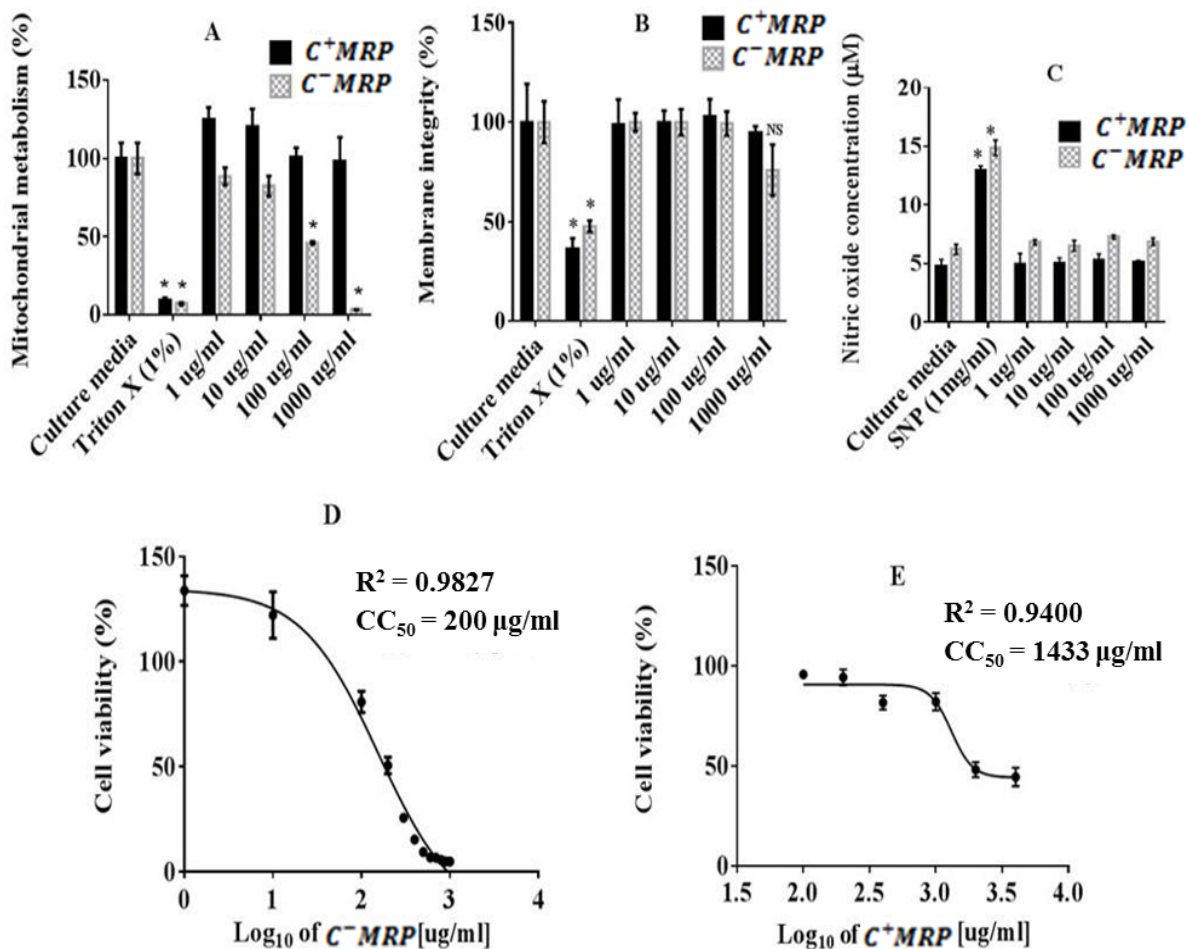


Figure 5-8: VK2 cytotoxicity. A, B and C shows the mitochondrial metabolism, cellular membrane integrity and nitric oxide production, respectively, for C^+MRP and C^-MRP . D and E represent the CC_{50} curves for C^+MRP and C^-MRP , respectively. Values are computed from quintuplicates (n=5). One-way anova test is performed in GraphPad (version 6.0) to determine statistical significance. * ($P \leq 0.05$) shows statistically significant difference from the negative control (culture media). NS indicates non-significance ($P > 0.05$).

Upon murine macrophages RAW 264.7 cells' treatment with both MRP, C^+MRP is found to be non-cytotoxic and does not induce any loss in cell viability nor in membrane

integrity in the concentration range tested in 24h (figure 5-9). The CC_{50} value for C^+MRP treatment associated with murine macrophages RAW 264.7 is 1413 $\mu\text{g/ml}$. C^-MRP formulation is non-cytotoxic up to 100 $\mu\text{g/ml}$ and slightly cytotoxic at 1000 $\mu\text{g/ml}$, when

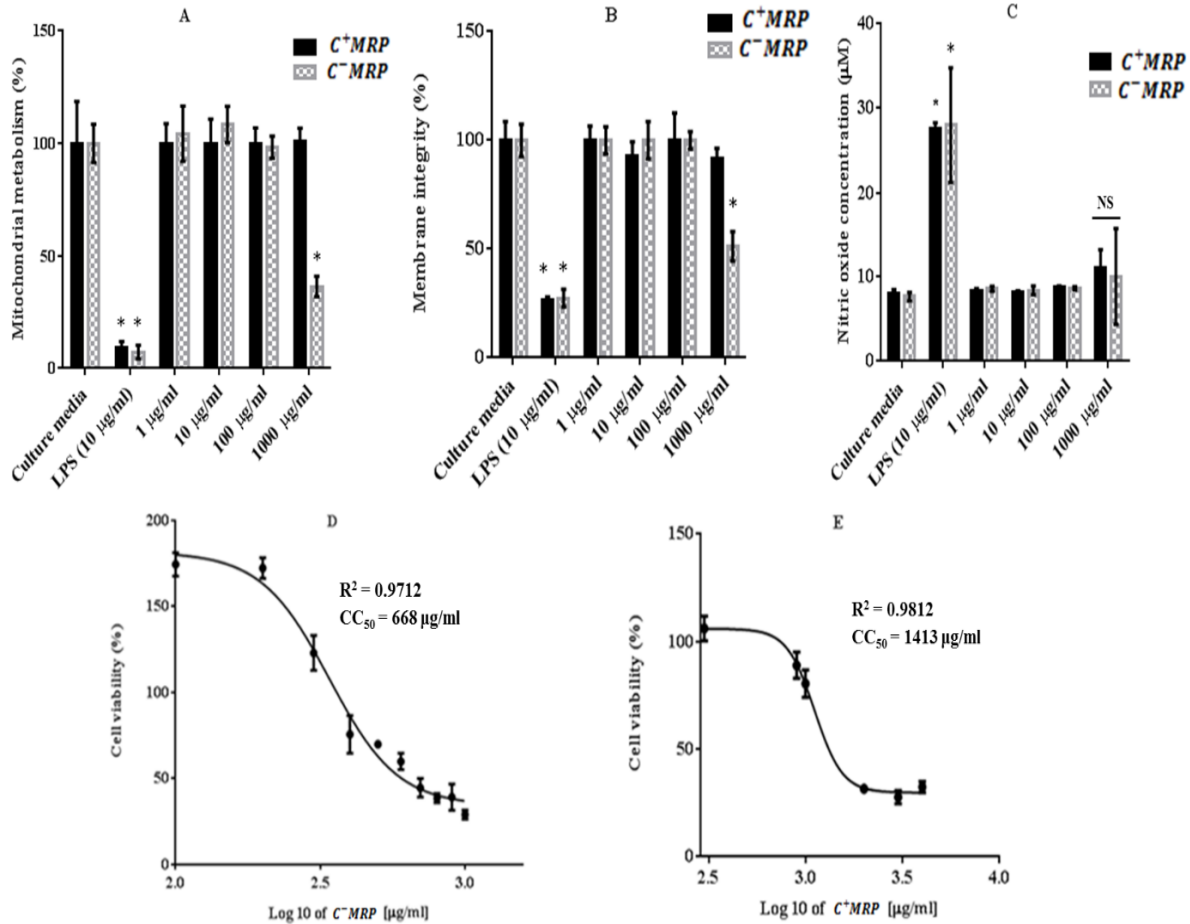


Figure 5-9: RAW 264.7 cytotoxicity. A, B and C shows the mitochondrial metabolism, cellular membrane integrity and nitric oxide production, respectively, for C^+MRP and C^-MRP . D and E represent the CC_{50} curves for C^+MRP and C^-MRP , respectively. Values are computed from quintuplicates (n=5). One-way anova test is performed in GraphPad (version 6.0) to determine statistical significance. * ($P \leq 0.05$) shows statistically significant difference from the negative control (culture media). NS indicates non-significance ($P > 0.05$).

tested on murine macrophages RAW 264.7 cells. Similar to VK2 cells, C^-MRP cell viability result is consistent with the membrane integrity test measured in the same conditions. Indeed, a significant decrease in cell membrane integrity is observed for C^-MRP at 1000 $\mu\text{g/ml}$ which could explain the low viability observed at the same concentration. Moreover, potential EDTA residues present in C^-MRP formulation might explain the inherent cytotoxicity observed at 1000 $\mu\text{g/ml}$. In fact, when tested on murine resident macrophages culture, EDTA (17%) induced 50% to 70% reduction in cell viability during 0–24h³⁵⁴. The CC_{50} value calculated for C^-MRP on murine macrophages RAW 264.7 cells is 668 $\mu\text{g/ml}$ and is twofold lower than the value obtained for C^+MRP in the same conditions. For both C^+MRP and C^-MRP , no significant nitric oxide release is observed compared to the negative control (culture media) in the concentration range tested, suggesting that no inflammation is associated with both MRPs' treatment of RAW 264.7 for 24h. However, to further confirm this result, pro-inflammatory cytokines ($\text{IL}1\alpha$, $\text{IL}1\beta$, $\text{IL}6$, $\text{TNF}\alpha$) and the mouse functional analogue of human IL-8, MKC³⁵⁵, as well as $\text{IL}7$ and $\text{IP}10$ levels are determined in RAW 264.7 cells culture supernatant (figure 5-10). $\text{IL}-1$, the first discovered and most studied cytokine consists of two distinct subtypes ($\text{IL}1\alpha$ and $\text{IL}1\beta$).³⁵⁶ Binding of these subtypes to the $\text{IL}-1$ receptor ($\text{IL}-1\text{R}1$) activates the $\text{NF-}\kappa\text{B}$ pathway which can result in more pro-inflammatory cytokines secretion, such as $\text{TNF}\alpha$, $\text{IL}6$ or $\text{IL}8$.^{357, 358} $\text{TNF}\alpha$, which is associated with free radical production, is well known for its contrasting role as both HIV entry inhibitor and replication facilitator in chronically infected cells.^{359, 360} $\text{IL}6$ and $\text{IL}8$ have also been shown to induce HIV upregulation.³⁶¹ Similarly, $\text{IL}7$ facilitates HIV infection mainly by prolonging the life of infected cells and preventing apoptosis of non-infected $\text{CD}4^+$ T cells³⁶². Interferon- γ -inducible protein 10 ($\text{IP}10$) stimulates HIV replication by attracting

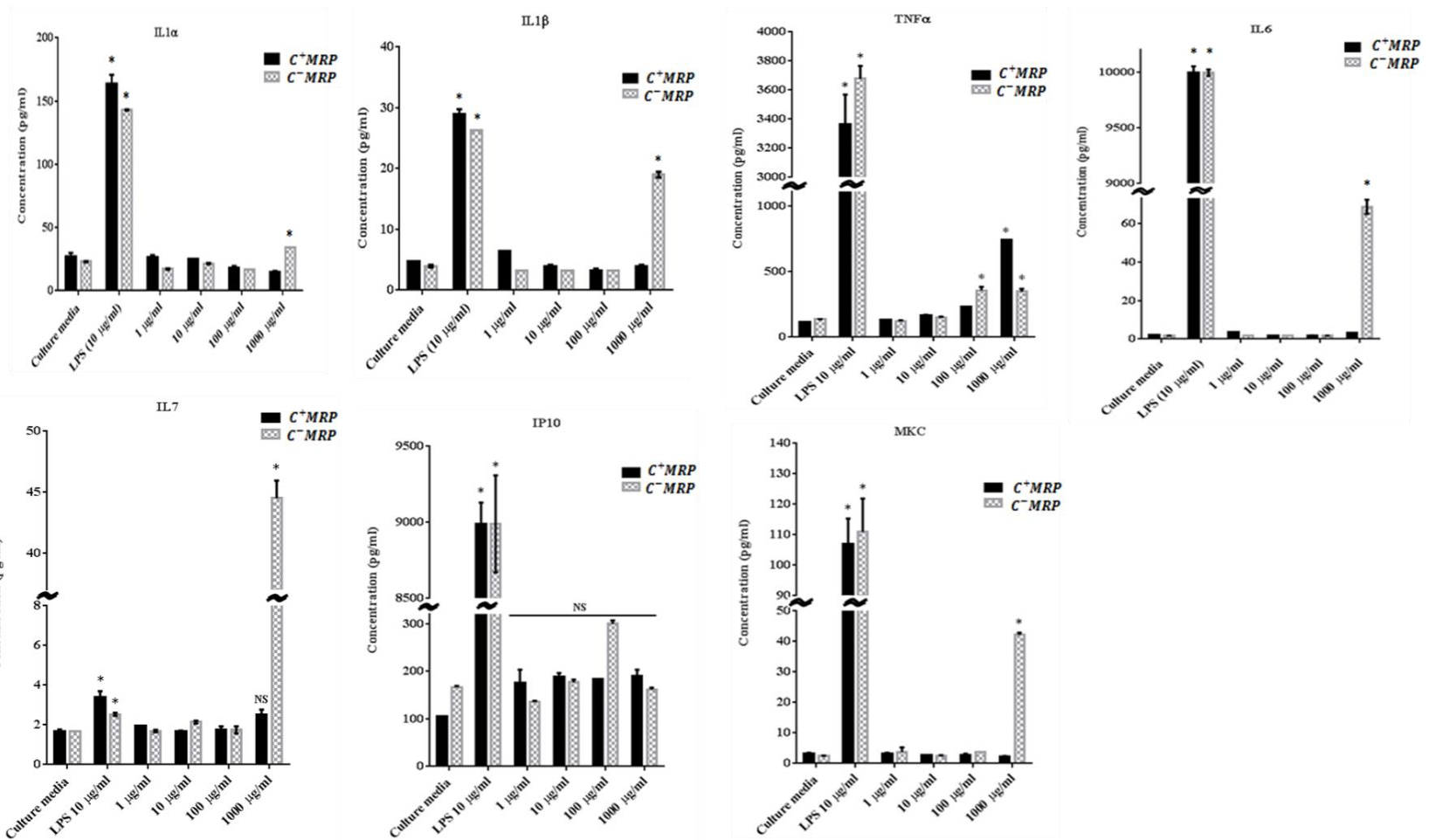


Figure 5-10: IL1 α , IL1 β , TNF α , IL6, IL7, IP10 and MKC cytokines levels measured in RAW 264.7 cell culture supernatant for C^+MRP and C^-MRP . Values are computed from quintuplicates (n=5). One-way anova test is performed in GraphPad (version 6.0) to determine statistical significance. * ($P \leq 0.05$) shows statistically significant difference from the negative control (culture media). NS indicates non-significance ($P > 0.05$).

activated T lymphocytes and monocytes.^{363, 364} No significant differences in pro-inflammatory cytokines IL1 α , IL2, MCP and IL6 levels was observed when macrophage RAW 264.7 are treated with C^+MRP for 24h. Although, no significant increase in TNF α level is observed for C^+MRP treatment, between 1-100 $\mu\text{g/ml}$; nonetheless, a significant increase of this cytokine is associated with C^+MRP at 1000 $\mu\text{g/ml}$. Similarly, C^+MRP did not induce a significant change in IL 7 and IP10 levels suggesting that this formulation might be safe for topical application in the concentration range tested for 24h. Conversely, other than IP10, where it did not induce any significant changes in the cytokine levels, C^-MRP formulation is associated with significantly high pro-inflammatory cytokines production at 1000 $\mu\text{g/ml}$. In fact, this formulation is non-cytotoxic only at concentration ranging between 1-100 $\mu\text{g/ml}$ as previously suggested by the cell viability testing. These results suggest that C^+MRP formulation might be safer for *in vivo* applications compare to C^-MRP which is not only associated with cell death, but also induces pro-inflammatory cytokines release at concentration above 100 $\mu\text{g/ml}$.

Assessment of HIV-1 gp120-triggered drug release. Due to the pronounced cytotoxicity observed for on both VK2 and RAW RAW 264.7, as well as the pro-inflammatory cytokines release it induced; C^-MRP formulation was not tested for HIV-1 gp120-triggered drug release. Thus, stimuli sensitivity was tested by monitoring TFV release from C^+MRP , up to 24 h, in the presence of Man and mannose-rich HIV-1 rgp120 (figure 5-11 and 5-12). In general, a maximum drug release was reached within 4 to 8 h. An increasing dose response effect was also observed with increasing HIV-1 rgp120 concentration. HIV-1 virus is known to cross the mucosal barrier in 2 to 6 h and, during the first 3 to 6 days, disseminates locally to reach draining lymph nodes.³⁶⁵ Thus C^+MRP could potentially offer the advantage of

neutralizing HIV-1 virus in the vaginal or rectal track before completion of its migration through the mucosal barrier. For C^+MRP formulation containing three Con A layers (3L) (figure 5-11), a maximum drug release ($(75\% \pm 6.5)$ [$176.75 \mu\text{g/ml}$]) was observed in the presence of Man ($1000 \mu\text{g/ml}$) while HIV-1 rgp120 induced $61\% \pm 3.7$ [$143.75 \mu\text{g/ml}$], $39\% \pm 1.7$ [$91.91 \mu\text{g/ml}$] and $22\% \pm 1.4$ [$51.84 \mu\text{g/ml}$] of TFV release at $1000 \mu\text{g/ml}$, $500 \mu\text{g/ml}$ and $100 \mu\text{g/ml}$, respectively. Previous studies show that TFV intravaginal ring completely protected macaques from multiple vaginal HIV challenges for average TFV vaginal fluid concentration of $180 \mu\text{g/ml}$ and a range stretching from 11 - $660 \mu\text{g/ml}$.³⁶⁶ Similarly, 1% TFV gel offered 76% protection against HIV infection for TFV vaginal fluid concentrations higher than $1 \mu\text{g/ml}$.³⁶⁷ Moreover, TFV EC_{50} values range from $0.021 \mu\text{g/ml}$ to $4.4 \mu\text{g/ml}$. These studies strongly suggest that TFV concentrations achieved with C^+MRP could effectively protect against HIV infections. The maximal drug release observed with Man could be due, in part, to a higher binding affinity of Con A for the monosaccharide, as previously shown by Goldstein et al.²⁶⁰ Moreover, Man smaller molecular weight might favor a better diffusion through Con A/glycogen layers resulting in a faster and greater layer degradation which

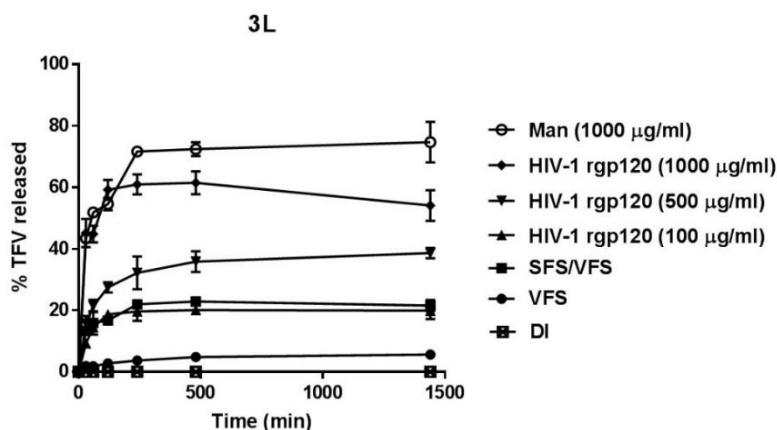


Figure 5-11: TFV release profiles from C^+MRP (3L) in the presence of Man ($1000 \mu\text{g/ml}$) and HIV-1 rgp120 (100 - $1000 \mu\text{g/ml}$).

translates into higher drug release and release rate constants (Table 2: Hixson–Crowell and Hopfenberg release kinetic models). Although a therapeutic concentration of TFV [51.84 µg/ml] was released from C^+MRP (3L), when exposed to 100 µg/ml of HIV-1 rgp120, this was, however, not significantly different from the drug release observed in the untreated conditions [SFS:VSF]. In fact, the model-independent method yielded dissimilarity factor (f_1) and similarity factor (f_2) values of 15.58 and 77.62, respectively for the release profile observed for HIV-1 rgp120 (100 µg/ml) (Table 5-1). According to the FDA guideline, f_1 values lower than 15 (0-15) and f_2 values higher than 50 (50-100) show the similarity of two release profiles.

Optimization of C^+MRP . This study is justified due to the lack of significant drug release observed for HIV-1 rgp120 concentrations ≤ 100 µg/ml, and the relatively lower *in vitro* HIV-1 gp120 levels reported in various studies [0.12 ng/ml to 120 µg/ml].³²³ After fitting TFV release from C^+MRP (3L) to various release kinetics models (Table 5-2), it was observed that TFV release profiles best follow Hixson–Crowell and Hopfenberg kinetic models. Traditionally, Hixson–Crowell model has been used to describe drug release profiles from diminishing surfaces of drug particles.³⁶⁸ Likewise, Hopfenberg kinetic model explains drug release profiles from matrix eroding drug particles. More specifically, Hopfenberg kinetic model assumes matrix erosion to be the rate-limiting step of drug release, instead of time dependent diffusional resistance (internal or external) to the eroding matrix.³⁶⁹ This suggested that drug release from C^+MRP occurred through an erosion of the Con A/Glycogen layers, primarily due to the binding of mannose moieties in Man and HIV-1 rgp120 to Con A. This competitive binding is possible due to the preference of Con A for mannose

Table 5-1: FDA similarity and dissimilarity factors for TFV release from C^+MRP (1L, 2L and 3L)^a.

Release conditions	1L		2L		3L	
	f1	f2	f1	f2	f1	f2
SFS:VFS (4.5V:1V)	NA	NA	NA	NA	NA	NA
Man (100 µg/ml)	80.04	36.39	51.11	46.75	NA	NA
Man (1000 µg/ml)	NA	NA	NA	NA	69.33	20.43
HIV-1 rgp120 (25 µg/ml)	51.86	49.31	30.99	67.64	NA	NA
HIV-1 rgp120 (50 µg/ml)	56.67	46.42	49.50	52.10	NA	NA
HIV-1 rgp120 (100 µg/ml)	67.46	40.60	62.68	48.03	15.58	77.62
HIV-1 rgp120 (500 µg/ml)	NA	NA	NA	NA	33.46	47.95
HIV-1 rgp120 (1000 µg/ml)	NA	NA	NA	NA	67.68	22.20

^aThe number of Con A layers (1, 2 and 3) in the C^+MRP formulations are referred to as 1L, 2L and 3L, respectively.

Table 5-2: Kinetic models describing TFV *in vitro* release profiles from C^+MRP (3L)^a.

	Zero order		First order		Higuchi		Hixson–Crowell		Hopfenberg	
	K_0	r^2	K_1	r^2	K_H	r^2	K_β	r^2	K_2	r^2
	($\mu\text{g}/\text{min}$)		(min^{-1})		($\mu\text{g}/\text{min}$)		(min^{-1})		($\mu\text{g}\cdot\mu\text{m}^{-2}\cdot\text{min}^{-1}$)	
SFS/VFS (4.5v/1v)	0.014	0.36	0.0002	0.36	0.8	0.56	0.0001	0.97	0.0002	0.97
Man (1000 $\mu\text{g}/\text{ml}$)	0.054	0.55	0.0003	0.51	2.78	0.69	0.0008	0.97	0.0019	0.95
HIV-1 rgp120 (1000 $\mu\text{g}/\text{ml}$)	0.01	0.05	0.00007	0.06	0.83	0.16	0.0005	0.78	0.0009	0.79
HIV-1 rgp120 (500 $\mu\text{g}/\text{ml}$)	0.042	0.60	0.0005	0.52	2.18	0.79	0.0003	0.96	0.0004	0.97
HIV-1 rgp120 (100 $\mu\text{g}/\text{ml}$)	0.013	0.25	0.0003	0.22	0.75	0.42	0.0004	0.94	0.0005	0.94

^aThree Con A inlayers containing C^+MRP is referred to as 3L.

compared to glucose.³⁷⁰ As a result, C^+MRP coating undergo a degradation, exposing TFV loaded $CaCO_3$ core particle to calcium chelating agents, such as citric acid and lactic acid, present in the seminal and vaginal fluid simulants. The calcium chelating property of citric acid and lactic acid has previously been established. Amaral et al.³⁵⁴ have shown that 10% citric acid has a greater chelating power compared to 17% EDTA. Citric acid concentration in seminal fluid varies from 300 mg/100 ml to 750 mg/100 ml and was 523 mg/100 ml in the present study.³²² Although the primary role of citric acid in semen is not well understood; several studies have suggested that it plays a major role in preventing the premature capacitation of sperm by chelating calcium ions in the seminal fluid.³⁷¹ In the present study, citric acid chelates calcium ions from $CaCO_3$ core particles contributing to core dissolution and enhanced drug release. This was further proved by exposing C^+MRP to citric acid and lactic acid free DI water with no quantifiable drug release observed, up to 24 h (figure 5-11). In contrast, 6% [$\sim 14 \mu\text{g/ml}$] of TFV was released in vaginal fluid simulant alone, probably due to its lactic acid content 200 mg/100 ml.³²¹ This non-specific drug release observed in vaginal fluid could potentially provide a basal drug level and a protecting barrier against HIV-1 vaginal infection.

In regard to results obtained with Hixson–Crowell and Hopfenberg kinetic models, C^+MRP was optimized by decreasing the number of Con A layers in C^+MRP formulation. Thus, one (1) and two (2) Con A layers containing formulations (1L & 2L) were prepared and tested for TFV release at HIV-1 rgp120 concentrations $\leq 100 \mu\text{g/ml}$ (figure 5-12; 1L & 2L). For C^+MRP (2L), a maximum drug release of $33\% \pm 3.9$ [$77.8 \mu\text{g/ml}$] was observed in the presence of Man. Although up to $28\% \pm 1.8$ [$66.88 \mu\text{g/ml}$] and $22\% \pm 1.7$ [$52.5 \mu\text{g/ml}$] drug release were observed for 50 and 25 $\mu\text{g/ml}$ HIV-1 rgp120, respectively; statistically significant

drug release was only obtained for 100 $\mu\text{g/ml}$ HIV-1 rgp120, compared to control blank vaginal and seminal fluids mixture (SFS:VFS) (Table 5-1). Nonetheless, TFV levels released from C^+MRP (2L) at 50 and 25 $\mu\text{g/ml}$ HIV-1 rgp120 were therapeutically relevant (cumulative drug released at 2 h ranged from 35.83 to 45.38 $\mu\text{g/ml}$), given that TFV EC_{50} values range from 0.021 to 4.4 $\mu\text{g/ml}$. Upon testing C^+MRP (1L), compared to SFS:VFS release profile,

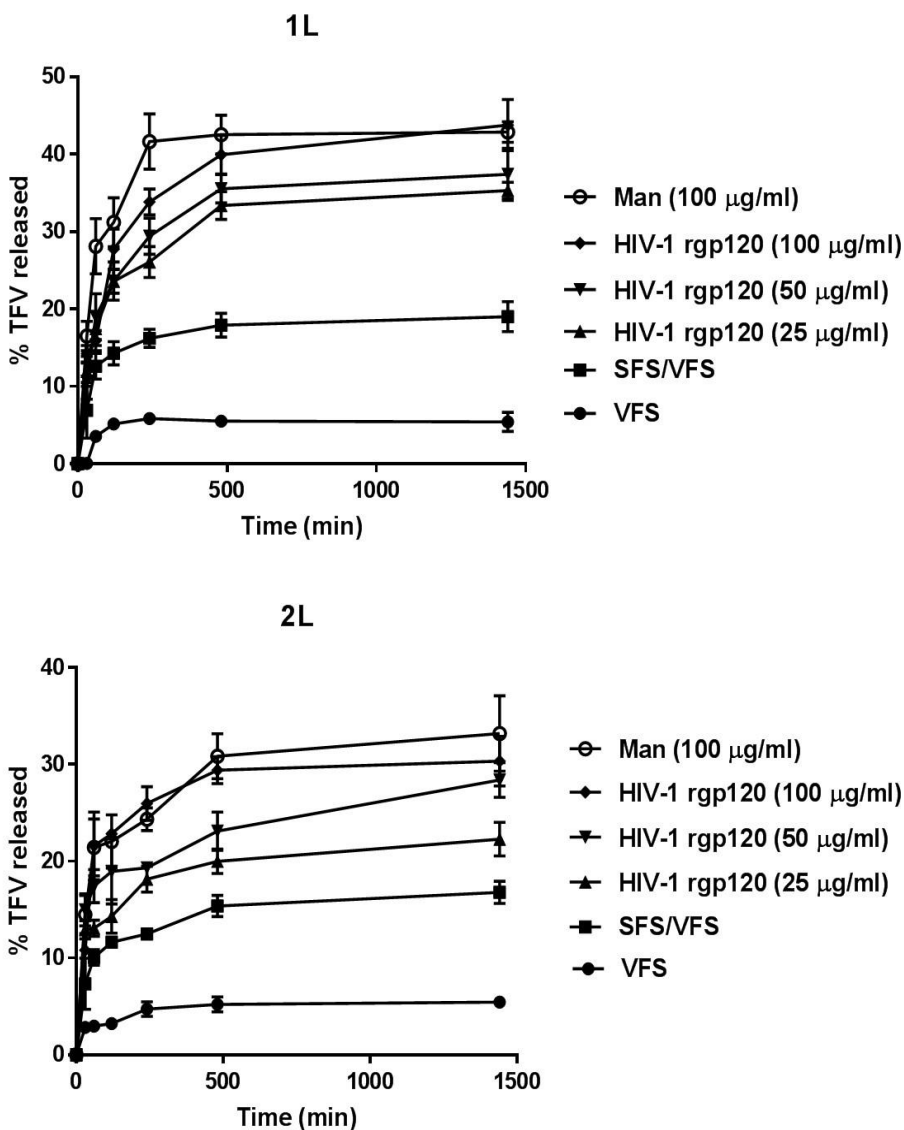


Figure 5-12: TFV release profiles from C^+MRP (2L & 1L) in the presence of Man (1000 $\mu\text{g/ml}$) and HIV-1 rgp120.

significant drug release was achieved for all three HIV-1 rgp120 concentrations ($\leq 100 \mu\text{g/ml}$) with a slight increase in cumulated TFV released (Table 5-1). This difference in drug release profile, relative to the number of Con A layers in C^+MRP formulation (decreased layer thickness), was consistent with the diminishing surface or matrix eroding drug particles, as explained above.

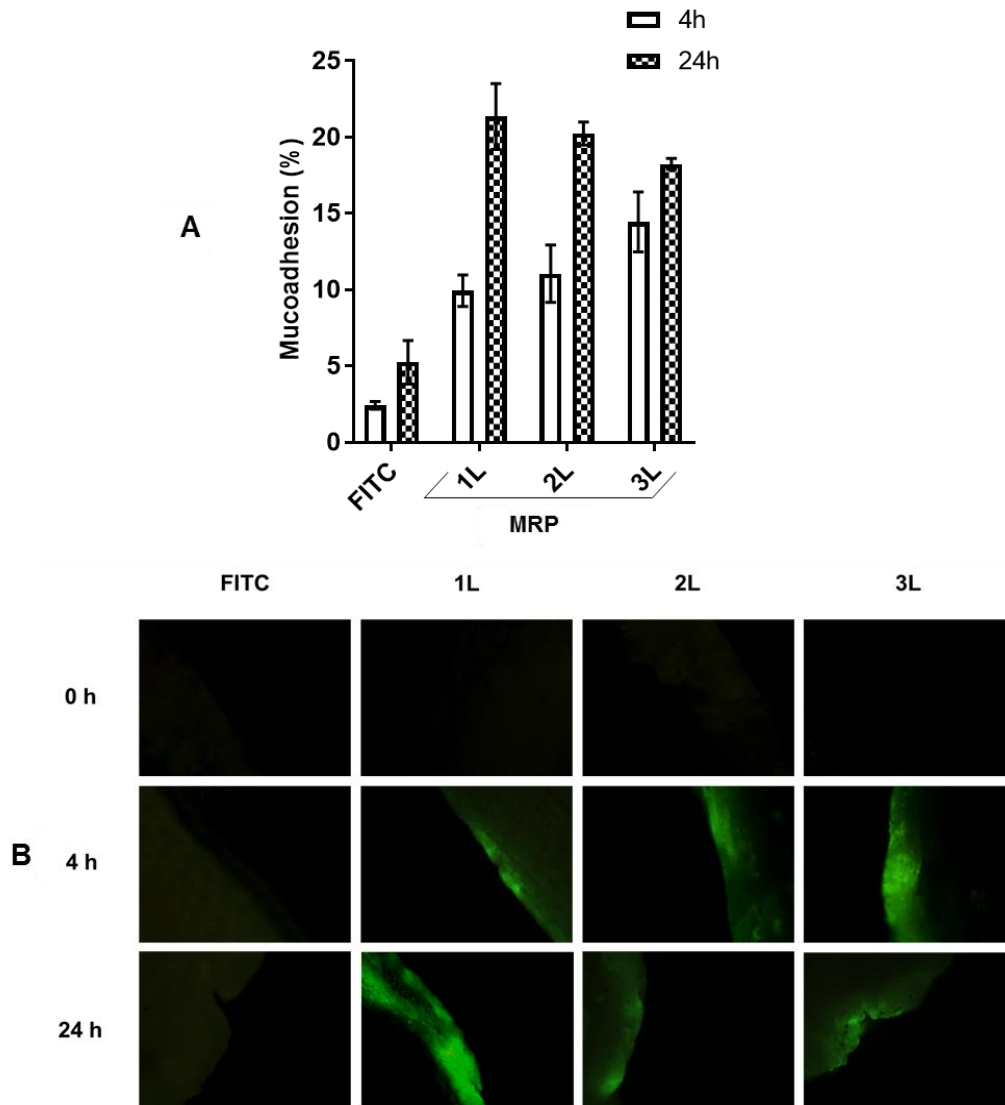


Figure 5-13: C^+MRP mucoadhesion to porcine vaginal tissue (A) with corresponding thin sections fluorescent images (B).

Bioadhesion. C^+MRP (1L, 2L and 3L) mucoadhesion was tested *ex vivo* on porcine vaginal tissue. Previous studies have demonstrated strong similarities between porcine vaginal and human vaginal tissues. These similarities are found in: histology, ultrastructural organization, lipid composition, secretions, pH and inflammatory responses.³⁷² The similarity between both tissues was also shown to translate into strong correlations between *ex vivo* studies on porcine vaginal tissue and human vaginal tissue.³²⁶ When exposed to porcine vaginal tissue, C^+MRP showed mucoadhesion ranging from $10\% \pm 1$ to $21\% \pm 2$ (figure 5-13A). Porcine tissues images also showed FITC labeled C^+MRP ' green fluorescence onto tissues surface (figure 5-13B). C^+MRP mucoadhesion was attributed to the presence of Con A in the self-assembly. Numerous studies have shown that Con A significantly improves mucoadhesion of drug delivery systems.³⁷³⁻³⁷⁵ Lectins, such as Con A, increase bioadhesion by binding to carbohydrates and glycans in glycoproteins found on mucus layer.^{376, 377}

5.4 Conclusion

HIV-1 gp120 and mannose responsive microbicide drug delivery system (MRP) was prepared through the layer-by-layer deposition of Con A and glycogen onto a $CaCO_3$ -PSS core particle. Tenofovir is encapsulated in $CaCO_3$ and the encapsulation efficiency is 74.4%. TFV was successfully loaded in MRP owing to $CaCO_3$ phosphate binding properties and the coprecipitation process involved in $CaCO_3$ crystallization. TFV loading efficiency in core containing MRP (C^+MRP) and core removed MRP (C^-MRP) are 16.3% w/w and 6.0% w/w, respectively. It is determined that C^-MRP , prepared through the layer-by-layer method followed by EDTA core dissolution, is cytotoxic to vaginal keratinocytes (VK2) and murine macrophage (RAW 264.7) cells at concentrations higher than 10 $\mu\text{g/ml}$. That is, C^-MRP might

not be appropriate for vaginal or rectal drug delivery. However, C^+MRP is non-cytotoxic to both VK2 and macrophage RAW 264.7 cells and does not induce any significant changes in pro-inflammatory cytokines or nitric oxide levels in 24h. Moreover, C^+MRP was non-cytotoxic to *L. crispatus*, suggesting a safe and suitable template for future *in vivo* testing. HIV-1 gp120 triggered TFV release from C^+MRP in a concentration dependent manner, which followed Hixson–Crowell and Hopfenberg kinetic models, consistent with diminishing surface or matrix eroding drug particles. C^+MRP also showed significant mucoadhesion to porcine vaginal tissue, *ex vivo*. The one Con A layer containing C^+MRP system was found to be the most sensitive (~2-fold increase in drug release vs. control SFS:VFS) at the lowest HIV gp120 concentration tested (25 $\mu\text{g}/\text{mL}$). Altogether, this study strongly suggests that C^+MRP formulation of TFV might be suitable for further *in vivo* toxicity, retention and efficacy testing. One of the limitations of this study is the use of reported *in vitro* HIV gp120 concentrations as basis for the *in vitro* optimization. Although HIV gp120 seminal and vaginal fluid concentrations are not well studied, Oh et al. reported HIV gp120 concentration in majority of HIV/AIDS patients' sera in the range of 0.1-0.8 nM.¹¹¹ Moreover, in its unbound state, Con A was reported to be unstable at 37 °C.¹¹² However, it is unclear how the lectin behaves in the C^+MRP system, given that Con A denaturation in the presence of carbohydrate ligands is reported to vary between 91 °C and 96 °C.¹¹³ Therefore, future studies will investigate MRP's stability and sensitivity optimization with respect to clinically relevant HIV gp120 concentrations.

CHAPTER 6

IN VIVO PRECLINICAL SAFETY EVALUATION OF A MICROBICIDE LOADED HIV-1 gp120 TARGETED VAGINAL FORMULATION IN FEMALE MOUSE REPRODUCTIVE TRACT

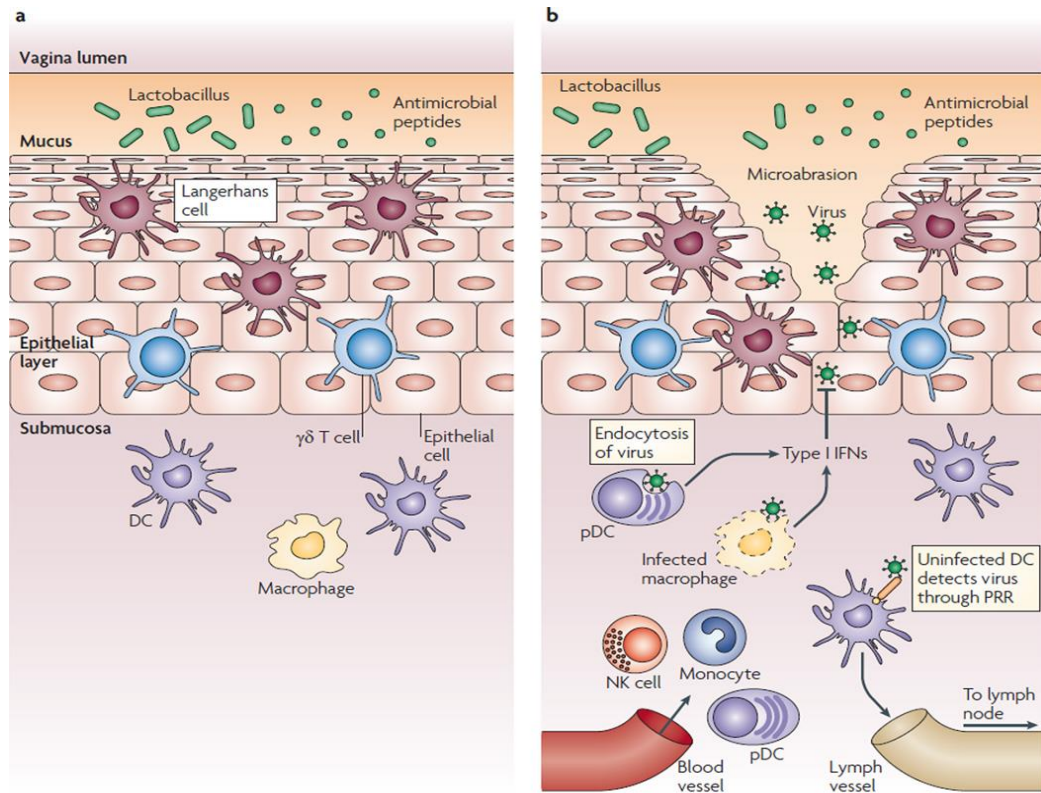
6.1 Introduction and rationale

In the past decades, numerous microbicides candidates have been proposed in the attempt to address HIV sexual transmission, with marginal success. Some of the microbicide formulation tested include gels, films and intravaginal ring.⁷³ Some of the most publicized microbicide clinical trials, such as CAPRISA 004, FACTS 001, VOICE, FAME-02 and CONRAD 128, have either failed due to safety concerns or remained to demonstrate their effectiveness in human.^{69, 71, 72, 378} For example, two first generation microbicide formulations, Nonoxynol-9 (N-9) and Cellulose Sulfate (CS) have failed to protect against HIV sexual transmission due to major safety issues, including mucosal inflammation and increase in pro-inflammatory mediators, which ultimately increased the risk of HIV infection.³⁷⁹ Furthermore, the VOICE study did not show any efficacy and was stopped early due to epithelial damage.³⁸⁰ Likewise, CAPRISA 004 trial showed that innate immunity activation increases HIV acquisition.³⁸¹ Nonetheless, these studies have greatly informed the scientific community and laid down the standards in microbicide research and testing.

As explained in chapter 2, it is widely accepted that physical damage to vaginal mucosa substantially increases vaginal susceptibility to HIV infection.⁴² An inflammation of the vaginal mucosa could lead to an increase in HIV infection by promoting the recruitment of HIV target cells, such as macrophages, CD4⁺ T cells, monocytes, natural killer cells and

dendritic cells at the site of inflammation.³⁸² In addition, the ability of pro-inflammatory cytokines to enhance HIV vaginal infectivity has been widely studied.³⁸³ Furthermore, the normal vaginal microbiota, dominated by *Lactobacillus* species, is known to provide an inherent antimicrobial protective layer in adult women compared to prepuberal girls and postmenopausal women.³⁸⁴ This is primarily due to the breakdown of glycogen into lactic acid, which maintains the vaginal acidic pH in adult women, as well as H₂O₂ production by *Lactobacillus* species, such as *L. crispatus* and *L. jensenii*.^{41, 51, 52} Therefore, the *in vivo* safety evaluation of vaginal microbicide formulations is of paramount importance to ensure, not only their suitability for the desired application, but ultimately to assess any potential adverse effects, such as vaginal mucosa damage, inflammations, irritations, localized and/or systemic toxicity, as well as any compromise of the vaginal microbiota.⁷³

The potential of lectins, a class of carbohydrate binding proteins, to prevent HIV infection has long been contemplated.⁸⁵ Lectins primarily exert their antiviral activity by recognizing and binding major glycan structures onto HIV surface. Considering the selectivity of mannose binding lectins to HIV gp120, we have previously reported a layer-by-layer engineered, lectin-based microbicide drug delivery system targeting HIV-1 gp120, for the prevention of HIV sexual transmission.³⁸³ Major physicochemical and biological properties of the proposed HIV-1 gp120 and mannose responsive particles (*C⁺MRP*) were also discussed. In the present study, we investigate the preclinical safety of Tenofovir (TFV) loaded *C⁺MRP* in C57BL/6 mice model. If successful, this study may represent a major advance in lectin-based microbicide formulation for the prevention of HIV sexual transmission.



Nature Reviews | Immunology

Figure 6-1: Model of HIV vaginal infection following mucosal disruption (b) from an intact mucosal layer (a).³⁸²

6.2 Material and methods

Reagents

The following reagents were purchased from Sigma-Aldrich (St. Louis, MO, USA); Concanavalin A (Con A) from *Canavalia ensiformis* (Jack bean) type VI, glycogen from Oyster, polyethylenimine (PEI) 50 wt. % solution in water, poly(sodium 4-styrenesulfonate) (PSS) average Mw ~70.000 powder, calcium chloride dehydrate ($\text{CaCl}_2 \cdot 2\text{H}_2\text{O}$, ACS reagent, $\geq 99\%$), sodium carbonate anhydrous ($\geq 99\%$), fluorescein isothiocyanate labeled Concanavalin A (FITC-Con A) type IV lyophilized powder, tetramethylrhodamine isothiocyanate–Dextran

(TRITC-Dextran), manganese (II) chloride tetrahydrate ($\text{MnCl}_2 \cdot 4\text{H}_2\text{O}$, Reagent Plus, $\geq 99\%$), methyl α -D-mannopyranoside (Man) ($\geq 99\%$), Benzalkonium chloride (BZK, 2 %v/v), Crystal Violet, Phosphate Buffered Saline (PBS) pH 7.4 and Tris Buffer Saline (TBS) pH 8.0. Fluorescein Isothiocyanate Isomer I (FITC) 90% pure ACROS Organics™ was purchased from Thermo Fisher Scientific (Waltham, MA, USA). Tenofovir (TFV) (99%) was purchased from Zhongshuo Pharmaceutical Co. Ltd. (Beijing, China). Medroxyprogesterone acetate (Depo-Provera®) was purchased from Greenstone, (Peapack, NJ, USA). Nonoxynol-9 (N-9, Conceptrol®) was from Revive Personal, (Madison, NJ, USA). Human Immunodeficiency Virus type 1 recombinant envelope glycoprotein (HIV-1 rgp120) is purchased from Sino Biological Inc. (Beijing, P. R. China). All other chemicals were reagent grade and used without further purifications.

Methods

Layer by layer preparation of C^+MRP

As detailed in chapter 5, C^+MRP was prepared by successively coating a calcium carbonate (CaCO_3)/PSS core particle with PEI, Glycogen and Con A. Prior to preparing (CaCO_3)/PSS, a saturated solution of TFV (3 mg/ml) was prepared in CaCl_2 . Then TFV loaded CaCO_3 /PSS was prepared by mixing equal volume (15 ml) of 0.2 M CaCl_2 /TFV and 0.2 M sodium carbonate (Na_2CO_3) in the presence of a dispersant (PSS). The mixture was vigorously stirred at 13,500 rpm for two (2) minutes with the IKA Ultra-Turax model T25 homogenizer (Wilmington, NC, USA). After an initial dispersion in PEI (4 mg/ml in 0.5 M NaCl, pH 8.0) for at least 30 minutes, particles were successively dispersed in Con A (1 mg/ml in TBS, pH 8.0) and Glycogen (1 mg/ml in TBS, pH 8.0) solutions, at room temperature. After preparation,

C⁺MRP was washed twice with DI water and freeze-dried for twelve (12) hours (Labconco FreeZone 1 Liter Benchtop Freeze Dry System, Kansas City, MO). Following freeze-drying, *C⁺MRP* was kept in refrigeration at 4°C. Particle mean diameter (size), zeta potential (ζ -potential), polydispersity index (PDI), percent encapsulation efficiency (%EE) and loading efficiency (%LD) measurements were all conducted as explained in chapter 5.

Osmolality determination of the tested samples. Osmolality, a measure of the number of osmoles of solute per kilogram of solvent, is a critical parameter in vaginal and rectal microbicide formulation development.³⁸⁵ Various vaginal microbicide formulation candidates were thought to have failed due to their hyperosmolality nature.^{386, 387} In fact, hyperosmolar (> 400 mOsm/kg)³⁸⁸ vaginal formulations can cause brisk transudation of fluid across the cervico-vaginal epithelium which can result in increase vaginal wetness and watery discharges.³⁸⁶ Vaginal epithelial damage and increase HIV transmission have also been associated with hyperosmolar vaginal formulations^{385-387, 389} Furthermore, hyposmolar vaginal formulations increase water uptake in epithelial cells, which can lead to vaginal dehydration, vaginal lesions, and epithelial cells' rupture (figure 6-2). Ideally, a microbicide formulation candidate should be isosmolar (280 - 400 mOsm/Kg).^{390, 391} Before mice treatments, samples osmolality was determined on a Vapor Pressure 5520 Osmometer (Wescor, Inc., UT, USA). The instrument was calibrated following the Maximum Calibration Accuracy protocol using the 100 mOsm/kg standard and according to the manufacturer instructions. Typically, a single 1/8" solute-free Whatman No.1 sample disc (Wescor, Inc., UT, USA) was placed onto the sample slide and 20 microliters of sample was allowed to fully cover the filter paper. The sample holder was then inserted into the instrument and the osmolality measurement conducted

for 80 s. Samples were measured in triplicates and average osmolality values recorded in mOsm/kg.

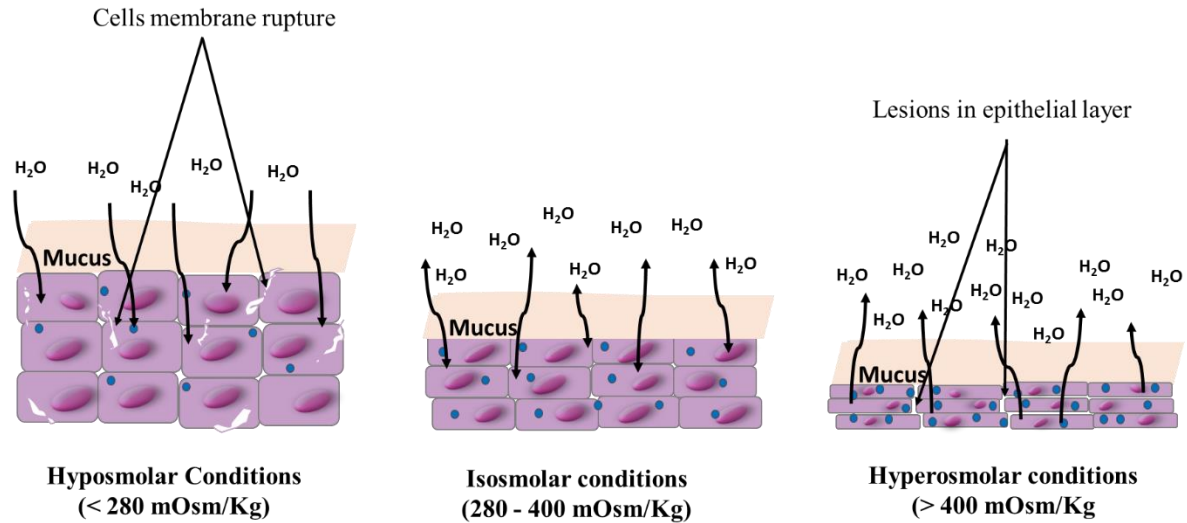


Figure 6-2: Vaginal epithelial layer in different osmolality conditions

***In Vivo* safety evaluation of *C⁺MRP* in mice Model.**

C⁺MRP *in vivo* safety evaluation was conducted following an approved University of Missouri - Kansas City Institutional Animal Care and Use Committee (IACUC) animal protocol, and according to methods described in previous publications.^{392, 393} Briefly, *C⁺MRP* safety was evaluated on 8-12 weeks old female C57BL/6 mice with an average body weight of 20 g. C57BL/6 mice, known for their easy breeding and robustness, were obtained from Jackson Laboratories (Harbor, ME) and allowed to acclimate for 7 days. Mice were housed (maximum of 5 per cage) in the UMKC Laboratory Animal Resource Center (LARC) under a 12 h light/dark regime. UMKC' LARC is a fully AAALAC (the Association for Assessment and Accreditation of Laboratory Animal Care) accredited with HEPA-filtered, temperature, humidity, and lighting control systems.

Mouse vaginal cytology

Unlike in humans, where the menstrual cycle last approximately 28 days, in female mice, the reproductive cycle (estrous cycle) lasts about 4-5 days and is divided into four main stages (proestrus, estrus, metestrus, and diestrus) (figure 6-3).³⁹⁴ The proestrus stage, which represents the pre-ovulatory day, is characterized by the predominance of nucleated epithelial cells, which can appear in cluster or individually. In this stage occasional cornified epithelial cells may appear (figure 6-3A). As the estrous cycle advances to the estrus stage, cells may

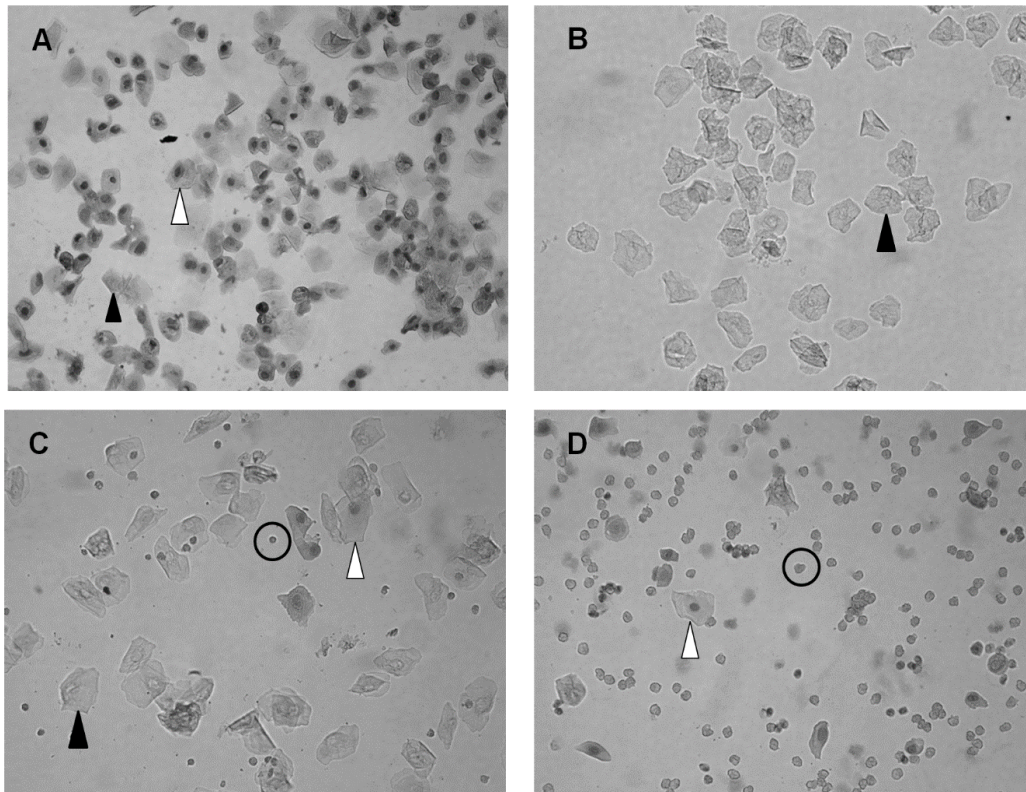


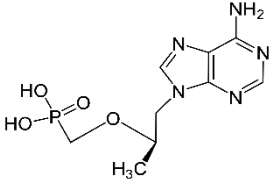
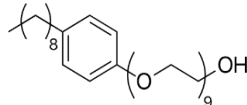
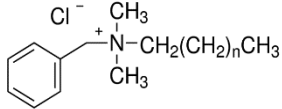
Figure 6-3: Mouse vaginal cytology representing each stage of estrous. The stages of estrous include proestrus (A), estrus (B), metestrus (C), diestrus (D). Three cell types are identified: leukocytes (circle), cornified epithelial (black arrow), and nucleated epithelial (white arrow)³⁹⁴

appear (figure 6-3A). As the estrous cycle advances to the estrus stage, cornified squamous epithelial cells, which occur in cluster, become predominant (figure 6-3B). Following the estrus stage (figure 6-3C), the metestrus stage will begin if the cycle is not interrupted by pregnancy, pseudopregnancy, or other phenomena. The metestrus stage is relatively brief and characterized by a mix of polymorphonuclear leukocytes and a few nucleated epithelial and/or cornified squamous epithelial cells. Diestrus (figure 6-3D) is the last and longest stage, lasting for more than 2 days. Vaginal swabs during diestrus show primarily polymorphonuclear leukocytes and a few epithelial cells during late diestrus. In this stage, leukocytes remain the predominant cell type after removing cellular debris.^{394, 395}

General protocol for mice treatment with C^+MRP

In the current study, mice were maintained in a constant diestrus-like vaginal cytology state, for reproducible experimental conditions and to avoid variability in vaginal histology data analysis. Thus, mice were subcutaneously injected with 2 mg of medroxyprogesterone acetate (Depo-Provera®, Greenstone, Peapack, NJ, USA) in 200 μ l of Lactated Ringer's saline solution, 4-5 days prior to C^+MRP exposure. To further confirm the diestrus-like state, vaginal cytology analysis was performed by visualizing nucleated and cornified squamous epithelial cells and polymorph nuclear leukocytes.³⁹⁶ Once the diestrus-like state was achieved, mice were divided in 4 groups (n=3). Group 1 and 2 were treated with N-9 (4% w/v) and BZK (2% v/v), respectively, and were used as positive control groups. N-9 and BZK were used as positive control because their toxic effects on genital tract are well established.^{397, 398} Group 3 was treated with PBS and taken as negative control. Group 4 represented the treatment group and was exposed to freshly prepared C^+MRP at a dose of 100 mg/kg corresponding to TFV

Table 6-1: Selected physico-chemical and biological properties of formulations tested.

Treatment formulation	API Physico-chemical properties	API Toxicology	API PK	Formulation properties
C⁺MRP Suspension	<p>Tenofovir ^{399, 400}</p>  <p>MW: 287.21 Da pKa : 3.8 LogP: -1.6</p>	<p>IC₅₀: 1.81 μM ⁴⁰¹ EC₅₀: 0.021 μg/mL⁴⁰² LD₅₀: 2.49 mol/kg⁴⁰³</p>	<p>Cmax: 247.87 ng/mL ⁴⁰⁴ Tmax: 0.87 h AUC: 2.11 μg·hr/mL T_{1/2}: 20.45 h</p>	<p>Dose: 100 mg/kg Size: 857.8 nm ζ-potential: +2.37 mV %EE: 70.1% %LD: 16.3% Osmol: 304.33 mOsm/kg</p>
	<p>Nonoxynol-9 ^{405, 406}</p>  <p>MW: 616.82 Da pKa: 15.12 LogP: 4.02</p>	<p>IC₅₀: 2 μg/ml ⁴⁰⁷ EC₅₀: 81 μM ⁴⁰⁸ LD₅₀: 2.24 mol/kg ⁴⁰⁶</p>	<p>Cmax: 4.87 ng/mL ⁴⁰⁹ Tmax: 1h AUC: 9.89 ng·hr/mL T_{1/2}: 1.45 h</p>	<p>Dose: 4% w/v ζ-potential: -27 mv Osmol: 745.33 mOsm/kg</p>
BZK solution	<p>Benzalkonium Chloride ^{410, 411}</p>  <p>MW: ~ 375 Da pKa: 12.77 LogP: 5.98</p> <p>(n = 7-18)</p>	<p>IC₅₀: ND EC₅₀: < 0.025% ⁴¹² LD₅₀: 150 mg/kg</p>	<p>ND</p>	<p>Dose: 2% v/v ζ-potential: +25.14 mV Osmol: 382.2 mOsm/kg</p>

dose of 16.3 mg/kg. C^+MRP exposure was conducted up to 24 h before mice are euthanized by carbon dioxide (CO₂) asphyxiation [70% (v/v) CO₂ and 30% (v/v) O₂]. Following animal sacrifice, vaginal tissues were collected, formalin fixed, embedded in paraffin, cut into 5-mm sections and analyzed, according to standard tissue processing procedures.

Hematoxylin and eosin (H&E) staining

To assess histopathological parameters such as epithelial cells morphology, cell populations and possible erosion in epithelial cell layer, mice reproductive system' (vagina, cervix, fallopian tube, uterus and ovary) tissue sections were stained with hematoxylin and eosin (H&E) (Sigma, Saint Louis, MO, USA). Stained tissue section were visualized on Nikon Labophot-2 microscope (Nikon Instruments, Inc., Melville, NY, USA) equipped with a PAXCam digital microscope camera and PAX-it! image management and analysis software (version 7.9, Midwest Information Systems, Inc., Villa Park, IL, USA).

Immunohistochemical staining

Immunohistochemistry staining was perform on vaginal tissue section to identify possible inflammation of mice genital tract following C^+MRP treatment (24 h). It is generally accepted that an increased lymphocytes infiltration within the vagina epithelium is indicative of vaginal inflammation.^{413, 414} Furthermore, CD45, a receptor-linked protein, is a lymphocyte common antigen.⁴¹⁵ Therefore, lymphocyte infiltration was assessed by staining the tissue using a primary anti-CD45 antibody and following the method described in immunohistochemistry protocol (ImmunoCruz™ mouse ABC Staining System, Santa Cruz Biotechnology, Dallas, TX, USA). Briefly, paraffin-embedded vaginal tissue sections were

deparaffinized and rehydrated in xylene, decreasing ethanol gradient (100%, 90%, and 70%) and deionized water. Antigen retrieval method was then conducted using heat steam method in citrate buffer/0.05% Tween-20 for 20 min. Tissue slides are further rinsed three times with TBS/0.05% Tween-20, incubated in 3% v/v H₂O₂ in PBS for 10 min, and blocked with 10% normal goat serum for 2 h (Vector Laboratories, Burlingame, CA, USA). Following the blocking step, vaginal tissue slides are incubated in the primary Anti-CD45 antibody (Santa Cruz Biotechnology, Inc., Dallas, TX, USA) diluted in 1.5% normal goat serum to 5 µg/mL. Slides were incubated overnight at 4 °C in a humidified chamber, rinsed with PBS and incubated in the biotinylated secondary antibody solution (5 µg/mL, Santa Cruz Biotechnology, Inc., Dallas, TX) at room temperature for 1 h. Tissues are then visualized using the DAB: Peroxidase Substrate Kit on Nikon Labophot-2 microscope (Nikon Instruments, Inc., Melville, NY, USA). Tissues were counter-stained with hematoxylin and treated with alcohol gradient and xylene before application of a coverslip mounted using cyto seal 60 mounting media (Richard Allan Scientific, Kalamazoo, MI).^{392, 393}

Cytokines secretion in mice cervicovaginal lavage (CVL) and cervicovaginal tissue

Following mice treatment with *C⁺MRP*, cervicovaginal lavage fluid (CVL) and cervicovaginal (CV) tissue were collected after 24 h and analyzed for pro-inflammatory cytokines secretion. Thus, IL-1 α , IL-1 β , IL-6, Interferon gamma-induced protein 10 (IP-10), IL-7, tumor necrosis factor-alpha (TNF- α) and mice keratinocyte-derived chemokine (MKC) levels were determined using a high-sensitivity multiplexed bead-based immunoassay (Milliplex MAP Mouse Cytokine/Chemokine Magnetic Bead Panel, Millipore Corp., Billerica, MA; and Luminex MAGPIX instrument, Luminex Corp., Austin, TX, USA).³¹⁹ Briefly, crude

vaginal lavage was performed by flushing mouse vaginal tract twice with 50 μ L of PBS. The vaginal lavage was then centrifuge at 1000 rpm for 10 min at 4 °C, and the supernatant (CVL) was collected. After the vaginal lavage was collected, mice were euthanized by CO₂ asphyxiation and the CV tissues were collected. When not being used, CV tissues and CVL samples were stored at -20°C to avoid any cytokines denaturation. For CV tissue extraction purposes, the homogenization buffer was prepared by mixing the protease inhibitors cocktail (Sigma, St. Louis, MO, USA) with the Tissue Extraction Reagent I (Invitrogen, Carlsbad, CA, USA). CV tissues samples were further homogenized in the homogenization buffer at 100 mg/mL using the Omni Homogenizer (Omni International, Kennesaw, GA, USA) at full speed. For maximized protein extraction ,CV tissue homogenates were kept on ice for 1 h and tissue debris were further removed by centrifuging the extract cocktail at 14,000 rpm, for 15 min at 4°C. The supernatant was then collected and kept on ice. The extraction medium was used as matrix solution, and cytokines level were assayed from CV tissue extracts and CVL following the manufacturer protocol on Luminex MAGPIX instrument equipped with xPONENT® version 4.2 software (Luminex Corp., Austin, TX), as described in chapter 5. Thus, pre-mixed magnetic beads conjugated to antibodies for all 7 cytokines analytes were mixed with equal volumes (25 μ l) of CV tissue extract and CVL supernatant (25 μ l) in 96-well plates. Plates were protected from light and incubated on a microplate shaker overnight at 4 °C. Then, magnetic beads were washed twice with 200 μ l of washing buffer. The detection antibodies were added to each well and the mixtures incubated at room temperature for 1 h. Streptavidin-phycoerythrin conjugate compound was added to each well, and the mixtures were incubated for an additional 30 min at room temperature. The magnetic beads were subsequently washed and resuspended in the washing buffer for 5 min. Plates were then assayed on the Magpix

system with Luminex xPONENT software (version 4.2, Austin, TX). Median fluorescence intensities were analyzed using a 5-parameter logistic method from a standard curve of respective analytes to determine cytokines concentration in the supernatants. All assays were conducted in duplicate.^{383, 392}

Bio-retention of FITC labelled C^+MRP in mouse genital tract

C^+MRP bio-retention in mice vaginal tract was assessed by treating C57Bl6 female mice with FITC labeled C^+MRP at a concentration of 25 mg/kg. FITC labeled C^+MRP bio-retention in mice vaginal tract was studied at two different time points (15 min and 24 h), and data were compared to FITC labeled 1% hydroxyethylcellulose (HEC) gel at the same time points. Post exposure, animals were sacrificed and the vaginal tract was removed, opened lengthwise and mounted on microscope glass slides. Fluorescence images of vaginal tissues were further acquired on Nikon Labophot-2 microscope (Nikon Instruments, Inc., Melville, NY, USA) equipped with PAXCam digital microscope camera and PAX-it! image management and analysis software (version 7.9, Midwest Information Systems, Inc., Villa Park, IL, USA).

6.3 Results and discussion

Figure 6-4 summarizes C^+MRP average particle size (diameter), surface charge density (ζ -potential) and morphology information. Single Con A layer containing C^+MRP formulation was previously shown to have a better *in vitro* mucoadhesion and an optimal drug release profile at low HIV-1 rgp120 concentrations (25 $\mu\text{g/ml}$).³⁸³ Therefore, a single Con A and glycogen layers containing C^+MRP formulation was prepared and tested in this study. C^+MRP

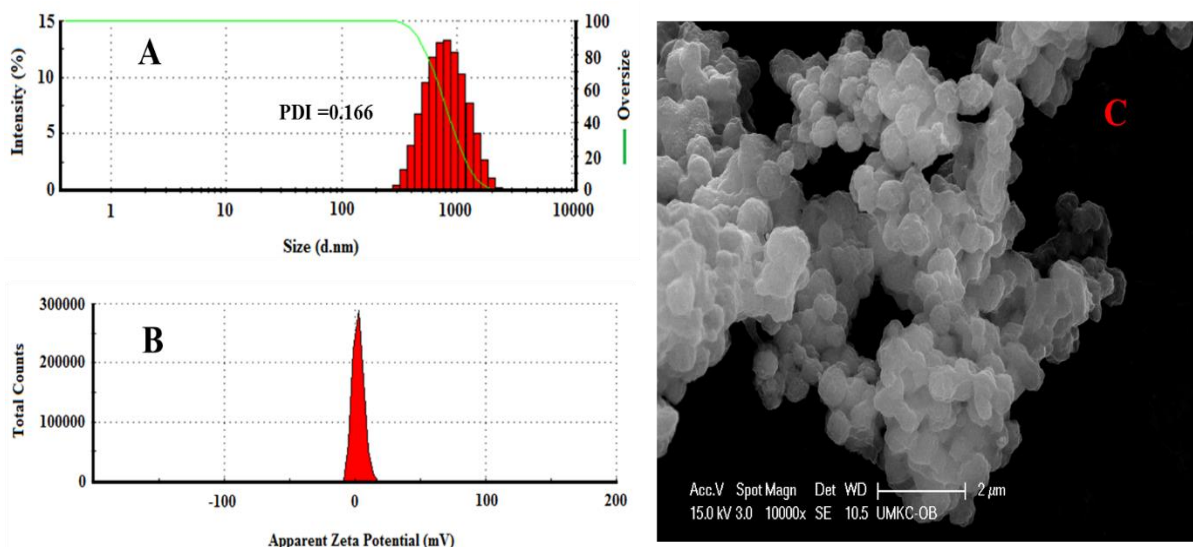


Figure 6-4: C^+ MRP average particle size (A), surface charge density (B) and SEM imaging (C). SEM image scale bar is 2 μ m.

average particle size was 857.8 ± 93.1 nm ($n=3$) (figure 6-4A) with a polydispersity index of 0.166. Although rarely attained with conventional layer-by-layer preparation techniques, PDI value lower than 0.05 is characteristic of monodispersed samples.⁴¹⁶ Nonetheless, PDI value of 0.1 to 0.7 represents nearly monodisperse preparation, whereas $PDI > 0.7$ suggests broadly distributed samples.⁴¹⁷ The ζ -potential was 2.37 ± 4.12 mV (figure 6-4B), characteristic of a neutrally charge nanoparticle formulation.⁴¹⁸ The neutral charge was probably due to the presence of glycogen onto C^+ MRP surface. The SEM image (figure 6-4C) shows $CaCO_3$ particles covered with a distinctive, smooth layer of Con A/glycogen. The feature was similar to previously reported C^+ MRP particles.³⁸³ Furthermore, particle size approximated from SEM imaging (~ 800 nm, $n=10$) was consistent with DLS size measurements data.

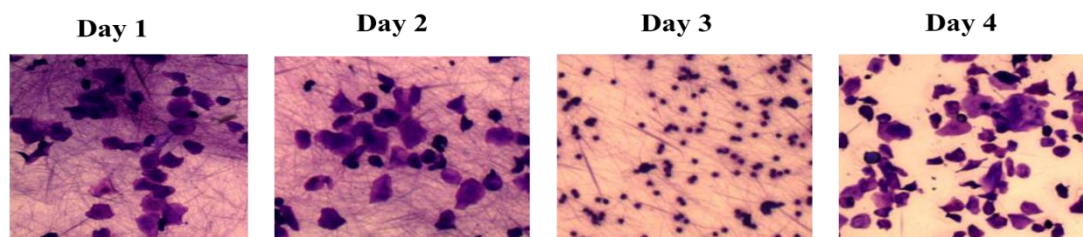
Owing to $CaCO_3$ phosphate binding properties and the co-precipitation process inherent to $CaCO_3$ crystallization, TFV was encapsulated in C^+ MRP at 70.1%. TFV drug loading in C^+ MRP was determined to be 16.3% w/w. The ability for phosphate binders, such

as CaCO_3 , to form stable complex with phosphate containing molecules has previously been demonstrated and used as drug entrapment strategy.⁴¹⁹⁻⁴²¹

The normal osmolality of vaginal and seminal secretions range between 250–380 mOsm/kg and vaginal microbicide candidates' osmolality should not exceed 400 mOsm/kg.^{321, 322, 390} Hyperosmolar vaginal formulations are known to induce vaginal epithelial damage and increase the rate and extent of watery discharges.^{386, 389} C^+MRP osmolality was 304.33 ± 0.58 mOsm/kg and was similar to normal osmolality recorded for vaginal and seminal secretions. Thus, C^+MRP is not expected to induce any pronounce vaginal discharge or epithelial damage. PBS, N-9 and BZK osmolality were were 295 ± 0 , 745.33 ± 45 and 482.2 ± 6.12 mOsm/k, respectively. In addition, mice behavior, body weight and temperature were evaluated daily during C^+MRP treatment and no significant alterations were noted.

In order to confirm the diestrus-like state of mice treated with Depo-Provera; mice CVL were constantly collected, for up to 9 days, and analyzed for evidence of nucleated and cornified squamous epithelial cells and polymorph nuclear leukocytes. After each collection, CVL was stained with crystal violet and images showed a maintained diestrus-like state in treated mice, starting from day 3 (figure 6-5). Control mice (not treated with Depo-Provera) showed distinctive changes in the estrous cycle with different cell types at different days (figure 6-5). In fact, in non-treated mice's CVL, image acquired on days 1 showed evidence of predominantly nucleated epithelial cells, with some cornified squamous epithelial cells, these features are characteristic of the proestrus stage of the estrous cycle. Similar features were also noticeable in the Depo-Provera treated group on day 1. On day 2, a mixture of cornified squamous epithelial cells and leukocyte cells were visible in non-treated mice CVL, characteristic of the late estrus and metestrus stages of the estrous cycle. These cell types

Control mice



Depo-Provera treated mice

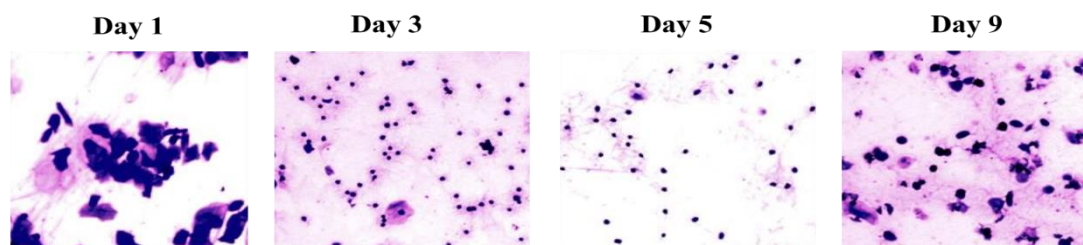


Figure 6-5: Vaginal cytology assessment of the estrous stages in Depo-Provera treated and non-treated mice. Three cell types are identified: leukocytes (blue circle), cornified epithelial (red arrow), and nucleated epithelial (white arrow).

remained visible on day 3 in non-treated mice CVL. On day 4, nucleated epithelial cells, cornified squamous epithelial cells and leukocytes were all visible in non-treated mice CVL, characteristic of diestrus-like stage, of the estrous cycle. As shown in figure 6-5, leukocytes were predominately present in the Depo-Provera treated group from day 3 through 9, which confirmed the constant diestrus-like state in that group.^{394, 395}

When mice were treated with C^+MRP for 24 h, histology analysis (figure 6-6) of reproductive organs (vagina, cervix, uterus, ovary and fallopian tube) did not show signs of abrasion of epithelial cell layer. In fact, the thickness of the vaginal epithelial cell layer (dark purple) was maintained in C^+MRP treated mice and was comparable to the negative control (PBS) treated mice in all the reproductive organs analyzed. Similar observations were also

made in cervix, uterus, ovary and fallopian tube tissues. However, visible signs of epithelial damage, including thinning and stripping were noticeable in the positive control (N-9 and BZK) groups. These observation suggested that C^+MRP treatment does not lead to an abrasion of the vaginal epithelial cell layer.

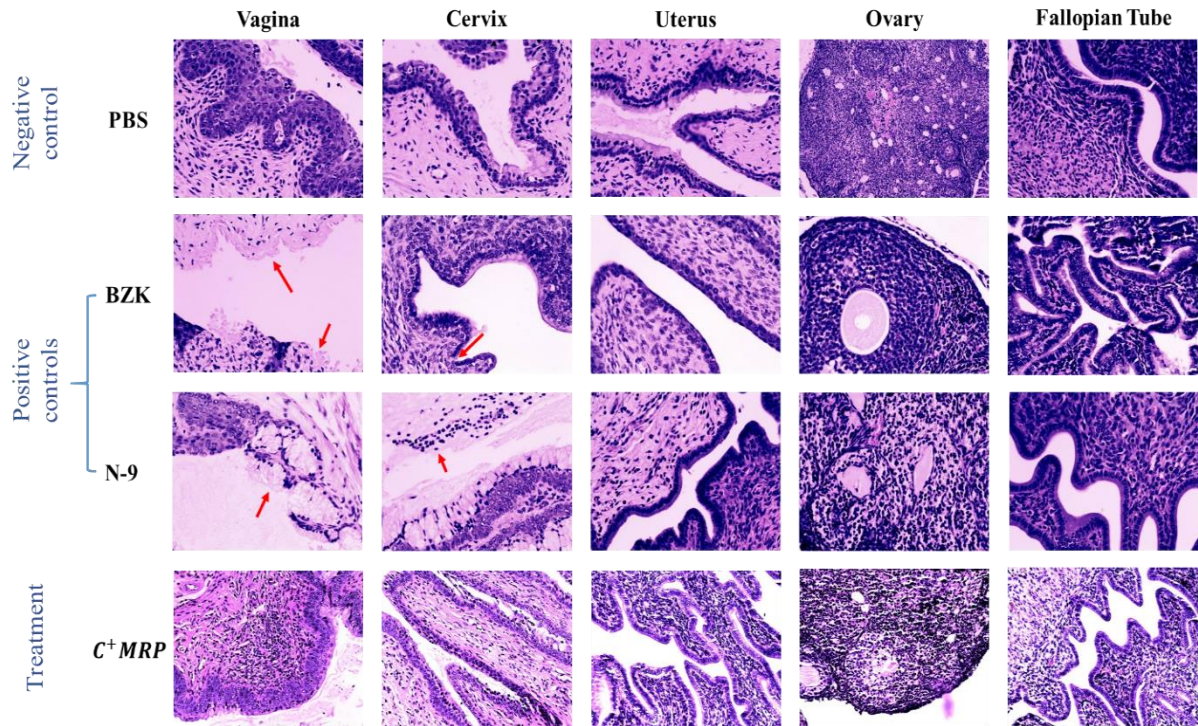


Figure 6-6: Histology (H&E staining) of mouse reproductive organs' tissues following treatment with C^+MRP for 24 h. Thinning and stripping of epithelial cell layer in positive controls is indicated by red arrows.

Immunohistochemistry analysis of vaginal tissue sections revealed minimal (not significant) CD45+ cells infiltration in the epithelial cell layer of C^+MRP treated mice. In fact, the leukocyte infiltration observed in C^+MRP treated mice was similar to the one observed in PBS treated mice, suggesting that this may not be directly related to C^+MRP .

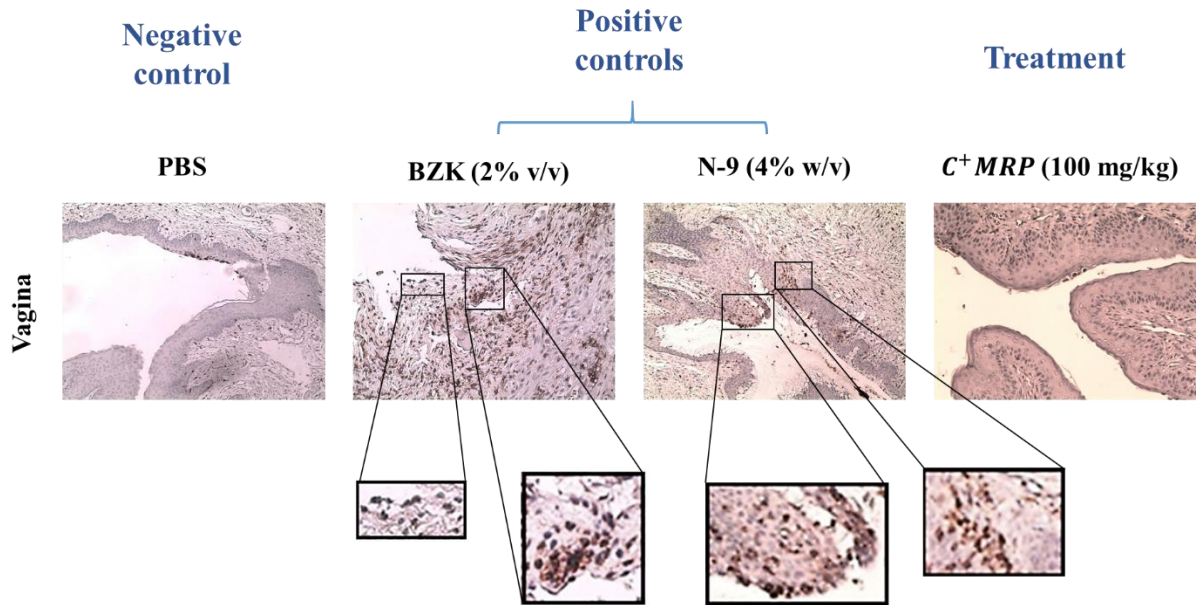


Figure 6-7: Immunohistochemistry evaluation of vaginal tissue sections following treatment with C^+MRP for 24 h. Black boxes indicated by red arrows show significant leukocyte (CD45+ cells) infiltration.

In contrast, positive controls (N-9 and BZK) treated mice showed significant leukocytes infiltration in the vaginal epithelial cell layer (figure 6-7). These immunohistochemistry observations were consistent with the histology (H&E) observations. Thus, C^+MRP does not induce major vaginal tissue inflammation in mice for up to 24 h.

A direct correlation between pro-inflammatory cytokine release and HIV vaginal infection/replication has been established.⁴²²⁻⁴²⁴ For example, binding of IL1 (α and β) to its receptor, IL1R1, results in an upregulation of other pro-inflammatory cytokines (TNF α , IL6 or IL8) release.^{357, 358} Many reports have also associated TNF α with an increase in HIV replication.^{359, 360} The pro-inflammatory cytokine IL7 is also known to facilitate HIV infection by prolonging the life of infected cells and preventing apoptosis of non-infected CD4⁺ T cells.³⁶² Likewise, IL6 and IL8 have been shown to induce an upregulation in HIV

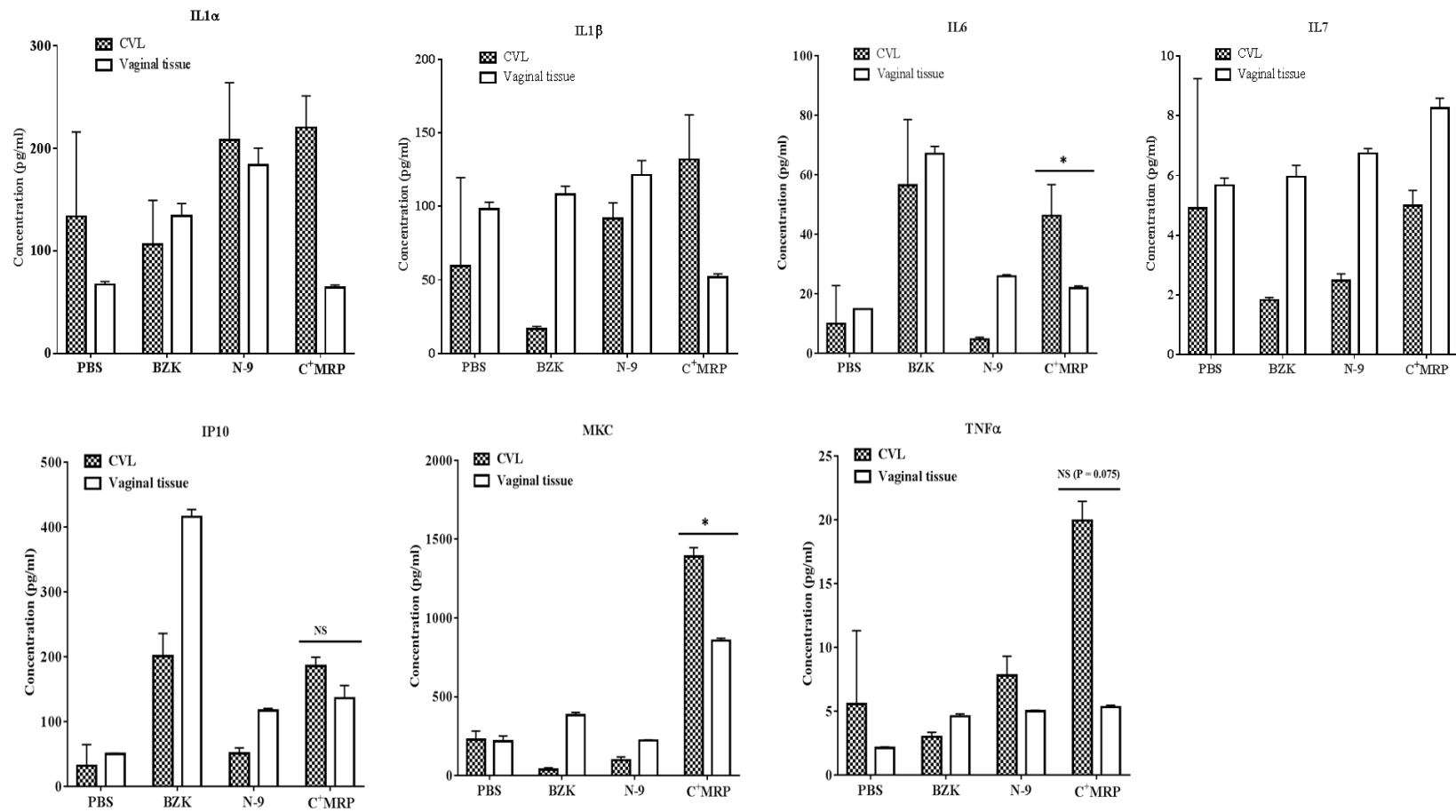


Figure 6-8: Pro-inflammatory cytokines (IL1 α , IL1 β , IL6, IL7, IP10, MKC and TNF α) levels measured in mice cervicovaginal lavage and vaginal tissue extract, following C⁺MRP treatment for 24 h, at a dose of 100 mg/kg. Values are computed from triplicates (n=3 animals). One-way anova test is performed in GraphPad (version 6.0) to determine statistical significance. * ($P \leq 0.05$) shows statistically significant difference from the negative control (PBS treated group). NS indicates non-significance ($P > 0.05$).

replication.^{425, 426} Furthermore, interferon- γ -inducible protein 10 (IP10) stimulates HIV replication by attracting activated T lymphocytes and monocytes.^{363, 364} Thus, vaginal HIV microbicide formulations should not induce an increase in pro-inflammatory cytokines' level.⁴²⁷ In this study, seven (7) pro-inflammatory cytokines including, IL1 α , IL1 β , IL6, IL7, IP10, TNF α , as well as, the mouse functional analogue of human IL-8, MKC are evaluated in *C⁺MRP* treated mice cervicovaginal lavage and vaginal tissue extract. As summarized in figure 6-8, no significant difference in pro-inflammatory cytokines IL1 α , IL1 β , IL7, IP10 and TNF α levels was noticed between *C⁺MRP* treated mice and the negative control group (PBS). Although statistically significant increases were observed in IL6 and MKC levels in both the cervicovaginal lavage and vaginal tissue extract, these were nonetheless within their standard value ranges in accordance with the homeostasis state.⁶⁹⁻⁷³ With the absence of visible signs of inflammations in vaginal and major reproductive organs, the increase in both cytokines could be due to external factors not investigated in this study (e.g. time dependent body metabolism of individual animal). In fact, stress and the normal circadian rhythm have been associated with strong variation in cytokines' level, even in healthy individuals.⁴²⁸⁻⁴³² The relative safety of MRP formulation, compared to the positive controls, could be due, in part, to its biocompatibility. In fact, it was shown that implantable Con A-based biosensors for sugar detection do not cause any health risks at Con A concentration < 10 mg/ml.¹⁸⁷ In addition, glycogen, which is used as the principal storage form of glucose (energy) in animal cells, is well known for its safety and biocompatibility.^{433, 434} Furthermore, MRP isosmolality (304.33 mOsmo/Kg) might also explain its relative safety in C57BL/6 mice. Hyposmolar and hyperosmolar vaginal formulations can induce severe epithelial damage (vaginal lesions and

epithelial cells' rupture) and discomforts (increased vaginal discharge or dehydration) which could result in pronounce HIV infection.^{386, 389, 390}

Figure 6-9 summarizes FITC labeled C^+MRP distribution (retention) in mice vaginal tract. Although a significant short time retention was initially observed, only few FITC labeled C^+MRP particles were visible after 24 h. In fact, compared to FITC labeled HEC gel, the result shows a significantly low long-term vaginal retention of FITC labeled C^+MRP . Thus, in contrast to the *in vitro* findings on porcine vaginal tissue (chapter 5), FITC labeled C^+MRP does not have a long residence time in mice vaginal tract. This could be due to structural or physiological differences between both vaginal tissues. Moreover, FITC labeled C^+MRP may

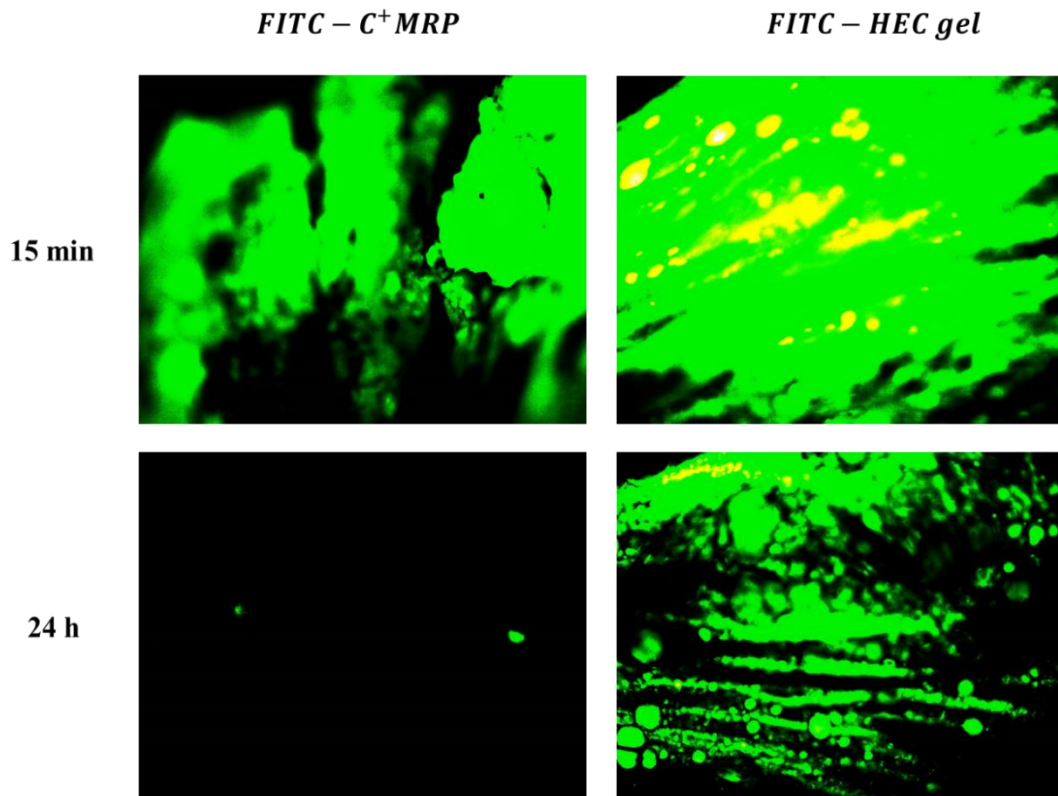


Figure 6-9: Vaginal retention of FITC labeled C^+MRP and HEC gel in mice after 24 h. C^+MRP was applied at a dose of 25 mg/kg.

leak out of mice vaginal tract due to the natural mucus renewal cycle.²⁵ This result also suggest that a potential clinical use of C^+MRP will probably require either a precoital or multiple vaginal applications to ensure enough C^+MRP particles and TFV in the vaginal cavity capable of eliciting a desired HIV preventive activity.

6.4 Conclusion

In this study, the preclinical safety of mannose and HIV-1 gp120 responsive microbicide drug delivery system (C^+MRP) was investigated on C57BL/6 mice model. TFV loaded C^+MRP was prepared through the layer-by-layer deposition of Con A and glycogen onto a $CaCO_3$ -PSS core particle. The microbicide formulation was delivered vaginally at a dose of 100 mg/kg in PBS, and vaginal histology, immunohistochemistry evaluations and pro-inflammatory cytokines release were investigated after 24 h. The vaginal retention of FITC labeled C^+MRP was also evaluated, up to 24 h. Vaginal and major reproductive organs' histology did not show major damage of the epithelial layer. This result was also consistent with immunohistochemistry evaluation of CD45+ cells infiltration in the vaginal epithelial layer, unlike the positive control treated groups (BZK and N-9). Thus, no visible signs of inflammation were observable after 24 h exposure. Furthermore, Furthermore, no biologically significant increase was observed in all the pro-inflammatory cytokines tested. In addition, it was also observed that FITC labeled C^+MRP does not have a long-term retention in mice vaginal tract. This result suggested that a precoital or multiple vaginal application (i.e., BID) approaches of C^+MRP should be investigated.

CHAPTER 7

SUMMARY AND FUTURE STUDIES

7.1 Summary

Since its discovery in 1983, Human Immunodeficiency Virus infection and Acquired Immune Deficiency Syndrome (HIV/AIDS) has remained a global epidemic threat. Unfortunately, despite intensive global campaigns aimed at raising awareness among the most vulnerable communities, a complete cure and eradication strategy is yet to be effective against HIV/AIDS. In fact, according to the 2017 UNAIDS fact sheet, it is estimated that 36.7 million [34. million – 39.8 million] of people are currently living with HIV worldwide. Advances in antiretroviral therapy research have significantly improve HIV/AIDS patients live and survival. Nonetheless, sexual transmission of HIV remains the major route (75 to 85%) by which all new HIV infections occur. In addition, women remain the most vulnerable population affected by HIV/AIDS infection. Novel vaginal and rectally applicable microbicide formulations have been proposed as a potential solution for the prevention of HIV sexual transmission with limited success. The current dissertation aimed to test the hypothesis that a lectin-based vaginal microbicide formulation can be developed to target HIV envelope glycoprotein (HIV gp120) for a safer and controlled drug release therapy.

In chapter 1 and 2, the scope of HIV epidemic, the general hypothesis of this dissertation and major considerations in vaginal microbicides formulation development are presented. Chapter 3 focuses on the review of anti-HIV lectins and their delivery strategies currently investigated. In Chapter 4, we investigated the use of quartz crystal microbalance (QCM) to study the binding affinity of the mannose binding lectin concanavalin A (Con A) to

a glucose based polysaccharide (glycogen from Oyster) and a mannose based polysaccharide (mannan from *Saccharomyces cerevisiae*). It was observed that the equilibrium dissociation constant for the interaction between Con A and glycogen ($K_D = 0.25 \mu\text{M}$) was about 12 fold lower than the equilibrium dissociation constant describing the binding between Con A and mannan ($K_D = 2.89 \mu\text{M}$). Thus Con A, a mannose specific lectin, was found to have a higher affinity to glycogen from Oyster, a glucose-base polysaccharide, than to mannan from *Saccharomyces cerevisiae*, a mannose-based polysaccharide. This observation was mainly attributed to steric effects, the molecular weight difference and the branching pattern of both polysaccharides.

Knowledge learned from the QCM study was applied in Chapter 5 for the development of a lectin-based mannose sensitive drug delivery system. Thus, HIV-1 gp120 and mannose responsive particles (MRP) were prepared via the layer-by-layer coating of a calcium carbonate (CaCO_3) core template with the mannose specific lectin (Con A) and a polysaccharide cross-linker (Glycogen). Core dissolved MRP (C^-MRP) and core containing MRP (C^+MRP) were prepared, characterized and tested in vitro on *Lactobacillus crispatus*, Human vaginal keratinocytes (VK2/E6E7) and murine macrophage [RAW 264.7 (TIB-71)] cell lines. C^+MRP average size and ζ -potential were $1130 \pm 15.72 \text{ nm}$ [PDI = 0.153] and $-15.1 \pm 0.55 \text{ mV}$, (n=3). Similarly, C^-MRP average size and ζ -potential were $1089 \pm 23.33 \text{ nm}$ (n=3) and $-14.2 \pm 0.25 \text{ mV}$ (n=3). Tenofovir (TFV) encapsulation efficiency in CaCO_3 core particle was 74.4% with drug loading of 16.3% w/w and 6.0% w/w in C^+MRP and C^-MRP , respectively. Both C^-MRP and C^+MRP were nontoxic to *L. crispatus* and did not induce any significant pro-inflammatory nitric oxide release in VK2 and RAW 264.7 cell culture. Nonetheless, C^-MRP was found to significantly affect VK2 and RAW 264.7 cells viability at

concentrations ≥ 100 $\mu\text{g/ml}$. Similarly, C^-MRP significantly increased pro-inflammatory cytokines (IL1 α , IL1 β , IL6, IL7, MKC and TNF α) release at concentrations ≥ 100 $\mu\text{g/ml}$. Conversely, C^+MRP did not induce any significant changes in VK2 and RAW 264.7 cells viability nor in pro-inflammatory cytokines' levels, in the concentration range tested (≤ 1000 $\mu\text{g/ml}$), for 24 h. Therefore, C^+MRP was selected for further *in vitro* drug release studies as well as *ex vivo* vaginal mucoadhesion studies. In fact, it was observed that HIV gp120 triggers TFV release from C^+MRP in a concentration dependent manner. TFV was released from C^+MRP which following Hixson–Crowell and Hopfenberg kinetic models, consistent with drug release from diminishing surface or matrix eroding drug particles. C^+MRP was further optimized by varying the number of Con A layer in the formulation, and in order to achieve lower HIV gp120 sensitivity (≤ 100 $\mu\text{g/ml}$). Furthermore, bioadhesion studies, performed *ex vivo* on porcine vaginal tissue, demonstrated that fluorescein (FITC) labeled C^+MRP adhere to vaginal tissue at rates varying between $10\% \pm 1$ and $20\% \pm 2$, depending on the number of Con A layers in the formulation. Thus, it was determined that the optimal MRP formulation consisted of C^+MRP containing 1 Con A/glycogen bilayer with a TFV %LD of 16.3%, an %EE of $\geq 70\%$, an average size of ~ 850 nm and a surface charge density of +2.4 mV.

In chapter 6, the optimal C^+MRP preclinical safety was evaluated in C57BL/6 mice model. Mice were initially treated with Depo-Provera to maintain them in a diestrus-like state. The microbicide formulation was delivered vaginally at a dose of 100 mg/kg in PBS, and vaginal histology, immunohistochemistry evaluations, as well as pro-inflammatory cytokines release (vaginal lavage and tissue extract) were investigated after 24 h. The vaginal retention of FITC labeled C^+MRP was also evaluated, up to 24 h. Vaginal and major reproductive organs' histology did not show major damage of the epithelial layer. This result was also

consistent with immunohistochemistry evaluation of CD45+ cells infiltration in the vaginal epithelial layer, unlike the positive control treated groups (BZK and N-9). Furthermore, no statistically significant increase was observed in, pro-inflammatory cytokines (IL1 α , IL1 β , IL7, IP10 and TNF α). In addition, it was observed that FITC labeled *C⁺MRP* does not have a long-term retention in mice vaginal tract. This result suggested that a precoital or multiple vaginal application approaches of *C⁺MRP* should be investigated. Overall, the preclinical data suggested that *C⁺MRP* induces minor vaginal cytotoxicity at 100 mg/kg.

7.2. Future studies

The development and preclinical testing of *C⁺MRP* represents a major step in lectin-based vaginal microbicide drug delivery and their potential to prevent HIV sexual transmission. However, further in-depth investigations of *C⁺MRP* are needed. In fact, *C⁺MRP* long and short term stability needs to be thoroughly investigated. Furthermore, future studies also need to investigate a dose escalation of *C⁺MRP* to identify its MTD in C57BL/6 mice model. In addition, the pharmacokinetic of TFV released from *C⁺MRP* needs be investigated in C57BL/6 mice. More importantly, *C⁺MRP* efficacy against HIV virus replication will need to be investigated and compared to free TFV drug.

Although this dissertation focused on a model natural lectin (Con A), synthetic lectins, such as phenylboronic acids (PBA), could be evaluated for the prevention of HIV transmission through the so-called HIV virion capture therapy. The success of synthetic lectins will probably rely on novel drug delivery carriers such as closomers, dendrimers and liposomes, capable of achieving higher surface density of PBA, which was been shown to be critical for their microbicidal activity.

APPENDIX

12/15/2017

Rightslink® by Copyright Clearance Center



RightsLink®

Home

Create Account

Help



Title: Concanavalin A–Polysaccharides binding affinity analysis using a quartz crystal microbalance

Author: Fohona S. Coulibaly, Bi-Botti C. Youan

Publication: Biosensors and Bioelectronics

Publisher: Elsevier

Date: 15 September 2014

Copyright © 2014 Elsevier B.V. Published by Elsevier B.V. All rights reserved.

LOGIN

If you're a [copyright.com](#) user, you can login to RightsLink using your [copyright.com](#) credentials. Already a [RightsLink](#) user or want to [learn more?](#)

Please note that, as the author of this Elsevier article, you retain the right to include it in a thesis or dissertation, provided it is not published commercially. Permission is not required, but please ensure that you reference the journal as the original source. For more information on this and on your other retained rights, please visit: <https://www.elsevier.com/about/our-business/policies/copyright#Author-rights>

BACK

CLOSE WINDOW

Copyright © 2017 [Copyright Clearance Center, Inc.](#) All Rights Reserved. [Privacy statement](#). [Terms and Conditions](#). Comments? We would like to hear from you. E-mail us at customercare@copyright.com



RightsLink®

[Home](#)[Create Account](#)[Help](#)

ACS Publications
Most Trusted. Most Cited. Most Read.

Title: Layer-by-Layer Engineered Microbicide Drug Delivery System Targeting HIV-1 gp120: Physicochemical and Biological Properties

Author: Fohona S. Coulibaly, Miezán J. M. Ezoulin, Sudhaunshu S. Purohit, et al

Publication: Molecular Pharmaceutics

Publisher: American Chemical Society

Date: Oct 1, 2017

Copyright © 2017, American Chemical Society

[LOGIN](#)

If you're a [copyright.com](#) user, you can login to RightsLink using your [copyright.com](#) credentials. Already a [RightsLink](#) user or want to [learn more?](#)

PERMISSION/LICENSE IS GRANTED FOR YOUR ORDER AT NO CHARGE

This type of permission/license, instead of the standard Terms & Conditions, is sent to you because no fee is being charged for your order. Please note the following:

- Permission is granted for your request in both print and electronic formats, and translations.
- If figures and/or tables were requested, they may be adapted or used in part.
- Please print this page for your records and send a copy of it to your publisher/graduate school.
- Appropriate credit for the requested material should be given as follows: "Reprinted (adapted) with permission from (COMPLETE REFERENCE CITATION). Copyright (YEAR) American Chemical Society." Insert appropriate information in place of the capitalized words.
- One-time permission is granted only for the use specified in your request. No additional uses are granted (such as derivative works or other editions). For any other uses, please submit a new request.

[BACK](#)[CLOSE WINDOW](#)

REFERENCES

- (1) Grulich, A. E.; van Leeuwen, M. T.; Falster, M. O.; Vajdic, C. M. Incidence of Cancers in People With HIV/AIDS Compared With Immunosuppressed Transplant Recipients: A Meta-Analysis. *Lancet* **2007**, *370*, (9581), 59-67.
- (2) Hernandez-Ramirez, R. U.; Shiels, M. S.; Dubrow, R.; Engels, E. A. Cancer Risk in HIV-Infected People in the USA From 1996 To 2012: A Population-Based, Registry-Linkage Study. *Lancet HIV* **2017**.
- (3) Wang, C. C.; Silverberg, M. J.; Abrams, D. I. Non-AIDS-Defining Malignancies in the HIV-Infected Population. *Curr Infect Dis Rep* **2014**, *16*, (6), 406.
- (4) Silverberg, M. J.; Lau, B.; Achenbach, C. J.; Jing, Y.; Althoff, K. N.; D'Souza, G.; Engels, E. A.; Hessol, N. A.; Brooks, J. T.; Burchell, A. N.; Gill, M. J.; Goedert, J. J.; Hogg, R.; Horberg, M. A.; Kirk, G. D.; Kitahata, M. M.; Korthuis, P. T.; Mathews, W. C.; Mayor, A.; Modur, S. P.; Napravnik, S.; Novak, R. M.; Patel, P.; Rachlis, A. R.; Sterling, T. R.; Willig, J. H.; Justice, A. C.; Moore, R. D.; Dubrow, R. Cumulative Incidence of Cancer Among Persons With HIV in North America: A Cohort Study. *Ann Intern Med* **2015**, *163*, (7), 507-18.
- (5) Coghill, A. E.; Shiels, M. S.; Suneja, G.; Engels, E. A. Elevated Cancer-Specific Mortality Among HIV-Infected Patients in the United States. *J Clin Oncol* **2015**, *33*, (21), 2376-83.
- (6) Coghill, A. E.; Pfeiffer, R. M.; Shiels, M. S.; Engels, E. A. Excess Mortality among HIV-Infected Individuals With Cancer in the United States. *Cancer Epidemiol Biomarkers Prev* **2017**, *26*, (7), 1027-1033.
- (7) UNAIDS. Fact Sheet - Latest Statistics on the Status of the AIDS Epidemic. <http://www.unaids.org/en/resources/fact-sheet>. (10/23/2017).
- (8) UNAIDS. People Living With HIV. <http://aidsinfo.unaids.org/>. (10/23/2017).

- (9) Swanson, M. D.; Winter, H. C.; Goldstein, I. J.; Markovitz, D. M. A Lectin Isolated From Bananas is a Potent Inhibitor of HIV Replication. *J Biol Chem* **2010**, *285*, (12), 8646-55.
- (10) Murphy, E. M.; Greene, M. E.; Mihailovic, A.; Olupot-Olupot, P. Was the "ABC" Approach (Abstinence, Being Faithful, Using Condoms) Responsible for Uganda's Decline in HIV? *PLoS Med* **2006**, *3*, (9), e379.
- (11) Cohen, S. A. Promoting the 'B' in ABC: Its Value and Limitations in Fostering Reproductive Health. <https://www.guttmacher.org/gpr/2004/11/promoting-b-abc-its-value-and-limitations-fostering-reproductive-health>. (10/23/2017).
- (12) Sovran, S. Understanding Culture and HIV/AIDS in Sub-Saharan Africa. *Sahara J* **2013**, *10*, (1), 32-41.
- (13) Reniers, G.; Watkins, S. Polygyny and the Spread of HIV in Sub-Saharan Africa: A Case of Benign Concurrency. *Aids* **2010**, *24*, (2), 299-307.
- (14) Helweg-Larsen, M.; Collins, B. E. The UCLA Multidimensional Condom Attitudes Scale: Documenting the Complex Determinants of Condom Use in College Students. *Health Psychol* **1994**, *13*, (3), 224-37.
- (15) The World Bank. Women's Share of Population Ages 15+ Living With HIV (%). <https://data.worldbank.org/indicator/SH.DYN.AIDS.FE.ZS>. (10/23/2017).
- (16) Ramjee, G.; Daniels, B. Women and HIV in Sub-Saharan Africa. *AIDS Res Ther* **2013**, *10*, (1), 30.
- (17) Wira, C. R.; Fahey, J. V. A New Strategy to Understand How HIV Infects Women: Identification of a Window of Vulnerability During the Menstrual Cycle. *Aids* **2008**, *22*, (15), 1909-17.

- (18) Mabala, R. From HIV Prevention to HIV Protection: Addressing the Vulnerability of Girls and Young Women in Urban Areas. *Environment & Urbanization* **2006**, *18*, (2), 407-432.
- (19) Gupta, G. R. How Men's Power Over Women Fuels the HIV Epidemic. *Bmj* **2002**, *324*, (7331), 183-4.
- (20) Jewkes, R. K.; Levin, J. B.; Penn-Kekana, L. A. Gender Inequalities, Intimate Partner Violence and HIV Preventive Practices: Findings of a South African Cross-Sectional Study. *Soc Sci Med* **2003**, *56*, (1), 125-34.
- (21) Royce, R. A.; Sena, A.; Cates, W., Jr.; Cohen, M. S. Sexual Transmission of HIV. *N Engl J Med* **1997**, *336*, (15), 1072-8.
- (22) UNAIDS. Gap Report.
<http://www.unaids.org/en/resources/campaigns/2014/2014gapreport/gapreport>. (4/25/2016).
- (23) Hunter, D. J. AIDS in Sub-Saharan Africa: The Epidemiology of Heterosexual Transmission and the Prospects for Prevention. *Epidemiology* **1993**, *4*, (1), 63-72.
- (24) Heneine, W.; Kashuba, A. HIV Prevention by Oral Preexposure Prophylaxis. *Cold Spring Harb Perspect Med* **2012**, *2*, (3), a007419.
- (25) Rohan, L. C.; Sassi, A. B. Vaginal Drug Delivery Systems for HIV Prevention. *Aaps J* **2009**, *11*, (1), 78-87.
- (26) Valley-Omar, Z.; Sibeko, S.; Anderson, J.; Goodier, S.; Werner, L.; Arney, L.; Naranbhai, V.; Treurnicht, F.; Abrahams, M. R.; Bandawe, G.; Swanstrom, R.; Karim, Q. A.; Karim, S. S.; Williamson, C. CAPRISA 004 Tenofovir Microbicide Trial: No Impact of Tenofovir Gel on the HIV Transmission Bottleneck. *J Infect Dis* **2012**, *206*, (1), 35-40.

- (27) Xu, L.; Liu, Y.; Chen, Z.; Li, W.; Wang, L.; Wu, X.; Ji, Y.; Zhao, Y.; Ma, L.; Shao, Y.; Chen, C. Surface-Engineered Gold Nanorods: Promising DNA Vaccine Adjuvant for HIV-1 Treatment. *Nano Lett* **2012**, *12*, (4), 2003-12.
- (28) Baeten, J. M.; Palanee-Phillips, T.; Brown, E. R.; Schwartz, K.; Soto-Torres, L. E.; Govender, V.; Mgodhi, N. M.; Matovu Kiweewa, F.; Nair, G.; Mhlanga, F.; Siva, S.; Bekker, L. G.; Jeenarain, N.; Gaffoor, Z.; Martinson, F.; Makanani, B.; Pather, A.; Naidoo, L.; Husnik, M.; Richardson, B. A.; Parikh, U. M.; Mellors, J. W.; Marzinke, M. A.; Hendrix, C. W.; van der Straten, A.; Ramjee, G.; Chirenje, Z. M.; Nakabiito, C.; Taha, T. E.; Jones, J.; Mayo, A.; Scheckter, R.; Berthiaume, J.; Livant, E.; Jacobson, C.; Ndase, P.; White, R.; Patterson, K.; Germuga, D.; Galaska, B.; Bunge, K.; Singh, D.; Szydlo, D. W.; Montgomery, E. T.; Mensch, B. S.; Torjesen, K.; Grossman, C. I.; Chakhtoura, N.; Nel, A.; Rosenberg, Z.; McGowan, I.; Hillier, S. Use of a Vaginal Ring Containing Dapivirine for HIV-1 Prevention in Women. *N Engl J Med* **2016**, *375*, (22), 2121-2132.
- (29) UNAIDS. Global Report. http://www.unaids.org/globalreport/Global_report.htm. (10/25/2016).
- (30) NIH <https://aidsinfo.nih.gov/understanding-hiv-aids/glossary/3320/fusion>. (12/09/2017),
- (31) Melikyan, G. B. Common Principles and Intermediates of Viral Protein-Mediated Fusion: The HIV-1 Paradigm. *Retrovirology* **2008**, *5*, 111.
- (32) Wilen, C. B.; Tilton, J. C.; Doms, R. W. HIV: Cell Binding and Entry. *Cold Spring Harb Perspect Med* **2012**, *2*, (8).
- (33) Checkley, M. A.; Luttge, B. G.; Freed, E. O. HIV-1 Envelope Glycoprotein Biosynthesis, Trafficking, and Incorporation. *J Mol Biol* **2011**, *410*, (4), 582-608.

- (34) Campbell, E. M.; Hope, T. J. HIV-1 Capsid: The Multifaceted Key Player in HIV-1 Infection. *Nat Rev Microbiol* **2015**, *13*, (8), 471-83.
- (35) Craigie, R.; Bushman, F. D. HIV DNA Integration. *Cold Spring Harb Perspect Med* **2012**, *2*, (7), a006890.
- (36) Freed, E. O. HIV-1 Replication. *Somat Cell Mol Genet* **2001**, *26*, (1-6), 13-33.
- (37) Chen, H. Y.; Di Mascio, M.; Perelson, A. S.; Ho, D. D.; Zhang, L. Determination of Virus Burst Size in Vivo Using a Single-Cycle SIV In Rhesus Macaques. *Proc Natl Acad Sci U S A* **2007**, *104*, (48), 19079-84.
- (38) Cummins, N. W.; Badley, A. D. Making Sense of How HIV Kills Infected CD4 T Cells: Implications for HIV Cure. *Mol Cell Ther* **2014**, *2*, 20.
- (39) Elka Touitou, B. W. B., Enhancement in Drug Delivery. CRC Press Boca Raton, 2006.
- (40) Kenhub. Vagina. <https://www.kenhub.com/en/library/anatomy/vagina>. (12/09/2017),
- (41) Anderson, D. J.; Marathe, J.; Pudney, J. The Structure of the Human Vaginal Stratum Corneum and its Role in Immune Defense. *Am J Reprod Immunol* **2014**, *71*, (6), 618-23.
- (42) Petrova, M. I.; van den Broek, M.; Balzarini, J.; Vanderleyden, J.; Lebeer, S. Vaginal Microbiota and its Role in HIV Transmission and Infection. *FEMS Microbiol Rev* **2013**, *37*, (5), 762-92.
- (43) Dei, M.; Di Maggio, F.; Di Paolo, G.; Bruni, V. Vulvovaginitis in Childhood. *Best Pract Res Clin Obstet Gynaecol* **2010**, *24*, (2), 129-37.
- (44) Randelovic, G.; Mladenovic, V.; Ristic, L.; Otasevic, S.; Brankovic, S.; Mladenovic-Antic, S.; Bogdanovic, M.; Bogdanovic, D. Microbiological Aspects of Vulvovaginitis in Prepubertal Girls. *Eur J Pediatr* **2012**, *171*, (8), 1203-8.

- (45) Yamamoto, T.; Zhou, X.; Williams, C. J.; Hochwalt, A.; Forney, L. J. Bacterial Populations in the Vaginas of Healthy Adolescent Women. *J Pediatr Adolesc Gynecol* **2009**, *22*, (1), 11-8.
- (46) Brotman, R. M.; Shardell, M. D.; Gajer, P.; Fadrosh, D.; Chang, K.; Silver, M. I.; Viscidi, R. P.; Burke, A. E.; Ravel, J.; Gravitt, P. E. Association Between the Vaginal Microbiota, Menopause Status, and Signs of Vulvovaginal Atrophy. *Menopause* **2014**, *21*, (5), 450-8.
- (47) Muhleisen, A. L.; Herbst-Kralovetz, M. M. Menopause and the Vaginal Microbiome. *Maturitas* **2016**, *91*, 42-50.
- (48) Lawrence Impey, T. C., *Obstetrics and Gynaecology*. John Wiley and sons: 2016.
- (49) Bouvet, J. P.; Gresenguet, G.; Belec, L. Vaginal pH Neutralization by Semen as a Cofactor of HIV Transmission. *Clin Microbiol Infect* **1997**, *3*, (1), 19-23.
- (50) Lai, S. K.; Hida, K.; Shukair, S.; Wang, Y. Y.; Figueiredo, A.; Cone, R.; Hope, T. J.; Hanes, J. Human Immunodeficiency Virus Type 1 is Trapped by Acidic but Not by Neutralized Human Cervicovaginal Mucus. *J Virol* **2009**, *83*, (21), 11196-200.
- (51) Martin, H. L.; Richardson, B. A.; Nyange, P. M.; Lavreys, L.; Hillier, S. L.; Chohan, B.; Mandaliya, K.; Ndinya-Achola, J. O.; Bwayo, J.; Kreiss, J. Vaginal Lactobacilli, Microbial Flora, and Risk of Human Immunodeficiency Virus Type 1 and Sexually Transmitted Disease Acquisition. *J Infect Dis* **1999**, *180*, (6), 1863-8.
- (52) Dover, S. E.; Aroutcheva, A. A.; Faro, S.; Chikindas, M. L. Natural Antimicrobials and Their Role in Vaginal Health: A Short Review. *Int J Probiotics Prebiotics* **2008**, *3*, (4), 219-230.

- (53) Boily, M. C.; Baggaley, R. F.; Wang, L.; Masse, B.; White, R. G.; Hayes, R. J.; Alary, M. Heterosexual Risk of HIV-1 Infection per Sexual Act: Systematic Review and Meta-Analysis of Observational Studies. *Lancet Infect Dis* **2009**, *9*, (2), 118-29.
- (54) Conway, B.; Cameron, D. W.; Plummer, F. A.; Ronald, A. R. Heterosexual Transmission of Human Immunodeficiency Virus Infection - Strategies for Prevention. *Can J Infect Dis* **1991**, *2*, (1), 30-6.
- (55) Milam, J.; Richardson, J. L.; Espinoza, L.; Stoyanoff, S. Correlates of Unprotected Sex Among Adult Heterosexual Men Living With HIV. *J Urban Health* **2006**, *83*, (4), 669-81.
- (56) Szabo, R.; Short, R. V. How Does Male Circumcision Protect Against HIV Infection? *Bmj* **2000**, *320*, (7249), 1592-4.
- (57) Arts, E. J.; Hazuda, D. J. HIV-1 Antiretroviral Drug Therapy. *Cold Spring Harb Perspect Med* **2012**, *2*, (4), a007161.
- (58) Microbicide Trial Network. Studies. <http://www.mtnstopshiv.org/studies>. (12/14/2017).
- (59) Pau, A. K.; George, J. M. Antiretroviral Therapy: Current Drugs. *Infect Dis Clin North Am* **2014**, *28*, (3), 371-402.
- (60) Thenin-Houssier, S.; Valente, S. T. HIV-1 Capsid Inhibitors as Antiretroviral Agents. *Curr HIV Res* **2016**, *14*, (3), 270-82.
- (61) Healthline. HIV Treatments: List of Prescription Medications <https://www.healthline.com/health/hiv-aids/medications-list>. (12/14/2017).
- (62) Pirrone, V.; Thakkar, N.; Jacobson, J. M.; Wigdahl, B.; Krebs, F. C. Combinatorial Approaches to the Prevention and Treatment of HIV-1 Infection. *Antimicrob Agents Chemother* **2011**, *55*, (5), 1831-42.

- (63) Romano, J. W.; Robbiani, M.; Doncel, G. F.; Moench, T. Non-Specific Microbicide Product Development: Then and Now. *Curr HIV Res* **2012**, *10*, (1), 9-18.
- (64) Cutler, B.; Justman, J. Vaginal Microbicides and the Prevention of HIV Transmission. *Lancet Infect Dis* **2008**, *8*, (11), 685-97.
- (65) Cottrell, M. L.; Kashuba, A. D. Topical Microbicides and HIV Prevention in the Female Genital Tract. *J Clin Pharmacol* **2014**, *54*, (6), 603-15.
- (66) Abdool Karim, S. S.; Richardson, B. A.; Ramjee, G.; Hoffman, I. F.; Chirenje, Z. M.; Taha, T.; Kapina, M.; Maslankowski, L.; Coletti, A.; Profy, A.; Moench, T. R.; Piwowar-Manning, E.; Masse, B.; Hillier, S. L.; Soto-Torres, L. Safety and Effectiveness Of Buffergel and 0.5% PRO2000 Gel for the Prevention of HIV Infection in Women. *Aids* **2011**, *25*, (7), 957-66.
- (67) Fletcher, P. S.; Harman, S. J.; Boothe, A. R.; Doncel, G. F.; Shattock, R. J. Preclinical Evaluation of Lime Juice as a Topical Microbicide Candidate. *Retrovirology* **2008**, *5*, 3.
- (68) Bunge, K. E.; Dezzutti, C. S.; Rohan, L. C.; Hendrix, C. W.; Marzinke, M. A.; Richardson-Harman, N.; Moncla, B. J.; Devlin, B.; Meyn, L. A.; Spiegel, H. M.; Hillier, S. L. A Phase 1 Trial to Assess the Safety, Acceptability, Pharmacokinetics, and Pharmacodynamics of a Novel Dapivirine Vaginal Film. *J Acquir Immune Defic Syndr* **2016**, *71*, (5), 498-505.
- (69) Robinson, J. A.; Marzinke, M. A.; Bakshi, R. P.; Fuchs, E. J.; Radebaugh, C. L.; Aung, W.; Spiegel, H. M.; Coleman, J. S.; Rohan, L. C.; Hendrix, C. W. Comparison of Dapivirine Vaginal Gel and Film Formulation Pharmacokinetics and Pharmacodynamics (FAME 02B). *AIDS Res Hum Retroviruses* **2017**, *33*, (4), 339-346.

- (70) Luecke, E. H.; Cheng, H.; Woeber, K.; Nakyanzi, T.; Mudekunya-Mahaka, I. C.; van der Straten, A. Stated Product Formulation Preferences for HIV Pre-Exposure Prophylaxis Among Women in the VOICE-D (MTN-003D) Study. *J Int AIDS Soc* **2016**, *19*, (1), 20875.
- (71) Helen Rees, S. A. D.-M., Carl Lombard, Deborah Baron, Ravindre Panchia, Landon Myer, Jill L. Schwartz, Gustavo F. Doncel, Glenda Gray. FACTS 001 Phase III Trial of Pericoital Tenofovir 1% Gel for HIV Prevention in Women <http://www.croiconference.org/sessions/facts-001-phase-iii-trial-pericoital-tenofovir-1-gel-hiv-prevention-women>. (12/09/2017).
- (72) Notario-Perez, F.; Ruiz-Caro, R.; Veiga-Ochoa, M. D. Historical Development of Vaginal Microbicides to Prevent Sexual Transmission of HIV in Women: From Past Failures to Future hopes. *Drug Des Devel Ther* **2017**, *11*, 1767-1787.
- (73) Fernandez-Romero, J. A.; Teleshova, N.; Zydowsky, T. M.; Robbiani, M. Preclinical Assessments of Vaginal Microbicide Candidate Safety and Efficacy. *Adv Drug Deliv Rev* **2015**, *92*, 27-38.
- (74) Fox, C. A.; Meldrum, S. J.; Watson, B. W. Continuous Measurement by Radio-Telemetry of Vaginal pH During Human Coitus. *J Reprod Fertil* **1973**, *33*, (1), 69-75.
- (75) Tevi-Benissan, C.; Belec, L.; Levy, M.; Schneider-Fauveau, V.; Si Mohamed, A.; Hallouin, M. C.; Matta, M.; Gresenguet, G. In Vivo Semen-Associated pH Neutralization of Cervicovaginal Secretions. *Clin Diagn Lab Immunol* **1997**, *4*, (3), 367-74.
- (76) Agrahari, V., Formulation of Hyaluronidase Enzyme Sensitive Topical Nanomicrobicides for HIV Virus Transmission Prevention mospace.umsystem.edu: 2015; p 205.
- (77) Meng, J., Design and Evaluation of HIV Microbicides Loaded Mucoadhesive Nanoformulation. mospace.umsystem.edu: 2015; p 192.

- (78) Qian, K.; Morris-Natschke, S. L.; Lee, K. H. HIV Entry Inhibitors and Their Potential in HIV Therapy. *Med Res Rev* **2009**, *29*, (2), 369-93.
- (79) Fohona S. Coulibaly, B.-B. C. Y. Current Status of Lectin-Based Cancer Diagnosis and Therapy. *AIMS Molecular Science* **2017**, *4*, (1), 1-27.
- (80) Hansen, T. K.; Gall, M. A.; Tarnow, L.; Thiel, S.; Stehouwer, C. D.; Schalkwijk, C. G.; Parving, H. H.; Flyvbjerg, A. Mannose-Binding Lectin and Mortality in Type 2 Diabetes. *Arch Intern Med* **2006**, *166*, (18), 2007-13.
- (81) Guan, L. Z.; Tong, Q.; Xu, J. Elevated Serum Levels of Mannose-Binding Lectin and Diabetic Nephropathy in Type 2 Diabetes. *PLoS One* **2015**, *10*, (3), e0119699.
- (82) Losin, I. E.; Shakhnovich, R. M.; Zykov, K. A.; Ruda, M. Cardiovascular Diseases and Mannose-Binding Lectin. *Kardiologiia* **2014**, *54*, (3), 64-70.
- (83) Kelsall, A.; FitzGerald, A. J.; Howard, C. V.; Evans, R. C.; Singh, R.; Rhodes, J. M.; Goodlad, R. A. Dietary Lectins Can Stimulate Pancreatic Growth in the Rat. *Int J Exp Pathol* **2002**, *83*, (4), 203-8.
- (84) Hoyem, P. H.; Bruun, J. M.; Pedersen, S. B.; Thiel, S.; Richelsen, B.; Christiansen, J. S.; Hansen, T. K. The Effect of Weight Loss on Serum Mannose-Binding Lectin Levels. *Clin Dev Immunol* **2012**, *2012*, 354894.
- (85) Akkouh, O.; Ng, T. B.; Singh, S. S.; Yin, C.; Dan, X.; Chan, Y. S.; Pan, W.; Cheung, R. C. Lectins With Anti-HIV Activity: A Review. *Molecules* **2015**, *20*, (1), 648-68.
- (86) Koharudin, L. M.; Gronenborn, A. M. Antiviral Lectins as Potential HIV Microbicides. *Curr Opin Virol* **2014**, *7*, 95-100.

- (87) Balzarini, J.; Van Laethem, K.; Hatse, S.; Vermeire, K.; De Clercq, E.; Peumans, W.; Van Damme, E.; Vandamme, A. M.; Bolmstedt, A.; Schols, D. Profile of Resistance of Human Immunodeficiency Virus to Mannose-Specific Plant Lectins. *J Virol* **2004**, *78*, (19), 10617-27.
- (88) Huskens, D.; Van Laethem, K.; Vermeire, K.; Balzarini, J.; Schols, D. Resistance of HIV-1 to the Broadly HIV-1-Neutralizing, Anti-Carbohydrate Antibody 2G12. *Virology* **2007**, *360*, (2), 294-304.
- (89) Blumenthal, R.; Durell, S.; Viard, M. HIV Entry and Envelope Glycoprotein-Mediated Fusion. *J Biol Chem* **2012**, *287*, (49), 40841-9.
- (90) Ratner, L.; Haseltine, W.; Patarca, R.; Livak, K. J.; Starcich, B.; Josephs, S. F.; Doran, E. R.; Rafalski, J. A.; Whitehorn, E. A.; Baumeister, K.; et al. Complete Nucleotide Sequence of the AIDS Virus, HTLV-III. *Nature* **1985**, *313*, (6000), 277-84.
- (91) Allan, J. S.; Coligan, J. E.; Barin, F.; McLane, M. F.; Sodroski, J. G.; Rosen, C. A.; Haseltine, W. A.; Lee, T. H.; Essex, M. Major Glycoprotein Antigens that Induce Antibodies in AIDS Patients are Encoded By HTLV-III. *Science* **1985**, *228*, (4703), 1091-4.
- (92) Montagnier, L.; Clavel, F.; Krust, B.; Chamaret, S.; Rey, F.; Barre-Sinoussi, F.; Chermann, J. C. Identification and Antigenicity of the Major Envelope Glycoprotein of Lymphadenopathy-Associated Virus. *Virology* **1985**, *144*, (1), 283-9.
- (93) Wain-Hobson, S.; Sonigo, P.; Danos, O.; Cole, S.; Alizon, M. Nucleotide Sequence of the AIDS Virus, LAV. *Cell* **1985**, *40*, (1), 9-17.
- (94) Mizuochi, T.; Spellman, M. W.; Larkin, M.; Solomon, J.; Basa, L. J.; Feizi, T. Carbohydrate Structures of the Human-Immunodeficiency-Virus (HIV) Recombinant Envelope Glycoprotein Gp120 Produced in Chinese-Hamster Ovary Cells. *Biochem J* **1988**, *254*, (2), 599-603.

- (95) Mizuochi, T.; Spellman, M. W.; Larkin, M.; Solomon, J.; Basa, L. J.; Feizi, T. Structural Characterization by Chromatographic Profiling of the Oligosaccharides of Human Immunodeficiency Virus (HIV) Recombinant Envelope Glycoprotein gp120 Produced in Chinese Hamster Ovary Cells. *Biomed Chromatogr* **1988**, *2*, (6), 260-70.
- (96) Mizuochi, T.; Matthews, T. J.; Kato, M.; Hamako, J.; Titani, K.; Solomon, J.; Feizi, T. Diversity of Oligosaccharide Structures on the Envelope Glycoprotein gp 120 of Human Immunodeficiency Virus 1 From the Lymphoblastoid Cell Line H9. Presence of Complex-Type Oligosaccharides With Bisecting N-Acetylglucosamine Residues. *J Biol Chem* **1990**, *265*, (15), 8519-24.
- (97) Geyer, H.; Holschbach, C.; Hunsmann, G.; Schneider, J. Carbohydrates of Human Immunodeficiency Virus. Structures of Oligosaccharides Linked to the Envelope Glycoprotein 120. *J Biol Chem* **1988**, *263*, (24), 11760-7.
- (98) Go, E. P.; Hewawasam, G.; Liao, H. X.; Chen, H.; Ping, L. H.; Anderson, J. A.; Hua, D. C.; Haynes, B. F.; Desaire, H. Characterization of Glycosylation Profiles of HIV-1 Transmitted/Founder Envelopes by Mass Spectrometry. *J Virol* **2011**, *85*, (16), 8270-84.
- (99) Bonomelli, C.; Doores, K. J.; Dunlop, D. C.; Thaney, V.; Dwek, R. A.; Burton, D. R.; Crispin, M.; Scanlan, C. N. The Glycan Shield of HIV is Predominantly Oligomannose Independently of Production System or Viral Clade. *PLoS One* **2011**, *6*, (8), e23521.
- (100) Go, E. P.; Herschhorn, A.; Gu, C.; Castillo-Menendez, L.; Zhang, S.; Mao, Y.; Chen, H.; Ding, H.; Wakefield, J. K.; Hua, D.; Liao, H. X.; Kappes, J. C.; Sodroski, J.; Desaire, H. Comparative Analysis of the Glycosylation Profiles of Membrane-Anchored HIV-1 Envelope Glycoprotein Trimers and Soluble gp140. *J Virol* **2015**, *89*, (16), 8245-57.

- (101) Raska, M.; Takahashi, K.; Czernekova, L.; Zachova, K.; Hall, S.; Moldoveanu, Z.; Elliott, M. C.; Wilson, L.; Brown, R.; Jancova, D.; Barnes, S.; Vrbkova, J.; Tomana, M.; Smith, P. D.; Mestecky, J.; Renfrow, M. B.; Novak, J. Glycosylation Patterns of HIV-1 gp120 Depend on the Type of Expressing Cells and Affect Antibody Recognition. *J Biol Chem* **2010**, *285*, (27), 20860-9.
- (102) Zhu, X.; Borchers, C.; Bienstock, R. J.; Tomer, K. B. Mass Spectrometric Characterization of the Glycosylation Pattern of HIV-Gp120 Expressed in CHO Cells. *Biochemistry* **2000**, *39*, (37), 11194-204.
- (103) Doores, K. J.; Bonomelli, C.; Harvey, D. J.; Vasiljevic, S.; Dwek, R. A.; Burton, D. R.; Crispin, M.; Scanlan, C. N. Envelope Glycans of Immunodeficiency Virions are Almost Entirely Oligomannose Antigens. *Proc Natl Acad Sci U S A* **2010**, *107*, (31), 13800-5.
- (104) Behrens, A. J.; Harvey, D. J.; Milne, E.; Cupo, A.; Kumar, A.; Zitzmann, N.; Struwe, W. B.; Moore, J. P.; Crispin, M. Molecular Architecture of the Cleavage-Dependent Mannose Patch on a Soluble HIV-1 Envelope Glycoprotein Trimer. *J Virol* **2017**, *91*, (2).
- (105) Sok, D.; Doores, K. J.; Briney, B.; Le, K. M.; Saye-Francisco, K. L.; Ramos, A.; Kulp, D. W.; Julien, J. P.; Menis, S.; Wickramasinghe, L.; Seaman, M. S.; Schief, W. R.; Wilson, I. A.; Poignard, P.; Burton, D. R. Promiscuous Glycan Site Recognition by Antibodies to the High-Mannose Patch of gp120 Broadens Neutralization of HIV. *Sci Transl Med* **2014**, *6*, (236), 236ra63.
- (106) Pritchard, L. K.; Spencer, D. I.; Royle, L.; Bonomelli, C.; Seabright, G. E.; Behrens, A. J.; Kulp, D. W.; Menis, S.; Krumm, S. A.; Dunlop, D. C.; Crispin, D. J.; Bowden, T. A.; Scanlan, C. N.; Ward, A. B.; Schief, W. R.; Doores, K. J.; Crispin, M. Glycan Clustering

Stabilizes the Mannose Patch of HIV-1 and Preserves Vulnerability to Broadly Neutralizing Antibodies. *Nat Commun* **2015**, *6*, 7479.

(107) Coss, K. P.; Vasiljevic, S.; Pritchard, L. K.; Krumm, S. A.; Glaze, M.; Madzorera, S.; Moore, P. L.; Crispin, M.; Doores, K. J. HIV-1 Glycan Density Drives the Persistence of the Mannose Patch within an Infected Individual. *J Virol* **2016**, *90*, (24), 11132-11144.

(108) Raska, M.; Novak, J. Involvement of Envelope-Glycoprotein Glycans in HIV-1 Biology and Infection. *Arch Immunol Ther Exp (Warsz)* **2010**, *58*, (3), 191-208.

(109) Wang, S. K.; Liang, P. H.; Astronomo, R. D.; Hsu, T. L.; Hsieh, S. L.; Burton, D. R.; Wong, C. H. Targeting the Carbohydrates on HIV-1: Interaction of Oligomannose Dendrons With Human Monoclonal Antibody 2G12 and DC-SIGN. *Proc Natl Acad Sci U S A* **2008**, *105*, (10), 3690-5.

(110) Balzarini, J. Targeting the Glycans of gp120: A Novel Approach Aimed at the Achilles Heel of HIV. *Lancet Infect Dis* **2005**, *5*, (11), 726-31.

(111) Koch, M.; Pancera, M.; Kwong, P. D.; Kolchinsky, P.; Grundner, C.; Wang, L.; Hendrickson, W. A.; Sodroski, J.; Wyatt, R. Structure-Based, Targeted Deglycosylation of HIV-1 gp120 and Effects on Neutralization Sensitivity and Antibody Recognition. *Virology* **2003**, *313*, (2), 387-400.

(112) Rathore, U.; Saha, P.; Kesavardhana, S.; Kumar, A. A.; Datta, R.; Devanarayanan, S.; Das, R.; Mascola, J. R.; Varadarajan, R. Glycosylation of the Core of The HIV-1 Envelope Subunit Protein gp120 is Not Required for Native Trimer Formation or Viral Infectivity. *J Biol Chem* **2017**.

(113) Sanders, R. W.; van Anken, E.; Nabatov, A. A.; Liscaljet, I. M.; Bontjer, I.; Eggink, D.; Melchers, M.; Busser, E.; Dankers, M. M.; Groot, F.; Braakman, I.; Berkhout, B.; Paxton, W.

A. The Carbohydrate at Asparagine 386 on HIV-1 gp120 is Not Essential for Protein Folding and Function but is Involved in Immune Evasion. *Retrovirology* **2008**, *5*, 10.

(114) Montefiori, D. C.; Robinson, W. E., Jr.; Mitchell, W. M. Role of Protein N-Glycosylation in Pathogenesis of Human Immunodeficiency Virus Type 1. *Proc Natl Acad Sci U S A* **1988**, *85*, (23), 9248-52.

(115) Francois, K. O.; Balzarini, J. The highly Conserved Glycan at Asparagine 260 of HIV-1 gp120 is Indispensable for Viral Entry. *J Biol Chem* **2011**, *286*, (50), 42900-10.

(116) Mathys, L.; Francois, K. O.; Quandt, M.; Braakman, I.; Balzarini, J. Deletion of the Highly Conserved N-Glycan at Asn260 of HIV-1 gp120 Affects Folding and Lysosomal Degradation of gp120, and Results in Loss of Viral Infectivity. *PLoS One* **2014**, *9*, (6), e101181.

(117) Behrens, A. J.; Vasiljevic, S.; Pritchard, L. K.; Harvey, D. J.; Andev, R. S.; Krumm, S. A.; Struwe, W. B.; Cupo, A.; Kumar, A.; Zitzmann, N.; Seabright, G. E.; Kramer, H. B.; Spencer, D. I.; Royle, L.; Lee, J. H.; Klasse, P. J.; Burton, D. R.; Wilson, I. A.; Ward, A. B.; Sanders, R. W.; Moore, J. P.; Doores, K. J.; Crispin, M. Composition and Antigenic Effects of Individual Glycan Sites of a Trimeric HIV-1 Envelope Glycoprotein. *Cell Rep* **2016**, *14*, (11), 2695-706.

(118) Pritchard, L. K.; Vasiljevic, S.; Ozorowski, G.; Seabright, G. E.; Cupo, A.; Ringe, R.; Kim, H. J.; Sanders, R. W.; Doores, K. J.; Burton, D. R.; Wilson, I. A.; Ward, A. B.; Moore, J. P.; Crispin, M. Structural Constraints Determine the Glycosylation of HIV-1 Envelope Trimers. *Cell Rep* **2015**, *11*, (10), 1604-13.

- (119) Huang, X.; Jin, W.; Hu, K.; Luo, S.; Du, T.; Griffin, G. E.; Shattock, R. J.; Hu, Q. Highly Conserved HIV-1 gp120 Glycans Proximal to CD4-Binding Region Affect Viral Infectivity and Neutralizing Antibody Induction. *Virology* **2012**, *423*, (1), 97-106.
- (120) Binley, J. M.; Ban, Y. E.; Crooks, E. T.; Eggink, D.; Osawa, K.; Schief, W. R.; Sanders, R. W. Role of Complex Carbohydrates in Human Immunodeficiency Virus Type 1 Infection and Resistance to Antibody Neutralization. *J Virol* **2010**, *84*, (11), 5637-55.
- (121) Li, Y.; Luo, L.; Rasool, N.; Kang, C. Y. Glycosylation is Necessary for the Correct Folding of Human Immunodeficiency Virus Gp120 in CD4 Binding. *J Virol* **1993**, *67*, (1), 584-8.
- (122) Li, H.; Chien, P. C., Jr.; Tuen, M.; Visciano, M. L.; Cohen, S.; Blais, S.; Xu, C. F.; Zhang, H. T.; Hioe, C. E. Identification of An N-Linked Glycosylation in the C4 Region of HIV-1 Envelope gp120 that is Critical for Recognition of Neighboring CD4 T Cell Epitopes. *J Immunol* **2008**, *180*, (6), 4011-21.
- (123) Steckbeck, J. D.; Craigo, J. K.; Barnes, C. O.; Montelaro, R. C. Highly Conserved Structural Properties of the C-Terminal Tail of HIV-1 gp41 Protein Despite Substantial Sequence Variation Among Diverse Clades: Implications for Functions in Viral Replication. *J Biol Chem* **2011**, *286*, (31), 27156-66.
- (124) Dimonte, S.; Mercurio, F.; Svicher, V.; D'Arrigo, R.; Perno, C. F.; Ceccherini-Silberstein, F. Selected Amino Acid Mutations in HIV-1 B Subtype Gp41 are Associated With Specific Gp120v(3) Signatures in the Regulation of Co-Receptor Usage. *Retrovirology* **2011**, *8*, 33.

- (125) Perrin, C.; Fenouillet, E.; Jones, I. M. Role of Gp41 Glycosylation Sites in the Biological Activity of Human Immunodeficiency Virus Type 1 Envelope Glycoprotein. *Virology* **1998**, *242*, (2), 338-45.
- (126) Johnson, W. E.; Sauvron, J. M.; Desrosiers, R. C. Conserved, N-Linked Carbohydrates of Human Immunodeficiency Virus Type 1 gp41 are Largely Dispensable for Viral Replication. *J Virol* **2001**, *75*, (23), 11426-36.
- (127) Fenouillet, E. La N-glycosylation du VIH :Du Modèle Expérimental à l'Application Thérapeutique. *medecine/sciences* **1993**, *9*, 901-906.
- (128) Fenouillet, E.; Jones, I. M. The Glycosylation of Human Immunodeficiency Virus Type 1 Transmembrane Glycoprotein (Gp41) is Important for the Efficient Intracellular Transport of the Envelope Precursor gp160. *J Gen Virol* **1995**, *76* (Pt 6), 1509-14.
- (129) Lee, W. R.; Yu, X. F.; Syu, W. J.; Essex, M.; Lee, T. H. Mutational Analysis of Conserved N-Linked Glycosylation Sites of Human Immunodeficiency Virus Type 1 gp41. *J Virol* **1992**, *66*, (3), 1799-803.
- (130) Ma, B. J.; Alam, S. M.; Go, E. P.; Lu, X.; Desaire, H.; Tomaras, G. D.; Bowman, C.; Sutherland, L. L.; Scarce, R. M.; Santra, S.; Letvin, N. L.; Kepler, T. B.; Liao, H. X.; Haynes, B. F. Envelope Deglycosylation Enhances Antigenicity of HIV-1 gp41 Epitopes For Both Broad Neutralizing Antibodies and Their Unmutated Ancestor Antibodies. *PLoS Pathog* **2011**, *7*, (9), e1002200.
- (131) Wang, L. X.; Song, H.; Liu, S.; Lu, H.; Jiang, S.; Ni, J.; Li, H. Chemoenzymatic Synthesis of HIV-1 gp41 Glycopeptides: Effects of Glycosylation on the Anti-HIV Activity and Alpha-Helix Bundle-Forming Ability of Peptide C34. *ChemBiochem* **2005**, *6*, (6), 1068-74.

- (132) Balzarini, J.; Van Laethem, K.; Hatse, S.; Froeyen, M.; Peumans, W.; Van Damme, E.; Schols, D. Carbohydrate-Binding Agents Cause Deletions of Highly Conserved Glycosylation Sites in HIV GP120: A New Therapeutic Concept to Hit the Achilles Heel of HIV. *J Biol Chem* **2005**, *280*, (49), 41005-14.
- (133) van Anken, E.; Sanders, R. W.; Liscaljet, I. M.; Land, A.; Bontjer, I.; Tillemans, S.; Nabatov, A. A.; Paxton, W. A.; Berkhout, B.; Braakman, I. Only Five of 10 Strictly Conserved Disulfide Bonds are Essential for Folding and Eight for Function of the HIV-1 Envelope Glycoprotein. *Mol Biol Cell* **2008**, *19*, (10), 4298-309.
- (134) Mathys, L.; Balzarini, J. The Role of N-glycans of HIV-1 gp41 in Virus Infectivity and Susceptibility to the Suppressive Effects of Carbohydrate-Binding Agents. *Retrovirology* **2014**, *11*, 107.
- (135) Fenouillet, E.; Jones, I.; Powell, B.; Schmitt, D.; Kieny, M. P.; Gluckman, J. C. Functional Role of the Glycan Cluster of the Human Immunodeficiency Virus Type 1 Transmembrane Glycoprotein (Gp41) Ectodomain. *J Virol* **1993**, *67*, (1), 150-60.
- (136) Yuste, E.; Bixby, J.; Lifson, J.; Sato, S.; Johnson, W.; Desrosiers, R. Glycosylation of gp41 of Simian Immunodeficiency Virus Shields Epitopes that Can be Targets for Neutralizing Antibodies. *J Virol* **2008**, *82*, (24), 12472-86.
- (137) Tanaka, H.; Chiba, H.; Inokoshi, J.; Kuno, A.; Sugai, T.; Takahashi, A.; Ito, Y.; Tsunoda, M.; Suzuki, K.; Takenaka, A.; Sekiguchi, T.; Umeyama, H.; Hirabayashi, J.; Omura, S. Mechanism by Which the Lectin Actinohivin Blocks HIV Infection of Target Cells. *Proc Natl Acad Sci U S A* **2009**, *106*, (37), 15633-8.
- (138) Hoorelbeke, B.; Huskens, D.; Ferir, G.; Francois, K. O.; Takahashi, A.; Van Laethem, K.; Schols, D.; Tanaka, H.; Balzarini, J. Actinohivin, a Broadly Neutralizing Prokaryotic

Lectin, Inhibits HIV-1 Infection by Specifically Targeting High-Mannose-Type Glycans on the gp120 Envelope. *Antimicrob Agents Chemother* **2010**, *54*, (8), 3287-301.

(139) Zhang, F.; Hoque, M. M.; Jiang, J.; Suzuki, K.; Tsunoda, M.; Takeda, Y.; Ito, Y.; Kawai, G.; Tanaka, H.; Takenaka, A. The Characteristic Structure of Anti-HIV Actinohivin in Complex With Three HMTG D1 Chains of HIV-gp120. *ChemBiochem* **2014**, *15*, (18), 2766-73.

(140) Bewley, C. A.; Gustafson, K. R.; Boyd, M. R.; Covell, D. G.; Bax, A.; Clore, G. M.; Gronenborn, A. M. Solution Structure of Cyanovirin-N, a Potent HIV-Inactivating Protein. *Nat Struct Biol* **1998**, *5*, (7), 571-8.

(141) Barrientos, L. G.; Louis, J. M.; Ratner, D. M.; Seeberger, P. H.; Gronenborn, A. M. Solution Structure of a Circular-Permuted Variant of the Potent HIV-Inactivating Protein Cyanovirin-N: Structural Basis for Protein Stability and Oligosaccharide Interaction. *J Mol Biol* **2003**, *325*, (1), 211-23.

(142) Esser, M. T.; Mori, T.; Mondor, I.; Sattentau, Q. J.; Dey, B.; Berger, E. A.; Boyd, M. R.; Lifson, J. D. Cyanovirin-N Binds to Gp120 to Interfere With CD4-Dependent Human Immunodeficiency Virus Type 1 Virion Binding, Fusion, and Infectivity but Does Not Affect the CD4 Binding Site on gp120 or Soluble CD4-Induced Conformational Changes in gp120. *J Virol* **1999**, *73*, (5), 4360-71.

(143) Alexandre, K. B.; Gray, E. S.; Mufhandu, H.; McMahon, J. B.; Chakauya, E.; O'Keefe, B. R.; Chikwamba, R.; Morris, L. The Lectins Griffithsin, Cyanovirin-N and Scytovirin Inhibit HIV-1 Binding to the DC-SIGN Receptor and Transfer to CD4(+) Cells. *Virology* **2012**, *423*, (2), 175-86.

- (144) Buffa, V.; Stieh, D.; Mamhood, N.; Hu, Q.; Fletcher, P.; Shattock, R. J. Cyanovirin-N Potently Inhibits Human Immunodeficiency Virus Type 1 Infection in Cellular and Cervical Explant Models. *J Gen Virol* **2009**, *90*, (Pt 1), 234-43.
- (145) Boyd, M. R.; Gustafson, K. R.; McMahon, J. B.; Shoemaker, R. H.; O'Keefe, B. R.; Mori, T.; Gulakowski, R. J.; Wu, L.; Rivera, M. I.; Laurencot, C. M.; Currens, M. J.; Cardellina, J. H., 2nd; Buckheit, R. W., Jr.; Nara, P. L.; Pannell, L. K.; Sowder, R. C., 2nd; Henderson, L. E. Discovery of Cyanovirin-N, A Novel Human Immunodeficiency Virus-Inactivating Protein that Binds Viral Surface Envelope Glycoprotein gp120: Potential Applications to Microbicide Development. *Antimicrob Agents Chemother* **1997**, *41*, (7), 1521-30.
- (146) Hu, Q.; Mahmood, N.; Shattock, R. J. High-Mannose-Specific Deglycosylation of HIV-1 gp120 Induced by Resistance to Cyanovirin-N and the Impact on Antibody Neutralization. *Virology* **2007**, *368*, (1), 145-54.
- (147) Keefe, J. R.; Gnanapragasam, P. N.; Gillespie, S. K.; Yong, J.; Bjorkman, P. J.; Mayo, S. L. Designed Oligomers of Cyanovirin-N Show Enhanced HIV Neutralization. *Proc Natl Acad Sci U S A* **2011**, *108*, (34), 14079-84.
- (148) Dey, B.; Lerner, D. L.; Lusso, P.; Boyd, M. R.; Elder, J. H.; Berger, E. A. Multiple Antiviral Activities of Cyanovirin-N: Blocking of Human Immunodeficiency Virus Type 1 gp120 Interaction With CD4 and Coreceptor and Inhibition of Diverse Enveloped Viruses. *J Virol* **2000**, *74*, (10), 4562-9.
- (149) Ferir, G.; Huskens, D.; Noppen, S.; Koharudin, L. M.; Gronenborn, A. M.; Schols, D. Broad Anti-HIV Activity of the Oscillatoria Agardhii Agglutinin Homologue Lectin Family. *J Antimicrob Chemother* **2014**, *69*, (10), 2746-58.

- (150) Koharudin, L. M.; Gronenborn, A. M. Structural Basis of the Anti-HIV Activity of the Cyanobacterial Oscillatoria Agardhii Agglutinin. *Structure* **2011**, *19*, (8), 1170-81.
- (151) Koharudin, L. M.; Furey, W.; Gronenborn, A. M. Novel Fold and Carbohydrate Specificity of the Potent Anti-HIV Cyanobacterial Lectin From Oscillatoria Agardhii. *J Biol Chem* **2011**, *286*, (2), 1588-97.
- (152) Carneiro, M. G.; Koharudin, L. M.; Ban, D.; Sabo, T. M.; Trigo-Mourino, P.; Mazur, A.; Griesinger, C.; Gronenborn, A. M.; Lee, D. Sampling of Glycan-Bound Conformers by the Anti-HIV Lectin Oscillatoria Agardhii Agglutinin in the Absence of Sugar. *Angew Chem Int Ed Engl* **2015**, *54*, (22), 6462-5.
- (153) Bokesch, H. R.; O'Keefe, B. R.; McKee, T. C.; Pannell, L. K.; Patterson, G. M.; Gardella, R. S.; Sowder, R. C., 2nd; Turpin, J.; Watson, K.; Buckheit, R. W., Jr.; Boyd, M. R. a Potent Novel Anti-HIV Protein From the Cultured Cyanobacterium Scytonema Varium. *Biochemistry* **2003**, *42*, (9), 2578-84.
- (154) Adams, E. W.; Ratner, D. M.; Bokesch, H. R.; McMahon, J. B.; O'Keefe, B. R.; Seeberger, P. H. Oligosaccharide and Glycoprotein Microarrays as Tools in HIV Glycobiology; Glycan-Dependent gp120/Protein Interactions. *Chem Biol* **2004**, *11*, (6), 875-81.
- (155) McFeeters, R. L.; Xiong, C.; O'Keefe, B. R.; Bokesch, H. R.; McMahon, J. B.; Ratner, D. M.; Castelli, R.; Seeberger, P. H.; Byrd, R. A. The Novel Fold of Scytovirin Reveals a New Twist for Antiviral Entry Inhibitors. *J Mol Biol* **2007**, *369*, (2), 451-61.
- (156) Alexandre, K. B.; Gray, E. S.; Lambson, B. E.; Moore, P. L.; Choge, I. A.; Mlisana, K.; Karim, S. S.; McMahon, J.; O'Keefe, B.; Chikwamba, R.; Morris, L. Mannose-Rich

Glycosylation Patterns on HIV-1 Subtype C gp120 And Sensitivity to the Lectins, Griffithsin, Cyanovirin-N and Scytovirin. *Virology* **2010**, *402*, (1), 187-96.

(157) Williams, D. C., Jr.; Lee, J. Y.; Cai, M.; Bewley, C. A.; Clore, G. M. Crystal Structures of the HIV-1 Inhibitory Cyanobacterial Protein MVL Free and Bound to Man₃GlcNAc₂: Structural Basis for Specificity and High-Affinity Binding to the Core Pentasaccharide From N-Linked Oligomannoside. *J Biol Chem* **2005**, *280*, (32), 29269-76.

(158) Ziolkowska, N. E.; Wlodawer, A. Structural Studies of Algal Lectins With Anti-HIV Activity. *Acta Biochim Pol* **2006**, *53*, (4), 617-26.

(159) Shahzad-ul-Hussan, S.; Gustchina, E.; Ghirlando, R.; Clore, G. M.; Bewley, C. A. Solution Structure of the Monovalent Lectin Microvirin in Complex With Man(Alpha)(1-2)Man Provides a Basis For Anti-HIV Activity With Low Toxicity. *J Biol Chem* **2011**, *286*, (23), 20788-96.

(160) Huskens, D.; Ferir, G.; Vermeire, K.; Kehr, J. C.; Balzarini, J.; Dittmann, E.; Schols, D. Microvirin, a Novel Alpha(1,2)-Mannose-Specific Lectin Isolated From *Microcystis Aeruginosa*, Has Anti-HIV-1 Activity Comparable With That of Cyanovirin-N But a Much Higher Safety Profile. *J Biol Chem* **2010**, *285*, (32), 24845-54.

(161) Lopez, S.; Armand-Ugon, M.; Bastida, J.; Viladomat, F.; Este, J. A.; Stewart, D.; Codina, C. Anti-Human Immunodeficiency Virus Type 1 (HIV-1) Activity of Lectins From *Narcissus* Species. *Planta Med* **2003**, *69*, (2), 109-12.

(162) Bachmann, W. E. G. M. M. S. F.-H. C. E. W. S. M. *Narcissus* and *Gerardia* Lectins: Tools for the Development of a Vaccine Against AIDS and a New ELISA To Quantify HIV-gp 120. *Lectins and Cancer* **1991**, 27-40.

- (163) Charan, R. D.; Munro, M. H.; O'Keefe, B. R.; Sowder, R.; McKee, T. C.; Currens, M. J.; Pannell, L. K.; Boyd, M. R. Isolation and Characterization of Myrianthus Holstii Lectin, a Potent HIV-1 Inhibitory Protein From the Plant Myrianthus Holstii(1). *J Nat Prod* **2000**, *63*, (8), 1170-4.
- (164) Coulibaly, F. S.; Youan, B. B. Concanavalin A-Polysaccharides Binding Affinity Analysis Using a Quartz Crystal Microbalance. *Biosens Bioelectron* **2014**, *59*, 404-11.
- (165) Bhattacharyya, L.; Brewer, C. F. Interactions of Concanavalin A With Asparagine-Linked Glycopeptides. Structure/Activity Relationships of the Binding and Precipitation of Oligomannose and Bisected Hybrid-Type Glycopeptides With Concanavalin A. *Eur J Biochem* **1989**, *178*, (3), 721-6.
- (166) Witvrouw, M.; Fikkert, V.; Hantson, A.; Pannecouque, C.; O'Keefe B, R.; McMahon, J.; Stamatatos, L.; de Clercq, E.; Bolmstedt, A. Resistance Of Human Immunodeficiency Virus Type 1 to the High-Mannose Binding Agents Cyanovirin N and Concanavalin A. *J Virol* **2005**, *79*, (12), 7777-84.
- (167) Hansen, J. E.; Nielsen, C. M.; Nielsen, C.; Heegaard, P.; Mathiesen, L. R.; Nielsen, J. O. Correlation Between Carbohydrate Structures on the Envelope Glycoprotein gp120 of HIV-1 And HIV-2 and Syncytium Inhibition With Lectins. *Aids* **1989**, *3*, (10), 635-41.
- (168) Matsui, T.; Kobayashi, S.; Yoshida, O.; Ishii, S.; Abe, Y.; Yamamoto, N. Effects of Succinylated Concanavalin A on Infectivity and Syncytial Formation of Human Immunodeficiency Virus. *Med Microbiol Immunol* **1990**, *179*, (5), 225-35.
- (169) Pashov, A.; MacLeod, S.; Saha, R.; Perry, M.; VanCott, T. C.; Kieber-Emmons, T. Concanavalin A Binding to HIV Envelope Protein is Less Sensitive to Mutations in Glycosylation Sites than Monoclonal Antibody 2G12. *Glycobiology* **2005**, *15*, (10), 994-1001.

- (170) Swanson, M. D.; Boudreaux, D. M.; Salmon, L.; Chugh, J.; Winter, H. C.; Meagher, J. L.; Andre, S.; Murphy, P. V.; Oscarson, S.; Roy, R.; King, S.; Kaplan, M. H.; Goldstein, I. J.; Taret, E. B.; Hurst, B. L.; Smee, D. F.; de la Fuente, C.; Hoffmann, H. H.; Xue, Y.; Rice, C. M.; Schols, D.; Garcia, J. V.; Stuckey, J. A.; Gabius, H. J.; Al-Hashimi, H. M.; Markovitz, D. M. Engineering a Therapeutic Lectin by Uncoupling Mitogenicity From Antiviral Activity. *Cell* **2015**, *163*, (3), 746-58.
- (171) Alexandre, K. B.; Gray, E. S.; Pantophlet, R.; Moore, P. L.; McMahon, J. B.; Chakauya, E.; O'Keefe, B. R.; Chikwamba, R.; Morris, L. Binding of the Mannose-Specific Lectin, Griffithsin, to HIV-1 Gp120 Exposes the CD4-Binding Site. *J Virol* **2011**, *85*, (17), 9039-50.
- (172) Mori, T.; O'Keefe, B. R.; Sowder, R. C., 2nd; Bringans, S.; Gardella, R.; Berg, S.; Cochran, P.; Turpin, J. A.; Buckheit, R. W., Jr.; McMahon, J. B.; Boyd, M. R. Isolation and Characterization of Griffithsin, a Novel HIV-Inactivating Protein, From the Red Alga *Griffithsia* sp. *J Biol Chem* **2005**, *280*, (10), 9345-53.
- (173) Emau, P.; Tian, B.; O'Keefe, B. R.; Mori, T.; McMahon, J. B.; Palmer, K. E.; Jiang, Y.; Bekele, G.; Tsai, C. C. Griffithsin, a Potent HIV Entry Inhibitor, is an Excellent Candidate for Anti-HIV Microbicide. *J Med Primatol* **2007**, *36*, (4-5), 244-53.
- (174) Moulaei, T.; Alexandre, K. B.; Shenoy, S. R.; Meyerson, J. R.; Krumpke, L. R.; Constantine, B.; Wilson, J.; Buckheit, R. W., Jr.; McMahon, J. B.; Subramaniam, S.; Wlodawer, A.; O'Keefe, B. R. Griffithsin Tandemers: Flexible and Potent Lectin Inhibitors of the Human Immunodeficiency Virus. *Retrovirology* **2015**, *12*, 6.
- (175) Zhou, X.; Liu, J.; Yang, B.; Lin, X.; Yang, X. W.; Liu, Y. Marine Natural Products With Anti-HIV Activities in the Last Decade. *Curr Med Chem* **2013**, *20*, (7), 953-73.

- (176) Wang, J. H.; Kong, J.; Li, W.; Molchanova, V.; Chikalovets, I.; Belogortseva, N.; Luk'yanov, P.; Zheng, Y. T. A Beta-Galactose-Specific Lectin Isolated From the Marine Worm *Chaetopterus Variopedatus* Possesses Anti-HIV-1 Activity. *Comp Biochem Physiol C Toxicol Pharmacol* **2006**, *142*, (1-2), 111-7.
- (177) Bulgheresi, S.; Schabussova, I.; Chen, T.; Mullin, N. P.; Maizels, R. M.; Ott, J. A. A New C-Type Lectin Similar to the Human Immunoreceptor DC-SIGN Mediates Symbiont Acquisition By a Marine Nematode. *Appl Environ Microbiol* **2006**, *72*, (4), 2950-6.
- (178) Nabatov, A. A.; de Jong, M. A.; de Witte, L.; Bulgheresi, S.; Geijtenbeek, T. B. C-type Lectin Mermaid Inhibits Dendritic Cell Mediated HIV-1 Transmission to CD4+ T cells. *Virology* **2008**, *378*, (2), 323-8.
- (179) Molchanova, V.; Chikalovets, I.; Chernikov, O.; Belogortseva, N.; Li, W.; Wang, J. H.; Yang, D. Y.; Zheng, Y. T.; Lukyanov, P. A New Lectin From the Sea Worm *Serpula Vermicularis*: Isolation, Characterization and Anti-HIV Activity. *Comp Biochem Physiol C Toxicol Pharmacol* **2007**, *145*, (2), 184-93.
- (180) Vo, T. S.; Kim, S. K. Potential Anti-HIV Agents From Marine Resources: An Overview. *Mar Drugs* **2010**, *8*, (12), 2871-92.
- (181) Mahalingam, A.; Geonnotti, A. R.; Balzarini, J.; Kiser, P. F. Activity and Safety of Synthetic Lectins Based on Benzoboroxole-Functionalized Polymers for Inhibition Of HIV Entry. *Mol Pharm* **2011**, *8*, (6), 2465-75.
- (182) Berube, M.; Dowlut, M.; Hall, D. G. Benzoboroxoles as Efficient Glycopyranoside-Binding Agents in Physiological Conditions: Structure and Selectivity of Complex Formation. *J Org Chem* **2008**, *73*, (17), 6471-9.

- (183) Trippier, P. C.; McGuigan, C.; Balzarini, J. Phenylboronic-Acid-Based Carbohydrate Binders as Antiviral Therapeutics: Monophenylboronic Acids. *Antivir Chem Chemother* **2010**, *20*, (6), 249-57.
- (184) Trippier, P. C.; Balzarini, J.; McGuigan, C. Phenylboronic-Acid-Based Carbohydrate Binders as Antiviral Therapeutics: Bisphenylboronic Acids. *Antivir Chem Chemother* **2011**, *21*, (3), 129-42.
- (185) Khan, J. M.; Qadeer, A.; Ahmad, E.; Ashraf, R.; Bhushan, B.; Chaturvedi, S. K.; Rabbani, G.; Khan, R. H. Monomeric Banana Lectin at Acidic pH Overrides Conformational Stability of its Native Dimeric Form. *PLoS One* **2013**, *8*, (4), e62428.
- (186) Suzuki, K.; Ohbayashi, N.; Jiang, J.; Zhang, X.; Hoque, M. M.; Tsunoda, M.; Murayama, K.; Tanaka, H.; Takenaka, A. Crystallographic Study of the Interaction of the Anti-HIV Lectin Actinohivin With the Alpha(1-2)Mannobiose Moiety of gp120 HMTG. *Acta Crystallogr Sect F Struct Biol Cryst Commun* **2012**, *68*, (Pt 9), 1060-3.
- (187) Ballerstadt, R.; Evans, C.; McNichols, R.; Gowda, A. Concanavalin a for In Vivo Glucose Sensing: A Biototoxicity Review. *Biosens Bioelectron* **2006**, *22*, (2), 275-84.
- (188) Krauss, S.; Buttgerit, F.; Brand, M. D. Effects of the Mitogen Concanavalin A on Pathways of Thymocyte Energy Metabolism. *Biochim Biophys Acta* **1999**, *1412*, (2), 129-38.
- (189) Balzarini, J.; Van Laethem, K.; Peumans, W. J.; Van Damme, E. J.; Bolmstedt, A.; Gago, F.; Schols, D. Mutational Pathways, Resistance Profile, and Side Effects of Cyanovirin Relative to Human Immunodeficiency Virus Type 1 Strains With N-Glycan Deletions in Their Gp120 Envelopes. *J Virol* **2006**, *80*, (17), 8411-21.
- (190) Gavrovic-Jankulovic, M.; Poulsen, K.; Brckalo, T.; Bobic, S.; Lindner, B.; Petersen, A. a Novel Recombinantly Produced Banana Lectin Isoform is a Valuable Tool for

- Glycoproteomics and a Potent Modulator of the Proliferation Response in CD3+, CD4+, and CD8+ Populations of Human PBMCs. *Int J Biochem Cell Biol* **2008**, *40*, (5), 929-41.
- (191) Mahalingam, A.; Geonnotti, A. R.; Balzarini, J.; Kiser, P. F. Activity and Safety of Synthetic Lectins Based on Benzoboroxole-Functionalized Polymers for Inhibition Of HIV Entry. *Mol Pharm* **2011**, *8*, (6), 2465-75.
- (192) Lam, S. K.; Ng, T. B. Lectins: Production and Practical Applications. *Appl Microbiol Biotechnol* **2011**, *89*, (1), 45-55.
- (193) Scanlan, C. N.; Offer, J.; Zitzmann, N.; Dwek, R. A. Exploiting the Defensive Sugars of HIV-1 for Drug and Vaccine Design. *Nature* **2007**, *446*, (7139), 1038-45.
- (194) Gupta A, G. R., Gupta GS. Targeting Cells for Drug and Gene Delivery: Emerging Applications of Mannans and Mannan Binding Lectins. *Journal of Scientific and Industrial Research* **2009**, *68*, 465–483.
- (195) Ghazarian, H.; Idoni, B.; Oppenheimer, S. B. A Glycobiology Review: Carbohydrates, Lectins and Implications in Cancer Therapeutics. *Acta Histochem* **2011**, *113*, (3), 236-47.
- (196) Apostolopoulos, V.; Thalhammer, T.; Tzakos, A. G.; Stojanovska, L. Targeting Antigens to Dendritic Cell Receptors for Vaccine Development. *J Drug Deliv* **2013**, *2013*, 869718.
- (197) Zelensky, A. N.; Gready, J. E. The C-Type Lectin-Like Domain Superfamily. *FEBS J* **2005**, *272*, (24), 6179-217.
- (198) Cui, Z.; Hsu, C. H.; Mumper, R. J. Physical Characterization and Macrophage Cell Uptake of Mannan-Coated Nanoparticles. *Drug Dev Ind Pharm* **2003**, *29*, (6), 689-700.

- (199) Espuelas, S.; Thumann, C.; Heurtault, B.; Schuber, F.; Frisch, B. Influence of Ligand Valency on the Targeting of Immature Human Dendritic Cells by Mannosylated Liposomes. *Bioconjug Chem* **2008**, *19*, (12), 2385-93.
- (200) Zhang, Q.; Su, L.; Collins, J.; Chen, G.; Wallis, R.; Mitchell, D. A.; Haddleton, D. M.; Becer, C. R. Dendritic Cell Lectin-Targeting Sentinel-Like Unimolecular Glycoconjugates to Release an Anti-HIV Drug. *J Am Chem Soc* **2014**, *136*, (11), 4325-32.
- (201) Hong, P. W.; Flummerfelt, K. B.; de Parseval, A.; Gurney, K.; Elder, J. H.; Lee, B. Human Immunodeficiency Virus Envelope (gp120) Binding to DC-SIGN and Primary Dendritic Cells is Carbohydrate Dependent but Does Not Involve 2G12 or Cyanovirin Binding Sites: Implications for Structural Analyses of Gp120-DC-SIGN Binding. *J Virol* **2002**, *76*, (24), 12855-65.
- (202) Cruz, L. J.; Tacke, P. J.; Fokkink, R.; Joosten, B.; Stuart, M. C.; Albericio, F.; Torensma, R.; Figdor, C. G. Targeted PLGA Nano- but Not Microparticles Specifically Deliver Antigen to Human Dendritic Cells Via DC-SIGN In Vitro. *J Control Release* **2010**, *144*, (2), 118-26.
- (203) Ingale, J.; Stano, A.; Guenaga, J.; Sharma, S. K.; Nemazee, D.; Zwick, M. B.; Wyatt, R. T. High-Density Array of Well-Ordered HIV-1 Spikes on Synthetic Liposomal Nanoparticles Efficiently Activate B Cells. *Cell Rep* **2016**, *15*, (9), 1986-99.
- (204) Akashi, M.; Niikawa, T.; Serizawa, T.; Hayakawa, T.; Baba, M. Capture of HIV-1 gp120 and Virions by Lectin-Immobilized Polystyrene Nanospheres. *Bioconjug Chem* **1998**, *9*, (1), 50-3.
- (205) Hayakawa, T.; Kawamura, M.; Okamoto, M.; Baba, M.; Niikawa, T.; Takehara, S.; Serizawa, T.; Akashi, M. Concanavalin A-Immobilized Polystyrene Nanospheres Capture

HIV-1 Virions and gp120: Potential Approach Towards Prevention of Viral Transmission. *J Med Virol* **1998**, *56*, (4), 327-31.

(206) He, L.; de Val, N.; Morris, C. D.; Vora, N.; Thinnes, T. C.; Kong, L.; Azadnia, P.; Sok, D.; Zhou, B.; Burton, D. R.; Wilson, I. A.; Nemazee, D.; Ward, A. B.; Zhu, J. Presenting Native-Like Trimeric HIV-1 Antigens With Self-Assembling Nanoparticles. *Nat Commun* **2016**, *7*, 12041.

(207) Takahashi, K.; Moyo, P.; Chigweshe, L.; Chang, W. C.; White, M. R.; Hartshorn, K. L. Efficacy of Recombinant Chimeric Lectins, Consisting of Mannose Binding Lectin And L-Ficolin, Against Influenza a Viral Infection in Mouse Model Study. *Virus Res* **2013**, *178*, (2), 495-501.

(208) Sato, Y.; Morimoto, K.; Kubo, T.; Sakaguchi, T.; Nishizono, A.; Hirayama, M.; Hori, K. Entry Inhibition of Influenza Viruses With High Mannose Binding Lectin ESA-2 From the Red Alga *Euclima Serra* Through the Recognition of Viral Hemagglutinin. *Mar Drugs* **2015**, *13*, (6), 3454-65.

(209) Kachko, A.; Loesgen, S.; Shahzad-Ul-Hussan, S.; Tan, W.; Zubkova, I.; Takeda, K.; Wells, F.; Rubin, S.; Bewley, C. A.; Major, M. E. Inhibition of Hepatitis C Virus By the Cyanobacterial Protein *Microcystis Viridis* Lectin: Mechanistic Differences Between the High-Mannose Specific Lectins MVL, CV-N, and GNA. *Mol Pharm* **2013**, *10*, (12), 4590-602.

(210) Gadjeva, M.; Paludan, S. R.; Thiel, S.; Slavov, V.; Ruseva, M.; Eriksson, K.; Lowhagen, G. B.; Shi, L.; Takahashi, K.; Ezekowitz, A.; Jensenius, J. C. Mannan-Binding Lectin Modulates the Response to HSV-2 Infection. *Clin Exp Immunol* **2004**, *138*, (2), 304-11.

(211) Eisen, S.; Dzwonek, A.; Klein, N. J. Mannose-Binding Lectin in HIV Infection. *Future Virol* **2008**, *3*, (3), 225-233.

- (212) Ji, X.; Olinger, G. G.; Aris, S.; Chen, Y.; Gewurz, H.; Spear, G. T. Mannose-Binding Lectin Binds to Ebola and Marburg Envelope Glycoproteins, Resulting in Blocking of Virus Interaction With DC-SIGN and Complement-Mediated Virus Neutralization. *J Gen Virol* **2005**, *86*, (Pt 9), 2535-42.
- (213) Keyaerts, E.; Vijgen, L.; Pannecouque, C.; Van Damme, E.; Peumans, W.; Egberink, H.; Balzarini, J.; Van Ranst, M. Plant Lectins are Potent Inhibitors of Coronaviruses by Interfering With Two Targets in the Viral Replication Cycle. *Antiviral Res* **2007**, *75*, (3), 179-87.
- (214) Hamel, R.; Dejarnac, O.; Wichit, S.; Ekchariyawat, P.; Neyret, A.; Luplertlop, N.; Perera-Lecoin, M.; Surasombatpattana, P.; Talignani, L.; Thomas, F.; Cao-Lormeau, V. M.; Choumet, V.; Briant, L.; Despres, P.; Amara, A.; Yssel, H.; Misse, D. Biology of Zika Virus Infection in Human Skin Cells. *J Virol* **2015**, *89*, (17), 8880-96.
- (215) Clement, F.; Venkatesh, Y. P. Dietary garlic (*Allium sativum*) lectins, ASA I and ASA II, are Highly Stable and Immunogenic. *Int Immunopharmacol* **2010**, *10*, (10), 1161-9.
- (216) Lusvarghi, S.; Bewley, C. A. Griffithsin: An Antiviral Lectin with Outstanding Therapeutic Potential. *Viruses* **2016**, *8*, (10).
- (217) (1), O. Y. N. K. F. H. M. H. A Highly Sensitive 27 MHz Quartz-Crystal Microbalance as a Device for Kinetic Measurements of Molecular Recognition on DNA Strands. *Analytical sciences* **2000**, *16*, (11), 1113-1119.
- (218) K. Lebed, A. J. K., L. Forro' and M. Lekka. Atomic Force Microscopy and Quartz Crystal Microbalance Study of the Lectin-Carbohydrate Interaction Kinetics. *ACTA PHYSICA POLONICA A* **2007**, *111*, (2).

- (219) Dam, T. K.; Roy, R.; Das, S. K.; Oscarson, S.; Brewer, C. F. Binding of Multivalent Carbohydrates to Concanavalin A and Dioclea Grandiflora Lectin. Thermodynamic Analysis of the "Multivalency Effect". *J Biol Chem* **2000**, *275*, (19), 14223-30.
- (220) Duverger, E.; Frison, N.; Roche, A. C.; Monsigny, M. Carbohydrate-Lectin Interactions Assessed By Surface Plasmon Resonance. *Biochimie* **2003**, *85*, (1-2), 167-79.
- (221) GLEW, R. D. G. A. R. H. The Kinetics of Carbohydrate Binding to Concanavalin A. *The Journal Of Biological Chemistry* **1973**, *248*, (21), 7547-7551.
- (222) Chinnayelka, S.; McShane, M. J. Glucose-Sensitive Nanoassemblies Comprising Affinity-Binding Complexes Trapped in Fuzzy Microshells. *J Fluoresc* **2004**, *14*, (5), 585-95.
- (223) Sato, K.; Kodama, D.; Anzai, J. Sugar-Sensitive Thin Films Composed of Concanavalin A and Sugar-Bearing Polymers. *Anal Sci* **2005**, *21*, (11), 1375-8.
- (224) Sato, K.; Takahashi, S.; Anzai, J. Layer-By-Layer Thin Films and Microcapsules for Biosensors and Controlled Release. *Anal Sci* **2012**, *28*, (10), 929-38.
- (225) Yi Zhu, W. T. a. C. G. Molecular-Engineered Polymeric Microcapsules Assembled From Concanavalin A and Glycogen With Specific Responses to Carbohydrates. *Soft Matter* **2011**, *7*, (12), 5805-5815.
- (226) Yuri Lvov, K. A., Izumi Ichinose and Toyoki Kunitake. Layer-By-Layer Architectures of Concanavalin a by Means of Electrostatic and Biospecific Interaction. *J. Chem. Soc., Chem. Commun.* **1995**, (22), 2313-2314.
- (227) Sauerbrey, G. The Use of Quartz Crystal Oscillators for Weighing Thin Layers and for Microweighing Applications. *Z. Phys* **1959**, (155), 206-222.
- (228) Paulo Tde, F.; de Sousa, T. P.; de Abreu, D. S.; Felicio, N. H.; Bernhardt, P. V.; Lopes, L. G.; Sousa, E. H.; Diogenes, I. C. Electrochemistry, Surface Plasmon Resonance, and Quartz

Crystal Microbalance: An Associative Study on Cytochrome C Adsorption on Pyridine Tail-Group Monolayers on Gold. *J Phys Chem B* **2013**, *117*, (29), 8673-80.

(229) Sun, Y. X.; Ren, K. F.; Wang, J. L.; Chang, G. X.; Ji, J. Electrochemically Controlled Stiffness of Multilayers for Manipulation of Cell Adhesion. *ACS Appl Mater Interfaces* **2013**, *5*, (11), 4597-602.

(230) Sun, Y. X.; Ren, K. F.; Zhao, Y. X.; Liu, X. S.; Chang, G. X.; Ji, J. Construction of Redox-Active Multilayer Film for Electrochemically Controlled Release. *Langmuir* **2013**, *29*, (35), 11163-8.

(231) Pejcic, B.; Myers, M.; Ranwala, N.; Boyd, L.; Baker, M.; Ross, A. Modifying the Response of a Polymer-Based Quartz Crystal Microbalance Hydrocarbon Sensor With Functionalized Carbon Nanotubes. *Talanta* **2011**, *85*, (3), 1648-57.

(232) Ueyama, S.; Hijikata, K.; Hirotsuji, J. Water Monitoring System for Oil Contamination Using Polymer-Coated Quartz Crystal Microbalance Chemical Sensor. *Water Sci Technol* **2002**, *45*, (4-5), 175-80.

(233) Nicolini, C.; Adami, M.; Sartore, M.; Bragazzi, N. L.; Bavastrello, V.; Spera, R.; Pechkova, E. Prototypes of Newly Conceived Inorganic and Biological Sensors for Health and Environmental Applications. *Sensors (Basel)* **2012**, *12*, (12), 17112-27.

(234) Pei, Z.; Ma, X.; Ding, P.; Zhang, W.; Luo, Z.; Li, G. Study of a QCM Dimethyl Methylphosphonate Sensor Based on a ZnO-Modified Nanowire-Structured Manganese Dioxide Film. *Sensors (Basel)* **2010**, *10*, (9), 8275-90.

(235) Bouchet-Spinelli, A.; Reuillard, B.; Coche-Guerente, L.; Armand, S.; Labbe, P.; Fort, S. Oligosaccharide Biosensor for Direct Monitoring of Enzymatic Activities Using QCM-D. *Biosens Bioelectron* **2013**, *49*, 290-6.

- (236) Eom, S.; Yu, E.; Choi, S. J. Functionalization of Quartz Crystal Microbalances With Liposomes Containing the N-Hydroxysuccinimide Ester of Palmitic Acid. *Anal Biochem* **2013**, *443*, (1), 78-80.
- (237) Guntupalli, R.; Sorokulova, I.; Olsen, E.; Globa, L.; Pustovyy, O.; Vodyanoy, V. Biosensor for Detection of Antibiotic Resistant Staphylococcus Bacteria. *J Vis Exp* **2013**, (75).
- (238) Wangchareansak, T.; Sangma, C.; Ngermmeesri, P.; Thitithanyanont, A.; Lieberzeit, P. A. Self-Assembled Glucosamine Monolayers as Biomimetic Receptors for Detecting WGA Lectin And Influenza Virus With a Quartz Crystal Microbalance. *Anal Bioanal Chem* **2013**, *405*, (20), 6471-8.
- (239) Lebed, K.; Kulik, A. J.; Forro, L.; Lekka, M. Lectin-Carbohydrate Affinity Measured Using a Quartz Crystal Microbalance. *J Colloid Interface Sci* **2006**, *299*, (1), 41-8.
- (240) Li, X.; Pei, Y.; Zhang, R.; Shuai, Q.; Wang, F.; Aastrup, T.; Pei, Z. A Suspension-Cell Biosensor for Real-Time Determination of Binding Kinetics of Protein-Carbohydrate Interactions on Cancer Cell Surfaces. *Chem Commun (Camb)* **2013**, *49*, (85), 9908-10.
- (241) Mori, T.; Toyoda, M.; Ohtsuka, T.; Okahata, Y. Kinetic Analyses for Bindings of Concanavalin A to Dispersed and Condensed Mannose Surfaces on a Quartz Crystal Microbalance. *Anal Biochem* **2009**, *395*, (2), 211-6.
- (242) Tan, L.; Lin, P.; Chisti, M. M.; Rehman, A.; Zeng, X. Real Time Analysis of Binding Between Rituximab (Anti-CD20 Antibody) and B Lymphoma Cells. *Anal Chem* **2013**, *85*, (18), 8543-51.
- (243) Cho, Y. K.; Kim, S.; Kim, Y. A.; Lim, H. K.; Lee, K.; Yoon, D.; Lim, G.; Pak, Y. E.; Ha, T. H.; Kim, K. Characterization of DNA Immobilization and Subsequent Hybridization

Using in Situ Quartz Crystal Microbalance, Fluorescence Spectroscopy, and Surface Plasmon Resonance. *J Colloid Interface Sci* **2004**, 278, (1), 44-52.

(244) Laricchia-Robbio, L.; Revoltella, R. P. Comparison Between the Surface Plasmon Resonance (SPR) and the Quartz Crystal Microbalance (QCM) Method in a Structural Analysis of Human Endothelin-1. *Biosens Bioelectron* **2004**, 19, (12), 1753-8.

(245) Ha, T. H.; Kim, S.; Lim, G.; Kim, K. Influence of Liquid Medium and Surface Morphology on the Response of QCM During Immobilization and Hybridization of Short Oligonucleotides. *Biosens Bioelectron* **2004**, 20, (2), 378-89.

(246) Caruso, F.; Rodda, E.; Furlong, D. N.; Niikura, K.; Okahata, Y. Quartz Crystal Microbalance Study of DNA Immobilization and Hybridization for Nucleic Acid Sensor Development. *Anal Chem* **1997**, 69, (11), 2043-9.

(247) T. Coffey, M. A., and J. Krim. A Scanning Probe and Quartz Crystal Microbalance Study of the Impact of C60 on Friction at Solid-Liquid Interfaces. *Journal of Physics:Condensed Matter* **2001**, 13, (21), 4991-4999.

(248) Kristensen, E. M.; Rensmo, H.; Larsson, R.; Siegbahn, H. Characterization of Heparin Surfaces Using Photoelectron Spectroscopy and Quartz Crystal Microbalance. *Biomaterials* **2003**, 24, (23), 4153-9.

(249) Pei, Z.; Anderson, H.; Aastrup, T.; Ramstrom, O. Study of Real-Time Lectin-Carbohydrate Interactions on the Surface of a Quartz Crystal Microbalance. *Biosens Bioelectron* **2005**, 21, (1), 60-6.

(250) Compain, P.; Martin, O. R. Carbohydrate Mimetics-Based Glycosyltransferase Inhibitors. *Bioorg Med Chem* **2001**, 9, (12), 3077-92.

- (251) Koeller, K. M.; Wong, C. H. Emerging Themes in Medicinal Glycoscience. *Nat Biotechnol* **2000**, *18*, (8), 835-41.
- (252) Varki, A. Biological Roles of Oligosaccharides: All of the Theories are Correct. *Glycobiology* **1993**, *3*, (2), 97-130.
- (253) Flatt, J. P. Use and Storage of Carbohydrate and Fat. *Am J Clin Nutr* **1995**, *61*, (4), 952S-959S.
- (254) Zhang, S. Z.; Zhao, F. L.; Li, K. A.; Tong, S. Y. A Study on the Interaction Between Concanavalin A and Glycogen By Light Scattering Technique and its Analytical Application. *Talanta* **2001**, *54*, (2), 333-42.
- (255) Alberti, K. G.; Batstone, G. F.; Foster, K. J.; Johnston, D. G. Relative Role of Various Hormones in Mediating the Metabolic Response to Injury. *JPEN J Parenter Enteral Nutr* **1980**, *4*, (2), 141-6.
- (256) Hochachka, P. W.; Storey, K. B. Metabolic Consequences of Diving In Animals and Man. *Science* **1975**, *187*, (4177), 613-21.
- (257) Kong, J.; Shepel, P. N.; Holden, C. P.; Mackiewicz, M.; Pack, A. I.; Geiger, J. D. Brain Glycogen Decreases With Increased Periods of Wakefulness: Implications for Homeostatic Drive To Sleep. *J Neurosci* **2002**, *22*, (13), 5581-7.
- (258) Brewer, F. Studies of the Carbohydrate Binding Specificity of Concanavalin A Using Nuclear Magnetic Resonance Spectroscopy. *The Einstein Quarterly Journal of Biology and Medicine* **1985**, *3*, (1), 55-60.
- (259) Goldstein, I. J.; Hollerman, C. E.; Merrick, J. M. Protein-Carbohydrate Interaction. I. The Interaction of Polysaccharides with Concanavalin A. *Biochim Biophys Acta* **1965**, *97*, 68-76.

- (260) Goldstein, I. J.; Hollerman, C. E.; Smith, E. E. Protein-Carbohydrate Interaction. II. Inhibition Studies on the Interaction of Concanavalin A With Polysaccharides. *Biochemistry* **1965**, *4*, 876-83.
- (261) Agrawal, B. B.; Goldstein, I. J. Protein-carbohydrate interaction. VII. Physical And Chemical Studies on Concanavalin A, the Hemagglutinin of the Jack Bean. *Arch Biochem Biophys* **1968**, *124*, (1), 218-29.
- (262) Pensa, E.; Cortes, E.; Corthey, G.; Carro, P.; Vericat, C.; Fonticelli, M. H.; Benitez, G.; Rubert, A. A.; Salvarezza, R. C. The Chemistry of the Sulfur-Gold Interface: In Search of a Unified Model. *Acc Chem Res* **2012**, *45*, (8), 1183-92.
- (263) Love, J. C.; Estroff, L. A.; Kriebel, J. K.; Nuzzo, R. G.; Whitesides, G. M. Self-Assembled Monolayers of Thiolates on Metals as a Form of Nanotechnology. *Chem Rev* **2005**, *105*, (4), 1103-69.
- (264) Corn, B. L. F. a. R. M. Covalent Attachment and Derivatization Of Poly(L-Lysine) Monolayers on Gold Surfaces as Characterized by Polarization-Modulation FT-IR Spectroscopy. *Anal. Chem* **1996**, *68*, (18), 3187-3193.
- (265) Plant, D. J. V. C. W. M. V. I. S. A. L. Synthesis and Characterization of Self-Assembled Monolayers of Alkylated 1-Thiahexa(Ethylene Oxide) Compounds on Gold. *Organic Analytical Chemistry* **1998**, *14*, (24), 6916 - 6923.
- (266) Ojamae, L.; Aulin, C.; Pedersen, H.; Kall, P. O. IR And Quantum-Chemical Studies of Carboxylic Acid and Glycine Adsorption on Rutile TiO₂ Nanoparticles. *J Colloid Interface Sci* **2006**, *296*, (1), 71-8.

- (267) Yi, C.; Sun, Y.; Song, B.; Tian, W.; Qi, Q.; Zheng, Y.; Dai, Y.; Jiang, W. Efficient Energy Transfer in a New Hybrid Diphenylfluorene Derivative-Cds Quantum Dot Nanocomposite. *Nanotechnology* **2013**, *24*, (43), 435704.
- (268) Sam, S.; Touahir, L.; Salvador Andresa, J.; Allongue, P.; Chazalviel, J. N.; Gouget-Laemmel, A. C.; Henry de Villeneuve, C.; Morailon, A.; Ozanam, F.; Gabouze, N.; Djebbar, S. Semiquantitative Study of the EDC/NHS Activation of Acid Terminal Groups at Modified Porous Silicon Surfaces. *Langmuir* **2010**, *26*, (2), 809-14.
- (269) Hulme, E. C.; Trevethick, M. A. Ligand Binding Assays at Equilibrium: Validation and Interpretation. *Br J Pharmacol* **2010**, *161*, (6), 1219-37.
- (270) Tan, L.; Xie, Q.; Yao, S. Electrochemical Piezoelectric Quartz Crystal Impedance Study on the Interaction Between Concanavalin A and Glycogen at Au Electrodes. *Bioelectrochemistry* **2007**, *70*, (2), 348-55.
- (271) Horisberger, M. An Application Of Ellipsometry. Assessment of Polysaccharide and Glycoprotein Interaction With Lectin at a Liquid/Solid Interface. *Biochim Biophys Acta* **1980**, *632*, (2), 298-309.
- (272) Mislovicova, D.; Masarova, J.; Svitel, J.; Mendichi, R.; Soltes, L.; Gemeiner, P.; Danielsson, B. Neoglycoconjugates of Mannan With Bovine Serum Albumin and Their Interaction With Lectin Concanavalin A. *Bioconjug Chem* **2002**, *13*, (1), 136-42.
- (273) Ohyama, Y.; Kasai, K.; Nomoto, H.; Inoue, Y. Frontal Affinity Chromatography of Ovalbumin Glycoasparagines on A Concanavalin A-Sepharose Column. A Quantitative Study of the Binding Specificity of the Lectin. *J Biol Chem* **1985**, *260*, (11), 6882-7.
- (274) Mueller, A.; Raptis, J.; Rice, P. J.; Kalbfleisch, J. H.; Stout, R. D.; Ensley, H. E.; Browder, W.; Williams, D. L. The Influence of Glucan Polymer Structure and Solution

Conformation on Binding To (1->3)-Beta-D-Glucan Receptors in A Human Monocyte-Like Cell Line. *Glycobiology* **2000**, *10*, (4), 339-46.

(275) kemasa Kojima, K. T.; and, W. I.; Yanaki, T. Molecular Weight Dependence of the Antitumor Activity of Schizophyllan. *Agric. Biol Chem.* **1985**, *1*, (50), 231-232.

(276) Goldstein, I. J.; Reichert, C. M.; Misaki, A. Interaction of Concanavalin A With Model Substrates. *Ann N Y Acad Sci* **1974**, *234*, (0), 283-96.

(277) Roach, P. J.; Depaoli-Roach, A. A.; Hurley, T. D.; Tagliabracci, V. S. Glycogen and its Metabolism: Some New Developments and Old Themes. *Biochem J* **2012**, *441*, (3), 763-87.

(278) Cawley, T. N.; Ballou, C. E. Identification of Two *Saccharomyces Cerevisiae* Cell Wall Mannan Chemotypes. *J Bacteriol* **1972**, *111*, (3), 690-5.

(279) Jones, G. H.; Ballou, C. E. Studies on the Structure of Yeast Mannan. II. Mode Of Action of the *Arthrobacter* Alpha-Mannosidase on Yeast Mannan. *J Biol Chem* **1969**, *244*, (3), 1052-9.

(280) Nakajima, T.; Ballou, C. E. Characterization of the Carbohydrate Fragments Obtained From *Saccharomyces Cerevisiae* Mannan by Alkaline Degradation. *J Biol Chem* **1974**, *249*, (23), 7679-84.

(281) Kwiatkowski, S. K. a. S. E., Yeast (*Saccharomyces cerevisiae*) Glucan Polysaccharides – Occurrence, Separation and Application in Food, Feed and Health Industries. In *THE COMPLEX WORLD OF POLYSACCHARIDES* Karunaratne, D. N., Ed. InTech: 2012; pp 47-70.

(282) Stephen J. Martin, V. E. G., and Gregory C. Frye. Characterization of a Quartz Crystal Microbalance With Simultaneous Mass and Liquid Loading. *Anal. Chem* **1991**, *63*, (20), 2272-2281.

- (283) Fu, Y.; Chen, C.; Xie, Q.; Xu, X.; Zou, C.; Zhou, Q.; Tan, L.; Tang, H.; Zhang, Y.; Yao, S. Immobilization of Enzymes Through One-Pot Chemical Preoxidation and Electropolymerization of Dithiols in Enzyme-Containing Aqueous Suspensions to Develop Biosensors With Improved Performance. *Anal Chem* **2008**, *80*, (15), 5829-38.
- (284) Mamo, T.; Moseman, E. A.; Kolishetti, N.; Salvador-Morales, C.; Shi, J.; Kuritzkes, D. R.; Langer, R.; von Andrian, U.; Farokhzad, O. C. Emerging Nanotechnology Approaches for HIV/AIDS Treatment and Prevention. *Nanomedicine* **2010**, *5*, (2), 269-85.
- (285) Tian, Y.; Wang, H.; Liu, Y.; Mao, L.; Chen, W.; Zhu, Z.; Liu, W.; Zheng, W.; Zhao, Y.; Kong, D.; Yang, Z.; Zhang, W.; Shao, Y.; Jiang, X. A Peptide-Based Nanofibrous Hydrogel as a Promising DNA Nanovector for Optimizing the Efficacy of HIV Vaccine. *Nano Lett* **2014**, *14*, (3), 1439-45.
- (286) UNAIDS. Fact Sheet. <http://www.unaids.org/en/resources/fact-sheet>. (03/28/2017).
- (287) Balzarini, J. Carbohydrate-Binding Agents: A Potential Future Cornerstone for the Chemotherapy of Enveloped Viruses? *Antivir Chem Chemother* **2007**, *18*, (1), 1-11.
- (288) Balzarini, J. V. L., K. Hatse, S. Froeyen, M. Peumans, W. Van Damme, E. Schols, D. Carbohydrate-Binding Agents Cause Deletions of Highly Conserved Glycosylation Sites in HIV GP120: A New Therapeutic Concept to Hit the Achilles Heel Of HIV. *J Biol Chem* **2005**, *280*, (49), 41005-14.
- (289) Pollicita, M.; Schols, D.; Aquaro, S.; Peumans, W. J.; Van Damme, E. J.; Perno, C. F.; Balzarini, J. Carbohydrate-Binding Agents (Cbas) Inhibit HIV-1 Infection in Human Primary Monocyte-Derived Macrophages (Mdms) and Efficiently Prevent MDM-Directed Viral Capture and Subsequent Transmission to CD4+ T Lymphocytes. *Virology* **2008**, *370*, (2), 382-91.

- (290) Balzarini, J. Targeting the Glycans of Glycoproteins: A Novel Paradigm for Antiviral Therapy. *Nat Rev Microbiol* **2007**, *5*, (8), 583-97.
- (291) Xue, J.; Gao, Y.; Hoorelbeke, B.; Kagiampakis, I.; Zhao, B.; Demeler, B.; Balzarini, J.; Liwang, P. J. The Role Of Individual Carbohydrate-Binding Sites in the Function of the Potent Anti-HIV Lectin Griffithsin. *Mol Pharm* **2012**, *9*, (9), 2613-25.
- (292) Mandal, D. K.; Brewer, C. F. Interactions of Concanavalin A With Glycoproteins: Formation of Homogeneous Glycoprotein-Lectin Cross-Linked Complexes in Mixed Precipitation Systems. *Biochemistry* **1992**, *31*, (50), 12602-9.
- (293) Mondor, I.; Moulard, M.; Ugolini, S.; Klasse, P. J.; Hoxie, J.; Amara, A.; Delaunay, T.; Wyatt, R.; Sodroski, J.; Sattentau, Q. J. Interactions Among HIV Gp120, CD4, and CXCR4: Dependence on CD4 Expression Level, Gp120 Viral Origin, Conservation of The Gp120 COOH- and NH₂-Termini and V1/V2 And V3 Loops, and Sensitivity to Neutralizing Antibodies. *Virology* **1998**, *248*, (2), 394-405.
- (294) Leonard, C. K.; Spellman, M. W.; Riddle, L.; Harris, R. J.; Thomas, J. N.; Gregory, T. J. Assignment of Intrachain Disulfide Bonds and Characterization of Potential Glycosylation Sites of the Type 1 Recombinant Human Immunodeficiency Virus Envelope Glycoprotein (Gp120) Expressed in Chinese Hamster Ovary Cells. *J Biol Chem* **1990**, *265*, (18), 10373-82.
- (295) Bhattacharyya, L.; Brewer, C. F. Interactions of Concanavalin A With Asparagine-Linked Glycopeptides. Structure/Activity Relationships of the Binding And Precipitation of Oligomannose and Bisected Hybrid-Type Glycopeptides With Concanavalin A. *Eur J Biochem* **1989**, *178*, (3), 721-26.

- (296) Parekh, G.; Pattekari, P.; Joshi, C.; Shutava, T.; DeCoster, M.; Levchenko, T.; Torchilin, V.; Lvov, Y. Layer-By-Layer Nanoencapsulation Of Camptothecin With Improved Activity. *Int J Pharm* **2014**, *465*, (1-2), 218-27.
- (297) Ruttala, H. B.; Ramasamy, T.; Shin, B. S.; Choi, H. G.; Yong, C. S.; Kim, J. O. Layer-By-Layer Assembly of Hierarchical Nanoarchitectures to Enhance the Systemic Performance of Nanoparticle Albumin-Bound Paclitaxel. *Int J Pharm* **2017**, *519*, (1-2), 11-21.
- (298) Kittitheeranun, P.; Sajomsang, W.; Phanpee, S.; Treetong, A.; Wutikhun, T.; Suktham, K.; Puttipipatkachorn, S.; Ruktanonchai, U. R. Layer-By-Layer Engineered Nanocapsules of Curcumin With Improved Cell Activity. *Int J Pharm* **2015**, *492*, (1-2), 92-102.
- (299) Labala, S.; Mandapalli, P. K.; Kurumaddali, A.; Venuganti, V. V. Layer-By-Layer Polymer Coated Gold Nanoparticles for Topical Delivery of Imatinib Mesylate to Treat Melanoma. *Mol Pharm* **2015**, *12*, (3), 878-88.
- (300) Beyer, S.; Mak, W. C.; Trau, D. Reverse-Phase LBL-Encapsulation of Highly Water Soluble Materials by Layer-By-Layer Polyelectrolyte Self-Assembly. *Langmuir* **2007**, *23*, (17), 8827-32.
- (301) Richardson, J. J.; Bjornmalm, M.; Caruso, F. Multilayer Assembly. Technology-Driven Layer-By-Layer Assembly of Nanofilms. *Science* **2015**, *348*, (6233), aaa2491.
- (302) Zhang, C.; Zhang, T.; Oyler, N. A.; Youan, B. B. Direct and Real-Time Quantification of Tenofovir Release From Ph-Sensitive Microparticles into Simulated Biological Fluids Using $(1)H$ Nuclear Magnetic Resonance. *J Pharm Sci* **2014**, *103*, (4), 1170-7.
- (303) Agrahari, V. M., Jianing; Purohit, Sudhaunshu; Oyler, Nathan and Youan, Bi-Botti. Real-Time Analysis of Tenofovir Release Kinetics Using Quantitative Phosphorus ($31P$) Nuclear Magnetic Resonance Spectroscopy. *J Pharm Sci* **2017**, *in press*.

- (304) Lackman-Smith, C.; Osterling, C.; Luckenbaugh, K.; Mankowski, M.; Snyder, B.; Lewis, G.; Paull, J.; Profy, A.; Ptak, R. G.; Buckheit, R. W., Jr.; Watson, K. M.; Cummins, J. E., Jr.; Sanders-Bear, B. E. Development of a Comprehensive Human Immunodeficiency Virus Type 1 Screening Algorithm for Discovery and Preclinical Testing of Topical Microbicides. *Antimicrob Agents Chemother* **2008**, *52*, (5), 1768-81.
- (305) Ma, B.; Forney, L. J.; Ravel, J. Vaginal Microbiome: Rethinking Health and Disease. *Annu Rev Microbiol* **2012**, *66*, 371-89.
- (306) Meng, J.; Sturgis, T. F.; Youan, B. B. Engineering Tenofovir Loaded Chitosan Nanoparticles to Maximize Microbicide Mucoadhesion. *Eur J Pharm Sci* **2011**, *44*, (1-2), 57-67.
- (307) Bural, C.; Aktas, E.; Deniz, G.; Unlucerci, Y.; Bayraktar, G. Effect of Leaching Residual Methyl Methacrylate Concentrations on In Vitro Cytotoxicity of Heat Polymerized Denture Base Acrylic Resin Processed With Different Polymerization Cycles. *J Appl Oral Sci* **2011**, *19*, (4), 306-12.
- (308) Jiao, Y.; Ma, S.; Li, J.; Shan, L.; Yang, Y.; Li, M.; Chen, J. The Influences of N-Acetyl Cysteine (NAC) on the Cytotoxicity and Mechanical Properties of Poly-Methylmethacrylate (PMMA)-Based Dental Resin. *PeerJ* **2015**, *3*, e868.
- (309) Fichorova, R. N.; Cronin, A. O.; Lien, E.; Anderson, D. J.; Ingalls, R. R. Response to Neisseria Gonorrhoeae by Cervicovaginal Epithelial Cells Occurs in the Absence Of Toll-Like Receptor 4-Mediated Signaling. *J Immunol* **2002**, *168*, (5), 2424-32.
- (310) Borenfreund, E.; Puerner, J. A. Toxicity Determined In Vitro by Morphological Alterations and Neutral Red Absorption. *Toxicol Lett* **1985**, *24*, (2-3), 119-24.

- (311) Lanone, S.; Rogerieux, F.; Geys, J.; Dupont, A.; Maillot-Marechal, E.; Boczkowski, J.; Lacroix, G.; Hoet, P. Comparative Toxicity of 24 Manufactured Nanoparticles in Human Alveolar Epithelial and Macrophage Cell Lines. *Part Fibre Toxicol* **2009**, *6*, 14.
- (312) Ivanova, L.; Uhlig, S. A Bioassay for the Simultaneous Measurement of Metabolic Activity, Membrane Integrity, and Lysosomal Activity in Cell Cultures. *Anal Biochem* **2008**, *379*, (1), 16-9.
- (313) Repetto, G.; del Peso, A.; Zurita, J. L. Neutral Red Uptake Assay for the Estimation Of Cell Viability/Cytotoxicity. *Nat Protoc* **2008**, *3*, (7), 1125-31.
- (314) Riss, T. L.; Moravec, R. A.; Niles, A. L.; Duellman, S.; Benink, H. A.; Worzella, T. J.; Minor, L., Cell Viability Assays. In *Assay Guidance Manual*, Sittampalam, G. S.; Coussens, N. P.; Brimacombe, K.; Grossman, A.; Arkin, M.; Auld, D.; Austin, C.; Baell, J.; Bejcek, B.; Chung, T. D. Y.; Dahlin, J. L.; Devanaryan, V.; Foley, T. L.; Glicksman, M.; Hall, M. D.; Hass, J. V.; Inglese, J.; Iversen, P. W.; Kahl, S. D.; Lal-Nag, M.; Li, Z.; McGee, J.; McManus, O.; Riss, T.; Trask, O. J., Jr.; Weidner, J. R.; Xia, M.; Xu, X., Eds. Bethesda (MD), 2004.
- (315) Vega-Avila, E.; Pugsley, M. K. An Overview of Colorimetric Assay Methods Used to Assess Survival or Proliferation of Mammalian Cells. *Proc West Pharmacol Soc* **2011**, *54*, 10-4.
- (316) Kacimi, R.; Giffard, R. G.; Yenari, M. A. Endotoxin-Activated Microglia Injure Brain Derived Endothelial Cells Via NF-Kappab, JAK-STAT and JNK Stress Kinase Pathways. *J Inflamm (Lond)* **2011**, *8*, (7), 1-15.
- (317) Nurhasni, H.; Cao, J.; Choi, M.; Kim, I.; Lee, B. L.; Jung, Y.; Yoo, J. W. Nitric Oxide-Releasing Poly(Lactic-Co-Glycolic Acid)-Polyethylenimine Nanoparticles for Prolonged

Nitric Oxide Release, Antibacterial Efficacy, and in Vivo Wound Healing Activity. *Int J Nanomedicine* **2015**, *10*, 3065-80.

(318) Heigold, S.; Sers, C.; Bechtel, W.; Ivanovas, B.; Schafer, R.; Bauer, G. Nitric Oxide Mediates Apoptosis Induction Selectively in Transformed Fibroblasts Compared to Nontransformed Fibroblasts. *Carcinogenesis* **2002**, *23*, (6), 929-41.

(319) Lee, V.; McMahan, R. S.; Hu, X.; Gao, X.; Faustman, E. M.; Griffith, W. C.; Kavanagh, T. J.; Eaton, D. L.; McGuire, J. K.; Parks, W. C. Amphiphilic Polymer-Coated Cdse/Zns Quantum Dots Induce Pro-Inflammatory Cytokine Expression in Mouse Lung Epithelial Cells and Macrophages. *Nanotoxicology* **2015**, *9*, (3), 336-43.

(320) Guo, J.; Meng, F.; Li, L.; Zhong, B.; Zhao, Y. Development and Validation of an LC/MS/MS Method for the Determination of Tenofovir in Monkey Plasma. *Biol Pharm Bull* **2011**, *34*, (6), 877-82.

(321) Owen, D. H.; Katz, D. F. A Vaginal Fluid Simulant. *Contraception* **1999**, *59*, (2), 91-5.

(322) Owen, D. H.; Katz, D. F. A Review of the Physical and Chemical Properties of Human Semen and the Formulation of a Semen Simulant. *J Androl* **2005**, *26*, (4), 459-69.

(323) Klasse, P. J.; Moore, J. P. Is There Enough Gp120 in the Body Fluids of HIV-1-Infected Individuals to Have Biologically Significant Effects? *Virology* **2004**, *323*, (1), 1-8.

(324) Costa, P.; Sousa Lobo, J. M. Modeling and Comparison of Dissolution Profiles. *Eur J Pharm Sci* **2001**, *13*, (2), 123-33.

(325) Grabovac, V.; Guggi, D.; Bernkop-Schnurch, A. Comparison of the Mucoadhesive Properties of Various Polymers. *Adv Drug Deliv Rev* **2005**, *57*, (11), 1713-23.

- (326) Meng, J.; Zhang, T.; Agrahari, V.; Ezoulin, M. J.; Youan, B. B. Comparative Biophysical Properties of Tenofovir-Loaded, Thiolated and Nonthiolated Chitosan Nanoparticles Intended for HIV Prevention. *Nanomedicine* **2014**, *9*, (11), 1595-612.
- (327) Changyou Gao, S. M., Edwin Donath, Helmuth Möhwald. Melamine Formaldehyde Core Decomposition as the Key Step Controlling Capsule Integrity: Optimizing the Polyelectrolyte Capsule Fabrication. *Macromol. Chem. Phys* **2002**, *203*, (7), 953-960.
- (328) Petrov, A. I.; Volodkin, D. V.; Sukhorukov, G. B. Protein-Calcium Carbonate Coprecipitation: A Tool for Protein Encapsulation. *Biotechnol Prog* **2005**, *21*, (3), 918-25.
- (329) Ma, J.; Meng, J.; Simonet, M.; Stingelin, N.; Peijs, T.; Sukhorukov, G. B. Biodegradable Fibre Scaffolds Incorporating Water-Soluble Drugs and Proteins. *J Mater Sci Mater Med* **2015**, *26*, (7), 205.
- (330) Ergul Yilmaz, Z.; Cordonnier, T.; Debuigne, A.; Calvignac, B.; Jerome, C.; Boury, F. Protein Encapsulation and Release From PEO-B-Polyphosphoester Templated Calcium Carbonate Particles. *Int J Pharm* **2016**, *513*, (1-2), 130-137.
- (331) Locatelli, F.; Del Vecchio, L.; Violo, L.; Pontoriero, G. Phosphate Binders for the Treatment of Hyperphosphatemia in Chronic Kidney Disease Patients on Dialysis: A Comparison of Safety Profiles. *Expert Opin Drug Saf* **2014**, *13*, (5), 551-61.
- (332) Friedman, E. A. Calcium-Based Phosphate Binders are Appropriate in Chronic Renal Failure. *Clin J Am Soc Nephrol* **2006**, *1*, (4), 704-9.
- (333) Friedman, E. A. An Introduction to Phosphate Binders for the Treatment of Hyperphosphatemia in Patients With Chronic Kidney Disease. *Kidney Int Suppl* **2005**, (96), S2-6.

- (334) Nguyen, T. M.; Muller, R. H.; Taupitz, M.; Schnorr, J.; Hamm, B.; Wagner, S. Novel Oral Phosphate Binder With Nanocrystalline Maghemite-Phosphate Binding Capacity and pH Effect. *Int J Pharm* **2015**, *482*, (1-2), 21-6.
- (335) Ueno, Y.; Futagawa, H.; Takagi, Y.; Ueno, A.; Mizushima, Y. Drug-Incorporating Calcium Carbonate Nanoparticles for a New Delivery System. *J Control Release* **2005**, *103*, (1), 93-8.
- (336) Mahaguna, V.; McDermott, J. M.; Zhang, F.; Ochoa, F. Investigation of Product Quality Between Extemporaneously Compounded Progesterone Vaginal Suppositories And an Approved Progesterone Vaginal Gel. *Drug Dev Ind Pharm* **2004**, *30*, (10), 1069-78.
- (337) Shanmugam, S.; Kim, Y. H.; Park, J. H.; Im, H. T.; Sohn, Y. T.; Kim, K. S.; Kim, Y. I.; Yong, C. S.; Kim, J. O.; Choi, H. G.; Woo, J. S. Sildenafil Vaginal Suppositories: Preparation, Characterization, in Vitro and in Vivo Evaluation. *Drug Dev Ind Pharm* **2014**, *40*, (6), 803-12.
- (338) Johnson, T. J.; Clark, M. R.; Albright, T. H.; Nebeker, J. S.; Tuitupou, A. L.; Clark, J. T.; Fabian, J.; McCabe, R. T.; Chandra, N.; Doncel, G. F.; Friend, D. R.; Kiser, P. F. A 90-Day Tenofovir Reservoir Intravaginal Ring for Mucosal HIV Prophylaxis. *Antimicrob Agents Chemother* **2012**, *56*, (12), 6272-83.
- (339) Hendrix, C. W.; Chen, B. A.; Guddera, V.; Hoesley, C.; Justman, J.; Nakabiito, C.; Salata, R.; Soto-Torres, L.; Patterson, K.; Minnis, A. M.; Gandham, S.; Gomez, K.; Richardson, B. A.; Bumpus, N. N. MTN-001: Randomized Pharmacokinetic Cross-Over Study Comparing Tenofovir Vaginal Gel and Oral Tablets in Vaginal Tissue and Other Compartments. *PLoS One* **2013**, *8*, (1), e55013.
- (340) Gilberto Íñiguez, A. V., Ricardo Manríquez and María V. Moreno. Utilization of By-Products From the Tequila Industry. Part 10: Characterization of Different Decomposition

Stages of *Agave Tequilana* Webber Bagasse Using Ftir Spectroscopy, Thermogravimetric Analysis and Scanning Electron Microscopy. *Rev. Int. Contam. Ambie.* **2011**, *27*, (1), 61-74.

(341) M. Grube, E. Z., E. Gromozova, M. Fomina. Comparative Investigation of the Macromolecular Composition of Mycelia Forms *Thielaõia Terrestris* by Infrared Spectroscopy. *Vibrational Spectroscopy* **1999**, *19*, 301–306.

(342) Deflores, L. P.; Ganim, Z.; Nicodemus, R. A.; Tokmakoff, A. Amide I-II' 2D IR Spectroscopy Provides Enhanced Protein Secondary Structural Sensitivity. *J Am Chem Soc* **2009**, *131*, (9), 3385-91.

(343) Ni, M.; Ratner, B. D. Differentiation of Calcium Carbonate Polymorphs by Surface Analysis Techniques - an XPS and TOF-SIMS study. *Surf Interface Anal* **2008**, *40*, (10), 1356-1361.

(344) Borba, A.; Gomez-Zavaglia, A.; Simoes, P. N.; Fausto, R. Matrix-Isolation FT-IR Spectra and Theoretical Study of Dimethyl Sulfate. *Spectrochim Acta A Mol Biomol Spectrosc* **2005**, *61*, (7), 1461-70.

(345) Dahl, M.; Castaneda, F.; Joo, J. B.; Reyes, V.; Goebel, J.; Yin, Y. Ethylene Glycol-Assisted Coating of Titania on Nanoparticles. *Dalton Trans* **2015**.

(346) Yi Zhu, W. T. a. C. G. Molecular-Engineered Polymeric Microcapsules Assembled From Concanavalin A and Glycogen With Specific Responses to Carbohydrates. *Soft Matter* **2011**, *7*, 5805–5815.

(347) Quayle, A. J. The Innate and Early Immune Response to Pathogen Challenge in the Female Genital Tract and the Pivotal Role of Epithelial Cells. *J Reprod Immunol* **2002**, *57*, (1-2), 61-79.

- (348) Klebanoff, S. J.; Coombs, R. W. Viricidal Effect of Lactobacillus Acidophilus on Human Immunodeficiency Virus Type 1: Possible Role in Heterosexual Transmission. *J Exp Med* **1991**, *174*, (1), 289-92.
- (349) Wilks, M.; Wiggins, R.; Whiley, A.; Hennessy, E.; Warwick, S.; Porter, H.; Corfield, A.; Millar, M. Identification And H₂O₂ Production of Vaginal Lactobacilli From Pregnant Women at High Risk of Preterm Birth and Relation With Outcome. *J Clin Microbiol* **2004**, *42*, (2), 713-7.
- (350) Galvin, S. R.; Cohen, M. S. The Role of Sexually Transmitted Diseases in HIV Transmission. *Nat Rev Microbiol* **2004**, *2*, (1), 33-42.
- (351) Boily-Larouche, G.; Kenyan, Y.; Fowke, K., Immune Activation and HIV Transmission. In *Encyclopedia of AIDS*, Hope, T. J.; Stevenson, M.; Richman, D., Eds. Springer New York: 2014; pp 1-11.
- (352) Sharma, J. N.; Al-Omran, A.; Parvathy, S. S. Role of Nitric Oxide in Inflammatory Diseases. *Inflammopharmacology* **2007**, *15*, (6), 252-9.
- (353) Laroux, F. S.; Pavlick, K. P.; Hines, I. N.; Kawachi, S.; Harada, H.; Bharwani, S.; Hoffman, J. M.; Grisham, M. B. Role of Nitric Oxide in Inflammation. *Acta Physiol Scand* **2001**, *173*, (1), 113-8.
- (354) Amaral, K. F.; Rogero, M. M.; Fock, R. A.; Borelli, P.; Gavini, G. Cytotoxicity Analysis of EDTA and Citric Acid Applied on Murine Resident Macrophages Culture. *Int Endod J* **2007**, *40*, (5), 338-43.
- (355) Saric, J.; Li, J. V.; Swann, J. R.; Utzinger, J.; Calvert, G.; Nicholson, J. K.; Dirnhofer, S.; Dallman, M. J.; Bictash, M.; Holmes, E. Integrated Cytokine and Metabolic Analysis of

Pathological Responses to Parasite Exposure in Rodents. *J Proteome Res* **2010**, *9*, (5), 2255-64.

(356) Fantuzzi, G., *Cytokine Knockouts* 2nd ed.; Totowa, N.J. : Humana Press, c2003. : 2003.

(357) Nambu, A.; Nakae, S. IL-1 and Allergy. *Allergol Int* **2010**, *59*, (2), 125-35.

(358) Bujak, M.; Frangogiannis, N. G. The Role of IL-1 in the Pathogenesis of Heart Disease. *Arch Immunol Ther Exp (Warsz)* **2009**, *57*, (3), 165-76.

(359) Kumar, A.; Abbas, W.; Herbein, G. TNF And TNF Receptor Superfamily Members in HIV Infection: New Cellular Targets for Therapy? *Mediators Inflamm* **2013**, *2013*, 484378.

(360) Bahia, M. S.; Silakari, O. Tumor Necrosis Factor Alpha Converting Enzyme: An Encouraging Target for Various Inflammatory Disorders. *Chem Biol Drug Des* **2010**, *75*, (5), 415-43.

(361) Fernandez-Ortega, C.; Dubed, M.; Ramos, Y.; Navea, L.; Alvarez, G.; Lobaina, L.; Lopez, L.; Casillas, D.; Rodriguez, L. Non-Induced Leukocyte Extract Reduces HIV Replication and TNF Secretion. *Biochem Biophys Res Commun* **2004**, *325*, (3), 1075-81.

(362) Introini, A.; Vanpouille, C.; Lisco, A.; Grivel, J. C.; Margolis, L. Interleukin-7 Facilitates HIV-1 Transmission to Cervico-Vaginal Tissue Ex Vivo. *PLoS Pathog* **2013**, *9*, (2), e1003148.

(363) Lane, B. R.; King, S. R.; Bock, P. J.; Strieter, R. M.; Coffey, M. J.; Markovitz, D. M. The C-X-C Chemokine IP-10 Stimulates HIV-1 Replication. *Virology* **2003**, *307*, (1), 122-34.

(364) Jiao, Y.; Zhang, T.; Wang, R.; Zhang, H.; Huang, X.; Yin, J.; Zhang, L.; Xu, X.; Wu, H. Plasma IP-10 is Associated With Rapid Disease Progression in Early HIV-1 Infection. *Viral Immunol* **2012**, *25*, (4), 333-7.

- (365) Haynes, B. F.; Shattock, R. J. Critical Issues in Mucosal Immunity for HIV-1 Vaccine Development. *J Allergy Clin Immunol* **2008**, *122*, (1), 3-9; quiz 10-1.
- (366) Smith, J. M.; Rastogi, R.; Teller, R. S.; Srinivasan, P.; Mesquita, P. M.; Nagaraja, U.; McNicholl, J. M.; Hendry, R. M.; Dinh, C. T.; Martin, A.; Herold, B. C.; Kiser, P. F. Intravaginal Ring Eluting Tenofovir Disoproxil Fumarate Completely Protects Macaques From Multiple Vaginal Simian-HIV Challenges. *Proc Natl Acad Sci U S A* **2013**, *110*, (40), 16145-50.
- (367) Kashuba, A. D.; Gengiah, T. N.; Werner, L.; Yang, K. H.; White, N. R.; Karim, Q. A.; Abdool Karim, S. S. Genital Tenofovir Concentrations Correlate With Protection Against HIV Infection in the CAPRISA 004 Trial: Importance of Adherence for Microbicide Effectiveness. *J Acquir Immune Defic Syndr* **2015**, *69*, (3), 264-9.
- (368) Niebergall, P. J.; Milosovich, G.; Goyan, J. E. Dissolution Rate Studies. II. Dissolution of Particles Under Conditions Of Rapid Agitation. *J Pharm Sci* **1963**, *52*, 236-41.
- (369) Fu, Y.; Kao, W. J. Drug Release Kinetics and Transport Mechanisms of Non-Degradable and Degradable Polymeric Delivery Systems. *Expert Opin Drug Deliv* **2010**, *7*, (4), 429-44.
- (370) Yoshida, K.; Hasebe, Y.; Takahashi, S.; Sato, K.; Anzai, J. Layer-By-Layer Deposited Nano- and Micro-Assemblies for Insulin Delivery: A Review. *Mater Sci Eng C Mater Biol Appl* **2014**, *34*, 384-92.
- (371) Shindel, A. W., *Male Infertility: A Clinical Guide*. 2012; Vol. 98.
- (372) Squier, C. A.; Mantz, M. J.; Schlievert, P. M.; Davis, C. C. Porcine Vagina Ex Vivo as a Model for Studying Permeability and Pathogenesis in Mucosa. *J Pharm Sci* **2008**, *97*, (1), 9-21.

- (373) Adebisi, A. O.; Conway, B. R. Lectin-Conjugated Microspheres for Eradication of Helicobacter Pylori Infection and Interaction With Mucus. *Int J Pharm* **2014**, *470*, (1-2), 28-40.
- (374) Ning Ning Li, X. Y. C., Jiu Cun Chen, Xue Feng Hu, and Li Qun Xu. Conjugation of Lectin to Poly(ϵ -caprolactone)-blockglycopolymer Micelles for In Vitro Intravesical Drug Delivery. *Polymer* **2016**, *8*, (379), 2-15.
- (375) Anande, N. M.; Jain, S. K.; Jain, N. K. Con-A Conjugated Mucoadhesive Microspheres for the Colonic Delivery Of Diloxanide Furoate. *Int J Pharm* **2008**, *359*, (1-2), 182-9.
- (376) Kalb, A. J.; Levitzki, A. Metal-binding Sites of Concanavalin a and Their Role in the Binding of Alpha-Methyl D-Glucopyranoside. *Biochem J* **1968**, *109*, (4), 669-72.
- (377) Sunil K. Jain, M. G., Ashok K. Sahoo, Aditya N. Pandey and Akhlesh K. Jain. Lectin Conjugated Gastro-Retentive Microspheres of Amoxicillin for Effective Treatment of Helicobacter Pylori. *CURRENT SCIENCE* **2014**, *106*, (2), 267-276.
- (378) Nicol, M. R.; Adams, J. L.; Kashuba, A. D. HIV PrEP Trials: The Road to Success. *Clin Investig (Lond)* **2013**, *3*, (3).
- (379) Obiero, J.; Mwethera, P. G.; Wiysonge, C. S. Topical Microbicides For Prevention Of Sexually Transmitted Infections. *Cochrane Database Syst Rev* **2012**, (6), CD007961.
- (380) Fichorova, R. N., Safety Aspect of Topical Anti-HIV Microbicides. In *Drug Delivery and Development of Anti-HIV Microbicides*, José das Neves, B. S., Ed. Pan Stanford Publishing Pte. Ltd.: Singapore, 2015.
- (381) Naranbhai, V.; Abdool Karim, S. S.; Altfeld, M.; Samsunder, N.; Durgiah, R.; Sibeko, S.; Abdool Karim, Q.; Carr, W. H. Innate Immune Activation Enhances HIV Acquisition In

Women, Diminishing the Effectiveness of Tenofovir Microbicide Gel. *J Infect Dis* **2012**, *206*, (7), 993-1001.

(382) Iwasaki, A. Antiviral Immune Responses in the Genital Tract: Clues for Vaccines. *Nat Rev Immunol* **2010**, *10*, (10), 699-711.

(383) Coulibaly, F. S.; Ezoulin, M. J. M.; Purohit, S. S.; Ayon, N. J.; Oyler, N. A.; Youan, B. C. Layer-by-Layer Engineered Microbicide Drug Delivery System Targeting HIV-1 gp120: Physicochemical and Biological Properties. *Mol Pharm* **2017**, *14*, (10), 3512-3527.

(384) Cone, R. A. Vaginal Microbiota and Sexually Transmitted Infections that May Influence Transmission of Cell-Associated HIV. *J Infect Dis* **2014**, *210 Suppl 3*, S616-21.

(385) Cunha, A. R.; Machado, R. M.; Palmeira-de-Oliveira, A.; Martinez-de-Oliveira, J.; das Neves, J.; Palmeira-de-Oliveira, R. Characterization of Commercially Available Vaginal Lubricants: A Safety Perspective. *Pharmaceutics* **2014**, *6*, (3), 530-42.

(386) Lacey, C. J.; Woodhall, S.; Qi, Z.; Sawant, S.; Cowen, M.; McCormack, S.; Jiang, S. Unacceptable Side-Effects Associated With a Hyperosmolar Vaginal Microbicide in a Phase 1 trial. *Int J STD AIDS* **2010**, *21*, (10), 714-7.

(387) Dezzutti, C. S.; Rohan, L. C.; Wang, L.; Uranker, K.; Shetler, C.; Cost, M.; Lynam, J. D.; Friend, D. Reformulated Tenofovir Gel for Use as a Dual Compartment Microbicide. *J Antimicrob Chemother* **2012**, *67*, (9), 2139-42.

(388) Pasquel, F. J.; Umpierrez, G. E. Hyperosmolar Hyperglycemic State: A Historic Review of the Clinical Presentation, Diagnosis, and Treatment. *Diabetes Care* **2014**, *37*, (11), 3124-31.

- (389) Fuchs, E. J.; Lee, L. A.; Torbenson, M. S.; Parsons, T. L.; Bakshi, R. P.; Guidos, A. M.; Wahl, R. L.; Hendrix, C. W. Hyperosmolar Sexual Lubricant Causes Epithelial Damage in the Distal Colon: Potential Implication for HIV Transmission. *J Infect Dis* **2007**, *195*, (5), 703-10.
- (390) Ham, A. S.; Nugent, S. T.; Peters, J. J.; Katz, D. F.; Shelter, C. M.; Dezzutti, C. S.; Boczar, A. D.; Buckheit, K. W.; Buckheit, R. W., Jr. The Rational Design and Development of a Dual Chamber Vaginal/Rectal Microbicide Gel Formulation for HIV Prevention. *Antiviral Res* **2015**, *120*, 153-64.
- (391) Milionis, H. J.; Liamis, G. L.; Elisaf, M. S. The Hyponatremic Patient: A Systematic Approach to Laboratory Diagnosis. *Cmaj* **2002**, *166*, (8), 1056-62.
- (392) Agrahari, V. Formulation Of Hyaluronidase Enzyme Sensitive Topical Nanomicrobicides for HIV Virus Transmission Prevention University Of Missouri-Kansas City, Kansas City, Missouri, 2015.
- (393) Meng, J. Design and Evaluation of HIV Microbicides Loaded Mucoadhesive Nanoformulation University Of Missouri-Kansas City, Kansas City, Missouri 2015.
- (394) Byers, S. L.; Wiles, M. V.; Dunn, S. L.; Taft, R. A. Mouse Estrous Cycle Identification Tool and Images. *PLoS One* **2012**, *7*, (4), e35538.
- (395) Caligioni, C. S. Assessing Reproductive Status/Stages in Mice. *Curr Protoc Neurosci* **2009**, *Appendix 4*, Appendix 4I.
- (396) McLean, A. C.; Valenzuela, N.; Fai, S.; Bennett, S. A. Performing Vaginal Lavage, Crystal Violet Staining, and Vaginal Cytological Evaluation for Mouse Estrous Cycle Staging Identification. *J Vis Exp* **2012**, (67), e4389.

- (397) Patton, D. L.; Kidder, G. G.; Sweeney, Y. C.; Rabe, L. K.; Hillier, S. L. Effects of Multiple Applications of Benzalkonium Chloride And Nonoxynol 9 on the Vaginal Epithelium in the Pigtailed Macaque (*Macaca Nemestrina*). *Am J Obstet Gynecol* **1999**, *180*, (5), 1080-7.
- (398) Schreiber, C. A.; Meyn, L. A.; Creinin, M. D.; Barnhart, K. T.; Hillier, S. L. Effects of Long-Term Use of Nonoxynol-9 on Vaginal Flora. *Obstet Gynecol* **2006**, *107*, (1), 136-43.
- (399) Zhang, T.; Sturgis, T. F.; Youan, B. B. pH-Responsive Nanoparticles Releasing Tenofovir Intended for the Prevention Of HIV Transmission. *Eur J Pharm Biopharm* **2011**, *79*, (3), 526-36.
- (400) Qingxin Mu, J. Y., Lisa A. McConnachie, John C. Kraft, Yu Gao, Gaurav K. Gulati & Rodney J. Y. Translation of Combination Nanodrugs into Nanomedicines: Lessons Learned and Future Outlook. *Journal of Drug Targeting* **2018**, *26*, (5), 435-447
- (401) Chaowanachan, T.; Krogstad, E.; Ball, C.; Woodrow, K. A. Drug Synergy of Tenofovir and Nanoparticle-Based Antiretrovirals for HIV Prophylaxis. *PLoS One* **2013**, *8*, (4), e61416.
- (402) Nakata, H.; Amano, M.; Koh, Y.; Kodama, E.; Yang, G.; Bailey, C. M.; Kohgo, S.; Hayakawa, H.; Matsuoka, M.; Anderson, K. S.; Cheng, Y. C.; Mitsuya, H. Activity Against Human Immunodeficiency Virus Type 1, Intracellular Metabolism, and Effects on Human DNA Polymerases of 4'-Ethyne-2-Fluoro-2'-Deoxyadenosine. *Antimicrob Agents Chemother* **2007**, *51*, (8), 2701-8.
- (403) DrugBank. Tenofovir Disoproxil. <https://www.drugbank.ca/drugs/DB00300>. (3/29/2018).
- (404) Kim, Y. K.; Choi, M. J.; Oh, T. Y.; Yu, K. S.; Lee, S. A Comparative Pharmacokinetic and Tolerability Analysis of the Novel Orotic Acid Salt Form of Tenofovir Disoproxil and the Fumaric Acid Salt Form in Healthy Subjects. *Drug Des Devel Ther* **2017**, *11*, 3171-3177.

- (405) ChEMBL. Nonoxynol-9.
<https://www.ebi.ac.uk/chembl/db/index.php/compound/inspect/CHEMBL1410>. (3/29/2018).
- (406) DrugBank. Nonoxynol-9. <https://www.drugbank.ca/drugs/DB06804>. (3/29/2018),
- (407) Weber, J.; Desai, K.; Darbyshire, J. The Development of Vaginal Microbicides for the Prevention of HIV Transmission. *PLoS Med* **2005**, *2*, (5), e142.
- (408) D'Cruz, O. J.; Ghosh, P.; Uckun, F. M. Spermicidal Activity of Chelated Complexes of Bis(Cyclopentadienyl)Vanadium(IV). *Mol Hum Reprod* **1998**, *4*, (7), 683-93.
- (409) Chhonker, Y. S.; Chandasana, H.; Bala, V.; Kumar, L.; Sharma, V. L.; Gupta, G.; Bhatta, R. S. Quantitative Determination Of Microbicidal Spermicide 'Nonoxynol-9' in Rabbit Plasma and Vaginal Fluid Using LC-ESI-MS/MS: Application to Pharmacokinetic Study. *J Chromatogr B Analyt Technol Biomed Life Sci* **2014**, *965*, 127-32.
- (410) ChEMBL. Benzalkonium Chloride.
<https://www.ebi.ac.uk/chembl/compound/inspect/CHEMBL502109>. (3/29/2018),
- (411) MPS. Benzalkonium Chloride. <https://mps.csb.pitt.edu/compounds/342/>. (3/29/2018).
- (412) Xun-cheng Ding, W.-h. L., Jie-fei LI, Qiang-yi Wang. Optimized Benzalkonium Chloride Gel: A Potential Vaginal Microbicides. *Journal of Reproduction and Contraception* **2007**, *18*, (2), 89-92.
- (413) Catalone, B. J.; Kish-Catalone, T. M.; Budgeon, L. R.; Neely, E. B.; Ferguson, M.; Krebs, F. C.; Howett, M. K.; Labib, M.; Rando, R.; Wigdahl, B. Mouse Model of Cervicovaginal Toxicity and Inflammation For Preclinical Evaluation of Topical Vaginal Microbicides. *Antimicrob Agents Chemother* **2004**, *48*, (5), 1837-47.
- (414) Catalone, B. J.; Kish-Catalone, T. M.; Neely, E. B.; Budgeon, L. R.; Ferguson, M. L.; Stiller, C.; Miller, S. R.; Malamud, D.; Krebs, F. C.; Howett, M. K.; Wigdahl, B. Comparative

Safety Evaluation of the Candidate Vaginal Microbicide C31G. *Antimicrob Agents Chemother* **2005**, *49*, (4), 1509-20.

(415) Altin, J. G.; Sloan, E. K. The Role Of CD45 And CD45-Associated Molecules in T Cell Activation. *Immunol Cell Biol* **1997**, *75*, (5), 430-45.

(416) Ngamcherdtrakul, W.; Morry, J.; Gu, S.; Castro, D. J.; Goodyear, S. M.; Sangvanich, T.; Reda, M. M.; Lee, R.; Mihelic, S. A.; Beckman, B. L.; Hu, Z.; Gray, J. W.; Yantasee, W. Cationic Polymer Modified Mesoporous Silica Nanoparticles for Targeted SiRNA Delivery to HER2+ Breast Cancer. *Adv Funct Mater* **2015**, *25*, (18), 2646-2659.

(417) Stetefeld, J.; McKenna, S. A.; Patel, T. R. Dynamic Light Scattering: A Practical Guide and Applications in Biomedical Sciences. *Biophys Rev* **2016**, *8*, (4), 409-427.

(418) Clogston, J. D.; Patri, A. K. Zeta Potential Measurement. *Methods Mol Biol* **2011**, *697*, 63-70.

(419) Slatopolsky, E.; Weerts, C.; Lopez-Hilker, S.; Norwood, K.; Zink, M.; Windus, D.; Delmez, J. Calcium Carbonate as a Phosphate Binder in Patients With Chronic Renal Failure Undergoing Dialysis. *N Engl J Med* **1986**, *315*, (3), 157-61.

(420) Skretting, G.; Prydz, H. An Amino Acid Exchange in Exon I of the Human Lecithin: Cholesterol Acyltransferase (LCAT) Gene is Associated With Fish Eye Disease. *Biochem Biophys Res Commun* **1992**, *182*, (2), 583-7.

(421) Chan, S.; Au, K.; Francis, R. S.; Mudge, D. W.; Johnson, D. W.; Pillans, P. I. Phosphate Binders in Patients With Chronic Kidney Disease. *Aust Prescr* **2017**, *40*, (1), 10-14.

(422) Connolly, N. C.; Riddler, S. A.; Rinaldo, C. R. Proinflammatory Cytokines in HIV Disease-A Review and Rationale for New Therapeutic Approaches. *AIDS Rev* **2005**, *7*, (3), 168-80.

- (423) Roberts, L.; Passmore, J. A.; Mlisana, K.; Williamson, C.; Little, F.; Bebell, L. M.; Walzl, G.; Abrahams, M. R.; Woodman, Z.; Abdool Karim, Q.; Abdool Karim, S. S. Genital Tract Inflammation During Early HIV-1 Infection Predicts Higher Plasma Viral Load Set Point In Women. *J Infect Dis* **2012**, *205*, (2), 194-203.
- (424) Belec, L.; Gherardi, R.; Payan, C.; Prazuck, T.; Malkin, J. E.; Tevi-Benissan, C.; Pillot, J. Proinflammatory Cytokine Expression in Cervicovaginal Secretions of Normal And HIV-Infected Women. *Cytokine* **1995**, *7*, (6), 568-74.
- (425) Mait-Kaufman, J.; Fakioglu, E.; Mesquita, P. M.; Elliott, J.; Lo, Y.; Madan, R. P. Chronic HIV Infection Is Associated With Upregulation of Proinflammatory Cytokine and Chemokine and Alpha Defensin Gene Expression in Colorectal Mucosa. *AIDS Res Hum Retroviruses* **2015**, *31*, (6), 615-22.
- (426) Poli, G.; Bressler, P.; Kinter, A.; Duh, E.; Timmer, W. C.; Rabson, A.; Justement, J. S.; Stanley, S.; Fauci, A. S. Interleukin 6 Induces Human Immunodeficiency Virus Expression In Infected Monocytic Cells Alone and in Synergy With Tumor Necrosis Factor Alpha By Transcriptional and Post-Transcriptional Mechanisms. *J Exp Med* **1990**, *172*, (1), 151-8.
- (427) Shattock, R. J.; Moore, J. P. Inhibiting Sexual Transmission of HIV-1 Infection. *Nat Rev Microbiol* **2003**, *1*, (1), 25-34.
- (428) Dominguez Rodriguez, A.; Abreu Gonzalez, P.; Garcia, M. J.; de la Rosa, A.; Vargas, M.; Marrero, F. Circadian Variations in Proinflammatory Cytokine Concentrations in Acute Myocardial Infarction. *Rev Esp Cardiol* **2003**, *56*, (6), 555-60.
- (429) Nakao, A. Temporal Regulation of Cytokines by the Circadian Clock. *Journal of Immunology Research* **2014**, *2014*, 1-4.

- (430) Keller, M.; Mazuch, J.; Abraham, U.; Eom, G. D.; Herzog, E. D.; Volk, H. D.; Kramer, A.; Maier, B. A Circadian Clock in Macrophages Controls Inflammatory Immune Responses. *Proc Natl Acad Sci U S A* **2009**, *106*, (50), 21407-12.
- (431) Monastero, R. N.; Pentylala, S. Cytokines as Biomarkers and Their Respective Clinical Cutoff Levels. *Int J Inflamm* **2017**, *2017*, 4309485.
- (432) Man Huang , X. P., Katia Karalis , Theoharis C. Theoharides. Stress-Induced Interleukin-6 Release in Mice is Mast Cell-Dependent and More Pronounced in Apolipoprotein E Knockout Mice. *Cardiovascular Research* **2003**, *59*, (2003), 241-249.
- (433) Priyapratim Patra, A. P. R., Dipankar Das, Santanu Dhara, Asit Baran Pandac and Sagar Pal. Stimuli-Responsive, Biocompatible Hydrogel Derived From Glycogen and Poly(N-Isopropylacrylamide) for Colon Targeted Delivery of Ornidazole and 5-Amino Salicylic Acid. *Polymer Chemistry* **2016**, *7*, (34), 5426-5435
- (434) Adeva-Andany, M. M.; Gonzalez-Lucan, M.; Donapetry-Garcia, C.; Fernandez-Fernandez, C.; Ameneiros-Rodriguez, E. Glycogen Metabolism in Humans. *BBA Clin* **2016**, *5*, 85-100.

VITA

Fohona Soumahila Coulibaly was born on November 13, 1984 in Korhogo, Côte d'Ivoire. He received his science focused high-school diploma in 2004 from Groupe Scolaire Offoumou Yapo in Abidjan, Côte d'Ivoire. He then joined the INSTITUT NATIONAL POLYTECHNIQUE Félix Houphouët Boigny (INP-HB) Yamoussoukro, Côte d'Ivoire, where he obtained an Associate's degree in Industrial Chemistry, in 2007, and a Bachelor of Science in Chemical Engineering, in 2011. After his B.S. degree, Mr. Fohona joined the interdisciplinary Ph.D. program in Pharmaceutical Sciences and Chemistry at the University of Missouri-Kansas City (UMKC) School of Pharmacy. Mr. Fohona is a member of American Association of Pharmaceutical Sciences (AAPS), American Chemical Society (ACS) and the Pharmaceutical Sciences Graduate Students Association (PSGSA). Throughout his Ph.D. educations, Mr. Fohona has received several awards including, Edith and Russell Nesbitt, Jr. Pharmaceutical Sciences Graduate Scholarship award (2015), the UMKC School of Graduate Studies Research Grant award (2016), and the 2017 Annual Meeting and Exposition travelship award. Mr. Fohona has also chaired the 48th Pharmaceutics Graduate Students Research Meeting in 2016. Mr. Fohona authored and co-authored several peer reviewed publications in renowned international journals and has presented his work in various scientific meetings.